Ultrasonic diagnostics of mechanical and structural degradation of concrete

Pawel Safinowski

N° d'ordre : 168

Ecole Centrale de Lille

THESE

présentée en vue
d'obtenir le grade de

DOCTEUR

Specialité : electronique

par

Paweł Safinowski

DOCTORAT DELIVERE PAR L'ECOLE CENTRALE DE LILLE

Titre de la thèse :

Diagnostic ultrasonore de la dégradation mécanique et structurale du béton
(Ultrasonic diagnostics of mechanical and structural degradation of concrete)

Soutenue en Pologne à Bydgoszcz le 25/11/2011 devant le jury d'examen :

Président **Rapporteur** Reviewer	*Zbigniew Ranachowski, Professor, Institute of Fundamental Technological Research, Polish Academy of Sciences, Warsaw (Poland)*
Rapporteur Reviewer	*Jean-Paul Balayssac, Professeur, Université de Toulouse (France)*
Directeur de thèse (France) PhD supervisor (France)	*Bogdan Piwakowski, Professeur, Ecole Centrale de Lille (France)*
Directeur de thèse (Pologne) PhD supervisor (Poland)	*Mariusz Kaczmarek, Professor, Kazimierz Wielki University, Bydgoszcz (Poland)*
Membre invité Invited Member	*Jozef Kubik, Professor, Kazimierz Wielki University, Bydgoszcz (Poland)*

Thèse préparée dans les Laboratoires:

Ecole Centrale de Lille ,IEMN UMR 8520 CNRS Groupe TPIA (Transduction, Propagation et Imagerie Acoustique) ,France
et
Kazimierz Wielki University, Institute of Mechanics and Applied Computer Science, Bydgoszcz Poland

Ecole Doctorale SPI 072 (Lille I, Lille III, Artois, ULCO, UVHC, EC Lille)
PRES Université Lille Nord-de-France

ACKNOWLEDGEMENTS

I would like to give thanks to the Advisors of the present doctoral thesis Professor Mariusz Kaczmarek and Professor Bogdan Piwakowski for the opportunity of realization of this thesis as well as for the constructive and spiritual support on every stage of its realization.

Moreover I would like to give thanks to all the employees of the Institute of Mechanics and Applied Computer Science of Kazimierz Wielki University as well as the Electronics and Acoustics Laboratory of École Central de Lille in France for openness and help in realization of the experimental part of this thesis.

I would like to give thanks to my colleague Arkadiusz Kosecki for his help with realization of the final version of the software controlling the SWMD system as well as for many valuable remarks considering this thesis.

I would also like to give thanks to my Parents for support in pursuing my goals and to all my Family and Friends who I can rely on in every moment of my life. And finally I would like to give special thanks to Edyta Wanat for her help and support.

Realization of a part of the work was possible thanks to the financial support within the project "SENSO" in France, developmental project N R04 009 02 in UKW in Bydgoszcz as well as scholarships „Krok w przyszłość – stypendia dla doktorantów" and „Les Bourses du Gouvernement Français (BGF)".

Table of contents

INDTRODUCTION

The need for the development of an automated measuring system which allows diagnosing the top layer of concrete in a completely noninvasive way is the motivation of this work. For the accomplishment of this task, computer-controlled, automated measurement systems, including data processing software must be developed. The system will be used to estimate certain parameters of the teste materials. The ultrasonic techniques are used in the experimental part of this work. The measurements realizations in the noninvasive way with a one side access only are the additional requirements. Such assumptions are necessary to create a measuring system which could be applied in the study of real objects. Non-contact ultrasonic techniques are a novel group of ultrasonic methods in which the air is used as a transducers-concrete coupling medium. This avoids adverse impact of conventional coupling substances such as gels or water, which in contact with porous concrete, locally change their properties. Moreover the gel drying causes unpredictable changes of the conditions of ultrasonic waves propagation.

Research for diagnosing methods of the top layer of concrete, is the answer for increasing demand of diagnosis of concrete structures and in consequence the safety of reliable civil engineering structures. The assessment of degradation especially is needed caused by influence of adverse environment. Diagnosis should give the answer to the question whether the structure is safe and can be used, whether it should be renovated or demolished. Creating a system, that will accurately and reliably assess the condition of the structure in a non-destructive way, carries a lot of measurable benefits. This can be illustrated by the example of a bridge, each day of its decommissioning entails significant costs. The best solution is to start renovations exactly when the state of the structure needs it. This prevents financial loss due to premature withdrawal of the facility from exploitation while providing the safety of its maintenance until renovation. The need to carry out research concerns mainly the older structures, for which there is often no sufficient technical documentation which provide to estimate their current condition. Years of neglect in monitoring the destruction /weakening of the structure can lead to tragic effects of building disasters. Economic analysis

shows, that only the U.S. will need to spend more than $ 27[1] trillion to repair roads and bridges in the years 2009-2014. In Canada, at the end of the twentieth century, it was estimated that 83% of bridges need repairs[2]. Similar situation is in Europe, where a large part of the infrastructure are the structures made of concrete from the 50's and 60's Detailed analysis of concrete structures not only allows avoiding tragic accidents, but also enable us to optimize the costs of the repairs carried out. Increasing demand for non-destructive tests of concrete for newly constructed buildings is also observed. It's caused by the need to reduce costs and time while carrying out the necessary expertise. Moreover, the traditional - destructive diagnostic methods can be applied not at all cases.

Concrete structures during exploitation are exposed to an adverse action by the surrounding environment. This applies both to the adverse effects of polluted air in case of free-standing buildings, as well as water or brine in case of concrete hydro infrastructure. The rate of degradation depends on many factors, but the biggest impacts on the progressive destruction have: the type of concrete used in construction, environmental pollution, temperature fluctuations, the age of a structure and the manner of its use. Large-scale studies in a field on concrete degradation show that the crucial information about the state of tested structure relates to the surface or subsurface layer. It has a direct contact with the environment, where the degradation starts and progresses with time into the material. As a subsurface layer, is considered material to a depth of reinforcement. This is usually a layer with a thickness from 3 cm to 5 cm from the surface. Assessing the extent and depth of degradation gives some important information from the diagnostic point of view. The most important thing is the answer to the question whether degradation has reached the first layer of reinforcement. If so, there is risk that the process of corrosion of reinforcing bars has began. In this situation, the next step is to set the degree of reinforcement corrosion using appropriate diagnostic methods. Mechanisms of degradation of concrete can be varied and depend on many factors. A summary of these mechanisms in literature shows among others Mehta [Mehta 1997]. The most common mechanism of degradation of concrete structures in civil engineering is caused by aging and the development of cracks in concrete caused by loads. Each concrete structure during exploitation is treated by different types of loads, depending on its purpose and location. Taking as an example, the construction of a bridge, it is obvious that it is treated to considerable mechanical loads, which in connection with ageing of concrete leads to the emergence of micro cracks. With time, micro cracks develop creating longer and deeper

[1] ASCE, http://www.infrastructurereportcard.org/report-cards
[2] FCM, http://www.fcm.ca/english/view.asp?x=1

cracks. Weakened surface layer begins to lose its tightness, allowing moisture to reach the reinforcing bars causing corrosion and subsequent weakening of the structure. Concrete structures which are in constant contact with sea water are even in worse situation, because they are vulnerable to degradation of chloride ions, which after reaching reinforcement cause significant acceleration of corrosion. If the depth of degradation and the state of the surface layer are known, it is possible to determine when and what means should be taken to prevent further destruction. Knowing such information the range and time of repairs can be optimally adapted to the actual state of the building. Therefore the information about the state of the top layer of concrete structure is very important.

Mostly, destructive methods are used to control degradation of concrete. Their application is always a disadvantage for the structure, because it leads to its weakening. Nowadays there is no non-destructive control system that allows reliable and also comprehensive diagnose of the state of the top layer of concrete. Some works on different of such solutions are carried out in several laboratories around the world [Reichling 2009]. Methods NDT (Non Destructive Testing) which was developed so far, did not gain sufficient confidence in the environment dealing with diagnosis of concrete, in order to determine an independent and reliable tests.

Chapter I

Characteristics of the chosen problem, objectives and the range of work

The diagnostic methods of the top layer of concrete are the objectives of this work. Short description of the process of concrete structures degradation and review of some nondestructive testing (NDT) methods, with focus on the acoustic ones, are presented in this chapter. The choice of two noncontact NDT methods used for future work is justified. The objectives of presented work and requirements for the final solution are clearly defined. The description of the dissertation contents is placed at the end of the chapter.

Concrete degradation mechanisms

As mentioned in the introduction, global tendencies show increasing demand in the concrete diagnostic area, especially for NDT methods. The need to conduct reliable research applies to both, new structures and the old ones. Respectively, in order to control correctness of workmanship, but also to assess the extent of degradation and anticipate terms of exploitation and maintenance of the structure. In the case of older concrete, existence of several mechanisms of degradation, dependent on both environmental and operational factors is observed. Classification below shows major causes of degradation of concrete seen in the literature [Neville, 2000]:

- mechanical damages caused by overloads, strikes, vibrations or abrasions,
- physical damages which contribute to eg. high temperature resulting in expansion of concrete ingredients, with different thermal expansion coefficients or freezing resulting in burst of concrete by frozen water,
- chemical degradation caused by the action of the ingredients present in the environment (aggressive ions, soft water, acids and also sea water).

Almost always, several different mechanisms of destruction occur simultaneously. The simplified process of degradation, as a result of aging and mechanical loading is shown in the Figure I.1.

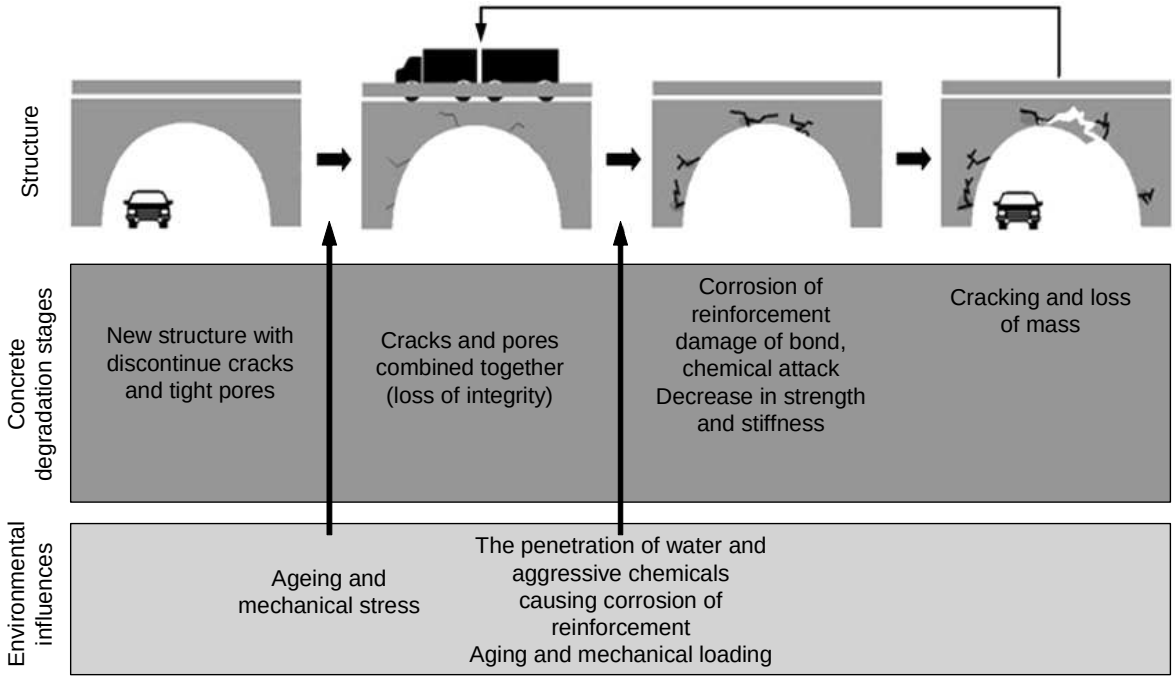

Figure I.1 Mechanisms of concrete degradation due to aging and fatigue mechanical loading [Mehta 1997].

Young concrete, although it is porous and not devoid of micro cracks is considered tight. Over time, as a result of interaction with the environment and due to mechanical stress, micro cracks begin to grow and join with each other leading to loss of water resistance. Increasing micro and larger cracks, allow water to penetrate into the material. When the leakage area spreads onto reinforcing bars, the process of corrosion begins, and thus gradually loss of strength and stiffness occurs. Deepen cracks and developing corrosion, cause peeling off the top layer of concrete. That causes a degradation of deeper zone in concrete. In particularly bad situations are concrete exposed to the substances chemically indifferent, such as chloride ions of sea water, or sulfur compounds (acid rain). Schematic process of environmental degradation in the salt water is shown in the Figure I.2. The stages of degradation in the presence of chloride ions are identical as in the previous case. The difference is that alkaline moisture reaction significantly accelerates the corrosion of steel reinforcement. The result is that degradation process accelerates rapidly, when leakage in concrete gets to reinforcement. Corroding steel swells, bursting concrete which surrounds the rods, and that results in faster weakening of the entire structure.

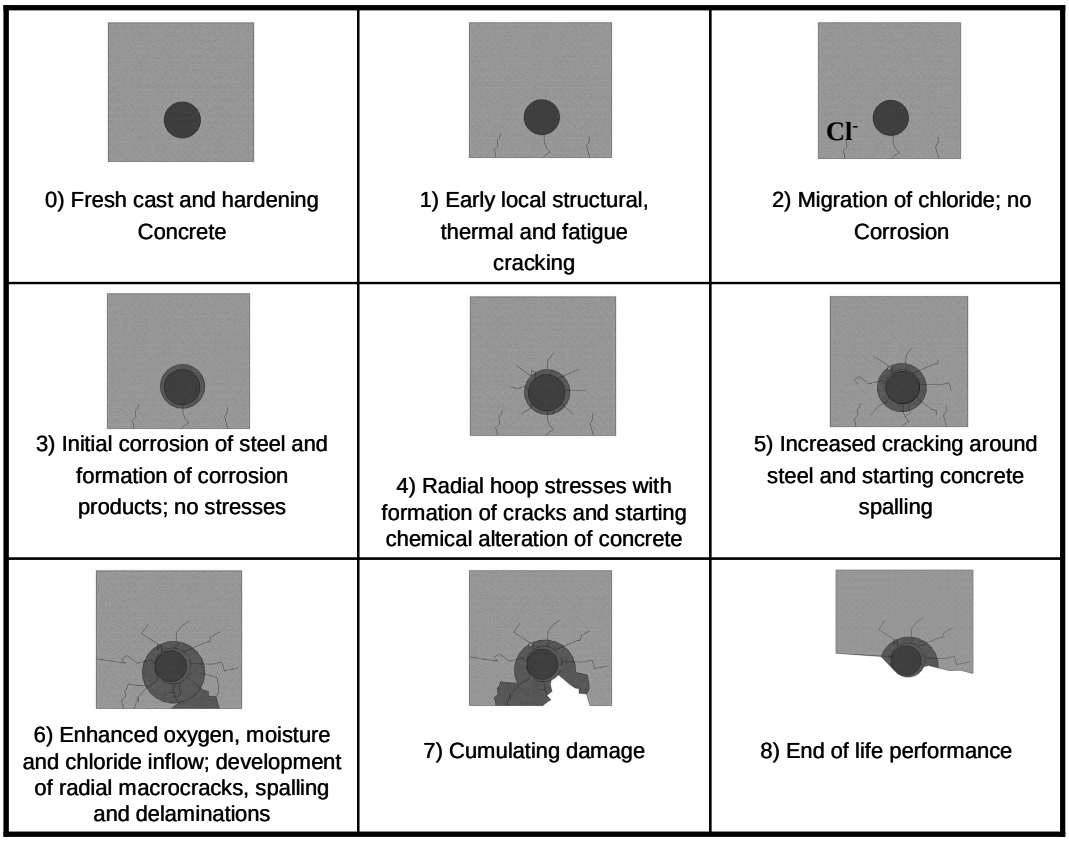

Figure I.2 Process of concrete degradation as a result of chlorine ions action [Arndt 2009].

As noted above, the degradation caused by the adverse impact of the environment accompanies mechanical degradation (overloads, vibrations). Regardless of the process which occurred before or has a greater share in the overall degradation, the final result is weakening of the concrete structure. The work is focused on developing a diagnostic method, which makes it possible to estimate the quality of the degraded material and the degree of this degradation whatever is the source of its origin is.

Major methods of non-destructive testing of concrete

Problems of concrete degradation outlined above, justify the need for their diagnosis. The following is a review of applied and further developed testing methods for concrete. Available diagnostic methods can be divided into three basic groups depending on the impact of the test material. These are destructive methods, non-destructive and pseudo non-destructive. A more detailed review of the methods used in the concrete diagnostic are presented in the monograph [Bungey at al. 1996] and publications [Moczko 2006, Mehta at al. 2006].

Destructive methods used for the diagnosis of concrete structures require a representative sample of material, often of relatively large size. The most commonly applied destructive testing method is the test of mechanical resistance of the given material. The sample is extracted from the tested construction. Thanks to the extensive tests, it is possible to determine, such parameters as Young's modulus E or compressive strength R_C. Furthermore, it is possible to measure porosity, for example, using mercury porosimetry [Cook 1991] and measurement of permeability. To study the permeability the gas method [Zoubeir at al. 2007] is one of the possible solutions. Taking a sample of material for diagnostic test weakens the structure. Moreover, quite often it turns out, that the major structural elements cannot be tested this way, because it would weaken the construction. In such cases, the samples are taken from elements not responsible for the safety of buildings with the assumption that the concrete in the remaining elements is in the same state. However, there is a risk that this assumption is unfulfilled. Moreover, it is worth noticing, that destructive methods are time consuming and require expensive laboratory equipment.

There are several methods for testing concrete parameters in a pseudo non-destructive way. Effects of measurements slightly damage testing structure, which excludes their use only in the case of more crucial elements of construction. Interference in such construction usually involves e. g. drilling a small hole. Such operations include for example permeability measurements by Figg [Figg 1989] or the concrete strength by Pullout test, inter alia, used in British Standard of Building and Construction [BS 1881].

The NDT methods are the most desirable and developed methods of concrete diagnosis. Among them stroke method, electrical, visual evaluation and acoustic methods can be distinguished. The latter called also as wave methods based mostly on the analysis of ultrasonic wave propagation. Acoustic methods can be divided into passive, in which the source of waves is only a construction with changing load (the method of acoustic emission) [Ranachowski 1990], and active methods of sending and receiving ultrasonic waves [Hola at al. 2007, Schabowicz at al. 2008, Kaszyński 2003]. Currently, the active methods are not so developed and tested, so that they can be widely used in the field, and in most cases, require access to two (opposite) sides of the test element or knowledge of its exact dimensions. The stroke methods in most cases are based on observation of responses given by the material due to the mechanical impact. For this type of study a common technique known as the Schmidt's hammer [ACI 228.1R-95 2002] is used. The essence of the method consists of using a weight bounce from the surface of the test material. The height of which the weight will be bounced is a quality indicator of the material. It is possible to estimate physical parameters of tested

material, such as surface hardness and compressive strength through the appropriate conversion relationships. Observations show that stroke method is not very reliable and repeatable primarily because of one-pointed impact and strong heterogeneity of concrete. In the group of electrical methods the electrical resistivity and capacity methods can be distinguished. Currently, these methods are used as complementary measurements, for example, to evaluate the humidity. Among visual testing methods testing methods in visible light and infrared can be distinguished. Methods of visual observation using special microscopes or endoscopes are used primarily to estimate the size and density of cracks or micro cracks. The Restriction in using visual methods stems from the fact, that when using these methods we cannot assess the depth of the observed cracks. Techniques based on the analysis of infrared images allow assessing the condition of the structure in the whole volume or in sufficiently large areas. These methods are also called infrared thermography, they use contrasts of heat flow while heating up and cooling down the structure during a day [Weil at al. 1991]. They allow to search the areas of weakened material, because the thermal radiation emitted from such areas is different from areas of a well conditioned healthy material. It should be noted that although infrared methods gives qualitative, not quantitative results. They allow detecting spots in structures, which require additional and more precise measurements. Another limitation of using infrared methods is fact that the test material has to change its temperature during the measurement, which sometimes is impossible or very difficult to implement.

Selection of diagnostic method depends on a few factors. The type, the range and the precision of the material parameters for the study should be selected first before choosing a diagnostic method. Each method has some limitations that might prevent its use in conditions in which the structure is situated. This kind of limitation is e.g. using destructive method for testing the key elements supporting the concrete structure. There is no incentive drilling, cutting or snap of samples form elements such as pillars, floor beams or binders. That’s could change the supporting structure of the building. It should be also noted that many of methods require additional information, which may be obtained using other NDT techniques. The characteristic of more important NDT methods used for concrete evaluation is presented in the Table I-1. The measurement capabilities or features of method are marked by “x”. The desired criteria of the NDT methods, mechanical and structural parameters of concrete relevant to his diagnosis are contained in the rows.

Table I-1 Parameters of more important NDT methods for concrete compared with destructive testing methods (x – measurement possible but no used in practice).

	Method / measurement capabilities	Acoustic methods	Radar	Capacity	Microwaves	Resisitivity	Thermography	Precussive	Traditional destructive test
1	*Possibility of in situ testing*	x	x	x	x	x	x	x	
2	*One side access*	x	x	x	x	x	x	x	x
3	*Non contact*	x	x	x	x	x	x		
4	*Velocity profile with depth*	x							x
5	*Information about reinforcement in concrete*	x*	x						x
6	*Porosity measurement*	x				x			x
7	*Permeability measurement*	x							x
8	*Tortuosity measurement*	x				x			
9	*Humidity*		x	x	x	x			x
10	*Elasticity parameters v and E*	x							x

The comparison in Table I-1 shows that acoustic methods fit most in to the desired criteria, beyond the destructive tests. Only for humidity measurement and location of reinforcements in concrete other techniques must be used. For humidity determination en electromagnetic method with the use of dielectric constant estimation ε could be utilized. ε measuring can be effectuate using the capacitive method or a more complicated microwaves beam method and the relationship between the velocity of waves propagation and dielectric constant ($c=f(\varepsilon)$). Humidity of porous material affect on its capacity as a capacitor via ε, where the skeleton of the material is a dielectric layer. Simultaneously, electrical methods are less sensitive to the mechanical properties of the material. During examination of concrete with steel reinforcement (most of cases) there is a risk of measurement disturbances because of presence of rebar. The imaging of reinforcing steel framework, and event thickness of used rods is a solution of this problem. For that task the radar method using Ground Penetration Radar (GPR) is applied [Hubbard at al. 2003, Clemena at al. 1991], which allows to locate reinforcement elements quickly and accurately. The high price of the measuring device is a disadvantage of the GPR method. Cheaper solution is to use precision metal detectors, allowing approximate positioning of the reinforcement bars without en information about

depth of its location. This avoids the influence of reinforcement during concrete measurements.

Table I-2 Features of more important acoustic methods for concrete
(x – measurement possible but no used in practice).

	Acoustic Methods / **Measurement features and obtained information**	Volumetric waves	Surface waves	Impact Echo	Backscattering	Reflectometry	Acoustic emission	Destructive tests
1	*Possibility of in situ testing*	x	x	x	x	x	x	
2	*One side access*		x	x	x	x	x	x
3	*Non contact*	x	x	x		x	x*	
4	*Velocity profile with depth*		x					x
5	*Gropu velocity V_P and V_S*	x		x				x
6	*Porosity measurement*					x		x
7	*Permeability measurement*					x		x
8	*Tortuosity measurement*					x		
9	*Humidity*							
10	*Elasticity parameters v and E*	x	x					x

The acoustic methods shown in Table I-1 represent a wide group of nondestructive testing methods. Table I-2 summarizes the most important acoustic methods and their comparison with destructive tests. For acoustic methods the ultrasonic frequency waves are most commonly used [Jung et al. 2002]. The mechanical and structural features of medium in which propagation occurs has a direct influence on acoustic waves considered as a mechanical disturbance. The velocity profile with depth (Table I-2) was highlighted because it lets directly estimate the degree and depth of degradation. If the velocity of waves propagations will be known it is possible to determine the material parameters such as Young's modulus E and Poisson's ration ν according to:

$$\nu = \frac{c_P^2 - 2c_S^2}{2\left(c_P^2 - c_S^2\right)} \tag{I.1}$$

$$E = c_P{}^2 \rho \frac{(1+\nu)(1-2\nu)}{1-\nu} \tag{I.2}$$

where c_P and c_S are longitudinal and transversal waves velocities respectively, and ρ is material density.

Measurement techniques based on analysis of surface waves propagation enable us to determine the wave velocity as a function of depth and only one side access is needed. The knowledge of the structural parameters such as porosity or permeability is also important information from diagnosing point of view. The ultrasonic reflectometry technique developed in this work gives the possibility to determine the surface porosity of material by nondestructive way with one side access only.

Finally the optimal solution is a combination of several complementary NDT methods. The GPR and capacitive methods have been recently developed and can be successfully applied to the above-mentioned tasks [Balayssac et al. 2009, Ploix et al. 2009, Villain et al. 2009] and combined with acoustic methods allow to meet all the criteria of comprehensive non-invasive diagnosis of concrete. In the SENSO project implementation of various NDT techniques for the study of concrete degradation was taken into consideration. The part of presented work was realized in frame of this project. The aim of the project was to determine the parameters of the tested concrete by the fusion of data obtained using different measurement techniques. For more information see chapter V.2.

Aim of the work

The main objective of the work described in this dissertation is the development of non-contact ultrasonic system for the nondestructive testing of top layer of concrete. Based on previous experiences with the diagnostics of concrete, and taking into account current trends in the range of requirements and exceptions to be met by developed system where established. Those are:

- possibility of evaluation the mechanical and structural parameters of the first 10 cm of concrete (the reinforcing bars are generally at 4-5 cm deep and in very few cases deeper then 10cm),
- totally nondestructive nature of diagnosis allowing to use the designed system for testing the important elements of structure (beams, pillars, binders, structural reinforcement, ceilings, etc.),
- non-contact operating, i.e. measurement does not require the application of additional substances like gels, glues, water, etc.). The measurement in which the waves transfer medium between transducers and concrete is air could be considered as a non-contact measurement,
- measurement with one side access only to the tested element,

- possibility of in site testing (mobility, compact size and weight of the system should let easy use regardless of shape and position of the tested element),
- repeatability and reliability of obtained data,
- safety of use – the system should not be dangerous for a user, environment and the tested structure,
- fast and easy system in use (economic aspect in carrying out the measurements).

Taking into account the above guidelines and analysis of existing NDT methods presented in Table I-1 and I-2 the surface waves and reflectometric techniques were chosen from the available methods for the future development. In presented work the solution of measurement configuration including hardware, signal processing and method of results interpretation is proposed. Measuring devices which allow realization of non-contact testing and illustrating the state of the material versus depth were built.

The relationship between frequency of surface wave and depth of its penetration into the material is used as a source of information about the sate of material versus depth. The models binding dispersion characteristics with mechanical and structural material parameters of surface layer (the distribution of heterogeneity) are adapted to interpret the measurements results using algorithms for solving the inverse problems. For determining the structural parameters of material such as porosity, tortuosity and permeability attempted to use method of ultrasonic reflectometry (reflectometric method). In this method the reflection coefficient of ultrasonic longitudinal wave in function of incident angle is determined (reflection coefficient characteristic). Wave propagation occur in the air and the wave is reflected by the measured surface. Based on a measured characteristic and the model the optimization algorithm is used for determining structural parameters. Measurement system configuration used for reflectometric method allows non-contact work with one side access to the tested item.

The realization of the tasks set in this introduction required:

- development of special measurement systems which provide non-contact measurement proceeded in field with one side access only,
- elaboration of appropriate methods for waves generation and processing of high damped signals in order to ensure high precision of obtained results,
- use of models describing mechanical waves propagation in micro- and macro-heterogeneous concrete,

- implementation of optimization methods for solving inverse problem in structure parameters identification. The parameters identification in this work mean estimation of material properties (i.e. micro- and macro-structural mechanical properties) obtained by solving inverse problem
- measurements of standard materials and real objects for verification of designed system functioning.

Contents of the thesis

Chapter I : presents an overview of the problem of concrete diagnosis as well as objectives and scope of the thesis. Main part of the chapter is the analysis of the available non-destructive control methods in concrete diagnosis and the substantiation of choice, among others, two methods of ultrasound research.

Chapter II : concerns the presentation of theoretical models used in the thesis. In modeling of dispersion phenomenon of surface waves two models were considered; the Haskell-Thomson model which describes layered center and the Gibson's model which assumes that shear modulus vary linearly with depth. Theoretical part was expanded with a proposal of a method considering dispersion derived from attenuation. To model the reflection coefficient from the concrete a modified Biot model was used.

Chapter III : is a description of measurement equipment designed and made for this work. Chapter consists of two parts. First part deals with all the issues concerning equipment used for propagation surface research. The second part is a description of the system to measure reflectance coefficient. Each section contains a description of the process of data acquisition and theirs processing, and also device tests for the known materials.

Chapter IV : presents a description of the estimating issues for searching model parameters by solving the reverse problem. The chapter describes two original algorithms for assessing and determining the depth of degradation structural parameters of the tested materials.

Chapter V : provides an overview of the most interesting results of the measurements using constructed diagnostic tools and discussion of the results. The presented results concern both laboratory and field measurements.

Chapter VI : provides a summary of the work, together with the presentation of results and perspectives.

Chapter II

Theoretical basis of considered models

In this chapter the models of ultrasonic waves propagation phenomena used for the developed concrete diagnostic methods are presented. Analysis of surface waves (SW) propagation in inhomogeneous medium and description of a reflection phenomena are mainly considered.

The first part of the chapter presents the theoretical basis of two models of macro-inhomogeneous media: the Haskell-Thomson model, in which a layered structure of medium is assumed (each layer is homogeneous, and heterogeneity is caused by differences between the layers), and the Gibson's model where shear modulus change linearly with depth. For each model a sensitivity analysis is made. The approach of taking into account the attenuation as an independent source of dispersion (exception material heterogeneity) is presented.

In the second part of the chapter the theoretical aspects of a reflection coefficient are presented. Waves propagated in the air and reflected from a porous media are considered and modified Biot's model without skeleton deformation is used. For that model also a sensitivity analysis is proceeded.

II.1 Surface waves propagation in heterogeneous media

Surface waves are the disturbances propagating along the surface of en elastic medium, when the surface bordered on another elastic medium or a vacuum. The disturbance consists in elliptical movement of the particles in a plane perpendicular to the surface of the material and parallel to the direction of propagation (Fig. II.1). The amplitude of the movement quickly decreases with depth. These types of waves propagating in a homogeneous elastic media are free form dispersion and are named Rayleigh waves (form the name of the author's of its mathematical description) [Rayleigh 1885]. Rayleigh wave propagation velocity in homogeneous media c_R is the root of the equation:

$$R(c_R) \equiv \left(2 - \frac{c_R^2}{c_S^2}\right)^2 - 4\sqrt{\left(1 - \frac{c_R^2}{c_P^2}\right)\left(1 - \frac{c_R^2}{c_S^2}\right)} = 0 \qquad \text{(II.1)}$$

where: ρ is the medium density and $c_P = \sqrt{(\lambda + 2\mu)/\sigma}$, $c_S = \sqrt{\mu/\sigma}$ are respectively velocity of a longitudinal and transversal wave propagation expressed as a function of Lame's constant μ and λ. In most of the cases an approximated solution of the Equation II.1 is used. For the Poisson coefficient in rang n $\eta \in [0,0.5]$ (the range valid for most materials and concrete also) the approximated solution of II.1 proposed by Bergmann is good enough [Bergmann 1948]:

$$c_R = c_S\left(\frac{0{,}87 + 1{,}12\nu}{1+\nu}\right) \tag{II.2}$$

For the Rayleigh wave the amplitude of the material particles displacements in the function of depth normalized to the wavelength λ is presented on the Figure II.1b. The *u* and *w*, are the displacements in the tangent and normal directions to the direction of propagation respectively. The characteristic shows that the amplitudes are strongly associated with depth and vanish in more than *82%* at a depth equal to the wavelength.

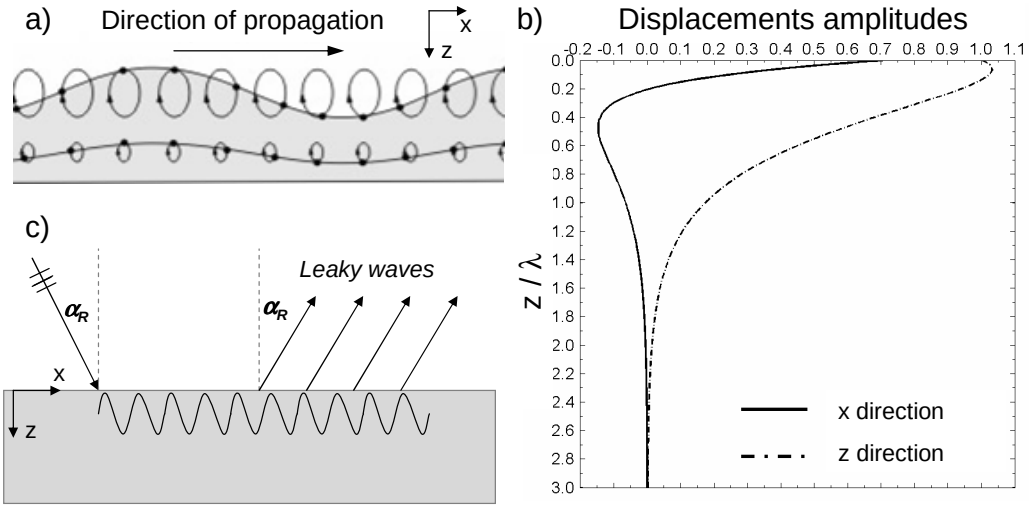

Figure II.1 Features of Rayleigh waves propagation in homogeneous media a) material particles displacement caused by surface wave propagation for different depths [wikipedia.pl], b) displacement amplitude for x and z direction versus depth normalized to the wavelength [Wardany 2005], c) schema of SW generate and receive.

One of method of SW generation is the emission of longitudinal wave in the air which incident to the surface with angle α_R. That is the third critical angle resulting form the Snell's low. The incidence angle for the case in which the wave propagates form the air to the material can be calculated as:

$$\alpha_R = \arcsin\left(\frac{c_{P\_AIR}}{c_R}\right) \tag{II.3}$$

with c_{P_AIR} as a velocity of acoustic wave in the air.

The wave propagating along the surface of material being in contact with another medium generates so-called leaky waves [Victorov 1967] where direction of the emission is inclined also with angle α_R from the normal. Observation and acquisition of leaky waves is possible in non-contact manner and what is, it important gives us indirect information about the surface waves.

Each wave could be characterized by a phase V and group V_{GR} velocities. The phase velocity of a monochromatic plane wave might be defined as:

$$V = \frac{\omega}{k} \tag{II.4}$$

with ω as an angular frequency and k as a wave number. Considering not monochromatic wave as a superposition of monochromatic waves with angular frequencies close to the central frequency the group velocity can by introduced as [Mavko et al 2003]:

$$V_{GR} = \left(\frac{d\omega}{dk} \right)_{\bar{\omega}} \tag{II.5}$$

In homogeneous half space without attenuation the Rayleigh waves of different frequencies (different wavelengths) propagate with the same velocity ($V(f)=const.$) In that case the phase and group velocities are equal ($V=V_{GR}=c$).

Modeling of the wave propagation phenomena in heterogeneous medium is developed since the 50' of XX century, mainly in geophysics. Usually, it is used to describe a propagation of seismic waves in rocks and soils for natural resources survey. The most common approach is the assumption of layered structure (eg Haskell model), where the heterogeneity arises from different mechanical parameters of the layers.

The model based on the concept of Gibson's elastic half-space (in short Gibson model) is an another model used for generating the theoretical dispersion characteristics of surface waves in a heterogeneous media (degraded material). The linear relation of Shear modulus versus depth is assumed.

II.1.1 SW in layered inhomogeneous medium (Haskell model)

The inhomogeneous half-space in which material properties abruptly change with depth in z direction is considered. The surface waves propagating such medium are called pseudo-Rayleigh waves and they are subject to dispersion, ie wave velocity depends on frequency. This can be described as a structural dispersion which originates from waves of

different lengths penetrate to different depths and related to that spread at different velocities (Fig. II.2a). In spectral domain it could be represented by a dispersion characteristic (Fig. II.2b), ie. the phase velocity characteristic in a function of frequency (or some times versus wavelength). In abrupt heterogeneity medium few modes can be generated which means existing of waves of different velocities at the same frequency. For a frequency tends to zero the first mode velocity (also referred to by the terms basic or fundamental mode) tends to the SW velocity in the half-space.

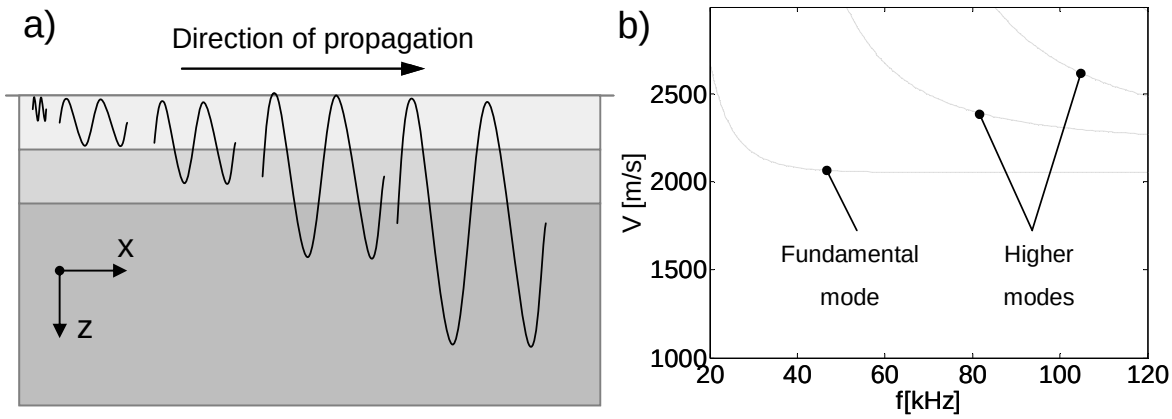

Figure II.2 The effect of structural dispersion a) propagation in heterogeneous material, b) the example of multimodal dispersion characteristic for the medium in which bulk waves velocity increase with depth.

For frequency tending to infinity, the velocities of all modes tend to the velocity of surface waves in half-space with properties of layer near the surface ($z=0$).

There are few possibilities of mathematical description for SW propagation in layered medium. Their comparison is presented inter alia in the paper [Lowe 1995]. Most of models were developed for geophysical applications and for the structural and mechanical parameters of soil. In that case thick layers and the waves of low velocities and low frequencies are considered. The conditions need for modeling of wave's propagation in depredated concrete diagnostic are considerably different and the thin layers and high frequencies are used. After bibliographic analysis the numerical implementation of Thomson-Haskell model (named Haskell model) was chosen as a model of pseudo-Rayleigh wave's propagation in a layered heterogeneous concrete. This model is also named shortly Haskell model or Transfer matrix model.

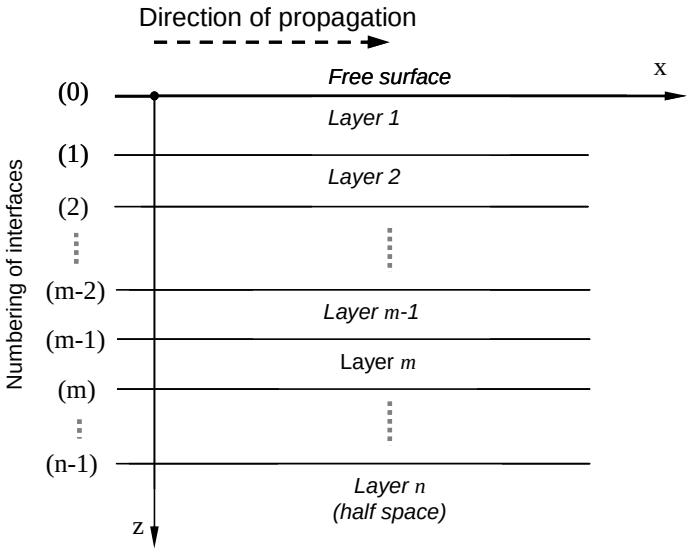

Figure II.3 Schema of modeled layered structure.

The model firstly developed by Thomson in 1950 and corrected by Haskell in 1953 [Haskell 1953] concern the SW's propagation in stratified heterogeneous material and the following assumptions must be fulfilled:

- the pseudo-Rayleigh waves (RW) are considered (shortly Rayleigh waves) with pulsation *p* and phase velocity *V*, and with the amplitude decreasing exponentially with depth *z*,
- there are *n* layers in considered system, and the last one is a half-space (layer of infinity depth),
- the stress and displacements are continues on the interfaces,
- there are no stresses across the free surface and there are no sources at infinity,
- each layer is isotropic and homogeneous solid,
- the particles displacements are in x-z plain.

Schema of considered structure is presented on the Figure II.3 and the properties of each layer are submitted in the Table II-1.

Table II-1 Layer parameters in Haskell model [Haskell 1953]

Symbol	Description
ρ_m	Density of m^{th} layer [kg/m^3]
d_m	Thickness of m^{th} layer [m]
$\lambda_m = \frac{E_m \nu_m}{(1-2\nu_m)(1+\nu_m)}$ $\mu_m = G_m = \frac{E_m}{2(1+\nu_m)}$	Lamé elastic constants for m^{th} layer (E_m – Young modulus for m^{th} layer G_m – Kirchhoff modulus for m^{th} layer ν_m – Poison coefficient for m^{th} layer)
$\alpha_m = \sqrt{\frac{\lambda_m + 2\mu_m}{\rho_m}}$	Longitudinal wave velocity V_P [m/s] for m^{th} layer (original naming)
$\beta_m = \sqrt{\frac{\mu_m}{\rho_m}}$	Transversal wave velocity V_S [m/s] for m^{th} layer (original naming)

To simplify writing of model equations the following additional parameters are introduced:

$$r_{\alpha m} = \begin{cases} +\sqrt{\left(\frac{V}{\alpha_m}\right)^2 - 1} & \text{dla} \quad V > \alpha_m \\ -i\sqrt{1-\left(\frac{V}{\alpha_m}\right)^2} & \text{dla} \quad V < \alpha_m \end{cases} \tag{II.6}$$

$$r_{\beta m} = \begin{cases} +\sqrt{\left(\frac{V}{\beta_m}\right)^2 - 1} & \text{dla} \quad V > \beta_m \\ -i\sqrt{1-\left(\frac{V}{\beta_m}\right)^2} & \text{dla} \quad V < \beta_m \end{cases} \tag{II.7}$$

$$\gamma_m = 2\left(\frac{\beta_m}{V}\right)^2 \tag{II.8}$$

where V is pseudo-Rayleigh waves velocity.

Given the assumptions, the relationships of dilatation Δ_m and rotation ω_m of the material particles for Rayleigh wave in m^{th} layer can be written:

$$\Delta_m = \frac{\partial u}{\partial x} + \frac{\partial w}{\partial z} = \exp[i(pt - kx)][\Delta'_m \exp(-ikr_{\alpha m} z) + \Delta''_m \exp(ikr_{\alpha m} z)] \tag{II.9}$$

$$\omega_m = \frac{1}{2}\left(\frac{\partial u}{\partial z} - \frac{\partial w}{\partial x}\right) = \exp[i(pt - kx)][\omega'_m \exp(-ikr_{\beta m} z) + \omega''_m \exp(ikr_{\beta m} z)] \tag{II.10}$$

where k is the wave number and the symbols Δ_m', Δ_m'', ω_m', ω_m'' represents constants corresponding to the amplitudes of dilatation and rotation in m^{th} layer. The relationship between angular frequency p and frequency f is $p=2\pi f$. The movements in x and z directions

marked as *u* i *w* respectively and corresponding stresses σ and τ are given by the Equations II.11-II-14:

$$u = -\left(\frac{\alpha_m}{p}\right)^2\left(\frac{\partial \Delta_m}{\partial x}\right) - 2\left(\frac{\beta_m}{p}\right)^2\left(\frac{\partial \omega_m}{\partial z}\right) \tag{II.11}$$

$$w = -\left(\frac{\alpha_m}{p}\right)^2\left(\frac{\partial \Delta_m}{\partial z}\right) + 2\left(\frac{\beta_m}{p}\right)^2\left(\frac{\partial \omega_m}{\partial x}\right) \tag{II.12}$$

$$\sigma = \rho_m\left[\alpha_m{}^2\Delta_m + 2\beta_m{}^2\left[\left(\frac{\alpha_m}{p}\right)^2\left(\frac{\partial^2 \Delta_m}{\partial x^2}\right) + 2\left(\frac{\beta_m}{p}\right)\left(\frac{\partial^2 \omega_m}{\partial x \partial z}\right)\right]\right] \tag{II.13}$$

$$\tau = 2\rho_m\beta_m{}^2\left[-\left(\frac{\alpha_m}{p}\right)^2\left(\frac{\partial^2 \Delta_m}{\partial x \partial z}\right) + \left(\frac{\beta_m}{p}\right)^2\left[\left(\frac{\partial^2 \omega_m}{\partial x^2}\right) - \left(\frac{\partial^2 \omega_m}{\partial z^2}\right)\right]\right] \tag{II.14}$$

There is no displacement in *y* direction in considered waves. There are not any stresses between 1^{th} layer and free surface. The stresses and strains on each interface are continues (except interface 0). Those conditions let to write *4m-2* equations, which are the basics of dispersion relations for considered pseudo-Rayleigh waves. Substituting the expressions II.9 and II.10 in the Equations II.11 – II.14 and differentiating at the time the equations of displacements (displacement continuity requirement is also met if their first derivatives at the time are continues) the relations for particles velocities and stresses are following:

$$\frac{1}{V}\frac{du}{dt} = -\frac{\alpha_m{}^2}{V^2}\left[(\Delta_m' + \Delta_m'')\cos(kr_{\alpha m}z) - i(\Delta_m' - \Delta_m'')\sin(kr_{\alpha m}z)\right] - \gamma_m r_{\beta m} \cdot \\ \cdot\left[(\omega_m' - \omega_m'')\cos(kr_{\beta m}z) - i(\omega_m' + \omega_m'')\sin(kr_{\beta m}z)\right] \tag{II.15}$$

$$\frac{1}{V}\frac{dw}{dt} = -\frac{\alpha_m{}^2}{V^2}r_{\alpha m}\left[-i(\Delta_m' + \Delta_m'')\sin(kr_{\alpha m}z) + (\Delta_m' - \Delta_m'')\cos(kr_{\alpha m}z)\right] + \gamma_m \cdot \\ \cdot\left[-i(\omega_m' - \omega_m'')\sin(kr_{\beta m}z) + (\omega_m' + \omega_m'')\cos(kr_{\beta m}z)\right] \tag{II.16}$$

$$\sigma = -\rho_m\alpha_m{}^2(\gamma_m - 1)\left[(\Delta_m' + \Delta_m'')\cos(kr_{\alpha m}z) - i(\Delta_m' - \Delta_m'')\sin(kr_{\alpha m}z)\right] + \\ - \rho_m V^2\gamma_m{}^2 r_{\beta m}\cdot\left[(\omega_m' - \omega_m'')\cos(kr_{\beta m}z) - i(\omega_m' + \omega_m'')\sin(kr_{\beta m}z)\right] \tag{II.17}$$

$$\tau = \rho_m\alpha_m{}^2\gamma_m{}^2 r_{\alpha m}\left[-i(\Delta_m' + \Delta_m'')\sin(kr_{\alpha m}z) + (\Delta_m' - \Delta_m'')\cos(kr_{\alpha m}z)\right] + \\ - \rho_m V^2\gamma_m(\gamma_m - 1)\cdot\left[-i(\omega_m' - \omega_m'')\sin(kr_{\beta m}z) + (\omega_m' + \omega_m'')\cos(kr_{\beta m}z)\right] \tag{II.18}$$

When the expressions $r_{\alpha m}$ and $r_{\beta m}$ becomes imaginary the corresponding trigonometric functions becomes hyperbolic.

According to the notation from the Figure II.3 the numbers of layers and interfaces at the bottom are equal. Placing the origin of *z* at the top of m^{th} layer (at the $(m\text{-}1)^{th}$ interface) from the Equations II-15 – II.18 for *z=0* the velocities of displacements and the stresses at $(m\text{-}1)^{th}$ interface can by expressed by the amplitudes of dilatation and rotation in m^{th} layer as

$$\left[\frac{1}{V}\left(\frac{du}{dt}\right)_{m-1} \quad \frac{1}{V}\left(\frac{dw}{dt}\right)_{m-1} \quad \sigma_{m-1} \quad \tau_{m-1}\right]^T = E_m\left[\Delta_m' + \Delta_m'' \quad \Delta_m' - \Delta_m'' \quad \omega_m' - \omega_m'' \quad \omega_m' + \omega_m''\right]^T \tag{II.19}$$

where expression E_m is a matrix

$$E_m = \begin{bmatrix} -\left(\frac{\alpha_m}{V}\right)^2 & 0 & -\gamma_m r_{\beta m} & 0 \\ 0 & -\left(\frac{\alpha_m}{V}\right)^2 r_{\alpha m} & 0 & \gamma_m \\ -\rho_m \alpha_m{}^2(\gamma_m - 1) & 0 & -\rho_m V^2 \gamma_m r_{\beta m} & 0 \\ 0 & \rho_m \alpha_m{}^2 \gamma_m r_{\alpha m} & 0 & -\rho_m V^2 \gamma_m(\gamma_m - 1) \end{bmatrix} \tag{II.20}$$

Moving the point of observation to the bottom of m^{th} layer i.e. $z=d_m$ the velocities and stresses at the bottom of the layer (m^{th} interface) in the function of dilatation and rotation amplitudes in the layer can by derived from the Equations II.15 – II.18 as

$$\left[\frac{1}{V}\left(\frac{du}{dt}\right)_{m} \quad \frac{1}{V}\left(\frac{dw}{dt}\right)_{m} \quad \sigma_{m} \quad \tau_{m}\right]^T = D_m\left[\Delta_m' + \Delta_m'' \quad \Delta_m' - \Delta_m'' \quad \omega_m' - \omega_m'' \quad \omega_m' + \omega_m''\right]^T \tag{II.21}$$

where expression D_m is a matrix

$$D_m = \begin{bmatrix} -\left(\frac{\alpha_m}{V}\right)^2 \cos(P_m) & i\left(\frac{\alpha_m}{V}\right)^2 \sin(P_m) & -\gamma_m r_{\beta m}\cos(Q_m) & i\gamma_m r_{\beta m}\sin(Q_m) \\ i\left(\frac{\alpha_m}{V}\right)^2 r_{\alpha m}\sin(P_m) & -\left(\frac{\alpha_m}{V}\right)^2 r_{\alpha m}\cos(P_m) & -i\gamma_m \sin(Q_m) & \gamma_m \cos(Q_m) \\ -\rho_m \alpha_m{}^2(\gamma_m - 1)\cos(P_m) & i\rho_m V_{ph}{}^2 \gamma_m r_{\beta m}\sin(P_m) & -\rho_m V^2 \gamma_m{}^2 r_{\beta m}\cos(Q_m) & i\rho_m V^2 \gamma_m{}^2 r_{\beta m}\sin(Q_m) \\ -i\rho_m \alpha_m{}^2 \gamma_m r_{\alpha m}\sin(P_m) & \rho_m \alpha_m{}^2 \gamma_m r_{\alpha m}\cos(P_m) & i\rho_m c^2 \gamma_m(\gamma_m - 1)\sin(Q_m) & -\rho_m V^2 \gamma_m(\gamma_m - 1)\cos(Q_m) \end{bmatrix} \tag{II.22}$$

where $P_m=kr_{\alpha m}d_m$ and $Q_m=kr_{\beta m}d_m$.

Equation of relations for the velocities and the stresses at the top and bottom interface of m^{th} layer (Eq. II.23) can be derived from II.19 and II.21.

$$\left[\frac{1}{V}\frac{du}{dt}_{m} \quad \frac{1}{V}\frac{dw}{dt}_{m} \quad \sigma_{m} \quad \tau_{m}\right]^T = a_m\left[\frac{1}{V}\frac{du}{dt}_{m-1} \quad \frac{1}{V}\frac{dw}{dt}_{m-1} \quad \sigma_{m-1} \quad \tau_{m-1}\right]^T \tag{II.23}$$

where $a_m=D_mE_m^{-1}$. Using the same reasoning the relation at $(m\text{-}2)^{th}$ and $(m\text{-}1)^{th}$ interfaces can be expressed analogously.

$$\left[\frac{1}{V}\frac{du}{dt}_{m-1} \quad \frac{1}{V}\frac{dw}{dt}_{m-1} \quad \sigma_{m-1} \quad \tau_{m-1}\right]^T = a_{m-1}\left[\frac{1}{V}\frac{du}{dt}_{m-2} \quad \frac{1}{V}\frac{dw}{dt}_{m-2} \quad \sigma_{m-2} \quad \tau_{m-2}\right]^T \tag{II.24}$$

The model assumptions required the continuity of displacements and stresses at the interfaces between $(m\text{-}1)^{th}$ and m^{th} layers. This assumption allows to link the velocities of displacements and the stresses at the $(m\text{-}2)^{th}$ interface (top of $(m\text{-}1)^{th}$ layer) and the m^{th} interface (bottom of m^{th} layer) as

$$\left[\frac{1}{V}\frac{du}{dt}_{m} \quad \frac{1}{V}\frac{dw}{dt}_{m} \quad \sigma_{m} \quad \tau_{m}\right]^T = a_m a_{m-1}\left[\frac{1}{V}\frac{du}{dt}_{m-2} \quad \frac{1}{V}\frac{dw}{dt}_{m-2} \quad \sigma_{m-2} \quad \tau_{m-2}\right]^T \tag{II.25}$$

In the same way the velocities and the stresses at any interfaces can be tie together. Thaws lets to write the relationship between the respective values at the top of first layer and the last interface (*m=n-1*) as

$$\left[\frac{1}{V}\frac{du}{dt}_{n-1} \quad \frac{1}{V}\frac{dw}{dt}_{n-1} \quad \sigma_{n-1} \quad \tau_{n-1}\right]^T = a_m a_{m-1} \ldots a_1 \left[\frac{1}{V}\frac{du}{dt}_{0} \quad \frac{1}{V}\frac{dw}{dt}_{0} \quad \sigma_0 \quad \tau_0\right]^T \qquad \text{(II.26)}$$

The relation above can be treated as a recursive equation and therefore a model with any number of layers can be considered.

Substituting II.19 to II.26 the velocities and the stresses at the free surface and the rotations and dilatations amplitudes in the last (*n*) layer can be linked as

$$\left[\Delta_n' + \Delta_n'' \quad \Delta_n' - \Delta_n'' \quad \omega_n' - \omega_n'' \quad \omega_n' + \omega_n''\right]^T = E_n^{-1} a_{n-1} a_{n-2} \ldots a_1 \cdot \left[\frac{1}{V}\frac{du}{dt_0} \quad \frac{1}{V}\frac{dw}{dt_0} \quad \sigma_0 \quad \tau_0\right]^T \qquad \text{(II.27)}$$

To simplify the notation the expression $J=E_n^{-1}a_n\text{-}1a_{n-2}\ldots a_1$ is assumed. Taking in to account that there is no sources of waves in infinity the assumption $\Delta_n''=\omega_n''=0$ is valid. Considering that there is no stresses at the free surface ($\sigma_0=\tau_0=0$) the equation II.27 can be expressed in a matrix form

$$\begin{bmatrix} \Delta_n' \\ \Delta_n' \\ \omega_n' \\ \omega_n' \end{bmatrix} = \begin{bmatrix} J_{11} & J_{12} & J_{13} & J_{14} \\ J_{21} & J_{22} & J_{23} & J_{24} \\ J_{31} & J_{32} & J_{33} & J_{34} \\ J_{41} & J_{42} & J_{43} & J_{44} \end{bmatrix} \begin{bmatrix} \frac{1}{V}\frac{du}{dt}_0 \\ \frac{1}{V}\frac{dw}{dt}_0 \\ 0 \\ 0 \end{bmatrix} \qquad \text{(II.28)}$$

The relationships between particles movement velocities at the free surface in normal and tangential directions can be derived from equation II.28

$$\frac{\dot{u}_0}{\dot{w}_0} = \frac{J_{22} - J_{12}}{J_{11} - J_{21}} = \frac{J_{42} - J_{32}}{J_{31} - J_{41}} \qquad \text{(II.29)}$$

Since the elements of the matrix *J* are dependent on the variables *V*, *k* i *p* the equation II.29 is considered as the dispersion function. That gives the relationship between wave velocity and frequency *V(f)* with the properties of each layer of the structure as a parameters. The roots of this equation presented on the velocity-frequency plain crates desired dispersion characteristic. Because there is no analytical determination of the *V(f)* function the numerical method of finding the roots of this equation is proposed.

II.1.2 Numerical solution of the dispersion equation

Obtaining the dispersion characteristics from Haskell model requires development of an algorithm which searches the roots of the dispersion equation in a numerical way. For this purpose, the Equation II.29 is converted to the products form

$$JJ = (J_{42} - J_{32})(J_{11} - J_{21}) - (J_{22} - J_{12})(J_{31} - J_{41}) = 0 \qquad \text{(II.30)}$$

Finding a solution of the Equation II.30 is realized on the velocity-frequency plane with fixed other models parameters. Elements of *J* matrix are depended on the system parameters and their complexity grows with the number of layers taken in the model, what could be well illustrated by the Equation II.27. Each layer is characterized by four parameters ρ_m, α_m, β_m, d_m (see Table II-1) and the last layer is the infinity depth (half space). Thus, having *n* layers in the model *4n-1* parameters must be placed. That is why the number of layers has significant influence on the problem of complexity and on computation time. The solution of dispersion equation is to find a set of such pairs of variables *V* and *f*, for which the relation II.30 is satisfied. The roots of the Equation II.30 can be found by many different ways. One of it is presented in the paper [Lowe 1995], where the author proposes *V(f)* plane scanning with simultaneously changing both velocity and frequency. In this study a little bit different approach of solving dispersion equation is taken. The details of this are presented below.

In the first stage of the discussed problem the course of *JJ* function versus frequency and velocity was analysed. For the ultrasonic concrete diagnostic the SW frequencies from several dozen to several hundred *kHz* and the velocities in range of *1500m/s* to *3000m/s* are used. These facts are taken into account for the future consideration. The real part JJ^{Re} of the function *JJ* versus *V* and *f* is shown in Figure II.4a. The analysis of imaginary part JJ^{Im} of the function *JJ* showed that JJ^{Im} takes zero value in considered domain ($JJ^{Im}=0$, Fig II.4.b) and therefore its consideration may be omitted [Lowe 1995].

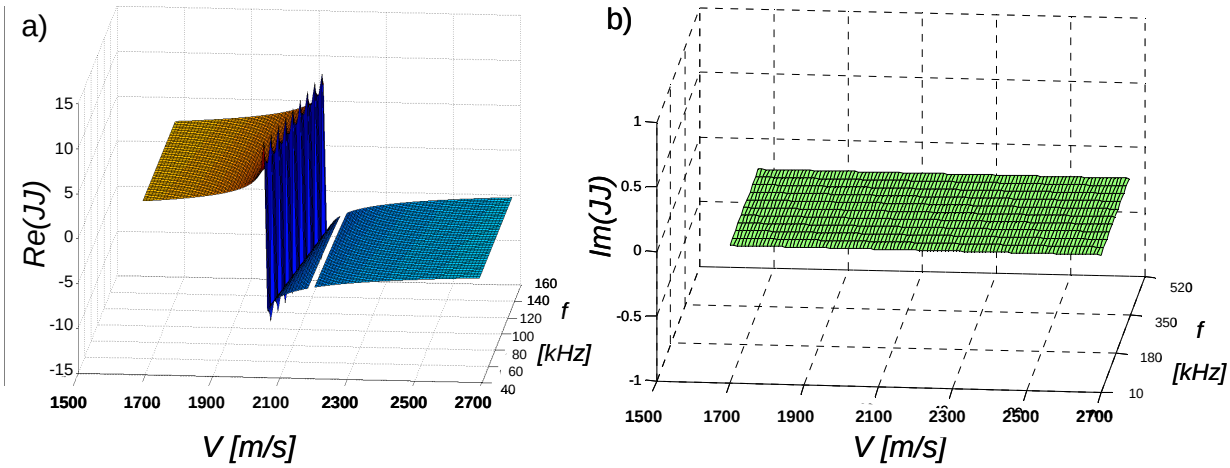

Figure II.4 *JJ* function in the *V-f* plain, a) real part, b) imaginary part.

In order to increase the efficiency of dispersion characteristics the search two variables function JJ^{RE} is simplified to one variable function. The phase velocity V of SW is the variable and the frequency is fixed (i.e. the considered equation is $JJ^{Re}(V,f=const.)$). In that case the desired roots of JJ^{Re} function are the values of velocity for which the function changes the sign. Depending on the considered values of model parameters and the range of V and f for one fixed frequency, few roots of the dispersion function could exists, which means the existence of several modes of wave function (Fig. II.2b). A complete multimodal dispersion characteristic at *V-f* is obtained by solving equation $JJ^{Re}=0$ for all considered frequencies.

For the purpose of this study a computer program named HASK was developed. The algorithm allows computing desired modes of dispersion characteristic to the roots of the function JJ^{Re} in selected *V-f* range.

The block diagram of the HASK program is shown in the Figure II.5. The first stage of the algorithm is configuration. In that moment the setup of the properties of each layer of modeled system is preceded (see Table II-1) and the range of V and f is chosen. The starting frequency f_S is an important parameter because the number of detected modes depends on it (STAGE I). Only detected modes can be searched in the next step. For example, for selected frequency f_S two modes are found on the diagram II.5. The third mod appears only for higher frequencies and hence for that range of SW velocity and the value of f_S the third mod can't be determined. Next, the user can select which of the detected modes will be determined. The velocity range for roots searching is limited by the values V_{min} and V_{max}. Searching the roots of JJ^{Re} function is performed using the bisection method which is also called the binary search

method [Annex I]. This is a relatively simple algorithm that gives fast and stable solution. Found roots are stocked to the vector V_M and are used as the initial points in searching (tracking) the selected modes. In a neighborhood of initial point of a search mod V_{MM} the interval $2\Delta V$ (STAGE II in the diagram II.5) is set as a region of research. To decrease the time of root finding by the bisection algorithm the interval should be as small as possible (STAGE III in the diagram II.5 shows that the root of function JJ^{Re} was found in $2\Delta V$ interval). In the next steps the roots of JJ^{Re} function are searched for the new frequencies f_i. For each new frequency f_i the root search also takes place in velocity range equal $2\Delta V$. The new initial point for new frequency fi is determined by linear regression method based on the previous roots (STAGE IV in the diagram II.5). If there is no root in $2\Delta V$ range, the range is gradually extended on both sides until a root will be found. The modes are tracked for the entire specified frequency range. The frequency band is swept firstly in left and then in right direction from the starting frequency f_S. The individual modes are determined recursively starting from the lowest ones. The algorithm terminates if all desired modes are determined (STAGE V in the diagram II.5 – in that case two lowest modes are determined).

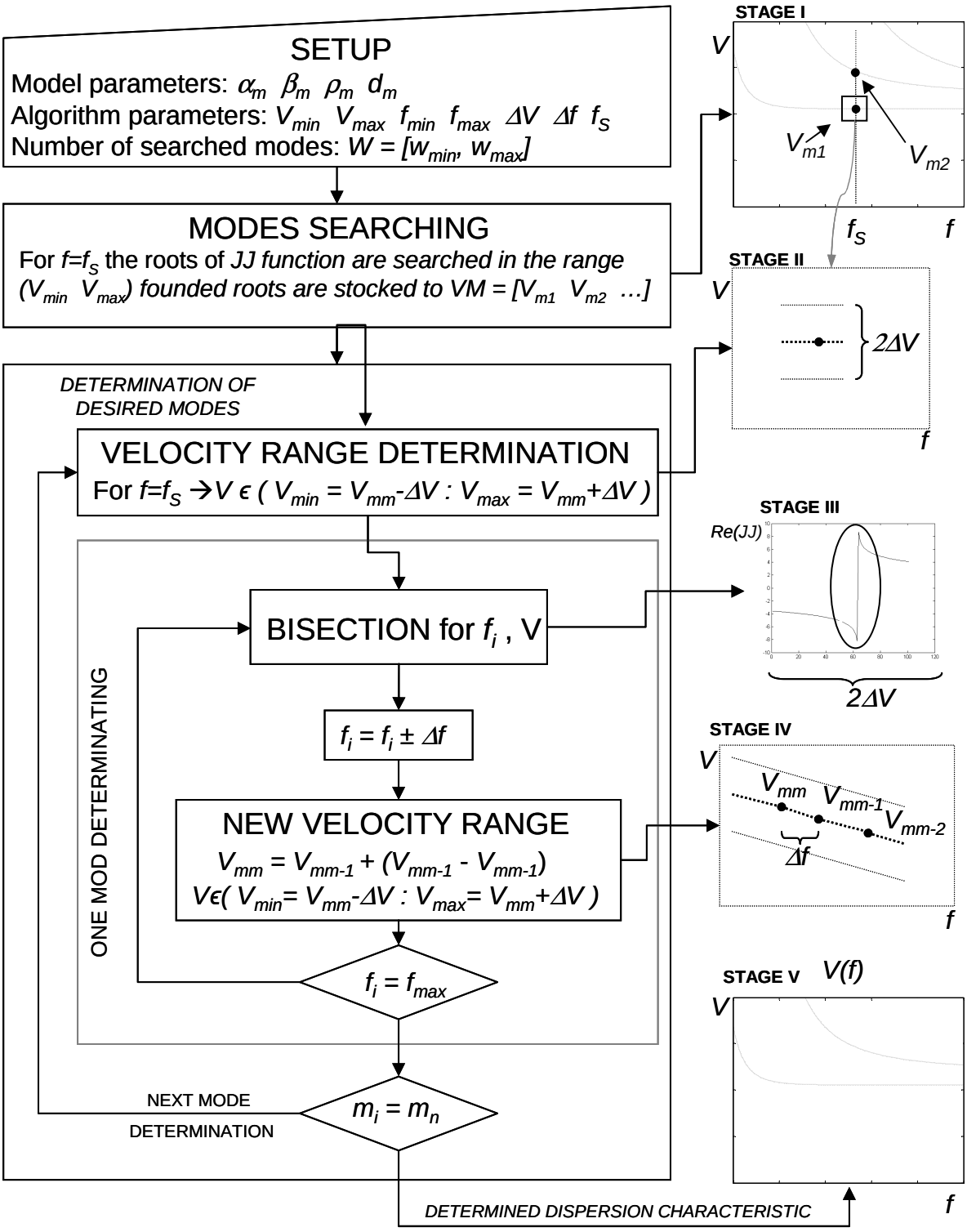

Figure II.5 The diagram of HASK program operating used for roots of dispersion equation determination based on Haskell model.

At the Figure II.6a the example of dispersion characteristic with one (first) mode obtained using Haskell model is shown. The range of $2\Delta V$ in which the roots are searched is

presented by dashed lines. Red dot on the characteristic (for frequency $f_S = 60\ kHz$) is the first found root of JJ^{Re} function.

Solving the Haskell model in the range of parameters used in the concrete requires overcoming a few problems. One of them is appearing a JJ^{Re} function discontinuity as shown in Figure II.4a. The problem occurs when the variable V takes the value equal to the velocities of longitudinal or transversal waves for any layer in model (i.e. α_m end β_m in Table II-1). Searching for solutions in a numerical way requires a velocity and frequency discretization. The solution for the problem is eliminating the value V equal to value of α or β for any layer. The elimination is realized by a little change of the value of the variable V, what lets us avoid a discontinuity. An error caused by this approach is negligibly small.

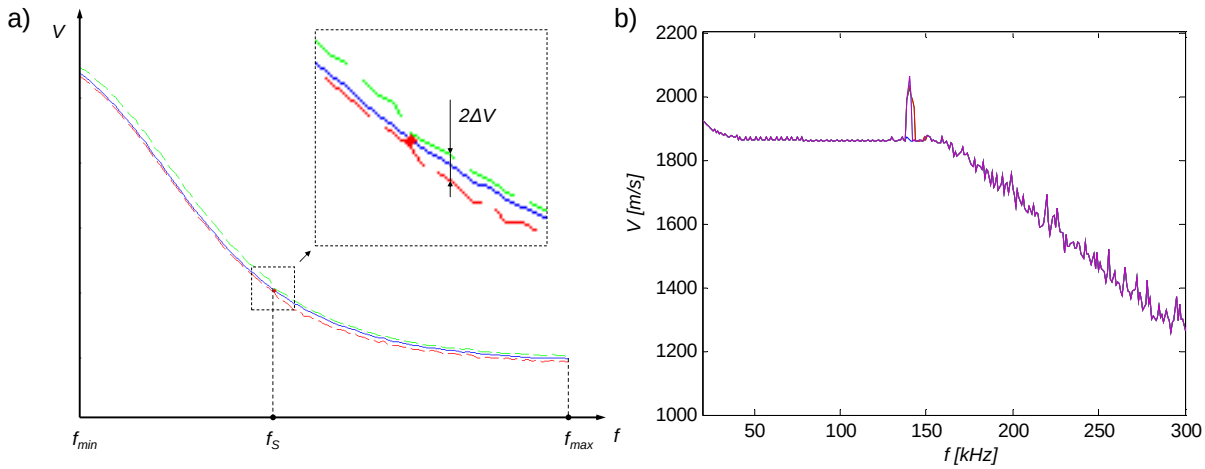

Figure II.6 a) Example of the fundamental mod of dispersion characteristic with the borders of search (dashed lines), b) the instability of model solution for higher frequencies.

In some cases the problem of instability of solving the $JJ^{Re}=0$ equation is presented. The example of dispersion characteristic generated for the parameters which it provides appears to be the problem for frequency over 140 kHz it is shown in the Figure II.6b. The graph shows that the first mod of dispersion characteristic does not tend to constant value above frequency of 140 kHz but decrease with oscillations for the higher frequencies. That model behaviour is caused due to its structure and is called a large *df* problem. In the model assumptions the stresses and strains at the one interface are expressed by the stresses and strains at the neighbouring interface. From a physical point of view, the problem stems form the rapid disappearance of the amplitude with depth. With sufficiently high frequency and enough thick layer the wave amplitude disappear before they reach from one interface to the other. From the mathematical point of view for the large f and d the matrix a_m becomes an ill

conditioned matrix. It is caused because the wave at one interface will have influence on the other only if the wave amplitude will be infinitely large. The tests carried out with the value of parameters for concrete shows that the upper limit *df* is *d*f=15 MHz·mm*. This means that for the layer thickness of *1 mm* the model will work properly until frequency of *15 MHz,* for thickness of *10 mm* until frequency *1,5 MHz,* etc. Considering assumptions in this study, it is required that the material will be checked to a depth of *10 cm* what reduces the maximum wave frequency to *150 kHz*. That occurs only when such thick layers are considered. The problem is more detailed in the paper [Lowe 1995], in which the author receives a similar boundary of the model for a titanium layers (*15 MHz-mm*). Despite the limitation described above the Haskell model is correct enough for modelling the heterogeneity of concrete structure, as the issue undertaken in this study.

II.1.3 Study of the sensitivity of the Haskell model

Information about how the different model parameters affect the model response (model solution) is very important during solving the inverse problem. The issue becomes complicated when the multi-parameter model is considered. Especially when a several parameters change simultaneously and their influences are abolished without a change or the model response. The objective of the study of the model sensitivity is determination of the influence of the mechanical and structural model parameters on a dispersion characteristic. The important question for the considered case is - which parameters are significant and should be optimized and which of them have a marginal effect on the dispersion characteristic and can be fixed as the constants. For that reason the systematic studies of the model sensitivity are proposed for determining the influence of each parameter on the shape of the dispersion characteristic. Based on the experimental measurements the frequency band and the ranges of the physical and structural model parameters were chosen. For simplicity of the study two-layered structure is considered. Main parameters of the simulations for all preceded tests are presented in Table II-2. It is assumed that the first layer of the model corresponds to degraded layer of concrete and the second one (half-space) is a healthy material. Only the fundamental mod of dispersion characteristic is analyzed because of experimental studies it is known that this mod is dominant in terms of energy. Moreover, in most of experiments only this mod is observed.

Table II-2 Main parameters of Haskell model sensitivity analysis.

Algorithm parameters		**Structure parameters**		
Number of layers (with half-space)	*2*		I layer	Half-space
Treated mod	*1*	Thickness *d [mm]*	*20*	+∞
Frequency band f_{min}/f_{max}	*1 kHz / 200 kHz*	Density ρ *[kg/m^3]*	*1900*	*2200*
Frequency step Δf	*2 kHz*	Velocity V_P *[m/s]*	*4300*	*4600*
Range of phase velocity V_{ph_min} / V_{ph_max}	*1600 m/s / 2500 m/s*	Velocity V_S *[m/s]*	*2370*	*2425*
Velocity step ΔV_{ph}	*0,1 m/s*			

The studies presented below include four tests. In each test the influence of one of the first layer parameters (d, ρ, V_P, V_S) on the SW velocity is analyzed and the parameters of half space are unchanged. The qualitative and quantitative comparisons of changes of the dispersion characteristics are preceded. In the qualitative assessment the changes of dispersion curve shape caused by changes of different model parameters are shown in the Figure II.7. The same range of axes for all graphs is taken to facilitate the comparison. In the quantitative assessment the normalized deviation measure *DBC* (Differences Between Characteristics) given by the Equation II.31 is considered. *DBC* represents a quantitative differences between the solution for the first and the *n-th* value of parameter *P* in a specific frequency range for *j=1* to *k*.

$$DBC(P_i, P_1) = \frac{\sum_{j=1}^{k} \sqrt{\left(V(f_j, P_1) - V(f_j, P_i)\right)^2}}{\sum_{j=1}^{k} V(f_j, P_1)} \cdot 100\% \qquad \text{(II.31)}$$

Pi – i-th parameter *P* value,

P1 – reference value of *P*,

f – frequency.

The span of changes of each parameter was chosen to cover the ranges found for the concrete. As a formality the tests are numbered form A to D. If one of the parameters is changed the values of the others parameters are as shown in the Table II-2. In the test A the values of thickness d_1 were chosen arbitrarily (according to the depth of degradation commonly found for concrete). In tests B, C and D the step of parameter changes is around

5% of the nominal value in the Table II-2. Firstly the qualitative and then quantitative results are described.

Test A shows the influence of the first layer thickness on the dispersion characteristic. Four curves generated for the thickness of *5 mm* to *50 mm* are presented in the Figure II.7a. Given the attention, that degraded layer in concrete is represented by the first layer in the model the thickness of the layer becoming one of the most interesting diagnostic parameters. The comparison of the curves shows that the SW phase velocity tends to the Rayleigh wave velocity in the deeper layer for low frequency. For the high frequencies the SW phase velocity tends to SW velocity in the first layer. The frequency region for which the SW velocity changes value form that for the fist layer to that for the deep layer clearly depends on the thickness *d*. Moreover it could be noticed that this transition abrupt for a thick first layer thick and very mild in the case of a thin layer.

Test B concerns the influence of changes of the first layer density on the shape of the dispersion curve (Fig. II.7b). Concrete density range rarely extends beyond the range from 1800 kg/m^3 to 2300 kg/m^3, and that range is taken into account. The obtained results show that the relatively small changes of dispersion characteristic are presented only for the low frequencies.

Test C presents the influence of longitudinal wave velocity on the dispersion characteristic (Fig. II.7c). The velocity range taken for analysis is between of 3800 m/s to 4800 m/s. The change of longitudinal wave velocity of the first layer caused a relatively small vertical shift of the characteristic without changing its shape.

Test D shows the influence of transversal wave velocity on the dispersion characteristic (Fig. II7d). The V_S velocity range takes the values from 2150 m/s to 2550 m/s with a step of 100 m/s. V_S change results with a significant shift of most part of the characteristic. For low frequencies all of the curves tend to SW velocity in the half space.

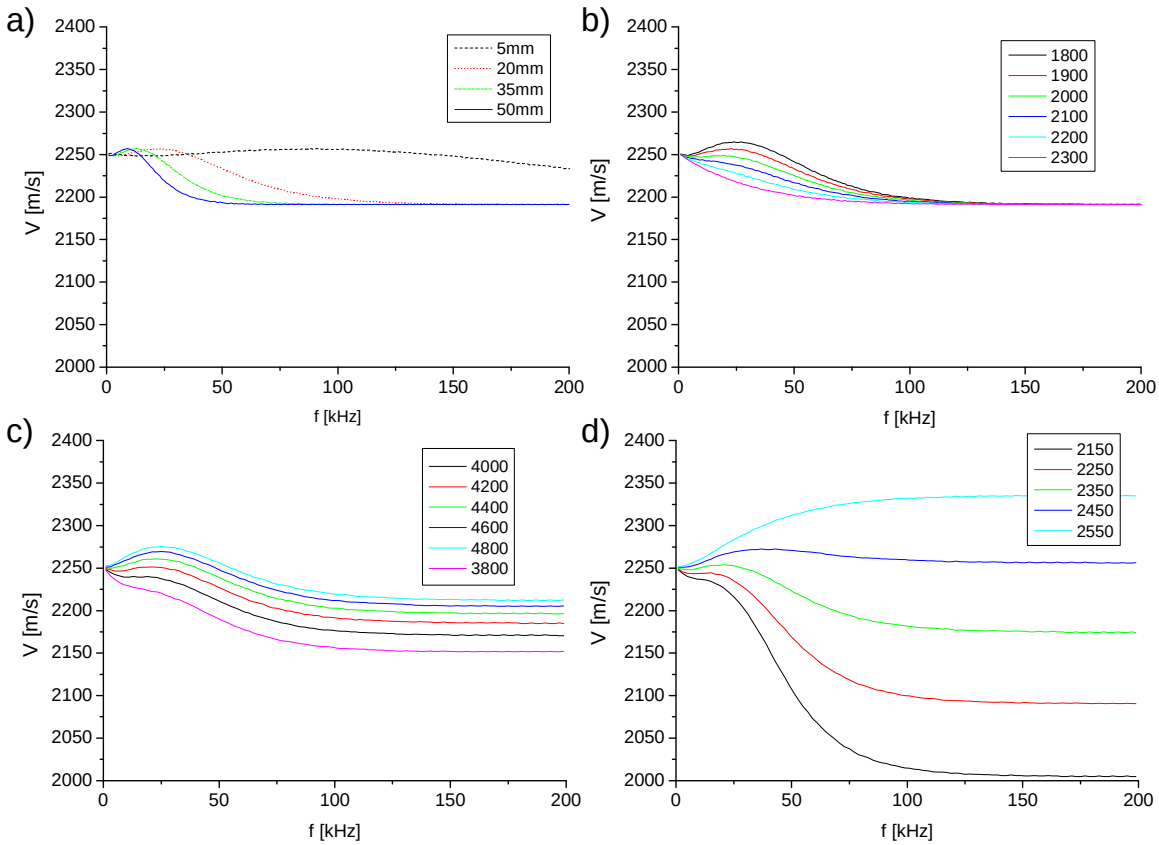

Figure II.7 Dispersion characteristic for two layers Haskell model for the case in which first layer parameters are changed a) the thickness *d*, b) the density ρ, c) V_P velocity, d) V_S velocity.

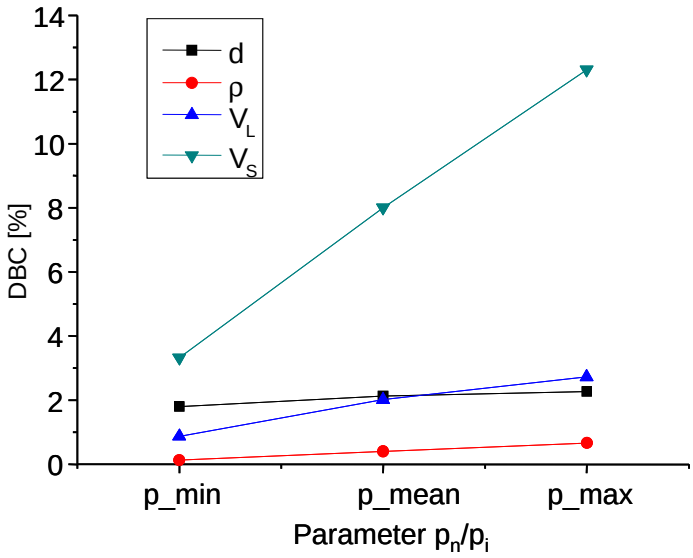

Figure II.8 The graphic representation of the quantitative assessment of the sensitivity test for Haskell model.

The results of the quantitative assessment of the model parameters influence on the dispersion characteristic is presented in the Figure II.8. The results confirm the observations of qualitative analysis (tests A-D). The changes of transversal wave velocity caused the greatest influence on the Haskell model with the maximum values of the relative measure DBC reaches *13%*. The density changes (Test B) have less influence on the dispersion curves (DBC value does not exceed *1%*). The influence of the layer thickness is comparable with the effect of the longitudinal wave velocity changes. The statement of proceeded tests shows that the inverse procedure (parameter value estimation procedure) should be focused on the V_S velocity and the thickness *d*. From the concrete diagnostic point of view the thickness of the first layer is the most important information. The limitation of the number of the model parameters is important for the speed of inverse procedure computation (in the identification process). Moreover the increase of the number of unknown parameters in inversion process caused the increased uniqueness of the solutions. The assessment of sensitivity should be taken into account during development of the algorithm for inversion.

II.1.4 Surface waves in the medium of a linear changes of a shear modulus (Gibson model)

In the Gibson model a linear and continuous change of a shear modulus *G* as a function of depth is assumed (Fig. II.9). In this work the Gibson model is used as a description of surface wave propagation in degraded concrete. This approach is justified if the degradation does not cause abrupt changes of properties, and the changes of shear modulus cause a dominant mechanical effect. Gibson half-space [Gibson 1967] is defined as an inhomogeneous elastic half-space with constant density ρ and constant Poisson ratio ν in the entire volume. The main assumption of the model is a linear increase of dynamic shear modulus *G* as a function of depth *z* in the form

$$G(z) = G_0(1 + mz) \tag{II.32}$$

where the parameter *m* can be considered as the degree of the material heterogeneity. It has direct influence on the rate of changes of shear modulus as a function of depth relative to values at the surface $G_0=G(z=0)$ (Fig. II.9).

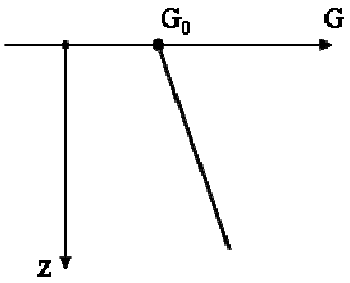

Figure II.9 The shear modulus *G* versus depth *z* in the Gibson model.

Using the relationship between shear modulus *G* and velocity of transversal wave propagation V_S, and based on II.32 V_S velocity can be presented as a function of depth [Xia and al.2006] in the form

$$V_s(z) = \sqrt{\frac{G(z)}{\rho}} = V_{S0}\sqrt{1+mz} \tag{II.33}$$

Approximation of surface waves propagation proposed in the paper [Vardoulakis and Verttos 1988] is based on Gibson model and allows us to formulate a dispersion equation for the fundamental mod of the Rayleigh wave in the form

$$V(f) \cong V_{S0}\left(\frac{1}{\Omega_V(f)} + \sqrt{\frac{1}{\Omega_V(f)^2} + \frac{1}{0.35(3.6-\nu)}}\right) \tag{II.34}$$

where

$$\Omega_V = \frac{0{,}56(3.6-\nu)\Omega}{(1.5+\nu)},\ \Omega = \frac{2\pi f}{mV_{S0}} \tag{II.35}$$

and

$V(f)$ – phase velocity of Rayleigh wave [m/s]

V_{S0} – transversal wave velocity at the surface ($z=0$) [m/s]

ν – Poisson ratio.

The model variables (V_{S0}, m, ν) link the changes of transversal wave velocity $V_S(z)$ versus depth with changes of surface wave phase velocity $V(f)$. Variable Ω is called dimensionless frequency. According to the paper [Vardoulakis and Verttos 1988] the error of presented approximation of the SW velocity related to accurate solution is up to *3%*.

The advantage of Gibson model to Haskell model is its simplicity and the existence of analytical solutions. That greatly accelerates the numerical calculation of dispersion characteristics. Presented model is implemented in GIBS program. The result of the program is a dispersion characteristics generated for any set of parameters V_{S0}, m and ν in chosen frequency range.

II.1.5 Study of the sensitivity of the Gibson model

The qualitative and quantitative changes of the dispersion characteristic caused by the changes of the parameters of the Gibson model are presented below. All tests of the model sensitivity were realised in the same way as presented in the Chapter II.1.3. The qualitative assessment was done by analyzing the dispersion characteristic shape changes caused by the changes of the model parameters. In each test only one parameter is changed and the others parameters are fixed. For the quantitative assessment the relation II.31 is used. The range of the changes for each parameter corresponds to the most common values for concrete. The qualitative and quantitative tests results are presented in the Figure II.10.

Test A shows the influence of the transversal wave velocity at the surface V_{S0} on the shape of dispersion curve. Three curves generated for the V_{S0} equal to *2000 m/s, 2300 m/s* and *2600 m/s* for fixed other parameters ($m=5$ and $\nu=0.2$) are presented in the Figure II.10a. The change of V_{S0} caused a perpendicular shift of the characteristics without significant changes of its shape.

Test B concerns the influence of changes of the heterogeneity factor *m* on the shape of the dispersion curve. The Figure II.10b shows the results for the *m* factor taking the values from *1* to *10*, while the other parameters take the values $V_{S0}=2200$ *m/s* and $\nu=0.2$. The comparison of the curves shows that the changes of the *m* factor affect mainly at the characteristics shape in the low frequencies. For higher frequencies all of the curves tend to the same velocity, which is close to V_{S0} value.

Test C presents the influence of the Poisson ratio value on the dispersion characteristics (Fig. II.10c). Poisson ratio for concrete has usually range from *0.20* to *0.22* and that range is considered. The $m=5$ and $V_{S0}=2200$ *m/s* is taken to generate the presented curves. The test shows that the effect of Poisson ratio changes is negligible.

Qualitative assessment shows that the model is much sensitive to the changes of the V_{S0} value and the *m* factor. Moreover there is no significant influence of the Poisson ratio changes. The same tendency is confirmed by the quantitative assessment, assumed that the parameters value vary within the ranges used in test A, B and C. The value of *DBC* deviation for each parameter is shown in the Figure II.10d. The V_{S0} velocity changes cause *DBC* changes of *32%*, while the Poison ration and heterogeneity factor cause *DBC* changes of *1%* and *6%* respectively. Conclusion of presented tests is that the Gibson model used in inversion process does not provide a reliable value of Poisson ratio.

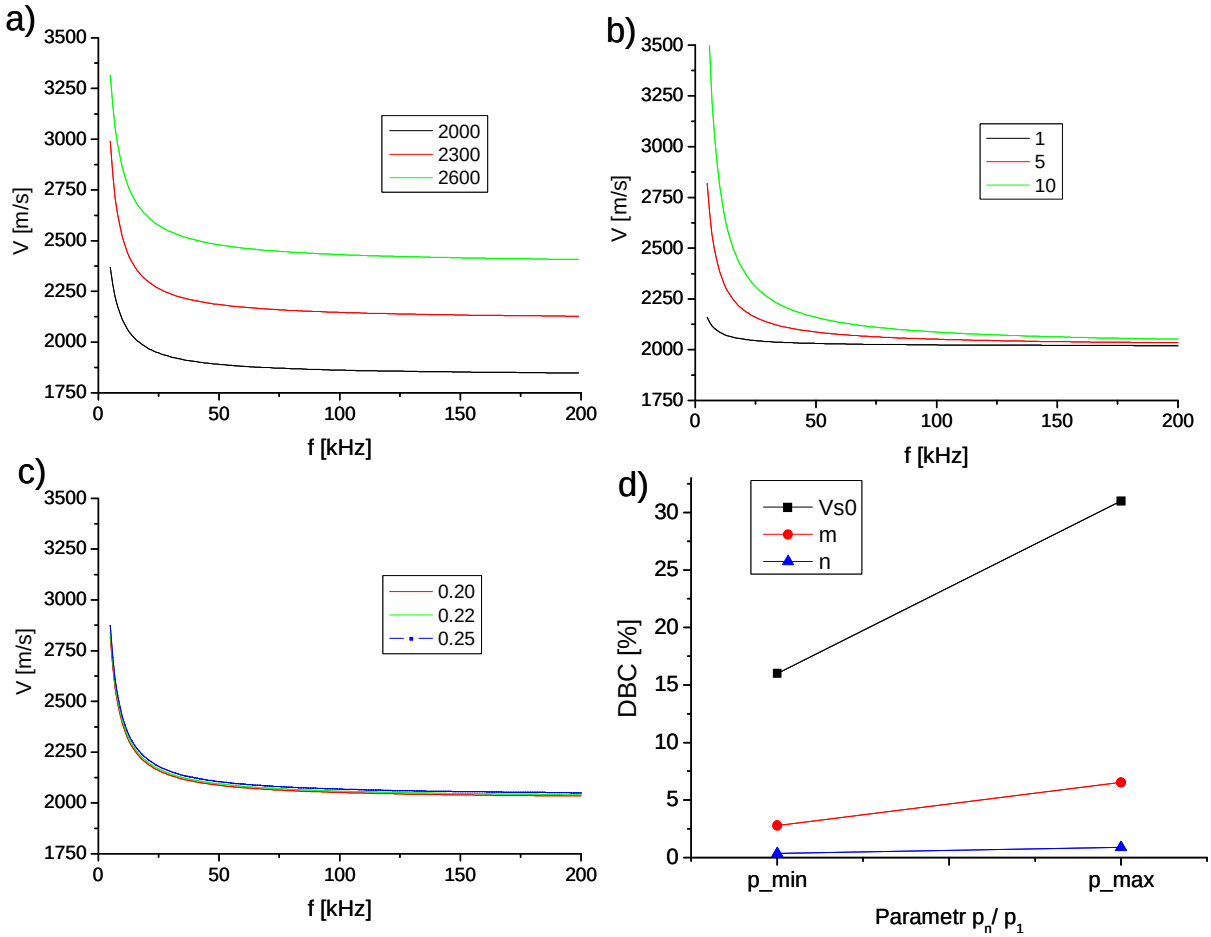

Figure II.10 The Gibson model dispersion characteristic with changed a) velocityV_{S0}, b) m factor, c) Poisson ration. d) Quantitative results.

II.1.6 Comparison of the Gibson's model with the Haskell's model

The two models discussed above (Haskell's and Gibson's models) are configured to map the same heterogeneous macrostructure. The objective of proceeded mapping is to compare the results obtained from these two models. The following assumptions are made:

- the Haskell's model consists of *11* layers (with halfspace),
- the parameters of 1^{st} layer of Haskell's model relates to the parameters at the edge of halfspace in the Gibson's model,
- the density ρ and the Poisson ration ν for each layer in Haskell's model are identical like in Gibson's halfspace,
- the thickness of layers in Haskell's model (excepting halfsapace) is the same and the sheer waves velocities in each layer result from the relation II.33.

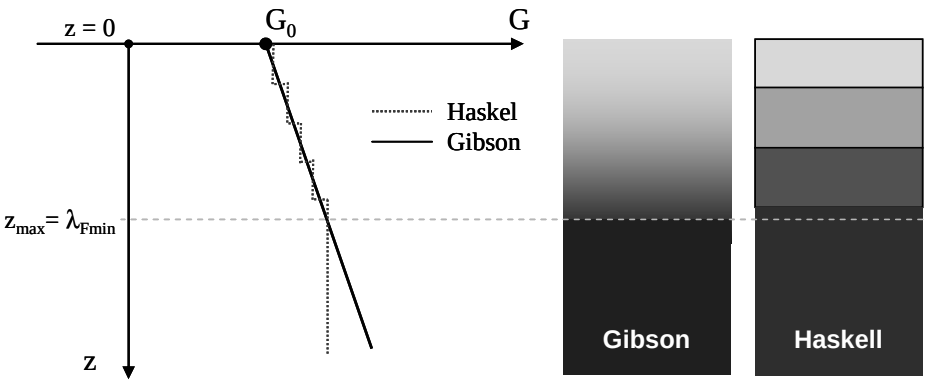

Figure II.11 The comparison of the shear modulus *G* for the structures modelled by the Gibson's and the Haskell's models and the G modulus visualisation for both cases.

Table II-3 The parameters of the Gibson's and Haskell's models used for the model comparison.

Gibson's model parameters		
Poison ratio ν	0,3	
Transversal wave velocity at the surface V_{s0}	2100 [m/s]	
Heterogeneity factor *m*	1,04	
Haskell's model parameters		
Poisona ratio ν (for each layer)	0,3	
Density ρ (for each layer)	2100[kg/m^3]	
Number of layers *n* (including halfspace)	11	
Thicknesses of layers (without halfspace)	0.01 [m]	
Velocities	V_S [m/s]	V_P [m/s]
I layer	2100	3929
II layer	2111	3949
n – 1 layer	2195	4107
n layer (halfspace)	2206	4126

The dispersion characteristics for Haskell's model were generated by the HASK program described above. The values of parameters used for calculations are presented in the Table II-3. The shear modulus versus depth for both cases are presented in Figure II.11. On the right side of the Figure II.11 the graphic interpretation of *G(z)* is presented and the range of the models coincidence z_{max} (limit of coincidence) is marked. That limit relates to the depth of degradation modelled by Haskell's model. Bellow the depth z_{max} the shear modulus *G* in

Gibson's model changes continuously with depth and in Haskell's model *G* remains constant (homogeneous halfspace). The comparison of dispersion characteristics for both models is presented in the Figure II.12. The relative differences between the two model's predictions are marked by curve *Dif* (with the axis on the right side) and were calculated according to the equation

$$Dif(f) = \left| \frac{V_H(f) - V_G(f)}{V_H(f)} \right| 100\% \qquad \text{(II.36)}$$

where V_H and V_G are the surface waves velocities for the Haskell's and Gibson's models respectively for the frequency *f*.

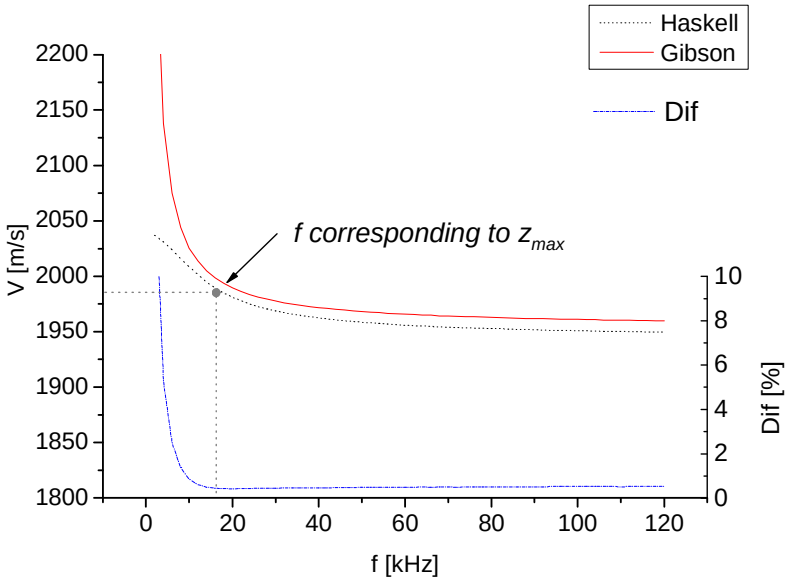

Figure II.12 The comparison of the dispersion characteristics obtained from Gibson's model (red continues line), and from Haskell's model (black doted line). The differences *Dif* between characteristics (the blue doted line).

The Figure II.12 shows that in the range from *18 kHz* to *120 kHz* the differences between the characteristics are insignificant. The relative differece *Dif* in this range is mostly constant and close to *0.5 %*. That small discrepancy may be caused by the approximations used in the Gibson's model (see Chapter II.1.4). For the frequency lower then *18 kHz* the characteristics became divergent (the *Dif* value increases). For this frequency the wave velocity is *1985 m/s*, and the wave longer $\lambda = 110{,}3$ *mm*. The Haskell's model parameters were set to represent the Gibson's model structure by the layered structure. The finite number of layers in Haskell's model caused that the model's results compatibility is fulfill to the deep $z_{max} = 110$ *mm* (*10* layers with *10 mm* thickness + first *10 mm* of half space – Fig. II.11). The depth z_{max} corresponds approximately to the wave length $\lambda = \lambda_{Fmin} = 110{,}3$ *mm* for which the

Dif value increases. The wave lengths λ_{Fmin} for which both characteristics are similar correlate with depth for the modeled structures are similar.

The comparison presented above confirms the compatibility of models and justifies the use of Gibson's model for materials with continuously (approximately linear) change of shear waves velocity profile. In the Chapter IV.5.2 more comparisons of the two models are presented. The use of Gibson's model instead of Haskell's model assures important acceleration of dispersion characteristics calculations because of simplicity of Gibson‘s model. This fact is very important during identification process executed for real experimental data. Moreover, the clear divergence between results of the models shown in the Figure II.12 is the base of the idea of the Degradation Depth Search (DDS) procedure in which the Gibson's model is used (see Chapter IV.5).

II.1.7 Attenuation modelling

The attenuation phenomena of mechanical waves exist in each real material. Sometimes attenuations have a very small influence and can be neglected without a big error. In many cases the value or the character of attenuation might contain important information, which is used in some research methods. Is knows that the attenuation caused additional dispersion of propagated waves. The value of dispersion caused by attenuation depends on the function of attenuation coefficient and frequency for the considered material. In this Chapter the influence of SW dispersion part caused by attenuation on entire dispersion for discussed material is considered. The analysis of this topic should show whether taking into account this phenomena during inversion process (show later, see Chapter IV) is necessary or not.

The range of attenuation values for materials such concrete is very large from dozens to hundreds of dB/m. There is not much knowledge about attenuation in heterogeneous and degraded concretes. There is possible that the effects which cause attenuation can have non-negligible influence on the shape of SW dispersion characteristic. The examples in which the dispersion caused by attenuation is taken into account can be found in articles [Schevenels et al. 2009, Lai 1998, Rix 2000].

The mathematical interpretation of the attenuation phenomena in concrete is very complex because of its heterogeneity. The heterogeneity is a reason of scattering and the attenuation in macroscopic view. The scattering part of attenuation depends on the ratio

between the wave length λ and the size of heterogeneities D [Garnier et al. 2000, Klimis et al. 1988]. Three ranges of λ/D ratio are considered in literature. The relations for attenuation are:

$\lambda >> D$ – Rayleigh range; $\alpha(f) = \overline{\alpha}_1 f + aD^3 f^4$,

$\lambda \approx D$ – stochastic range; $\alpha(f) = \overline{\alpha}_1 f + bDf^2$,

$\lambda << D$ – geometric range; $\alpha(f) = \overline{\alpha}_1 f + cD^{-1}$.

where $\overline{\alpha}_1$ dependent on the dissipative attenuation and a, b and c are the constants dependent on a structure of concrete. Taking into account relation between the range of waves length used in this work ($\lambda \approx$ 5 mm ÷ 40 mm) and the size of heterogeneities in concrete ($D \approx$ 10 nm ÷ 20 mm) the last range of λ/D can be excluded.

For the heterogeneous materials as rocks and concretes, simplified linear relations for attenuation depending frequency is frequently used. In this case only attenuation caused by absorption (dissipative process) is considered.

In the simplest case the spectrum $S(\omega,X)$ of the cylindrically spreading SW in a homogeneous and non attenuated medium $s(t,X)$ is given by relation II.37, where X is a distance form the source of wave.

$$S(\omega, X) = S_o(\omega)\frac{e^{-jkX}}{\sqrt{X}} \tag{II.37}$$

where $S_0(\omega)$ means complex amplitude, ω and k are the circular frequency and wave number respectively, the expression $1/\sqrt{X}$ relates to the amplitude decrees caused by cylindrical spreading of the wave.

In the attenuated medium the real wave number k must be replaced by the complex wave number k'

$$k' = k_\alpha(\omega) + j\alpha(\omega) \tag{II.38}$$

where both the real part k_α and the imaginary part α (related with attenuation) are generally the functions of frequency. The wave number k_α is related with phase velocity in attenuated material $V_\alpha(\omega)$.

$$k_\alpha(\omega) = \frac{\omega}{V_\alpha(\omega)} \tag{II.39}$$

Finally, taking into account the attenuation, the Equation II.37 can be written as

$$S(\omega, X) = S_o(\omega)\frac{e^{-\alpha(\omega)X}}{\sqrt{X}}e^{-jk_\alpha(\omega)X} \tag{II.40}$$

The introduction of the attenuation in the Haskell's model can be made in several ways. The assumption that the considered material has a visco elastic properties is the base for one of them. In that case the complex longitudinal and transversal wave velocities for all layers in model must be introduced. This causes the doubling of the number of model parameters. What is important, the increase in the number of parameters searched practically excludes the use of the model to solve the inverse problem. As already shown above the Haskell's model has no analytical solution, and for solving it, the optimization methods must be used. The forward solution of the model without attenuation is easy because it is two variables problem. For the model with attenuation the problem of three independent variables must be solved. That causes important increase of the computation time. The use of this approach for solving the inverse problem in which the "forward" problem must be solved many times is complicated. It was considered that this way of attenuation inclusion in Haskell's model, especially the inversion process, is not effective. For this reason the original method of including the dispersion caused by attenuation is proposed. The possibility to add a structural dispersion and dispersion caused by attenuation which source is the macroheterogeneity is assumed.

In the proposed solution the dispersion caused by attenuation is calculated and used to correct the experimental dispersion characteristic V_E. In this way the characteristic of the structural dispersion only is obtained. The corrected characteristic is used for inversion (for the model without attenuation). The possibility of use this approach for different models describe the phenomena of structural dispersion is an advantage. It is possible because in this method the operations are preceded on the dispersion characteristic, and not on the model equations.

Using the results obtained for the rocks, the assumption of the same level of attenuation as a function of depth is considered and then the relation between the attenuation and the frequency is given by equation [Aki et al 1990]

$$\alpha(\omega) = \frac{\alpha_1 \omega}{1 + \alpha_T \omega} \tag{II.41}$$

where α_1 is constant and α_T is constant which fulfills the relation $\alpha_T \omega << 1$. The assumptions above let us to express the quality factor $Q = \frac{\pi}{\lambda \alpha(f)}$ as fallowing approximation [Aki et al. 1990]

$$Q \approx \frac{1}{2V_\infty \cdot \alpha_1} \tag{II.42}$$

It was experimentally established that in the ultrasonic frequency range used in concrete diagnostic the value of $\alpha T\omega=0.1$ can be taken into account and gives the results equal to the observation. Besides, the causality rule for this value is performed [Kuc (1981,1983)]. Taking into account the assumption II.41 the relation between velocity and attenuation can be expressed as II.43 [Aki et al. 1990].

$$\frac{1}{V_\alpha(\omega)} = \frac{1}{V_\infty} + \frac{2\cdot\alpha_1}{\pi}\cdot\ln\left(\frac{1}{\alpha_T\cdot\omega}\right) \tag{II.43}$$

where V_∞ is the velocity for high frequencys ($\omega\rightarrow\infty$). Taking into account that for high frequencies the depth of the SW penetration into material is low and the dispersion is caused only by attenuation (the structural dispersion is negligible). The Equation II.43 can be transformed to the form

$$V_\alpha(f) = \frac{V_\infty}{1+\frac{1}{\pi\cdot Q}\cdot\ln\left(\frac{1}{\alpha_T\cdot 2\pi f}\right)} \tag{II.44}$$

where the phase velocity $V_\alpha(f)$ in function of quality factor Q and the velocity $V_\infty = V(f = \infty)$ is presented.

If the experimental dispersion characteristic which depends both on structural dispersion and the dispersion caused by attenuation is denoted as $V_E(f)$ the value of of V_∞ can be obtained by transformation of the Equations from II.44 to II45. Then as a $V_E(f_{max})$ the value of velocity for the highest frequency f_{max} obtained from V_E characteristic can be substituted.

$$V_\infty = V_E(f_{\max})\cdot\left[1+\frac{1}{\pi\cdot Q}\cdot\log\left(\frac{1}{\alpha_T\cdot 2\pi f_{\max}}\right)\right] \tag{II.45}$$

For known V_∞, Q, αT ($\alpha T\cdot 2\pi fmax << 1$) in the Equation II.44 the $V_\alpha(f)$ and then the vector $\Delta V_\alpha(f)$ can be calculated. This vector is a different between the velocity V_∞ and $V_\alpha(f)$ (always $V_\infty > V_\alpha(f)$)

$$\Delta V_\alpha(f) = V_\infty - V_\alpha(f) \tag{II.46}$$

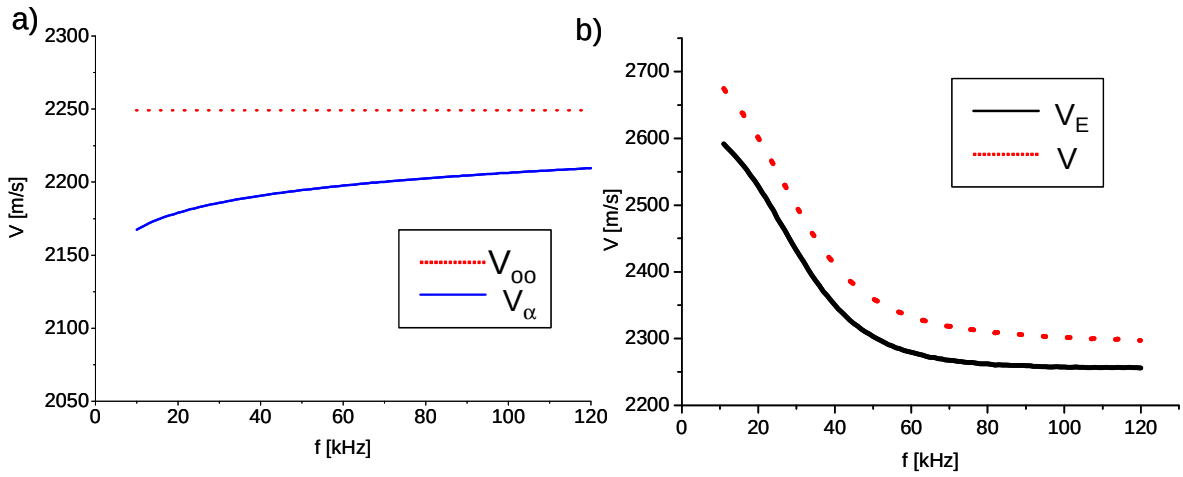

Figure II.13 Taking into account the dispersion caused by the attenuation: a) the V_∞ and V_α curves, b) the dispersion characteristics with and without attenuation influence (V_E and V curves respectively).

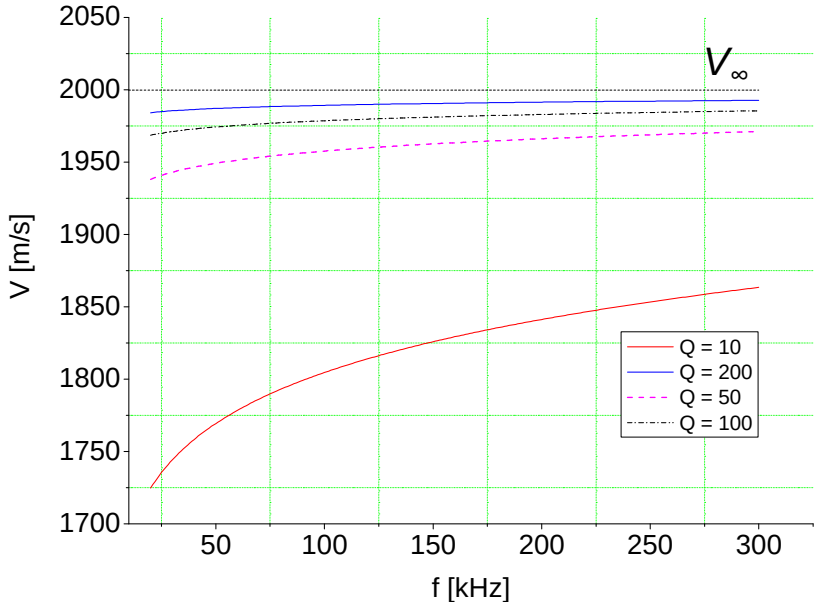

Figure II.14 The dispersion caused by attenuation for V_∞ =2000 m/s and Q = 10, 50, 100 and 200.

Using the model presented above (dispersion caused by attenuation) it is assumed that total dispersion of SW in macroheterogeneous media results from the superposition of the structural dispersion and the dispersion caused by attenuation. The value $\Delta V_\alpha(f)$ can be considered as an influence of attenuation on dispersion of SW. Finally, the dispersion of phase velocity of SW caused only by structure of a material $V(f)$ with a correction $\Delta V_\alpha(f)$ can be approximated in form as:

$$V(f) = V_E(f) + \Delta V_\alpha(f) \qquad \text{(II.47)}$$

The attenuation caused decrees of velocity and because of this a plus sign in equation II.47 is used. In the Figure II.13a the $\Delta V_\alpha(f)$ velocity curve is presented (for the following values $V_\infty = 2300$ *m/s*, $Q = 40$ and $\alpha T = 1{,}33 \cdot 10^{-8}$). In the Figure II.13b the example of the dispersion characteristic with and without dispersion caused by attenuation is presented (for $Q = 40$). In the example presented in figure II.13 mean absolute change of velocity is about *2.2 %*.

The experimental results shows that the values of quality factor Q for the most common concretes ranges from *10* (very weak concrete with high attenuation) to *200* (good quality concrete with low attenuation). The curves of dispersion caused by attenuation only (calculated on the base of equation II.44) for a few value of Q from the range form *10* to *200* are shown in Figure II.14. The velocity $V_\infty = 2000$*m/s* is taken for the calculations.

The mean change of SW velocity caused by attenuation (for the considered ranges of velocity and frequency) is in the range from *0.5%* for $Q = 200$ to *10%* for $Q = 10$, but this relationship is strongly nonlinear. Therefore it is necessary to consider whether its influence on the dispersion caused by attenuation on total dispersion is not negligible.

II.2 Modeling of the ultrasonic waves reflection from an interface of porous solid in the air

The considered reflectometric method is based on the measurement of the reflection coefficient R of the ultrasonic waves in function of the incident angle θ. The waves are reflected from the surface of the measured material. To use the results of reflectometric measurement to material diagnostics the mathematical model describing considered phenomena must be utilized. The reflection coefficient R is the ratio between the amplitudes of reflected A_r and emitted A_i signals for a given angle θ_i and can be written as

$$R(\theta) = \frac{A_r(\theta)}{A_i} \tag{II.48}$$

In the Figure II.15a the scheme of reflection phenomena on the fluid solid interface is presented. In the Figure II.15b the example of reflection coefficient in function of incident angle is shown.

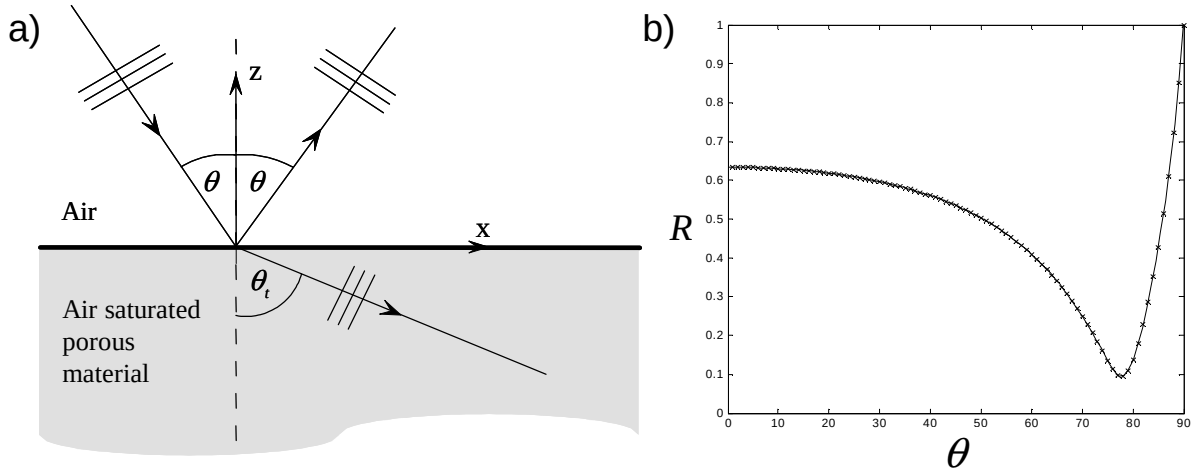

Figure II.15 Reflectometrie: a) the scheme of phenomena of reflection, b) the example of theoretical characteristic of reflection coefficient *R* versus incident/reflection angle θ.

The motivation for the use of the reflectometric method for concrete diagnosis are promising results of its use in tests of the structure parameters of other materials such as rocks and foam [Hoffren et al.2004, Hoffren et al. 2005, Fellach et al. 2003]. The presented method is a non-contact method, in which the air or water is used as a medium of propagation. In the presented work the measurement in the air are mainly considered because they have a chance to complement the measurements of SW propagation for real concrete structures. The reflectometric measurements in water could be used in the study of underwater structures, but for that the use of appropriate models and methods of identification is required. For the reflection coefficient measurement a special device called Refectometer was constructed. In the Chapter III.2 the details about the Reflectometer and the measurement technique is presented.

II.2.1 Description of the model with viscosity inclusion

A simplified variant of the presented approach omitting the impact of viscous forces can be found in the work of Fellach at al. [Fellach et al. 2003]. In this approach two structural parameters: porosity and tortuosity are determined from a measurement of two values of reflection coefficient at two different incidence/reflection angles θ in the range from 0° to 90° (referred to normal of measured surface). In real conditions the range of θ is limited because of the size of transducers (see Chapter III.2). The model used in this work is based on the simplified Biot's theory of the waves propagation by viscous liquid in a heterogeneous (rigid) porous material [Biot 1956]. The following assumptions for presented model are needed:

- the air saturated porous material is considered,
- the porous material is homogeneous and isotropic,
- the ultrasonic waves propagate only in a liquid filling the pores without the vibrations of skeleton because of a high difference of acoustic impedances,
- the viscous interactions between the air and porous material are included,
- the air viscosity outside the porous material (in border conditions) and the influence of temperature and humidity are neglected.

Model of waves propagation in the air saturated porous media

The macroscopic approach for modeling the waves reflection phenomena from fluid saturated porous materials is known as Biot's theory [Allard 1993, Attenborought 1982, Biot 1956]. It is applied here as a starting point to analyze reflection of waves from the air saturated porous material while the solid phase is assumed to be rigid. The linear momentum equation and the constitutive equation for viscous interaction force the stress in fluid phase are following [Allard 1993]

$$\sigma_{ij,j} + m_i + \rho_{12}\dot{v}_i = n\rho\dot{v}_i \tag{II.49}$$

$$\sigma_{ij} = -pn\delta_{ij} = Re\ \delta_{ij}\ ,\ m_i = -bn^2 G v_i \tag{II.50}$$

where σ_{ij}, m_i, v_i are components of macroscopic stress tensor, and vectors of viscous interaction force between phases and fluid velocity. The velocity is the local time derivative of fluid displacement *U*, i.e. $v_i = \dot{U}_i$, $e = U_{i,i}$ denotes dilatation of fluid, *p*, ρ, *n* are pressure, density and volume porosity (volume fraction of air). The flow resistivity *b* is expressed as the ratio of dynamic viscosity η and permeability k_0 , i.e. $b = \frac{\eta}{k_0}$. $R = Kn$ stands for the coefficient describing the pore fluid compressibility, while *K* is the bulk modulus of pore air. $\rho_{12} = -(\alpha - 1)n\rho$ is the coefficient of dynamic coupling, and α is tortuosity. The consequences of variation of distribution of microscopic velocities of fluid particles at different frequencies and the influence of the latter one on the macroscopic interaction force between fluid and solid phase which is represented by function *G*. For harmonic excitation with angular frequency $\omega = 2\pi f$ (*f* denotes frequency) the function *G* can be approximated using results for cylindrical pores [Biot 1956]

$$G(s) = -\frac{s}{4}\sqrt{-i}\,\frac{J_1\left(s\sqrt{-i}\right)}{J_0\left(s\sqrt{-i}\right)} \Big/ \left[1 - \frac{2}{s\sqrt{-i}}\,\frac{J_1\left(s\sqrt{-i}\right)}{J_0\left(s\sqrt{-i}\right)}\right] \tag{II.51}$$

where $s = c\left(\frac{8\omega\alpha\rho}{bn}\right)^{1/2}$ and c is the parameter depending on the shape of the cross-section of pores (for cylindrical circular pores $c = 1$) and J_n is Bessel's function of the first kind and n^{th} order.

Performing the operation of divergence to combined equations II.49 and II.50 the wave equation for dilatation of pore fluid in rigid porous material is obtained

$$R\nabla^2 e - bn^2 G\,\dot{e} = \rho_{22}\ddot{e} \tag{II.52}$$

where $\rho_{22} = n\rho - \rho_{12}$.

For harmonic waves the solution of equation II.52 may be written as

$$e = D\exp[i(kx - \omega t)] \tag{II.53}$$

The variable k is the wave number and D is the amplitude of oscillations. Substituting II.53 to II.52 the condition of non-trivial solution ($D \neq 0$) results in the dispersion equation, which solved for the wave number reads

$$k = \omega\sqrt{\frac{1}{R}\left[\rho_{22} + ibn^2\frac{G}{\omega}\right]} \tag{II.54}$$

from which the phase velocity in the air filler pores $V = \frac{\omega}{\mathrm{Re}(k)}$ and attenuation $a = \mathrm{Im}(k)$ can be found. When the viscous interaction between pore fluid and skeleton is neglected the wave velocity is $V = \frac{C}{\sqrt{\alpha}}$, where $C = \sqrt{\frac{K}{\rho}}$ is the wave velocity in air.

Incorporation of thermal effects due to heat generation and conduction in model of wave propagation in air saturated porous media can be indirectly represented through a form of a bulk modulus K. Then for harmonic disturbance and cylindrical pores of circular cross-section the thermal effects in air can be described by the following frequency dependent function for moduls , [Allard 1993]

$$K = K_0 \Big/ \left[g - (g-1)\left[1 + \frac{bn}{iB^2\omega\rho\alpha}G\,(Bs)\right]^{-1}\right] \tag{II.55}$$

where g stands for the specific heat ratio and B^2 is the Prandtl number (for air at $18^{\circ}C$ and pressure $p_0 = 1013\ hPa$ we have $g = 1.4$, $B^2 = 0.71$). The value of the modulus K in free air is assumed to be $K_0 = gp_0$.

Reflection of waves from air-saturated porous material

We consider the interaction of compressional wave coming from free air with the angle o incident θ which occupies the half space $z > 0$ with the porous material filled in air half space $z < 0$ (Fig. II.15). Within the adapted model the energy of the incident wave is divided into a reflected wave propagating at angle θ and a transmitted wave which propagates at the refraction angle θ_t in the air-saturated porous medium. The distribution of energy between the reflected and refracted waves is determined by appropriate boundary conditions.

Boundary conditions at the interface of free air and porous material

The mechanical boundary conditions at the interface between non-viscous fluid and pore fluid which saturates porous material, at $z = 0$, will be assumed as following [Gurevich et al 1997, Castagnede et al 19987]:

- The conservation of fluid mass is expressed as the condition of equal amount of mass displaced across the interface

$$\rho n U_z = \tilde{\rho}\,\tilde{U}_z \tag{II.56}$$

- The local balance of linear momentum reads as the proportionality between jump of the fluid pressure and the normal velocity of fluid in porous medium

$$p - \tilde{p} = Tn\dot{U}_z \tag{II.57}$$

where p and ρ are the intrinsic pore pressure and density of air in the pores, $\tilde{p}$ and $\tilde{\rho}$ are the pressure and density in free air ($z < 0$). $\tilde{U}_z$ and U_z are normal components of displacement vector in free fluid and fluid in porous material. T stands for a kind of surface flow impedance [Castagnede et al 1998] which is in general a complex function depended on wave frequency f proposed in the form $T = T_0 G(s)$. Constant T_0 ranges from zero (for open-pores) to infinity (for closed pores) and for $f \to 0$ tends to T_0.

The linearization of the Equation II.56 assuming equality of density of free air and of air in porous material gives

$$nU_z = \tilde{U}_z \tag{II.58}$$

Assuming that the pressure in free air can be expressed as $\tilde{p} = -K_0 \tilde{U}_{i,i}$ and using equation II.50 along with the formula between the velocity and displacement for harmonic motion $\dot{U}_z = -i\omega U_z$ the condition II.57 reads

$$KU_{i,i} - K_0\tilde{U}_{i,i} = i\omega nTU_z \tag{II.59}$$

For open pores $T = 0$ ($p = \tilde{p}$) and equation II.59 becomes

$$KU_{i,i} - K_0\tilde{U}_{i,i} = 0 \tag{II.60}$$

Reflection coefficient

To find the parameters describing properties of reflected harmonic plain waves at the interface between air and air-saturated porous solid two potentials $\tilde{\phi}$ and ϕ representing respectively displacements in free air due to superposition of incident and reflected waves and displacements related to transmitted wave. So then

$$\tilde{U}_i = \tilde{\phi}_{,i} \ , \ U_i = \phi_{,i} \tag{II.61}$$

For harmonic waves the potentials take form:

$$\tilde{\phi} = \left(e^{-i\tilde{\gamma}z} + Ae^{i\tilde{\gamma}z}\right)e^{i(\sigma x - \omega t)} \tag{II.62}$$

$$\phi = Be^{-i\gamma z}e^{i(\sigma x - \omega t)} \tag{II.63}$$

In the solutions II.62 and II.63 the amplitude of the incident wave is assumed to be equal to one, A is the amplitude of the reflected wave and B is the amplitude of the transmitted wave. The other wave parameters are related as following:

$$\sigma^2 + \gamma^2 = k^2 \tag{II.64}$$

$$\sigma^2 + \tilde{\gamma}^2 = \left(\frac{\omega}{c}\right)^2 \tag{II.65}$$

$$\gamma = k\cos\varphi \tag{II.66}$$

$$\tilde{\gamma} = (\omega / c)\cos\tilde{\theta} \tag{II.67}$$

where σ is the *x* component of all wave vectors, $\tilde{\gamma}$ denotes the *z* component of the wave vector of incident and reflected wave, γ is the *z* component of the wave vector for transmitted wave. Within the assumed model σ and $\tilde{\gamma}$ have real values and γ and φ are complex. The relation II.64 to II.67 comes form properties of heterogeneous waves [Declercq et al 2005]. The complex wave number *k* and the corresponding complex angle φ determine the refraction angle θ_t by the formula

$$tg\,\theta_t = \frac{\mathrm{Re}(k\sin\varphi)}{\mathrm{Re}(k\cos\varphi)}. \tag{II.68}$$

According to Snell's law the relationship between wave velocity in air *C*, incidence angle θ, wave number *k* and complex angle φ is

$$\sigma = (\omega / C)\sin\theta = k\sin\varphi \tag{II.69}$$

In order to calculate the amplitude reflection coefficient the Equations II.62 and II.63 were substituted into the Equations II.61 and then into boundary conditions II.58 and II.59. Neglecting the exponential factors that lead to the two algebraic equations

$$A\tilde{\gamma} + Bn\gamma = \tilde{\gamma} \tag{II.70}$$

$$-AK_0(\frac{\omega}{c})^2 + B(Kk^2 + T\omega n\gamma) = K_0(\frac{\omega}{c})^2 \tag{II.71}$$

the solution of which with respect to *A* gives the amplitude reflection coefficient

$$R = |A| = \sqrt{(\mathrm{Re}\,A)^2 + (\mathrm{Im}\,A)^2} \tag{II.72}$$

When the viscous interaction of air with porous material is neglected *Im A* = 0 and

$$A = \frac{\alpha\cos\theta + \dfrac{nT}{\sqrt{\rho K}}\cos\theta\sqrt{\alpha - \sin^2\theta} - n\sqrt{\alpha - \sin^2\theta}}{\alpha\cos\theta + \dfrac{nT}{\sqrt{\rho K}}\cos\theta\sqrt{\alpha - \sin^2\theta} + n\sqrt{\alpha - \sin^2\theta}} \tag{II.73}$$

If additionally the surface pores are open (*T = 0*) from equation above we have

$$A = \frac{\alpha\cos\theta - n\sqrt{\alpha - \sin^2\theta}}{\alpha\cos\theta + n\sqrt{\alpha - \sin^2\theta}} \tag{II.74}$$

The Equation II.74 with the left hand side erroneously replaced by the reflection coefficient which was used in the paper [Fellach et al 2003] to derive equations for tortuosity and porosity of porous materials from data for reflection coefficients R_1 and R_2 obtained for two different incidence angles θ_1 and θ_2 respectively. Taking into account that the real component of *A* can be positive or negative and $R = |A|$ the correct equation which should be used for calculation of the tortuosity is

$$\alpha = \frac{\left(\dfrac{(1\mp R_2)(1\pm R_1)\cos\theta_2}{(1\pm R_2)(1\mp R_1)\cos\theta_1}\right)^2 \sin^2\theta_1 - \sin^2\theta_2}{\left(\dfrac{(1\mp R_2)(1\pm R_1)\cos\theta_2}{(1\pm R_2)(1\mp R_1)\cos\theta_1}\right)^2 - 1} \tag{II.75}$$

and then finding the porosity *n* for any pair (θ_i , R_i) may be based on the formula derived also from II.74

$$n = \frac{\alpha(1\mp R_i)\cos\theta_i}{(1\pm R_i)\sqrt{\alpha - \sin^2\theta_i}} \tag{II.76}$$

where the upper and lower signs refer to $A > 0$ and $A < 0$, respectively. When the model includes the effects of surface flow impedance and/or viscous interaction there is no explicit analytical formulas for the structural parameters n and α.

II.2.2 Study of the model's sensitivity

The model of wave reflection from a porous material presented above and the measurement of reflection coefficient as a function of incident angle can be used to identify the structural parameters as, porosity n, α tortuosity, permeability k_0, and surface flow impedance T. The sensitivity tests let us determine ranges of model parameters in which they have important or neglected influence on the reflection coefficient, what is important in the identification process. A detailed analysis of the parameter influence for a wide range of porosities can be found in the report [RAP 2010]. In the presented work only low and medium porosities in the range occurred for concretes are considered. In each case the parametric study is done changing one parameter and preserving constant other (reference) parameters. The reference values of parameters are written in bold. The tests are grouped for low (Fig. II.16) and medium (Fig. II.17) porosities. In the Table II-4 model parameters for all cases are presented. The ranges of values for each parameter were chosen as the most common for concrete.

The quantitative assessment of model sensitivity in the range of low porosity (Fig. II.16) shows that whichever parameter causes the significant influence on the reflection coefficient characteristic. The graph axes are chosen so that the presented characteristics were comparable with further examples. Because of the low influence of material parameters on the reflection coefficient in the case of low porosity in the following analysis the qualitative and quantitative study of sensitivity only for medium porosity ranges is considered.

Table II-4 The structural parameters in the tests of reflection coefficient sensitivity.

Material	Porosity (n)	Tortuosity (α)	Permeability (k_0)	Surface flow impedance (T)
Low porosity	0.05/**0.1**/0.2	3/**5**/8	10^{-17}/**10^{-16}**/10^{-15}	0/**10^{3}**/10^{6}
Medium porosity	0.2/**0.3**/0.4	1.2/**1.6**/2	10^{-13}/**10^{-12}**/10^{-11}	0/5x**10^{3}**/10^{4}

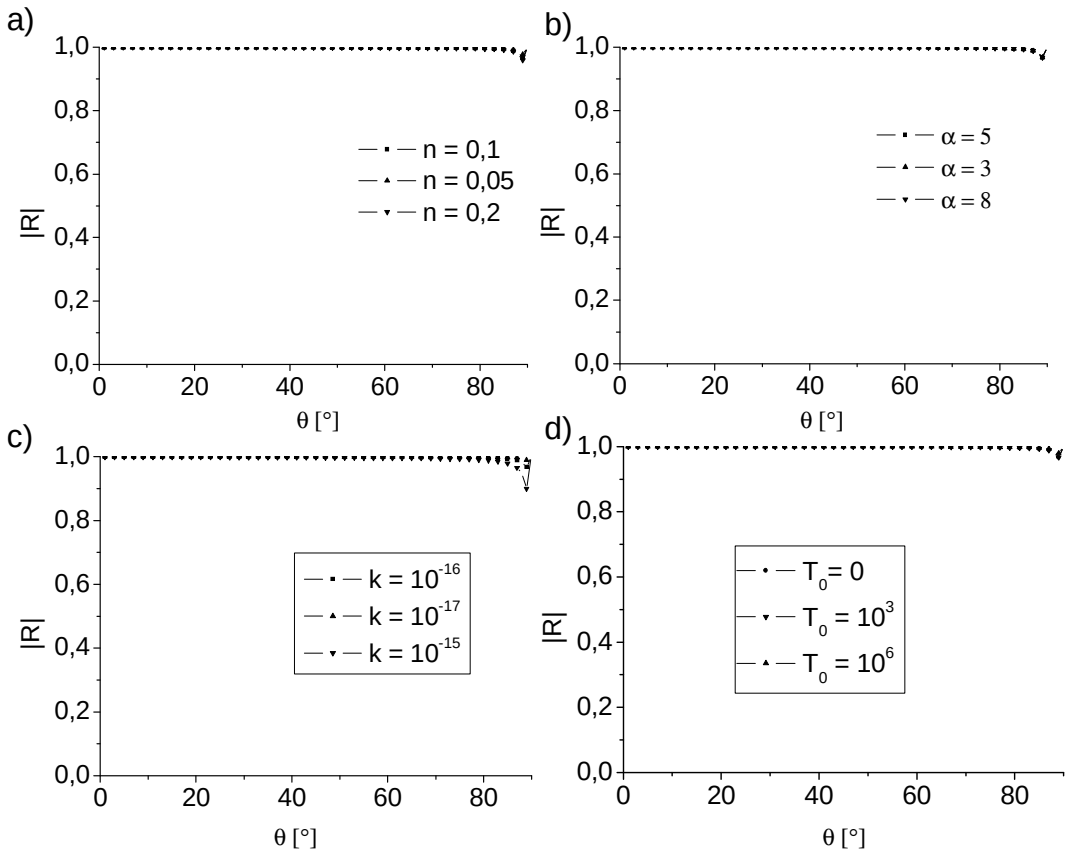

Figure II.16 The evaluation of *R* characteristic in the range of low porosity caused by the changes of a) porosity, b) tortuosity, c) permeability, d) surface flow impedance.

The sensitivity tests in the case of medium porosity are named by letters form A to D. The qualitative assumption is presented firstly before the quantitative one.

Test A shows the influence of the porosity (Fig. II.17a). Small vertical (along the *R* axis) displacements are caused by porosity changes. The increase of porosity causes the decrease of *R*.

Test B concerns the influence of tortuosity (Fig. II.17b). There is no significant influence of tortuosity on the *R* characteristic.

Test C concerns the influence of permeability (Fig. II.17c). The changes of permeability have significant influence on the reflection coefficient in the whole range of incident angles. The increase of permeability causes the decrease of *R*.

Test D presents the influence of surface flow impedance (Fig. II.17d). The changes of surface flow impedance have significant influence on the shape of reflection coefficient characteristic.

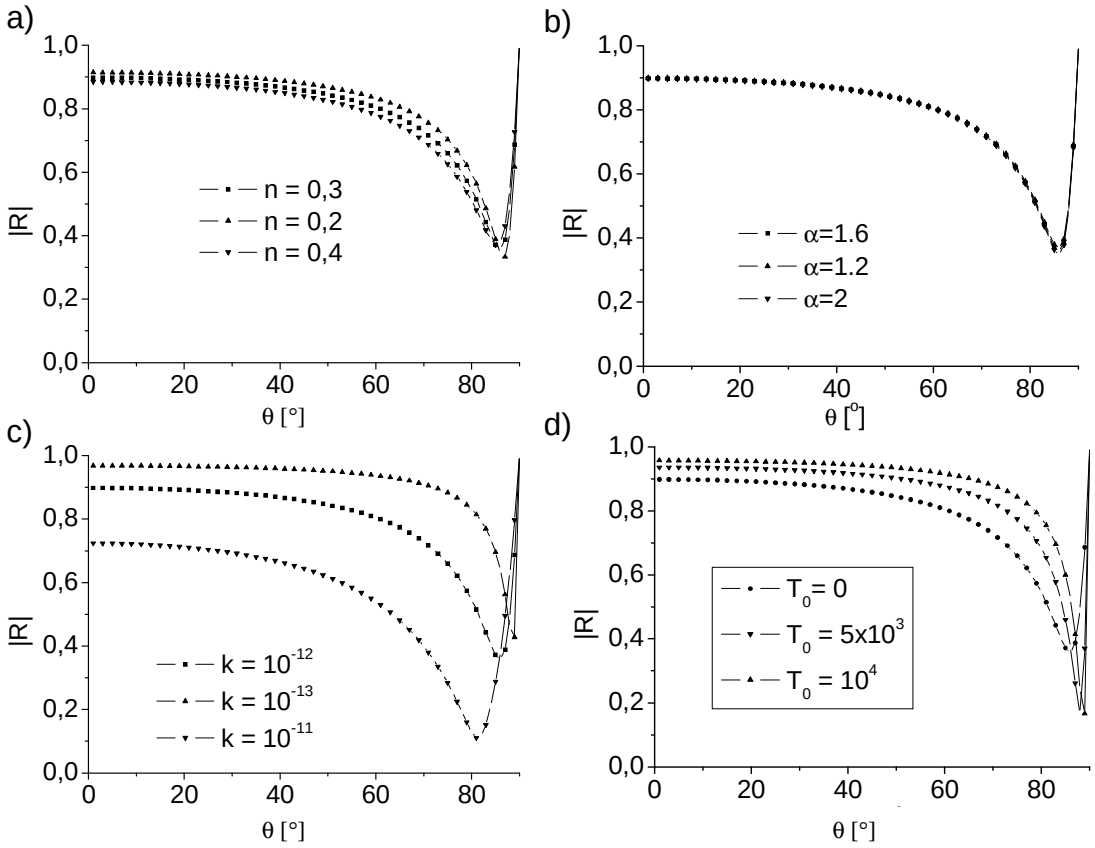

Figure II.17 The evaluation of *R* characteristic in the range of medium porosity caused by the changes of a) porosity, b) tortuosity, c) permeability, d) surface flow impedance.

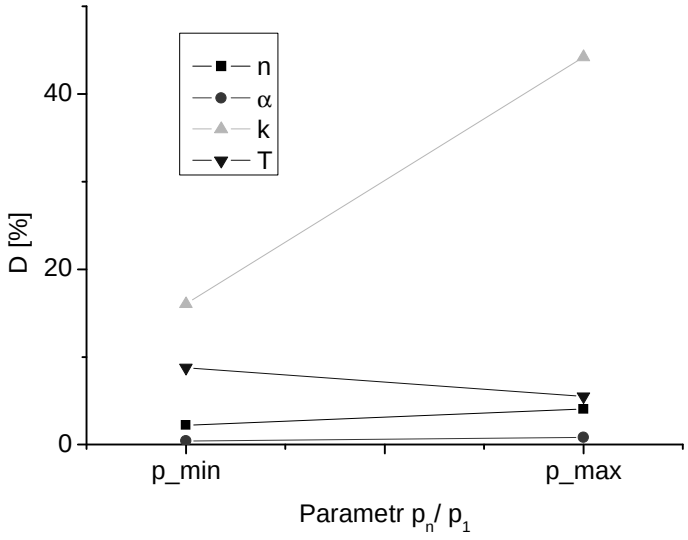

Figure II.18 The quantitative comparison of *R* characteristic evaluation caused by model parameters, where: n – porosity, α – torotuosity, k_0 – permeability and T – surface flow impedance.

The quantitative comparison was carried out in the same manner as in the case of models describing the SW propagation (eq. II.31). In the Figure II.18 the quantitative results of the sensitivity tests are presented.

Presented analyse confirm observations that the highest model sensitivity in the range of medium porosity is observed for changes of permeability. The surface flow impedance has secondary influence no the *R* characteristic. The changes of porosity have very low influence and influence of tortuosity is neglected. No changes in the reflection coefficient *R* caused by changes of model parameters in the range of low porosity (below 20%) means that this method can be used only for degraded concretes, which are characterized by higher porosity than "healthy" concretes.

II.3 Conclusions

In this chapter issues of modeling of surface wave propagation in heterogeneous materials and reflection of ultrasound wave at the interface of porous material and the air were presented.

In the section devoted to modeling of surface wave propagation:

- the use of Haskell's model (heterogeneous layered structure) and Gibson's model (heterogeneity linearly changed with depth) to determining the dispersion characteristics were discussed,
- the developed numerical approach of solving dispersion equation of Haskell's model was shown,
- the comparison of models prediction for discrete and linearly variable shear modulus were presented,
- the sensitivity study of both models, which allowed to determine (in a qualitative and quantitative manner) the influence of model parameters was performed. The analysis shows that for Haskell's model, the transversal waves velocity and thickness of layers have the greatest influence on the dispersion. The longitudinal waves velocity and density of layers have a secondary role. The sensitivity analysis of Gibson's model shows, that the greatest influence on dispersion characteristic has the velocity of propagation of transversal waves at the edge of halfspace. A much smaller role plays a coefficient of heterogeneity and almost negligible Poisson's ratio.

- the procedure of considering the dispersion component derived from attenuation was proposed. The analysis showed that for values of parameters mainly observed for concretes, the average relative influence of attenuation on dispersion does not exceed 5%.

In the section of the chapter dedicated to reflectometry The modeling of the phenomena of ultrasonic waves reflection from porous material was considered and:

- the assumptions of the model and its sensitivity testing were presented,
- it was shown, that the model can be applied to materials with average and higher porosity, which limits its application to degraded concrete only,
- it was observed, that the largest influence on the expected reflection coefficient firstly has changes of permeability, secondly surface flow impedance, and lastly porosity. The tortuosity has a neglected role.

Chapter III

Description and tests of the measurement devices

One of the major objectives of the presented work was to design and construct two measurement systems. These devices let to execute measurements of surface wave propagation and reflection coefficient and are called respectively SWMD (Surface Waves Measurement Device) and RMD (Reflectometry Mesurement Device). The main task of the constructed devices is to conduct the measurements and to provide relevant data for mechanical and structural properties of tested materials identification. The configuration of measurements (transducers positioning) should be faithful to the models assumptions presented in the Chapter II. The unique character of the developed devices and consequently, the lack of available knowledge sources, which would facilitate the development of these systems is worth to emphasizing. In this chapter the motivation and genesis of the formation of each of the measurement systems and the signal processing method are presented. An evaluation of their work on the basis of the tests with known materials is preceded.

III.1 Surface waves propagation measurement system

The study of surface wave propagation requires a system that is able to generate and receive ultrasonic waves in such rough materials for the US waves propagation as concrete. Depending on the specific application, there are several configurations which allow realizing such measurements [Szelążek 2001, Ryden et al. 2009]. In the simplest case the impulse excitation (et. seismic hammer) is used as a source. This let us generate all types of waves that may be presented in that medium. Subsequently, propagating waves are registered along the selected profile (area). As a measurement profile a set of observation points along a line running from the source of the signal to the receiver is considered. In seismic applications for observation of waves propagation geophones or hydrophones are used. In the material research domain the accelerometers are often used.

For high-frequency waves the ultrasonic transducers or laser sources/receivers can be used. From all of the received signals, it is necessary to isolate these associated with surface waves. Nowadays, this operation is performed frequently as a part of digital signal processing. The diagram of the simplest measuring configuration used for registration of surface waves is shown in the Figure III.1. The use of at least two receivers allows implementation of the relative measurement for two points of observation, because of that only the propagation over a distance x is taken into account. Using the fact of stationarity of the wave propagation in concrete, only one receiver moving along the measuring profile to consecutive positions can be used.

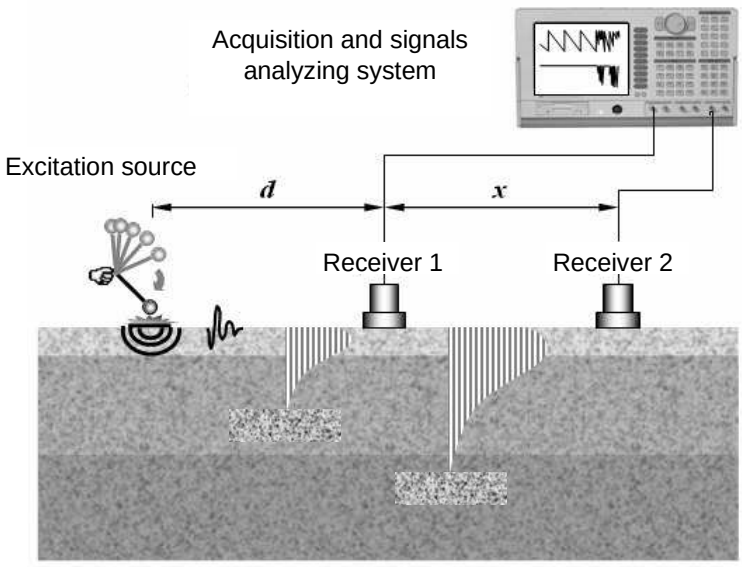

Figure III.1 Method of generation and measurement of surface waves [Wardany 2005].

A manual measurement of the surface wave propagation using ultrasonic contact transducers is problematic. The accuracy of transducers positioning has the key influence on the precise of measurements, while the quality of received signals is determined by the quality of transducers coupling with the tested surface. It was noticed, that the manual measurement is less repeatable, and the realization of a single profile is very time-consuming. In the study of porous materials, such as concrete, using the contact methods also presented a problem with stationarity of wave propagation phenomena. This results from the fact, that the tested material absorbs gel used for transducers coupling, and thus locally changes its properties. Taken it into account the remarks above it was necessary to improve measurement techniques. Modifications carried out were aimed at:

- increasing the precision of transducers positioning,

- increasing the repeatability of measurements,
- making implementation of measurements in field conditions easy,
- minimizing the influence of coupling substance on tested material or its total elimination,
- shortening the time of carrying out the measurements.

The first test of measurements of surface wave propagation on concrete samples were performed manually.

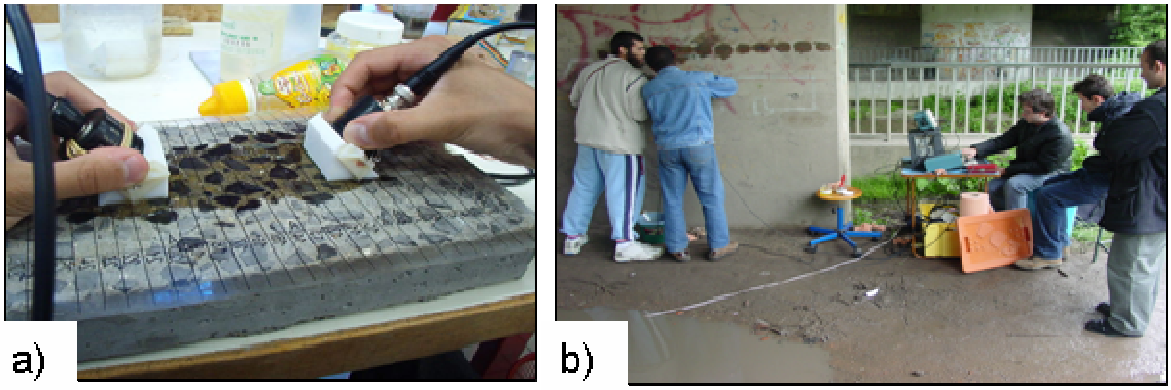

Figure III.2 Manual measurements of surface wave propagation; a) in the laboratory, b) in the field .

An example of measurements under laboratory conditions is shown in Figure III.2. The special Teflon adapters for ultrasonic transducers are used. Thanks to that the wave propagating in Teflon reaches the material with angle of incident slightly greater then the second critical angle. A similar situation occurs in the angle transducers (angular or wedge transducer) used in a non-destructive testing of metals. The use of Teflon was predicated by the fact that as one of the few solid materials is characterized by lower than in the concrete velocity of transverse wave propagation [Piwakowski 2004]. In such case, the angle of incidence wave can be determined from the relation

$$\sin\theta_c = \frac{c_{SW}}{c_{S2}} \qquad \text{(III.1)}$$

where c_{sw} is the transversal wave velocity in Teflon, and c_{S2} is the transversal wave velocity in concrete.

To get good coupling of transducers with tested material via Teflon adapters a coupled substance must be used. Usually as a coupled substance water-based gel or just water is used. Realization of measurement profile requires displacing one of the transducers in the successive points of observation (acquisition). Each new position requires a precise alignment of transducers relative to each other, to provide location of the receiving transducer in the

direction of wave propagation. The application of the new portion of the coupling gel is also necessary in each position. A larger number of measurement points (the next shifts) provides more accurate results obtained from signal processing. Much more difficult situation occurs in the implementation of research in the field (Fig. III. 2b), especially in vertical surfaces or ceilings. Using contact transducers on irregular concrete surfaces caused additional problems. Moreover, a long time of single profile acquisition makes that coupling gel dries up and thereby changes the wave propagation conditions.

The remarks above led us upgrade the measurement system, and one of results is the replacement of the contact receiver by a non-contact transducer. This is possible while using leaky waves phenomena caused by propagation of the surface wave (Fig. II.1) [Zhu at al 2001]. The membrane capacitive transducer of MicroAcoustic with very wide bandwidth (20-900 kHz) was used as the receiver. In this case coupling substance is the air, so the transducer can be set several millimetres above tested surface. Such configuration requires the use of gel only for the emitter, what facilitates automation of the receiver movements.

Configuration of the measurement system using a non-contact receiving transducer is shown on The Figure III.3. The movement of the receiver along the measurement profile (arrow) was carried out manually using a special trolley. The emitter was equipped with a Teflon adapter which allowed setting an angle of incidence of ultrasonic wave according to equation III.1. Non-contact receiving transducer has also an adjustment of receiving angle θ_R, which in case of coupling through the air is determined by the formula

$$\sin\theta_R \approx \frac{c_{P\_AIR}}{c_{S2}} \qquad \text{(III.2)}$$

The large difference between velocity of ultrasonic wave in the air c_{P_AIR} and transverse wave in concrete c_{S2}, makes that reception angle θ_R is small (about *8°-10°*), what is also seen on the Figure III.3. The disadvantage of discussed solution with one non-contact transducer is a need of using coupling gel for emitter, and also low precision and a lot of time-consumed for manual positioning of the receiving transducer. It is worth to noticing, that there occurs a large drop in the signal amplitude of leaky waves due to a significant difference of acoustic impedance between the concrete and the air (only *2 %* of emitted energy is received). Successfully carried out tests with the manual system, led to building a device that allows an automatic displacement of receiving transducer along the measuring profile, what let to shortening the duration of measurements significantly and increasing their accuracy. In the next modification, the emitting contact transducer was replaced by non-contact one, which

completely eliminates the need to use a coupling gel. Taking into account the fact, that in such solution, less than *0,1 %* of the send energy reaches to receiver the pulse excitation was replaced by excitation of frequently modulated signals such as chirp (see chapter III.1.2).

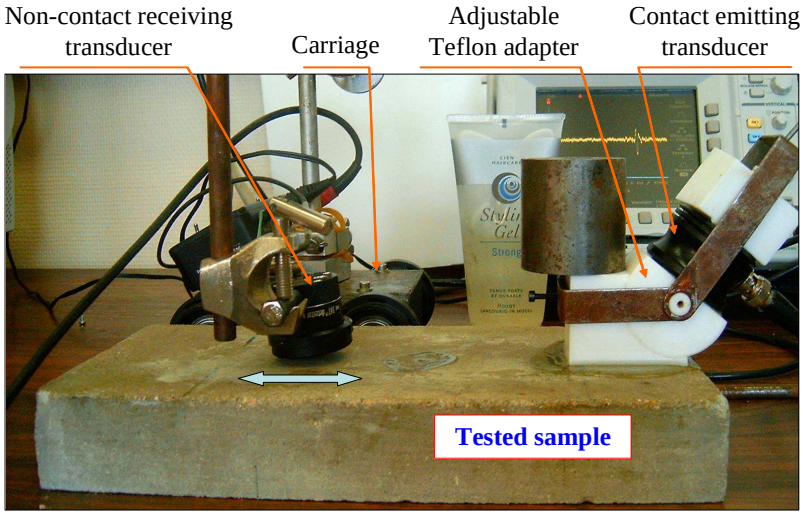

Figure III.3 Measurement configuration with use of non-contact receiving transducer.

III.1.1 Surface waves measurement device SWMD

The previous experiences and new modifications let us construct the final version of SWMD. In the Figure III.4 the block diagram is presented. The totally non contact measurements and the measurements with contact transducers can be effectuated by SWMD system. In the Figure III.5 the SWMD ready to work system is presented. The system operation is controlled by a PC, which through the stepper motor driver positions the receiving transducer. The emitter is positioned manually for the entire series of measurements. The chirp type signals emitted by the arbitrary function generator are amplified to the amplitude level needed for chosen emitting transducer. The received signal is acquired via an oscilloscopic card. The measured data for each point are stocked in the PC's hard disk. In the Figure III.6 the device for US transducer positioning of SWMD system in configuration of SW propagation measurement is presented.

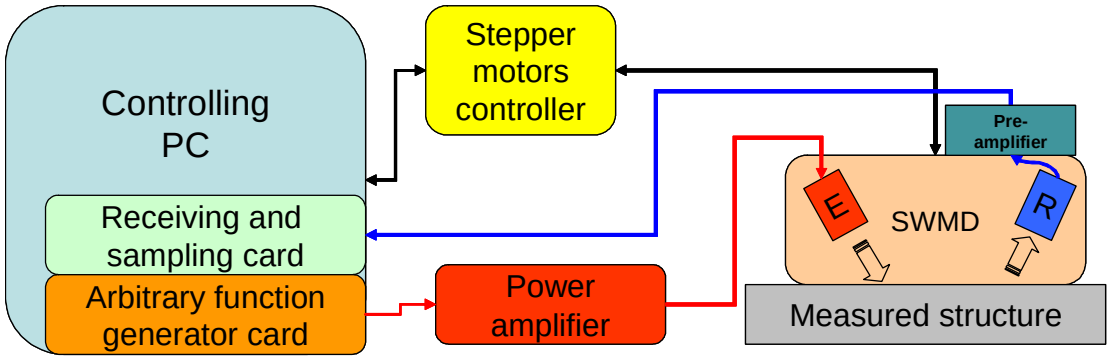

Figure III.4 The block diagram of SWMD system for surface waves measurement, SWMD – measuring device, E – emitter, R – receiver.

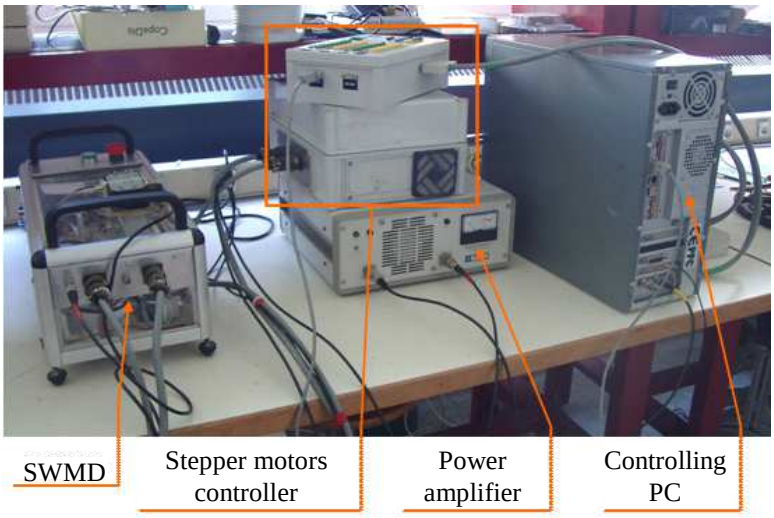

Figure III.5 The measuring system ready to work.

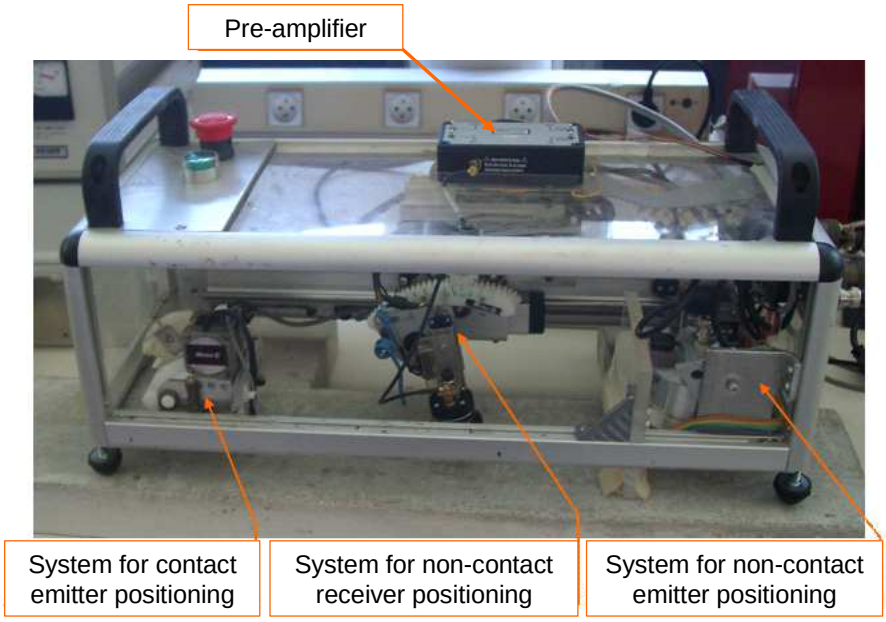

Figure III.6 SWMD during measurement of concrete sample.

The measuring system allows the user to select the mode of using contact or non-contact transducer. In each system of transducer positioning the angle between transducer axis and normal to surface can be adjusted (manually for the emitter and automatically or manually for the receiver). This angle is equal to the third critical angle and depends on the SW velocity in a studded material. The system of receiver positioning displaces the transducer horizontally into the following acquisition points in the way that the measuring profile was programmed.

In the LabVIEW environment the controlling software was created and the main tasks of it are:

- the arbitrary function generator cart configuration,
- the oscilloscope cart configuration,
- the measurement geometry composition (the set of numbers of measuring profiles and the number and the distribution of acquisition points in profile),
- controlling of the mechanical part of the system, e. i. the positioning of receiving transducer,
- measuring geometry realization,
- the registration of acquired signals.

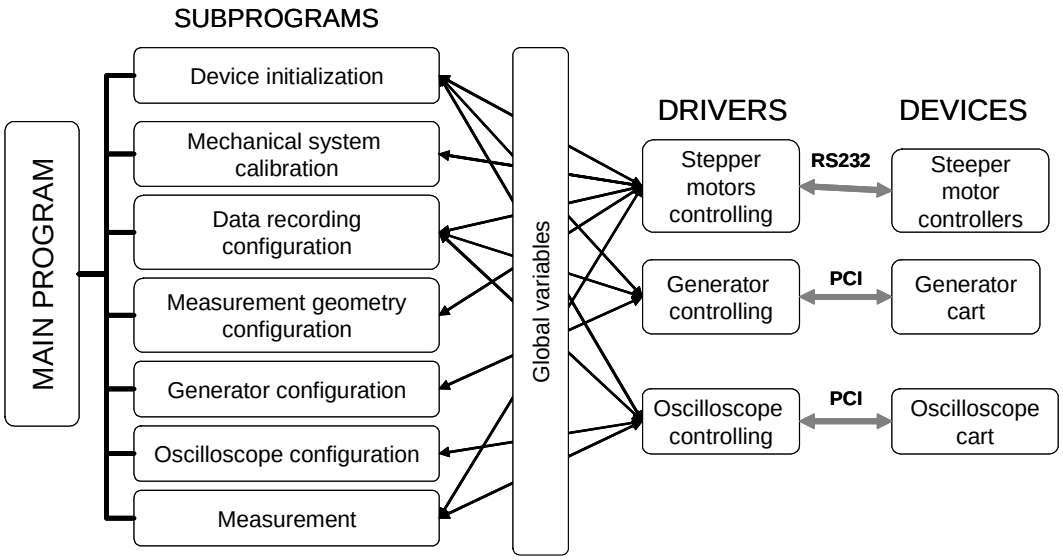

Figure III.7 The block diagram of controlling software..

In the Figure III.7 the block diagram of controlling software is presented. The main program consists of the group of subprograms responsible for preparing to work the various components of SWMD system (form component initialization to oscilloscope configuration).

For the communication between the subprograms and the device drivers the global variables are used. The task of the drivers is the communication between the devices and subprograms via the PCI bus and the RS232 port.

In the group of subprograms the “Generator configuration” one can be distinguished, in which the parameters of excitation chirp[3] signal are set. The parameters are optimally set in a function of the used transducer and the measured material. After the configuration process the subprogram “Measurement” is run, which is responsible for the measurement realization and signal data recording. In the Chapter III.1.2 the details of signal processing used in SWMD system are described. In the Figure III.8 the user interface during measurement sequence realization is presented (“Measurement” subprogram). The “Oscilloscope control and received signal” area refers to the oscilloscope card operating and the visualization of the signal before correlation (non correlated signal). In the “Scan B” area the image composed by till now recorded signals after correlation is presented. The “Measurement control” area lets us steer the measurement and shows the measurement progress.

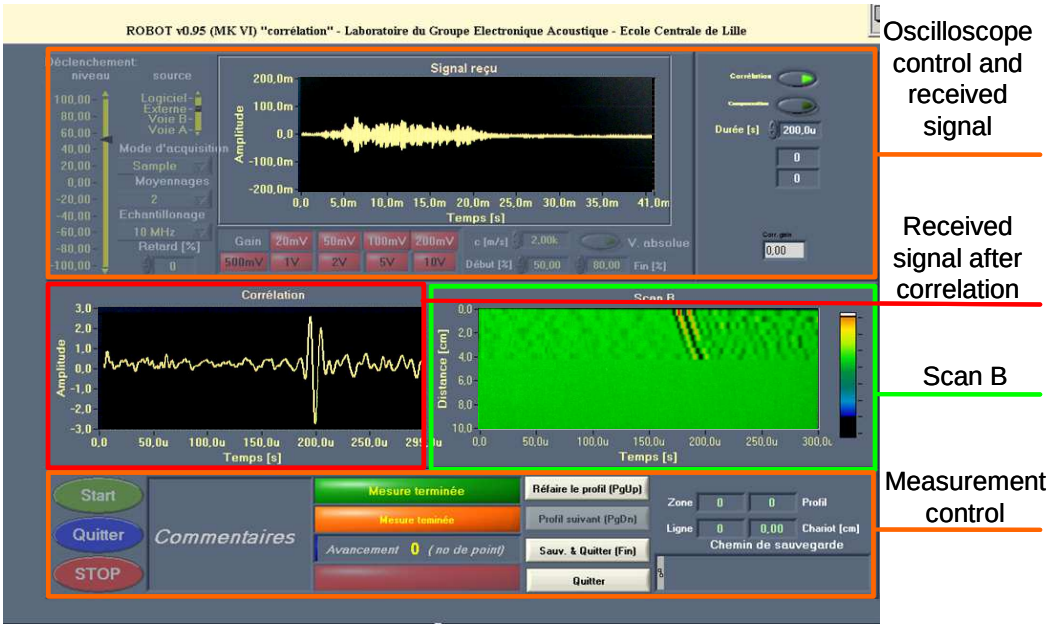

Figure III.8 The user interface during measurement.

In the block diagram III.9 the sequence of measuring process is presented. Before the measurements the software requires a system configuration in which the user sets a few elements like: the data storage configuration, geometry of measurements. The geometry of measurements contains of the information about the number of measurement points *N* in each

[3] only when non contact emitter is used.

profile, the number of profiles *P* and the distance of the first point of acquisition from the transmitter (offset). The oscilloscope card configuration concerns the set of sensitivity, time base and averaging. The generator card configuration mostly depends from the used transducer. At this stage excitation signal frequency and amplitude are determined

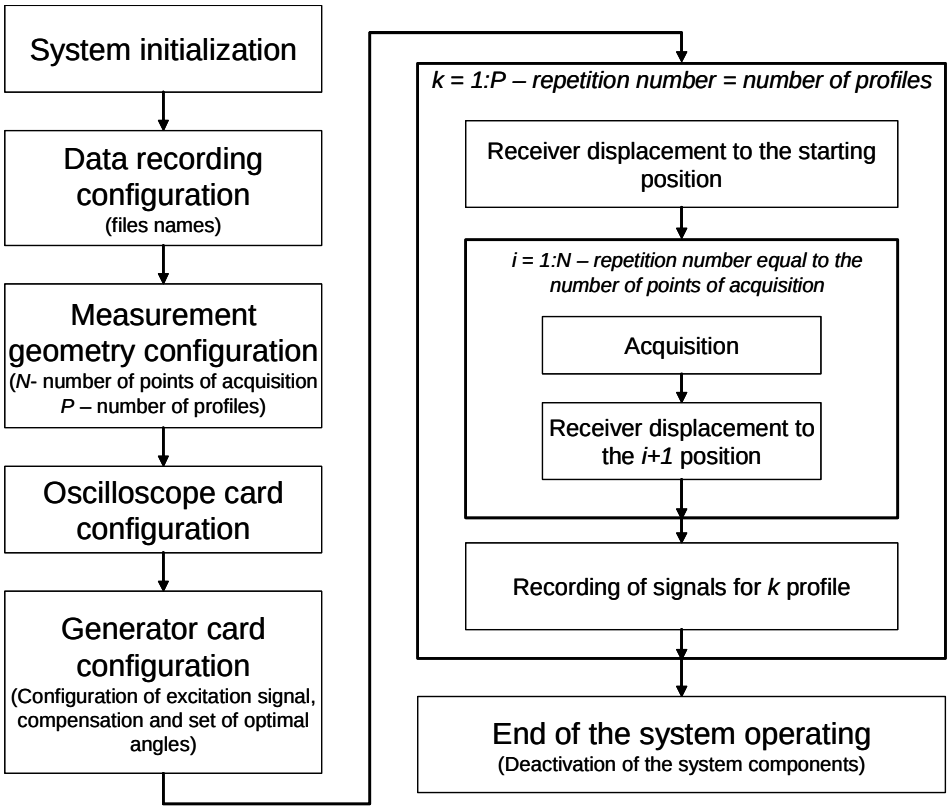

Figure III.9 The stages of measurement procedure of SWMD (details in text).

After configuring all the necessary elements of the system the measurement for a fixed number of profiles starts and each profile consists of *N* points of acquisition. The received signals are averaged M times and then correlated with the "pilot" signal (emitted signal). The correlated signals are recorded in binary file. The signal before correlation can be also recorded. For each profile a new file is created. That allows stopping the measurement in any moment without a loss of the data collected so far. Information related with the measurement necessary for the further signal processing is saved to a text file. In the Table III-1 the main parameters which characterized the positioning system of the SWMD and more important signal parameters are presented.

Table III-1 The operating parameters of SWMD system.

Parameter	Value
Mode	*Non contact* *(with possibility of contact emission)*
Location of measured surface	*Unrestricted* *horizontal (floor) / vertical (wall) / horizontal opposite (ceiling)*
Number of points of acquisition N	*any, smaller then N = ((24cm - X_{OFF})/Δx)+1*
Distance between point of acquisition Δx	*any (minimal: 0,3mm)*
Starting distance (Offset X_{OFF})	*minimal: 7cm, maximal 24cm*
Receiving band	*20 ÷ 900kHz*
Emitting band	*30 ÷ 500kHz* *(in function of emitting transducer)*
One profile acquisition time	*~20s* *(for N = 20 without averaging)*
Weight of the device	*~6kg*

III.1.2 Measured values and signal processing

Each profile consists of N points of measurement, which gives N $s_i(t)$ signals for N receiving positions (see Fig. III.10). The distance Δx between measuring points should meet the requirement of spatial resolution results from the theorem of spatial sampling according to the equation III.3 [Shannon 1949], where λ_{min} corresponds to the wavelength of the highest frequency.

$$\Delta x \leq \frac{\lambda_{\min}}{2} \qquad \text{(III.3)}$$

The device's design and transducers size cause that the shortest possible propagation distance is *7 cm*, and therefore the length propagation path for the *N-th* acquisition point is $X = 7\ cm + (N-1) * \Delta x$. The increase of length of the propagation path causes the increase of the delay of the received signal (Fig. III.10b).

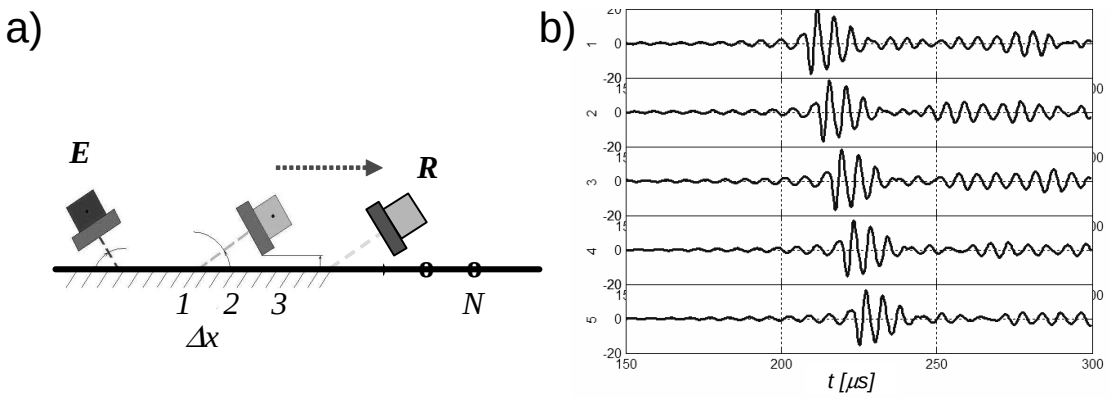

Figure III.10 The measure of a single profile; a) geometry (E –emitter, R – receiver), b) signals recorded for a few points of acquisition.

The one of the stages of signal processing is calculating the amplitude spectra of $S_i(\omega)$ for each of the signals $s_i(t)$, and the dispersion characteristics. The signal received in the position of X_i can be expressed as:

$$s(t, X_i) = \left[s(t - X_i / V_A)\right] e^{-\alpha X_i} \quad i = 1,2...N \tag{III.4}$$

where: Xi is the position of the acquisition point against to source,

α is the attenuation coefficient,

V_A is the observed velocity of the SW propagation (apparent velocity – close to the group velocity),

Performing the Fourier transformation operation on both sides of III.4, we get:

$$S(j, \omega, X_i) = \Im[s(t, X_i)] = \left|S(\omega, X_i)\right| \exp(-j\varphi(\omega X_i) \tag{III.5}$$

In the above equation the expression $|S(\omega)|$ represents the spectrum of the signal including attenuation, and $\varphi(\omega)$ is its phase spectrum.

For the dispersion characteristic determination the transform of p-τ (known in geophysics as the Slant Stack Transform (SL) is used [McMechan and others 1981, Yilmaz 1987]. The SL is based on the transformation of the signal s in a function of the linear delay $\tau = pX$,

$$\bar{s}(\tau, p) = \int_{-\infty}^{+\infty} s(t = \tau - pX, X)dX \tag{III.6}$$

where $p = 1/V$ is the inverse velocity (slowness). In reality, a discrete equivalent of the transformation III.6 is implemented and then the Fourier transform on the Equation III.6 is calculated

$$\bar{S}\left(\omega, \frac{1}{V}\right) = \bar{S}(\omega, p) = \Im\left[\bar{s}(\tau, p)\right] \tag{III.7}$$

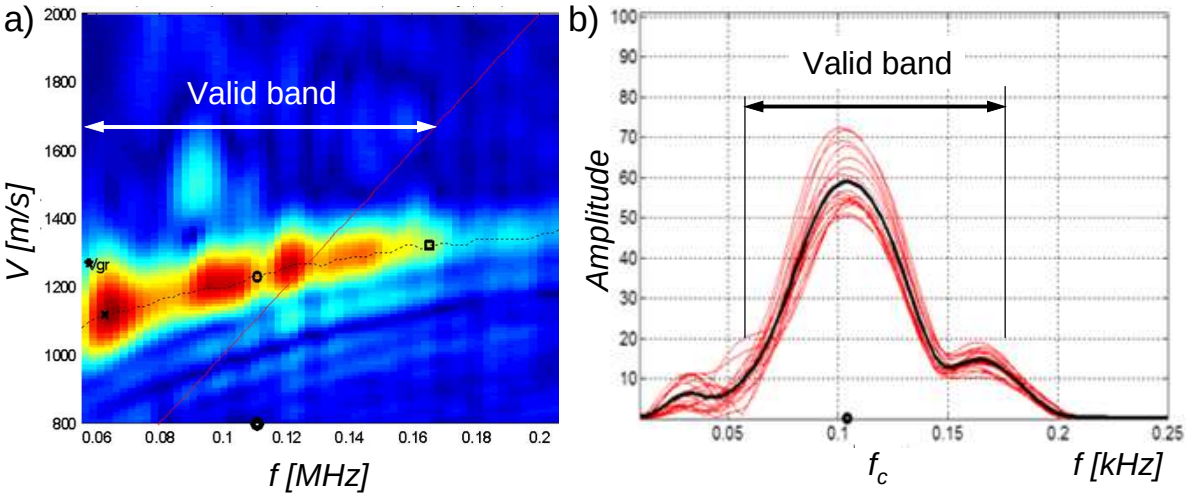

Figure III.11 The example of the dispersion map obtained from the SL and the Fourier transforms (a) and the example of spectral characteristics of received signals (b).

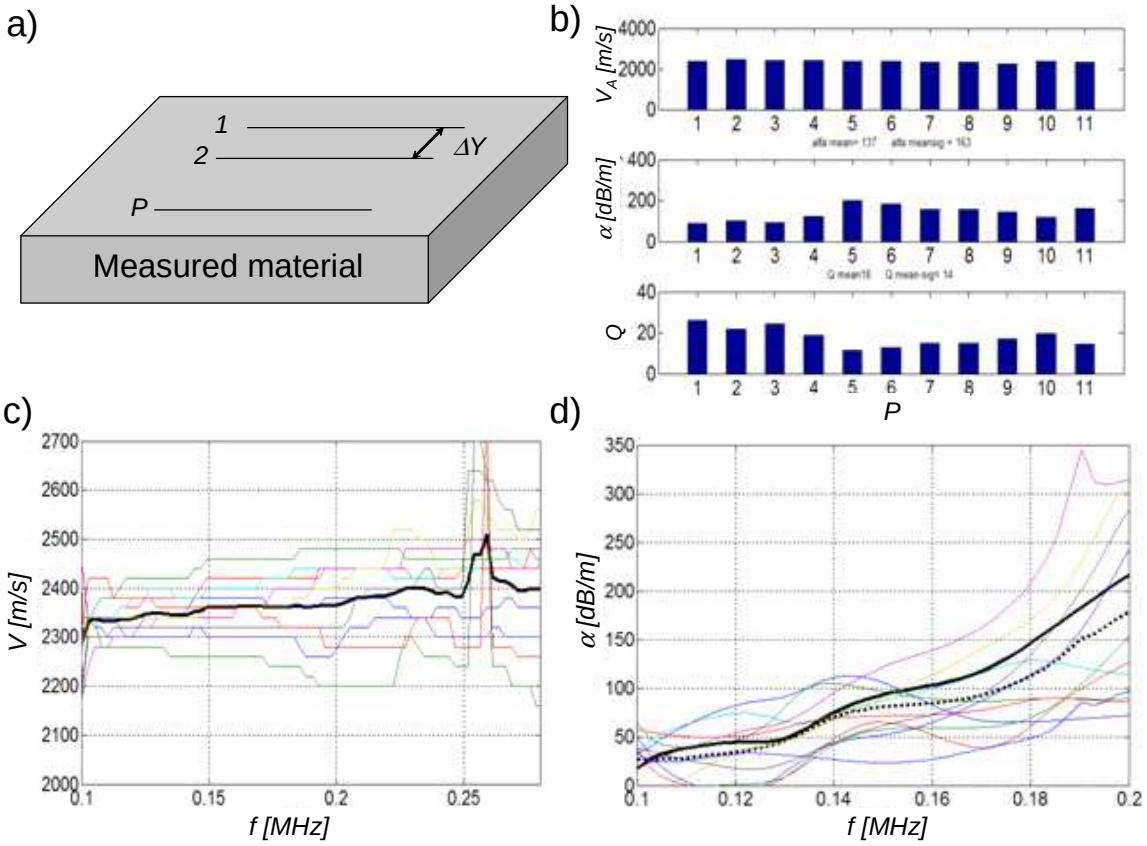

Figure III.12 The example of the measured profiles arranged on the measured surface (a), the results of measurements realized for 10 profiles (from top: velocity, attenuation, quality factor, 11th value in each row is a mean value) (b), the dispersion curves (bold line is a mean value) (c), the attenuation curves (bold line is a mean value) (d).

The results in the form of a module of the both (SL and Fourier) transforms of the signals $s(t,X_i)$ can be presented at the velocity/frequency plain (V,f). The local maximal values for each frequency determine phase velocities and form different wave modes. In the Figure III.11 the example of the use of both transforms to create the map of dispersion is presented. The line connecting the neighboring maxima determines the dispersion characteristics (in the case from the Figure III.11a only the basic mod is shown). In the Figure III.11b the spectrums for 20 received signals are presented. As a valid band the part of the spectrum with good signal noise ratio (SNR) is taken (in this case form *60 kHz* to *170 kHz*). Noticeable peaks shift of the spectra (Fig. III.11b) towards lower frequencies is due to the influence of attenuation [Kuc, 1983]. For the calculation of attenuation expressed in [*dB/m*] in the frequency domain the signals S_i and S_j (signals for X_i and X_j receiver positions) and the Equation III.8 are used. In order to improve the accuracy of the attenuation designation the calculations for all combinations of the positions of acquisition points *i* and *j* are carried out. Finally, the average value of the results is calculated [Goueygou et al 2002, Owino et al 1999].

$$a(f) = \frac{1}{X_j - X_i}\left[20\log\left(\frac{|S_i(f)|}{|S_j(f)|}\right) - 10\log\left(\frac{X_j}{X_i}\right)\right] \qquad \text{(III.8)}$$

In order to illustrate the signal processing procedure in the Figure III.12 the results of a sample measurement session are presented. In the Figure III.12a the arrangement of measurement profiles on the test material is shown (ΔY is a distance between profiles) [Piwakowski et al 2009]. Typically, the measurement of 10 profiles is preceded, and collected data is averaged. In the Figure III.12b the quantitative results for 10 registered profiles are presented (from the top: the SW observed velocity, the attenuation and the quality factor). In 11^{th} column the average value of all profiles is given. The Figure III.12c shows the dispersion curves obtained for all profiles with the average mean curve. The increase of velocity with the increase of frequency shows that for this material the average SW velocity decreases with depth (for measured areas). In the Figure III.12d the attenuation curves for each measured profile are shown. The mean value is presented by the bold continuous line and the value of attenuation for mean profile (11^{th} colon) is shown by bold pointed line. The attenuation evolution for lower and middle frequencies (in this case about *170 kHz*) can be considered as a quasi linear and could be approximated by the relation

$$\alpha(f) = \alpha_1 f \qquad \text{(III.9)}$$

In the function of attenuation (degree of degradation) and the heterogeneity size to the wavelength ratio in concrete the distance between profiles ΔY and number of profiles *P* are

determined. The research on the optimal values of these parameters is currently being pursued [Shiyan J. 2009].

The use of frequency-modulated signals

The SWMD system transition from contact to non-contact operation cause the loss of more than 99% of the emitted signal energy because of the high difference in the acoustic impedance of concrete and the air. For the wave incident at a small angle (*8° - 10°*) the energetic transmission coefficient *T* can be approximated by the relation for the *0°*.

$$T = 1 - \left(\frac{Z_2 - Z_1}{Z_2 + Z_1} \right)^2 \qquad \text{(III.10)}$$

where Z_1 and Z_2 are the acoustic impedances of the air and concrete. Substituting into equation III.10 numerical values for the air and concrete it can be seen that the receiving transducer reaches approximately *0,022 %* of the emitted energy. Moreover, the amount of the signal energy send by the transducer is limited due to the maximum amplitude of excitation, which could damage the transmitter if it is exceeded. This causes that the use of pulse excitation becomes inefficient due to the low energy of generated signal. The solution is to use a frequency-modulated signal (chirp-type signal or sweep [Klauder et al 1960]), and then the use of cross-correlation operation (for simplification hereinafter called correlation) (Fig. III.13b). This type of excitation in combination with the correlation can increase the energy of the emitted signal significantly (in this case from *100* to *200* times) without exceeding the allowed amplitude (Fig. III.13). This is the approach used in medicine [Nowicki 2010, Litniewski et al 2007], radar technologies, sonar technologies, in the deep geophysics and it is increasingly used in high-resolution seismic [Kosecki and others 2010, Rihaczek 1969, Goupillaud 1976].

The frequency modulated signal (chirp) can be expressed in the form [Brouwer et al 1998]

$$s(t) = A(t)\cos(\phi(t)) \qquad \text{(III.11)}$$

$$\phi(t) = 2\pi \int_0^t f(\tau) d\tau + \phi_0 \qquad \text{(III.12)}$$

where *A(t)* represents the changes of amplitude and *ϕ(t)* corresponds to the instantaneous phase shift of the signal resulting from the variable frequency *f(t)*.

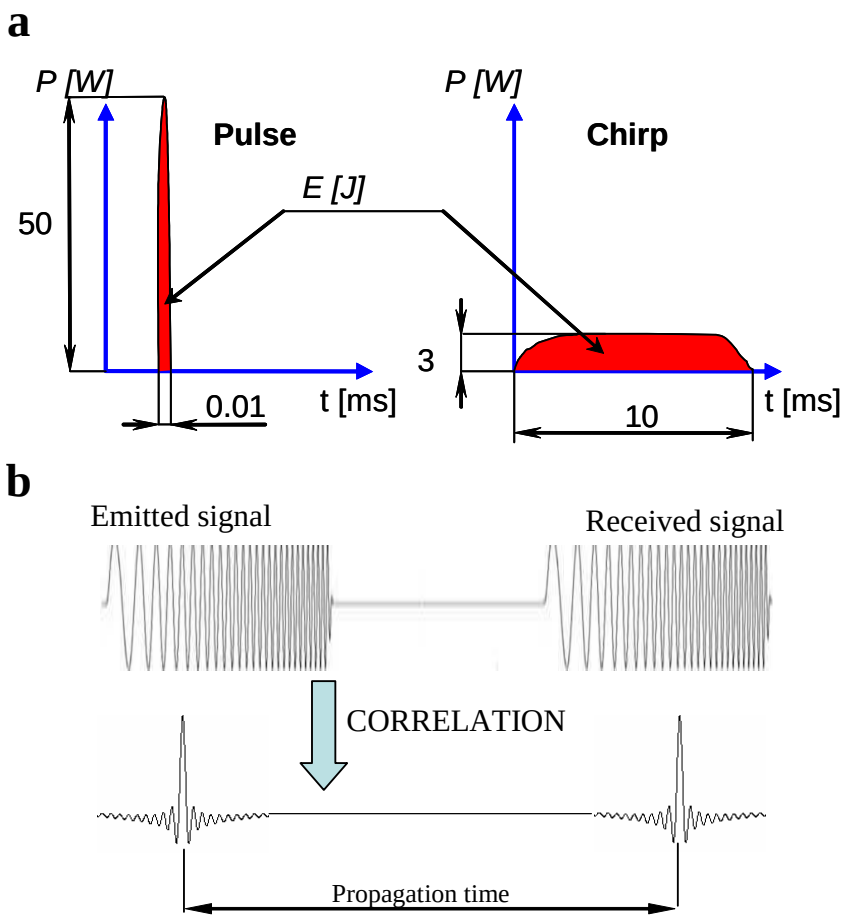

Figure III.13 The illustration of the frequency modulated signal type chirp and its signal processing: a) comparison of a pulse and chirp signals of the same energy, .the correlation process for the frequency modulated signals.

If we assume a constant amplitude in time $A(t) = 1$ and a linear change of frequency in time $f = at$, we get a linear chirp, in which the frequency changing in time can be expressed by the characteristic signal parameters

$$f(t) = f_{\min} + \frac{(f_{\max} - f_{\min})t}{T} \tag{III.13}$$

or

$$f(t) = f_0 - \frac{B}{2} + B\frac{t}{T} \tag{III.14}$$

where f_{min} and f_{max} mean lower and upper chirp frequencies, T its duration, f_0 corresponds to the center frequency and B is the frequency band. If the relationship $T \cdot B >> 1$ is satisfied, the spectrum of linear chirp $s(t)$ can be approximated by the relation

$$|S(f)| = a\frac{T}{B}\prod(f) \tag{III.15}$$

$$\prod(f) = u\left(f - \left(f_0 - \frac{B}{2}\right)\right) \cdot u\left(\left(f_0 + \frac{B}{2}\right) - f\right) \tag{III.16}$$

where $\prod(f)$ is a square function, and *u(f)* is a Heaviside step function. In the Figures III.14a and III.14b an example of the chirp signal in time domain and in frequency domain is shown respectively.

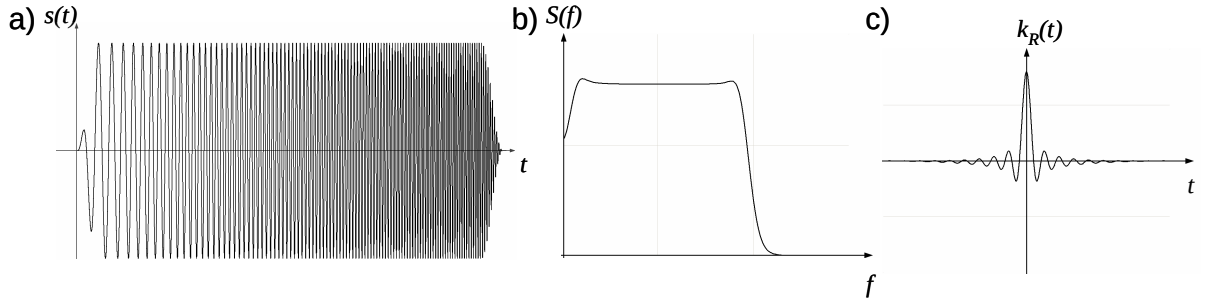

Figure III.14 The example of frequency modulated signal (chirp), a) in time domain, b) spectrum, c) autocorrelation ($k_R(t)$ (Klauder wavelet)) [Kosecki 2010].

The signal *s(t)* is the excitation signal also called "the pilot signal". The difference between the excitation signal and the signal propagating into the material $s_R(t)$ appears due to the specific spectral characteristic of the emitter and the characteristics of the transducer-material coupling. For simplicity, the transmittance associated with these two factors is indicated as *c(t)*. Description of the wave propagating into material $s_R(t)$ is obtained by convolution

$$s_R(t) = s(t) * c(t) \tag{III.17}$$

Performing an autocorrelation of the signal $s_R(t)$ results a function $k_R(t)$ (Klauder wavelet) (Fig. III.14c), also called the signature of the source

$$k_R(t) = s_R(t) \otimes s_R(t) = \int_{-T}^{T} s_R(\tau) \cdot s_R(t+\tau) d\tau = s_R(t) * s_R(-t) \tag{III.18}$$

The analytic solution for considered signal has a form [Misaridis et al 2005]

$$k_R(t) = T \cdot \cos(2\pi \cdot f_0 \cdot t) \cdot \frac{\sin\left(\left(1 - \frac{|t|}{T}\right) \cdot \pi \cdot B \cdot t\right)}{\pi \cdot B \cdot t} \tag{III.19}$$

The purpose of the correlation frequency-modulated signals is their "compression" in time. This operation allows us to present a long modulated signal $s_R(t)$ in the form of a short pulse $k_R(t)$ similar to the Dirac pulse $\delta(t)$. The result $k_R(t)$ of the *s(t)* signal correlation approach to the form of Dirac pulse $\delta(t)$ if the spectrum of *s(t)* signal becamess wider.

Taking into account the transmittance of the medium of propagation *e(t)* and the noise *n(t)* the received signal before correlation of *x(t)* can be written as

$$x(t) = s_R(t) * e(t) + n(t) \tag{III.20}$$

The correlation of the signal *x(t)* with the emitted modulated signal $s_R(t)$ results with the correlated received signal $x_C(t)$.

$$x_C(t) = x(t) \otimes s_R(t) \tag{III.21}$$

The form of the signal after correlation $x_C(t)$ resembles the shape of the received signal with the pulse excitation. Substituting III.20 into equation III.21 we get

$$x_C(t) = (e(t) * s_R(t) + n(t)) * s_R(-t) = s_R(t) * s_R(-t) * e(t) + n(t) * s_R(t) \tag{III.22}$$

and taking into account III.18

$$x_C(t) = e(t) * k_R(t) + n_c(t) \tag{III.23}$$

where $n_C(t)$ is a correlated noise.

As mentioned earlier, the most important advantage of using chirp signals is higher signal energy compared with the pulse signals. The equivalent of a pulse excitation is a signal *k(t)*, which energy is E_K

$$E_K = \int_{-T}^{T} |k(t)|^2 \, dt \tag{III.24}$$

where *T* is the length of the signal *s(t)* and *k(t)* is the autocorrelation signal *s(t)*. It follows that **increasing the chirp length without changing its amplitude the energy E_K of the signal *k(t)* will be increased** and consequently the energy of the signal $x_C(t)$ will also increase. The increase of energy E_K caused by the increase of time *T* grows faster than the increase of a noise energy at the same time, which is associated with improving the signal to noise ratio (*SNR*)

$$SNR = \frac{\int_{-\infty}^{+\infty} K_R^2(f) df}{\int_{-\infty}^{+\infty} N_{RC}^2(f) df} = \frac{E_K}{E_{NC}} \approx T \cdot B \tag{III.25}$$

where $K_R(f)$ is the spectrum of signal $k_R(t)$, E_{NC} is the energy of the correlated noise $n_C(t)$. Assuming that the $n_C(t)$ is a whit noise then the $N_{RC}(f)$ is the noise spectrum which is filtered by the spectrum of $S_R(f)$. This fact can be considered as the same kind of a matched filter.

$$N_{RC}(f) = N(f) \cdot S_R^*(f) \tag{III.26}$$

The equation III.25 shows that the *SNR* can be improved also by increasing the band *B* of the signal *s(t)*, but in reality *B* value is limited by the band of used transducers.

To improve the *SNR* in the measurement process three additional operations of averaging are used. The received signal is averaged *M* times in each point of acquisition, what improves *SNR* proportionally to $M^{0.5}$. Besides, in the SL algorithm the N received signals are averaging, what gives the improvement of *SNR* proportionally to $(NM)^{0.5}$. Moreover, during the measurement of *P* profiles the spatial averaging is performed, what finally gives the SNR improvement proportionally to $(MNP)^{0.5}$.

In the case of replacement the pulse signal excitation by the frequency modulated signal excitation the signal parameters must be adapted in the function of the installed transducer. The frequency band B of the *s(t)* signal is a most important parameter. In the simplest case, the band of *s(t)* signal should be exactly the same as the effective transmitter band, and thus the lower and upper frequencies of the *B* band should correspond to the same frequencies of the transmitter band.

The extension of *B* beyond that boundaries reduces the effectiveness of excitation because a part of the signal *s(t)* spectrum exceeds the transducer band and has much lower participation in the power of the emitted signal. In this case, the nature of the transmitter fulfills the role of the bandpass filter. Using a narrower band than the band of the transmitter also reduces the effectiveness of the source, but may be justified in situations where such high frequencies are strongly attenuated and have a negligible effect on the signal received, or if it is necessary to slightly shift the band in order to avoid the impact of some type of interference such as electromagnetic noise. The final precise selection of frequencies f_{min} and f_{max} depends largely on the ambient conditions and the tested material. Usually, the f_{min} and f_{max} frequencies are determined on the basis of observations of the correlation of the received signal $x_C(t)$ and its spectrum $X_C(f)$.

An important parameter of the *s(t)* signal is its amplitude, which should be as large as possible in order to improve *SNR*. A limitation of the amplitude of excitation is the acceptable voltage of transmitter excitation in continuous portioning, which is much lower than in the case of pulse excitation. The use of longtime excitation signal can lead to damaging the transducer by overheating, and therefore it is necessary to use both the limitations of mean power of signal as well as the use of pauses between successive emissions. For the safety reasons, it was assumed that the interval between emissions can not be shorter than the time of excitation. Maximum excitation voltage and the mean signal power are determined experimentally for each transmitter. A detailed analysis of the influence of different chirp

parameters on the correlation results can be found among others in the Kosecki's work [Kosecki 2010]. In the Table III-2 the more important parameters of excitation signal configuration are presented.

Table III-2 The parameters of configuration chirp signal.

Parameter	Value
Frequency f_{min} i f_{max}	*30 ÷ 500 [kHz]* *(in the fuction of used transducer)*
Signal length T	*5 ÷100 [ms]*
Pause between emissions	*1 ÷ 2·T [ms]*
RMS Power	*2 ÷ 10 [W]*
Excitation signal level *(at the output of amplifier)*	*100 [V]*
Excitation signal energy *(at the output of amplifier)*	*10 ÷ 1000 [mJ]*

The disadvantage of frequency-modulated signals is much longer acquisition time when the correlation is carried out continuously or the file size of the measured data is large when the correlation is performed in a separate procedure of the signal processing. In addition, the recording equipment (oscilloscope or oscilloscopic card) must have a sufficiently large memory able to record long signals. Using this type of excitatory signals also requires an appropriate solution in the system of emission. It is necessary to use a special programmable arbitrary function generator.

III.1.3 Test with the reference material

In order to verify the correct operation of the measuring system SWMD and software used for data processing a number of tests were proceeded. The results of one of them are discussed below. For this test the 100 mm thick homogeneous aluminum block was used. In the Table associated with the Figure III.15 more detail about the tested material is given, and a comparison of measured and calculated dispersion is shown. Theoretical characterization was generated using Haskell's model (assuming homogeneity of the material) for parameters as in the table (Figure III.14). The analyzed material is homogeneous (no layers), thus ignoring the dispersion caused by attenuation and the dispersion characteristics is the

horizontal straight line. In the measurement the transducer of center frequency f_C =*75 kHz* and a band from *60* to *200 kHz* was used.

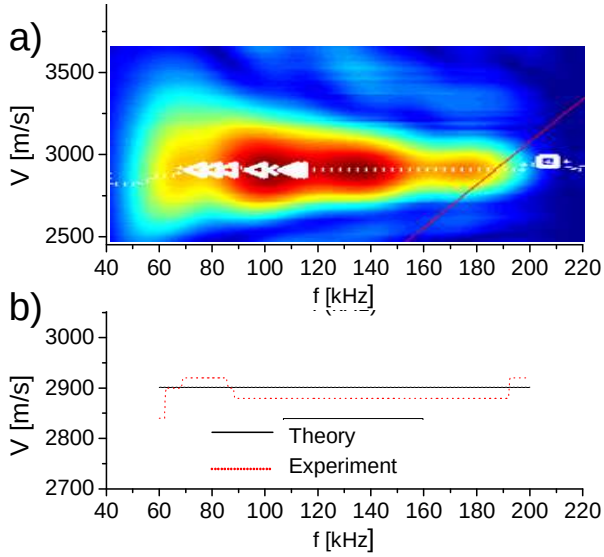

Characteristic of material	
Material	Aluminum
ρ [kg/m^3]	2800
V_P [m/s]	6420
V_S [m/s]	3104
V_R [m/s]	2910
d [mm]	100

Figure III.15 The comparison of the SW propagation velocity obtained from measurement via SWMD and from the model of homogeneous aluminium. a) SL characteristic, b) dispersion characteristic (theoretical and measured), table – the parameters of measured sample.

In the Figure III.14b the small differences between the dispersion characteristics in the central part of the band appear due to the SL procedures precision, while the differences at the ends of the band are also caused by deterioration of the SNR. The measured phase velocity was approximately *2890 m/s*, what gives the difference of only *1 %* from the theoretical value. The obtained result confirms the correctness of both the measuring system and the used data processing software.

III.2 Reflectometric measurement system

The Reflectometric Measurement Device (RMD) is the second measuring system developed in this work. The RMD is used in the measurement of reflection coefficient of the ultrasonic waves in the function of incident angle $R(\theta)$. The obtained characteristic $R(\theta)$ is used in the process of identification of structural parameters of the measured material. In the Figure III.16 the scheme of transducer positioning which must be ensured is presented. The signal *w(t)* is emitted by the transducer in the direction of the measured material. This signal is reflected from the surface of the measured material and then is received by the receiving

transducer as $s(t,\theta)$. Considering the harmonic waves the reflection coefficient R is determined as a ratio of the amplitudes of received end emitted signals. The reflection coefficient *R* in function of incident angle is obtained by the repetition of the measurement for all angles.

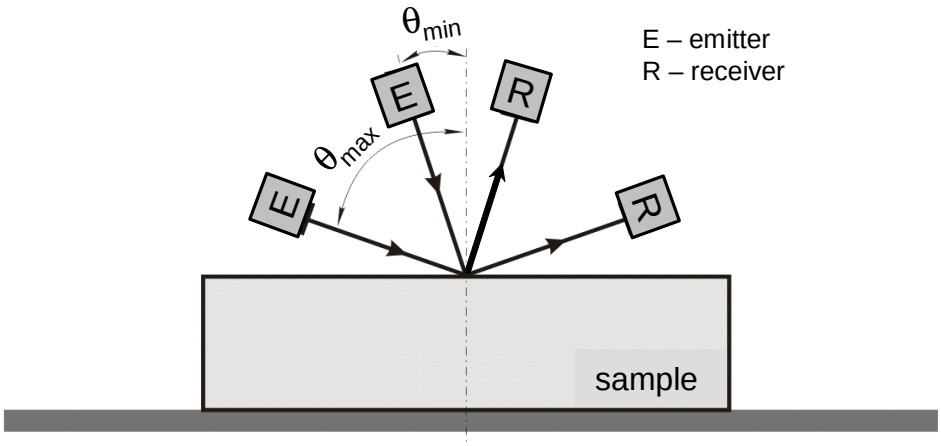

Figure III.16 The configuration of transducers and the sample in the reflectometric measurement.

The measurement procedure requires that the measuring transducers (the transmitter and the receiver) move at the curves of constant radii in the range of angles from θ_{min} to θ_{max}. It is important that the axes of rotation of the two transmitters overlap each other and lie on the surface of the test material. The angles of incidence and reflection relative to the normal to the surface must be equal.

III.2.1 Reflectometric Measuring Device (RMD)

The reflection coefficient *R* measurement requires acquisition of ultrasonic signals for at least several angular positions with high accuracy of both the angle and the distance from the center of rotation. Manual adjustments of the transducers while maintaining high position accuracy is very time consuming. The requirement of the measurements repetitions for their averaging multiplies the measurement duration up to several hours per sample. In this situation the implementation of an automatic measurement system was necessary.

Earlier laboratory researches of the reflection coefficient determination were carried out only under the water. The device used for these tests has such advantages as ease of

positioning the sample but has significant shortcomings, which prevented the research in the air. The main disadvantages are:

- too small range of angles θ,
- low precision of the transducers positioning,
- low motions repeatability,
- only one type of ultrasound transducers available in use.

The experience gained in solutions of both the mechanical part of the system and the software for device controlling and data processing was used to build the new version of the system, for which the following assumptions were taken into account:

- the ability to work both in water and air,
- high precision of angular positioning of transducers,
- the possibility of the regulation and precise determination of distance from the transducer to the measured surface,
- significant reduction of parasitic reflections caused by the device construction elements.

The above assumptions and previous experiences were designed and fabricated in the new measurement system [Safinowski et al 2008]. In the Figure III.17 the mechanical part of the system is presented. In this solution the transducers are attached to the rotating rams. Thanks to this, the possibility of moving transducers along the arm (the change of radius d) is assured. To the arms rotation two independent drives based on stepper motors are used. This allows rotating the transducers from $0°$ to $90°$ relative to the normal to the measured surface. The limit in rotation angle is caused only by the size of the used transducers. The angular transducers position can be set with accuracy $\Delta\theta = 0.018°$. For the system calibration procedure and for the direct wave measurement the opposite transducer position ($\theta = 90$) can by used. The radial transducers displacement in the range from $10\ mm$ to $300\ mm$ is possible. An important advantage is the ability to work both in air and in the water, which greatly expands the range of potential applications.

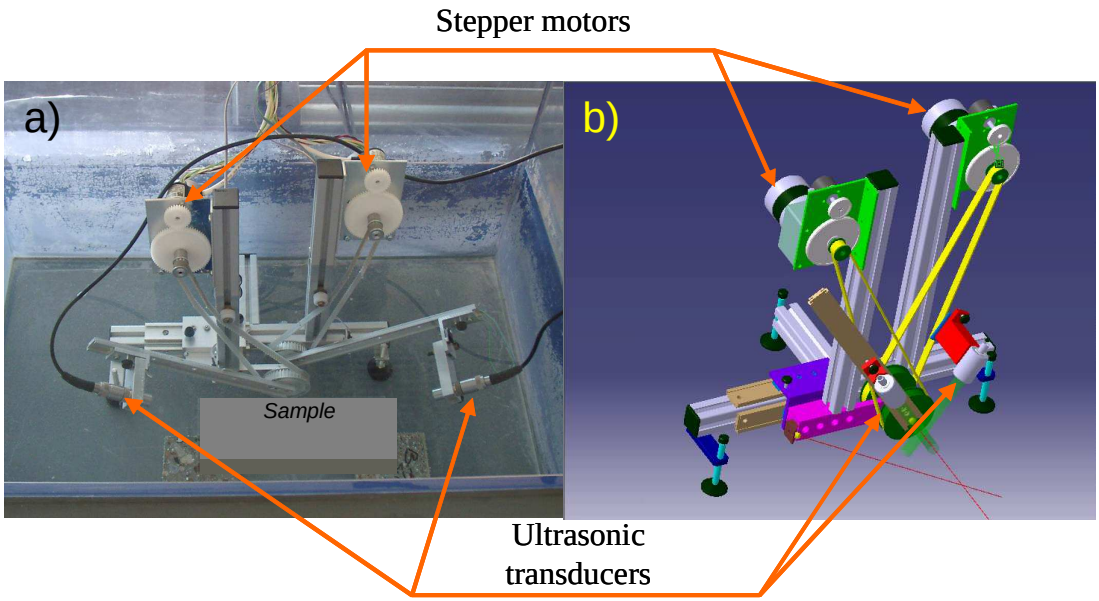

Figure III.17 The final solution of the RMD system; a) photo of device during measurement, b) 3D model.

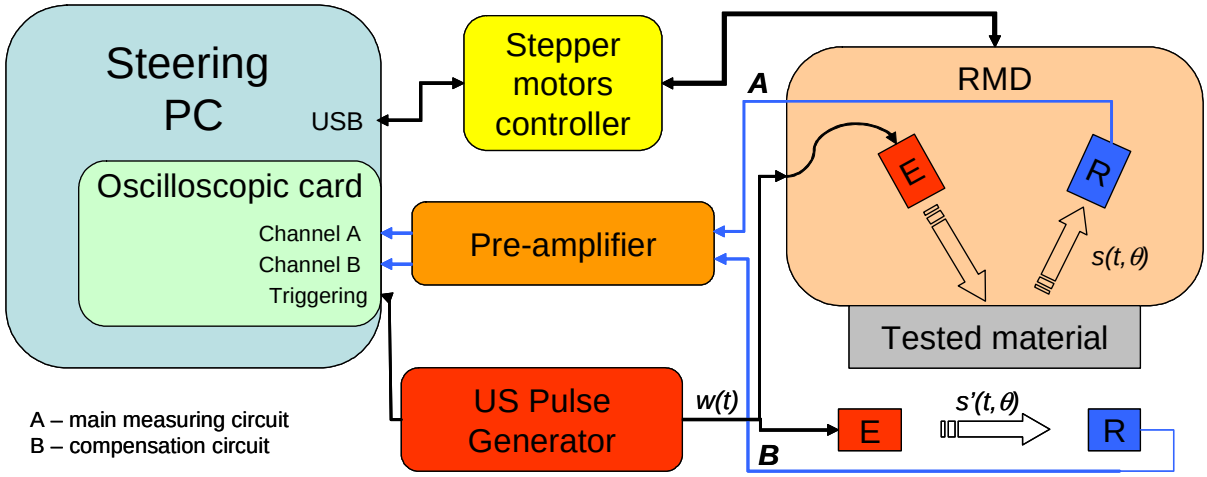

Figure III.18 The block diagram of the RMD system.

In the Figure III.18 the block diagram of a RMD system with marked circuits of measurement A and compensation B is shown. To take into account the influence of environmental conditions of the US waves propagation in the air the compensation circuit is added. In the Chapter III.2.2 the details of this issue are described

In the LabVIEW environment the special software for the RMD controlling called REFLECTO was developed. In Figure III.19 the user interface during the measurement is shown. This program performs the following tasks:

- the system initialization,
- the oscilloscope card configuration,

- the measurement geometry configuration (the range of angles, pitch, number of repetitions),
- the implementation of a programmed sequence of measurement
- saving of the data of measurement.

In the developed program different types of oscilloscopes can be used. The communication via USB ports improves system mobility by the use a laptop as a control unit. The method of measurement data recording is the same as for the SWMD. For each measurement channel the separate binary file containing the time signals for all angular positions is created. Every new repetition of the measurement is saved in a new pair of files, one for each of the measuring circuits. The noise visible on the sample of an amplitude versus angle waveform (Fig. III.19) follows from the adopted chart scale.

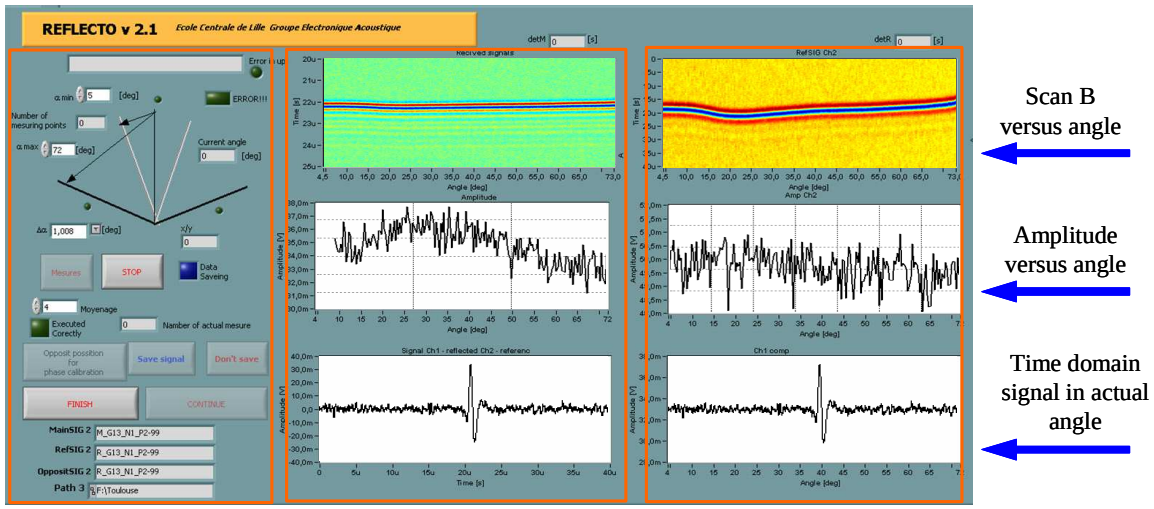

Figure III.19 The user interface of the REFLECTO program during measurements.

In the Figure III.20 the block diagram of the measurement realization is presented. After the start of the RMD system the correctness of communication with oscilloscope and the stepper motor driver is checked. Then, the parameters of signal recording and the parameters of measurement must be established. The most important parameters are the following:

N – the number of points of acquisition (the number of points in the characteristic $R(\theta)$, usually, a dozen points is enough for a good mapping of characteristic)

θ_{min} and θ_{max} - the starting and ending angles of measurement. The determination of the material parameters in the way of identification is more accurate if a wider range of angles

in *R* characteristic is covered (theoretically from *0°* to *90°*). A limitation of this range is the size of the transducer. In the real conditions the range of θ angle from *5°* to *70°* is achieved.

For the maximal distance from the sample ($d \approx 25\ cm$) such a large range of angles is achieved. This also provides the work in the far field. The disadvantage of larger distance *d* is the increase in attenuation and the noise from the air,

K - number of repetitions - in order to reduce the influence of a non-stationary noise (slow changes disturbances i.e. temperature change) the repetition of measurements for one device location (one tested area) is used. This gives *K* characteristics of $R(\theta)$, which are then averaged. The work on the optimal acquisition procedure due disturbances minimization is currently underway. In the paper [Kaczmarek et al 2009] this topic have been discussed. Usually no more than 10 repetitions are acquired.

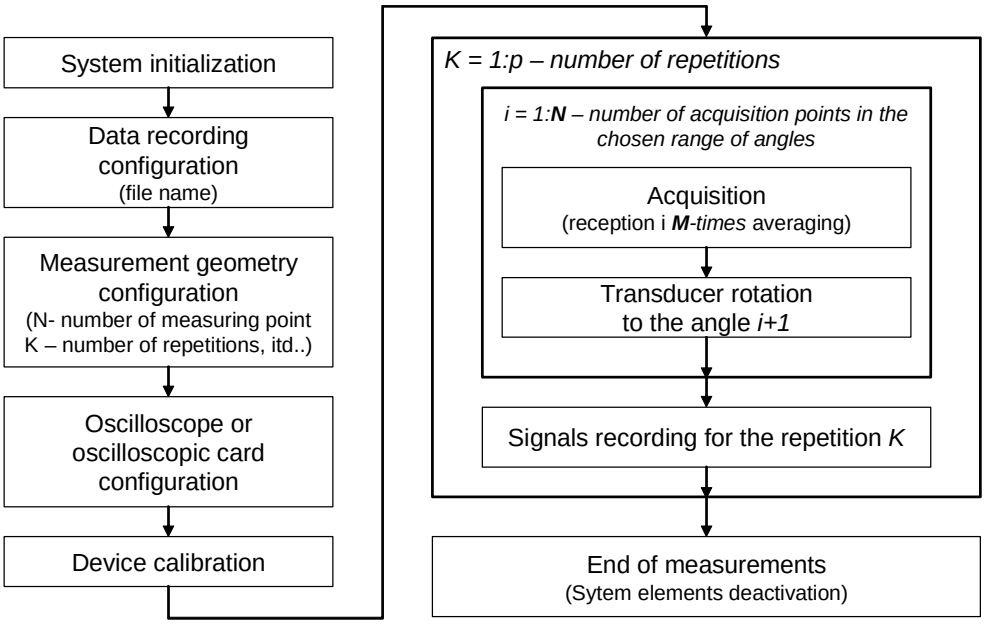

Figure III.20 The block diagram of the REFLECTO operating.

The oscilloscope configuration allows for optimal setting of the acquisition parameters (for example number of averaging *M* which affect the reduction of fast disturbances). For the signal $e(t,\theta)$ acquisition the device calibration on the glass reference sample is performed. After that, the RMD is placed on the measured surface for which *K* repetitions (measurements) are proceeded and the signals $s(t,\theta)$ and $s'(t,\theta)$ are recorded. After acquired (recorded) signals processing in the MATLAB the reflection characteristics $R(\theta)$ is obtained. In the Table III-3 the parameters of RMD system are summarized.

Table III-3 The RMD system operating parameters.

Parameter	Value
Operating mode	*Non-contact* *(in the water or in the air)*
Location of measured surface	*horizontal* *(special fixation needed if another)*
Number of points of acquisition N	*Any , less then* $N = ((\theta_{max} - \theta_{min})/\Delta\theta)+1$
Distance between point of acquisition $\Delta\theta$	*0,018°*
Range of angles	*minimal: 5°, maximal: 90°*
Operating band	*In function of used transducers* *(usually ~ 200kHz)*
One characteristic acquisition time	*~10min* *(for N = 11 without repetitions)*
Weight of the device	*~3kg*

III.2.2 Measured values and signal processing

In the RMD system pulse signal as an excitation of the emitting transmitter is applied. From the ratio of the received signal amplitude *s(t)* and emitted signal amplitude *w(t)* the reflection coefficient characteristic $R(\theta)$ is determined.

However, in this approach, the characteristics of $R(\theta)$ is not free form the supplementary errors resulting from additional influences on the $s(t,\theta)$ signal as, for example:

- the transmittance of the transducers *h(t)*,
- disturbances of the signal propagating through the air *u(t)*,
- not constant beam divergence versus angles $z(\theta)$.

Taking above into consideration, the reference signal *e(t)* can be expressed symbolically:

$$e(t,\theta) = w(t) * z(\theta) * u(t) \qquad \text{(III.27)}$$

Therefore, to obtain the reference signal *e(t)* free as much as possible form the influence of above factors, the following procedure is suggested.

Before the “exact” measurements the calibrating measurement is performed in which a reference sample of 14 mm glass thick glass is used. In comparison with the properties of the skeleton of a porous material the reference sample corresponds to the perfectly rigid and

smooth material. The calibration measurement is performed in the same configuration as the "exact" measurements and gives a group of reference signals $e(t,\theta)$ for a whole range of angles.

During the first tests quite substantial fluctuations in the received signal have been observed (in fixed transmitters position $\theta = const.$). The source of the fluctuation is the air in the area of propagation. In the actual configuration of the measurement device the wave propagation distance in the air is relatively long and is equal to $2d$, where d a distance from the transducer to the tested surface (usually from *20 cm* to *25 cm*). The changes in time of the air parameters on a such long distance of propagation may have a significant effect on the amplitude of the received signals $A_{S1}(\theta)$ and the reference signal $A_{S'}(\theta)$, and consequently on the reflection coefficient. To minimize the influence of these disturbances the second pair of transducers (transmitter and receiver) is added. This creates the second measuring circuit (circuit B, also referred to by the terms the compensating circuit) with two motionless transducers placed opposite each other at a distance $2d$. In this circuit the influence on the received signal $s'(t)$ is caused by the conditions of propagation in the air only (there is no reflection phenomena and transducers motions). As a formality the main measuring circuit (moving transducers) is called an A circuit. During the measurements the signals $s(t,\theta)$ and $s'(t,\theta)$ are recorded simultaneously. Using the amplitudes $A_{S'}(\theta)$ of the signals $s'(t,\theta)$ the amplitude changes $\Delta A(\theta)$ are calculated

$$\Delta A(\theta) = \frac{A_S'(\theta)}{A_S'(\theta_1)} \tag{III.28}$$

where $A_{S'}(\theta_1)$ denotes the amplitude of the signal $s'(t,\theta)$ for the first angular position.

Assuming that the air in the two measurement circuits subject to the same fluctuations the amplitude of the signal $s(t,\theta)$ is expressed as follows

$$A_S(\theta) = \frac{A_{S1}(\theta)}{\Delta A(\theta)} \tag{III.29}$$

For the signals $e(t,\theta)$ (for the perfect reflector) the analogous correction of amplitudes is performed.

For the calculation of the reflection coefficient $R(\theta)$ in the time domain the maximum value of the amplitudes of the signals $A_S(q) = max[A_S(t,\theta)]$ and $A_e = max[e(t)]$ or the peak to peak value $AS(\theta) = max[A_S(t,\theta)]-min[AS(t,\theta)]$ and $A_e = max[e(t)]-min[e(t)]$ are taken.

$$R(\theta) = \frac{A_S(\theta)}{A_e(\theta_1)} \tag{III.30}$$

When performing the Fourier transform on the emitted signal and on the group of received signals their spectrums can be expressed as

$$\Im(s(t,\theta)) = |S(f,\theta)|\exp(j\varphi(f)),\ E(f)\Im(e(t)) = |E(f)|\exp(j\varphi(f)) \qquad \text{(III.31)}$$

In general, the reflection coefficient can take complex values and can be a function of frequency. For the chosen frequencies the reflection coefficient can be expressed in the form

$$R(\theta, f_0) = \frac{|S(\theta, f_0)|}{|E(\theta, f_0)|} \qquad \text{(III.32)}$$

where f_0 is the desired frequency (usually the dominant frequency). An example of reflectance characteristics (phase and modulus of the time signals or their spectra) for a sample of gas concrete is shown in the Figure III.21a.

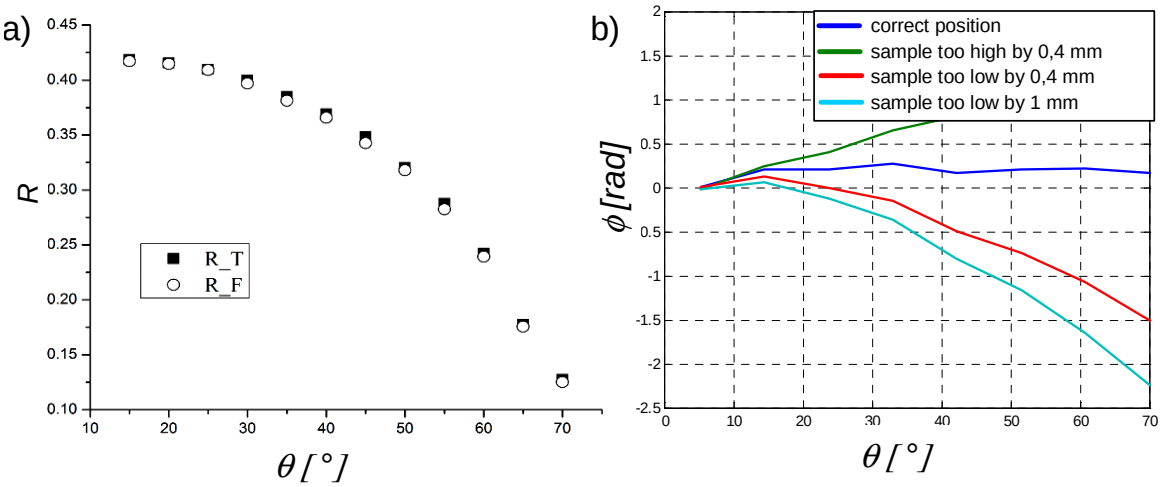

Figure III.21 a) The reflection coefficient characteristic R as a function of the angle θ, R_T – curve calculated from the amplitudes of signals in time domain, R_F – curve calculated on the basis of spectra, b) the phase characteristics of the signals $e(t,\theta)$ for glass sample placed with an error of a vertical position.

For the device positioning relative to the sample surface the phase of the signals $s(t,\theta)$, $e(t,\theta)$ is used. If the axis of the transducers rotation is located above or below the tested surface the length of the propagation path in the air is different for different angles of incidence. This causes the shift of signal phase depending on the angle θ.

$$\Delta\varphi(\theta, f) = \varphi(\theta_1, f) - \varphi(\theta, f) = \frac{2\pi f \cdot \Delta d}{c_{P\_air}} \qquad \text{(III.33)}$$

where c_{P_air} means propagation velocity of ultrasonic waves in the air, and Δd is the change in propagation path length. In the situation of ideal device positioning the signal phase shift should be the same as in the model (for the glass sample close to zero). In fact, the positioning

with the phase shift $\Delta\phi < 0.5\ rad$ is considered as a correct one. Otherwise the position of the device must be corrected. In the Figure III.21b the examples of the phase of the signal $e(t,\theta)$ for a different device versus sample positions are shown.

III.1.3 Test with the reference material

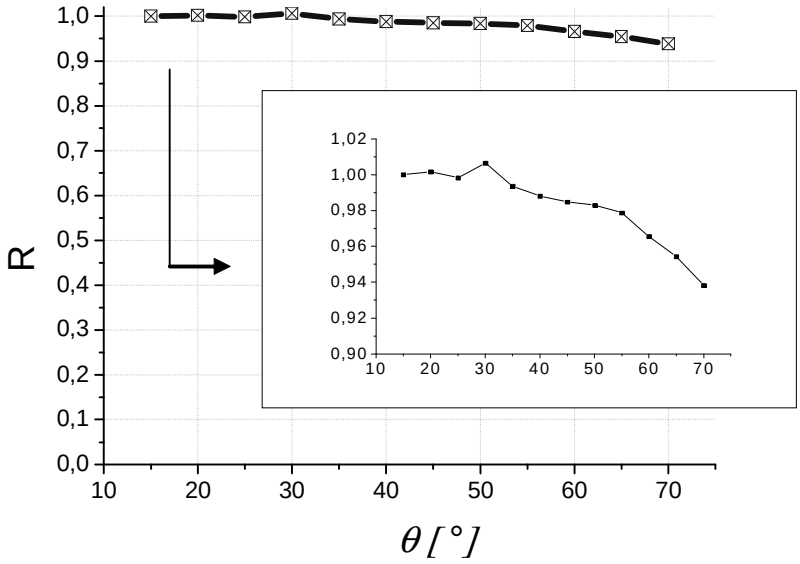

Figure III.22 The characteristics of the reflection coefficient R versus angle θ, measured for the glass standard.

One of the tests of the system was the measurement of the *R* characteristics for the-glass standard. The modelling shows that the reflection coefficient for the glass should be close to the one in the whole range of incident angles, due to the large difference in acoustic impedance between the air and the glass. In the Figure III.22 the *R* characteristics for the glass standard is presented. The scale of the *R* characteristic is chosen to be easily compared with the results for the other presented materials. The values of *R* for the small angles are close to the one as expected. For larger angles the slight decrease of *R* values (reaching up to the level of 0.94) is observed. This is consistent with the model of an unlimited plane wave reflection from an ideal material. That confirm the correct operating of the RMD system.

III.1 Conclusions

For the purpose of the presented research two original measurement systems were developed. The number of laboratory experiences with manually operated measurement systems helps in construction of the systems. The assumptions arising from the models (Chapter II) and the requirements mentioned in the introduction (Chapter I) were taken into account. The most important requirements are:

- non-contact measurements (completely non-invasive),
- material studies with a one side access only,
- feasibility of measuring both in the laboratory and field,
- sufficiently high precision and relatively short measurement duration.

These systems carry out the measurements of the surface wave propagation (SWMD System) and the measurements of the reflection coefficient as a function of angle of incidence (RMD System). In both cases, the transducers are precisely positioned by the computer controlled executive devices. For this purpose, specially software responsible for; the system configuration measurement realization and data acquisition was developed. For the requirement of totally non-contact measurements of SW propagations in the SWMD system the frequency-modulated signals (chirps) and special data processing have been applied. For the proper RMD system operating the special calibration procedure was developed and the second (compensative) measuring circuit which takes into account the environmental influence was added. The results of the tests performed on the reference materials for both systems confirm the methodology used for the measurement realization. The lightweight and compact devices design makes them easy to be used in the field.

Chapter IV

Identification of mechanical and structural parameters of concrete

This Chapter relates to identification of the material properties by solving the inverse problem, in short inversion. The procedure consists in finding the values of model parameters, for which its predictions (synthetic cure) best fit to experimental data. In order to find the best fit different types of optimization methods are used [Stachurski and al. 1999, Findeisen and al. 1987]. In the function of the model complexity (the number of searched parameters), and its characteristics (the importance of various parameters in the model), the solution for posed optimization problem may be more or less complex [Stadnicki 2006]. In any case, reaching the optimal solution requires lot of forward solutions of the model (Forward algorithm).

Development of optimization techniques began in the ‘40s of the twentieth century. The appearance of computers and fast growth of its computing power made, that the solve of very complex optimization problems became possible. Availability and efficiency of various types of optimization tools allows solving even multidimensional problems in a relatively short time. Topics related to solving inverse problems are strongly developed, among others for geophysical needs [Orozco 2003, Boiero and al. 2006, Feng and al. 2005] and medicine. That allows recognizing the structure of the ground or body internal organs on the basis of seismic or ultrasonic data respectively. There are also attempts to identify the concrete structure by inversion [Ward 2005]. In mostly of cases, the inversion process is carried out after the measurements, however, in the literature can be found the attempts of the real time inverse problem solving which is realized during the measurements [Lai and al. 2002]. Nowadays, even the choice of the optimization method can be a problem because of the numbers of available optimization tools.

In this work, the process of solving of the inverse problem was applied in the parameters identification based both on the registered surface wave propagation and the reflection coefficient. In each case, inversion requires defining the model, the objective function and the method of optimization. In the Figure IV.1 a functional diagram of procedure of inverse problem solving is shown. If in the identification procedure the multi-parameter

model is used, the number of unknowns can be reduced by establishing some of them as a constant. That can be done, on the basis of available knowledge or experience concerning model's sensitivity (e.g. Chapters: II.1.3, II.1.5, II.2.2). Decrease of unknown parameters in the optimization procedure causes decrease of computing time and increase the solution accuracy. If chosen optimization procedure makes it possible the limitations of searched parameters could be set in the base of available knowledge.

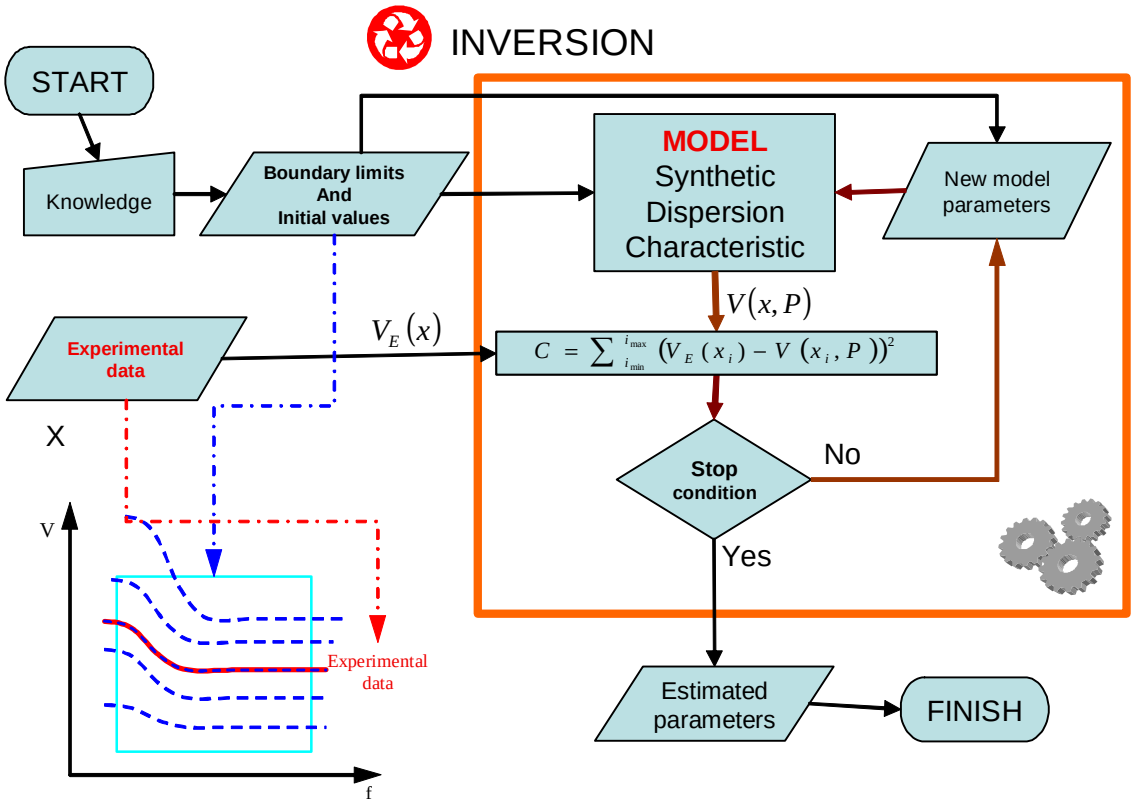

Figure IV.1 The functional diagram of the procedure of inverse problem solving.

According to the diagram shown in the Figure IV.1 the objective of optimization procedure is to find model parameters, for which the objective function *C* (Equation IV.1) meets one of the conditions of the end of optimization.

$$C(P) = \sum_{i_{\min}}^{i_{\max}} \left(V_E(x_i) - V(x_i, P)\right)^2 \qquad \text{(IV.1)}$$

where $V_E(x_i)$ is a set of experimental data, and $V(x_i,P)$ is a set of data obtained from the model for parameters *P*.

The determination of the minimum of objective function is obtained by the multiple solving of a direct problem (model solution) for different values of parameters vector *P*. On the basis of previous iteration the values of *P* vector are proposed by the optimization

algorithm. In considered cases, the objective function is defined as the sum of squared differences between the experimental data (V_E – on the diagram) and the model predictions (V - on the diagram). It's worth to notice, that the details of defining the objective function depends on the optimization algorithm which is used. In the optimization procedure the search for a solution is ended if one of required conditions will be fulfilled, such as attainment of; a specified value of C function, a maximal number of iteration, minimal increment of independent variables, etc. The types of conditions for procedure termination also depend on the chosen method of optimization, but in each case, the purpose of calculation is to find the minimum of the function C. This corresponds to the best matching of the model predictions to the experimental data. The parameters P of the model, for which the procedure was completed, determine a required solution.

In the following subsections a brief overview of optimization methods, which can be used in solving the identification problem is shown. The comparisons of their operating and implementation in considered issues with the use of Haskell's, Gibson's and reflection coefficient models are presented. The tests of the developed programs for the synthetic data are also shown.

IV.1 Brief review of the optimization methods

In the Figure IV.2 the one of the most frequently cited classification of optimization methods is shown. By the grey colour the methods used in the work are indicated. The main two groups of methods are the deterministic methods and the stochastic methods.

For the first group [Amborski 2009, Floudas et al 2009] the extremum of the objective function is searched according to the scheme, in which based on the results found in previous iterations the successive approximations are obtained. The advantage of this method is high speed, even for multi-parameter optimization. Moreover, the restrictions on the parameters values are easy to define. The disadvantage of deterministic methods is that the algorithms are local (ie that in which as the final solution the first found extremum is taken regardless of whether it is local or global extremum. Thus, this type of algorithms are suitable for multidimensional problems, where there is only one extremum of the objective function. There is no guarantee of correct results if this algorithm is used with the objective function, which has more than one local extremum. The stochastic methods are conted to the methods of global optimization. Therefore, the effect of their use should be a finding of the global

extremum of the objective function. However, there are always non-zero probability that the founded solution is a local extremum [Kusiak et al 2009]. A relatively long time of optimization problem resolve is a disadvantage of non-deterministic methods. This time increases significantly when the number of optimization parameters increase. The computation time using these methods is much longer than in the case in witch the deterministic methods are used. The another disadvantage is the difficulty in introducing restrictions on the optimization parameters. However, the introducing of a penalty function in the objective function is one of solutions of this problem. Among the stochastic methods the Genetic algorithms applied to solve various problems, eg in the field of geophysics have gained much popularity [Dal Morgo et al 2004].

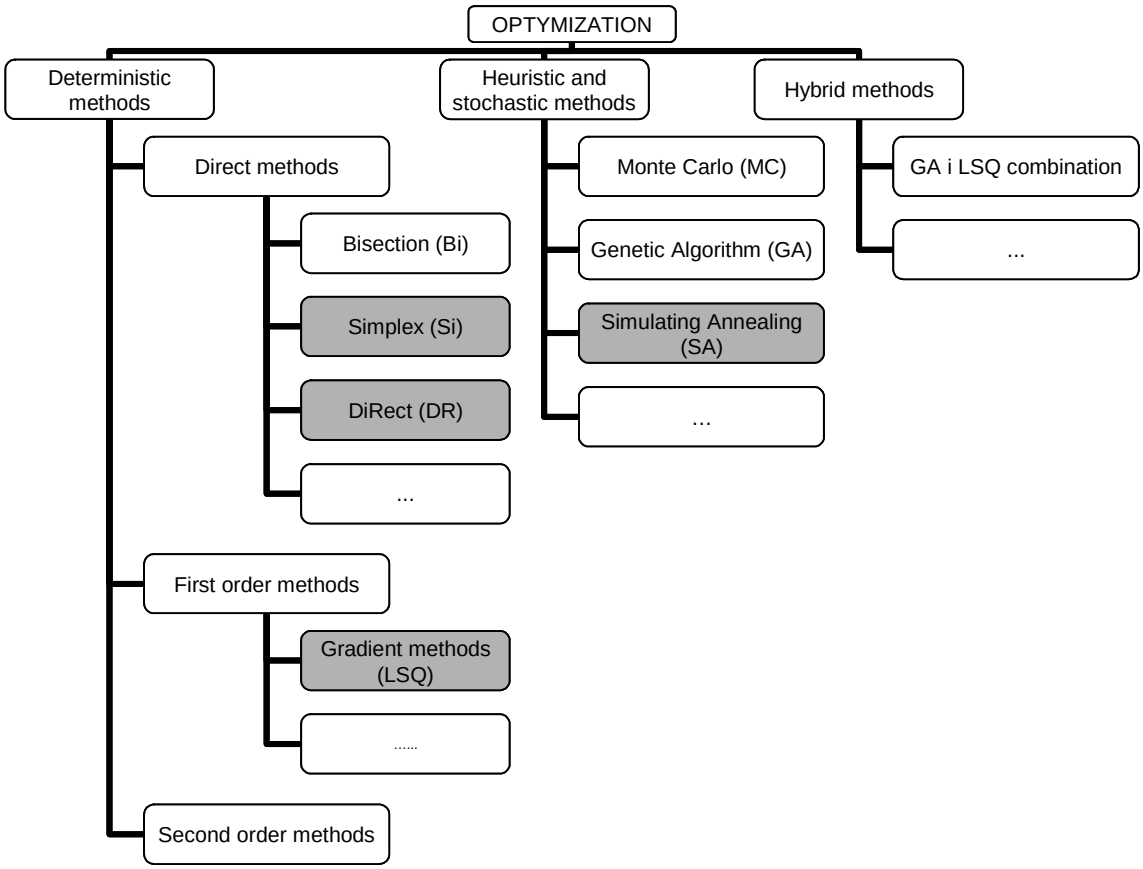

Figure IV.2 The classification of the optimization methods.

The use of a hybrid method can be a compromise between the two groups of optimization methods mentioned above. One of the solutions of such algorithm is the use of fast-acting deterministic procedure will be executed many times with different starting points. In each call the starting parameters will be chose by a stochastic method. In that case there is a

chance that one of the founded extremum will be a global solution. To distinguish the local and global solutions the value of the objective function - matching error should be compared. Global result corresponds to the lowest value (extremum) of the objective function. For the same optimization problem the hybrid method operating may be faster than for the stochastic algorithm. Another approach to the hybrid method is the rough searches of global extremum by one of the methods called „Artificial intelligence" such as Genetic Algorithms, and then apply the local method in order to accurately determination of this extremum. In most cases operation of such methods gives good results.

In the present study used several different optimization methods of both groups (deterministic and stochastic) are used. One hybrid algorithm is also developed. In the Chapter IV.6 the description of this algorithm is presented. In the Appendix I the selected optimization methods that were used in this work are briefly presented.

IV.2 Comparison of selected methods of optimization

Selection of appropriate optimization tools is relatively difficult and largely depends on the nature of the posed problem. The situation is relatively easy, if the objective function has only one minimum. Optimization tasks appearing in this work are the problems with many local extremes. This requires the combination of local and global optimizations.

In the case of a global optimization the question about type of method appears. What is better, the use of use time-consuming heuristic procedures or many repetitions of a local optimization started from a different starting points? If the second one, how many repetitions will be profitable in time in relation to global optimization. The aim of this chapter is to compare the performance of chosen optimization methods. All tests were performed for the same two-parameter model. For the tests the model for the reflection coefficient calculation (described in the Chapter II.2.1) is used. Instead to use the other test functions the one of the models considered in the work is chosen for the tests. In effect, the obtained results relate to the real problem considered in the work. The issue is solved as a best curve fit problem in witch the model to the real curve is fitted. For verification purpose the same model for the synthetic and "real" curve is used. The model parameters for a "real" curve are *x1 = 1.5* and *x2 = 0.5*. In the Tables below the results of search of the minimum of objective function are presented (Table IV-1 – ideal data, Table IV-2 – noised data). In the second case to the points of synthetic curves the noise (as the random values) is added.

To the considered problem solving four different optimization methods were used. Each of them is implemented in a separate program and solves the inverse problem. For the order the developed programs are named as follows:

- InvRefDR - algorithm with a global optimization Direct method
- InvRefSi – local optimization algorithm with the Simplex method
- InvRefLSQ - local optimization algorithm with the LSQ Matlab procedure (gradient method),
- InvRefSA – global optimization algorithm with the Simulated Annealing method.

Table IV-1 The comparison of results and efficiency of optimization algorithms for the case of ideal data.

Program	*InvRefDR*	*InvRefSi*	*InvRefLSQ*	*InvRefSA*
Parameter x1	1.5000	1.5016	1.5001	1.4981
Parameter x2	0.5000	4.9997	0.4998	0.49996
Time of calculations [s]	0.29	0.62	0.32	37.4
Number of the objective function calls	13	49	16	3312
Minimal value found for the objective function	6.92e-033	4.99e-008	6.23e-012	5.31e-008

Table IV-2 The comparison of results and efficiency of optimization algorithms for the case of noisy data.

Program	*InvRefDR*	*InvRefSi*	*InvRefLSQ*	*InvRefSA*
Parameter x1	1.5041	1.5013	1.5029	1.5037
Parameter x2	0.5000	0.5002	0.4996	0.5002
Time of calculations [s]	1.39	0.71	1,12	41.6
Number of the objective function calls	105	56	46	3312
Minimal value found for the objective function	1.508e-003	1.508e-003	1,508e-003	1.508e-003

The analysis of the results presented above shows that all methods found the same minimum of the objective function (the same parameters values). The only clear difference is the number of the objective function calls in the program InvRefSA, which is based on the Simulated Annealing method. This is directly linked with the calculations time, which was about 40 times longer than in this case of the other methods. Favourable results were obtained

for the program InvRefDR, which is based on the DiRect method. This method solves a global problem in a similar time as others algorithms of a local action. The disadvantage of this method is a difficulty of implementation for more than two-dimensional problems. Comparing the results for the programs based on the local optimization obtained results are better for the program InvRefLSQ in which the gradient method is used. Taking into account the results presented above, the gradient methods will be used for the local optimization and the Simulated Annealing for the global optimization.

Presented calculations were carried out on a personal computer HP Compaq 8510w with Intel Core 2 Duo T8300 2.4 GHz processor and 4GB RAM. All methods were implemented in Matlab 2007 on the system Windows Vista 32bit.

IV.3 Identification of the medium parameters using the Haskell's model - tests with synthetic data

The main objective of the diagnosis of the condition or quality of the materials is the identification of its parameters based on the measurement data. Quite often it is impossible to carry out the identification in a direct manner, like for example in the case of concrete diagnostic. In some of considered models the analytical determination of material or structural parameters describing the state of the concrete is impossible. One of these models is the Haskell's model, which is described in the Chapter II.1. The use of the Haskell's model in the identification process is doubly complex, because there is no analytical solution of this model and even for the solving of dispersion equation (the forward problem) the optimization procedure must be used. In the Chapter II.1.2 the details of the forward problems solving are shown. Examples of the parameters identification of the macrostructure medium with the Haskell's model are shown in studies of [Wathelet et al 2004, Orozco 2003, Krstulovic-Opara et al 1996].

Given the complexity of the problem of identification with the use of Haskell's model [Lowe 1995] the aim of this subsection is:

- the review of the effectiveness of the selected optimization procedures (LSQ and SA) in terms of computing time,
- the comparison of the accuracy of the obtained results,
- the verification of proper operation of the procedures depending on the complexity of the model (number on unknowns)

The information obtained in this way facilitates the correct configuration of the model and optimization procedures in terms of performance in the real conditions. The LSQ and SA procedures implemented in the developed programs are called InvHaskLSQ and InvHaskSA respectively. In the whole section the same method of results presentation is used for all of the tests performed. The objective function in the optimization procedure was defined according to the Equation IV.1. The quality of the identification was assessed on the basis of standard error as

$$BN = \frac{\sum_{f=f_{\min 1}}^{f_{\max}} \left| V(f) - V_E(f) \right|}{\sum_{f=f_{\min 1}}^{f_{\max}} V_E(f)} \cdot 100\,\% \qquad \text{(IV.2)}$$

where f_{min} and f_{max} correspond to the upper and lower frequency in dispersion characteristics, and the V_E is synthetic characteristic.

In the considered issues only the fundamental mod of the dispersion characteristic is taken into account. The use of higher order modes is also possible as long as they are measurable. The unlimited number of layers of the heterogeneous material can be taken when Haskell's model is used. However, each new layer of fine thickness adds four new parameters in the model (three parameters for last halfspace "layer"). Each layer is characterized by the propagation velocities of two types of waves (longitudinal and transverse), the density of the layer and its thickness. For example, in two layers model is seven variables (parameters) of optimization, in three layers model the number of parameters increase to eleven and so on. Such a large number of variables with a limited set of experimental data became a serious problem for the inversion. Each additional optimization parameter increases the computation time and the likelihood of ambiguity. The reduction of the number of the searched parameters can be achieved by the use of other measuring methods to set the values of some parameters. It is also possible that certain parameters (which values can be expected) can be taken as constants (not subject to identification), especially if they don't have a large influence on the model predictions. The sensitivity analysis presented in the Chapter II.1.3 shows that the density of the layers has a relatively small influence on the dispersion characteristics, the second parameter with small influence is longitudinal wave velocity. Similar observations can be found in the work in the geophysics field [Dal Moro et al 2006]. In experimental conditions the value of the longitudinal wave velocity can be estimated relatively easily, but for its accurate measurement much more complex techniques is required.

Solving the multiparameter issue of all the variables in the model should take the same order values. Thanks to this, the optimization procedure uses similar changes for all of the model parameters. For this reason, in the case of Haskell model (used to describe the waves in a heterogeneous medium) the thickness of layers in the *cm*, wave velocity in *km/s* and density t/m^3 were adopted.

For solving the inverse problem based on the Haskell model the Matlab algorithm "lsqnonlin" (LSQ) is used. The algorithm is in a configuration which allows the use of the variables limitations. In most cases the range of the measured material parameters are knows and the variables limitations can be set easy. This increases the calculations efficiency and reduces the risk that the local minimum corresponding to non physical solution will be found. The use of local optimization methods for problems with local minima the choice of starting point plays en important role. This choice can determine that the algorithm finds the global minimum, or incorrect local minimum. As has been written before, the solution to this problem can be booting the procedure repetitively from different starting points each time, as shown in the Chapter IV.6. In the Appendix II the details of the identification for the Haskell model and synthetic data are given.

Summary results of the tests preceded

In the Figure IV.3 the computation time and the standard error of identification for the preceded tests with synthetic data are presented (Appendix II). The summary allows us to evaluate the results of identification for the use of the Haskell's model in different optimization methods and in different model configurations. Jewels results can be summarized as follows:

- the use of global optimization increase the computation duration several times, without the confidence to obtain the correct solution,
- computation time increases in proportion to the quantity of the search parameters,
- the same task is solved several times longer by SA algorithm than the LSQ algorithm,
- for the synthetic data similar values of the objective function minimum (for the synthetic data *BN <0.1%*) and model parameters are found by both of algorithms (LSQ and SA).

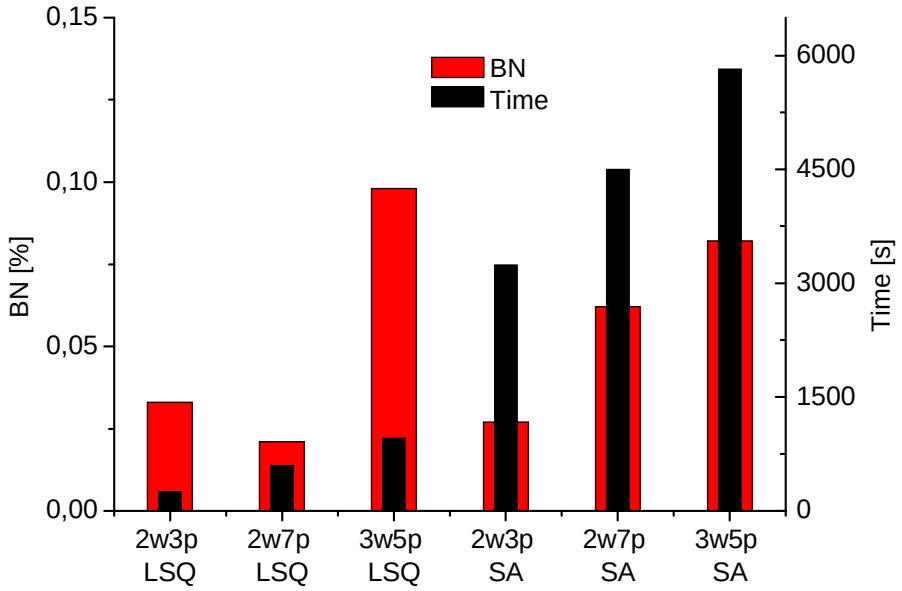

Figure IV.3 Summary of computational time and standard error in the synthetic data identification.

The tests duration presented above should be treated as estimation, because they can vary significantly depending on the starting point of the identification.

In the case of the use of experimental ("real") data into identification procedure slightly worse results might be obtained due to the measurement errors and the fact that the model is only an approximation of the measured material.

The overview presented above shows that the use of the repeatedly calling of the LSQ procedure is more advantageous in terms of computing time, and the accuracy obtained in both methods are similar. In the Chapter IV.6 the development of an algorithm that performs the repeatedly calling of the LSQ function is presented.

IV.4 Identification of the medium parameters using the Gibson's model - tests with synthetic data

In the following Chapter an analysis and tests of the Gibson's model inversion for the theoretical dispersion curves are presented. The detailed description of the model is shown in the Chapter II.1.4. In the comparison to the Haskell's model identification this case is much simpler, because the model has an analytic solution, and only three parameters must be optimized. There are also two ways to reduce the number of parameters form three to two.

In the first approach the fact that the Poisson's ratio has small influence on the dispersion curve. In the Chapter II.1.5 is shown that the changes of the Poisson's ratio in the range for the most common concretes modified the shape of the dispersion characteristic by a

maximum of *1%*. Therefore, if the value of the Poisson's ratio will be assumed as constant (for example, $\nu = 0.2$, the maximum error of this assumption not exceeding *1%*. Such error can be neglected taking into account the accuracy of the experimental dispersion characteristics. Moreover, the analytical approximation taken to solving the dispersion equation for the Gibson's model has an incompatibility of *1-3%* [Vardoulakis et al 1988]. In that case, for the identification the heterogeneity factor *m* and the transverse wave velocity at the edge V_{S0} are taken. The second possibility of the number of variables reduction is a determination of the speed V_{S0}. This can be achieved by the use of the approximation that the $V_R \approx 0.9V_S$, for example, if we assume that the surface wave phase velocity in the dispersion characteristics for the highest frequencies corresponds to the velocity of surface waves on the shore of the medium the V_{S0} can be estimated.

IV.4.1 Studies of the error function sensitivity

The studies of the error function sensitivity are useful in the optimization algorithm selection and configuration. For this aim the solutions of the model (the dispersion characteristics) must be calculated for all possible values (in considered ranges) of all model parameters. Then the group of characteristic obtained in that way must be compared with a synthetic characteristic generated for one set of parameters (the reference characteristic). The result of all comparisons is an error function (defined as in the Equation IV.2) which is a function of the model parameters *P*. The error function visualization shows its evolution with the changes of the model parameters. The Gibson's model is relatively simple and thus this kind of test can be proceeded. The complexity of the Haskell's model and greater number of parameters limits the uniqueness of the solution and for this studies where not performed for this model.

In the Gibson's model, parameters are three parameters. The transverse wave velocity V_{S0}, and the Poisson's ratio ν represents the properties of the material on the edge of half-space. The material homogeneity is represented by the coefficient *m*. In the Figure IV.4 the 3D graphs of the error function for the two cases is shown. The graphs are shown in a logarithmic scale for better illustration of the function extremum. Synthetic dispersion characteristic was generated for the following values of the parameters: $\nu = 0.2$, $V_{S0} = 2200$ m/s and $m = 3$. In the Figure IV.4a the case the constant value of the Poisson ratio ($\nu = 0.2$) is presented. It could be see that the error function obtained in this way has a

global minimum. In the Figure IV.4b the error function is calculated for a fixed $V_{S0} = 2200\ m/s$. In this case also the error function has the single minimum.

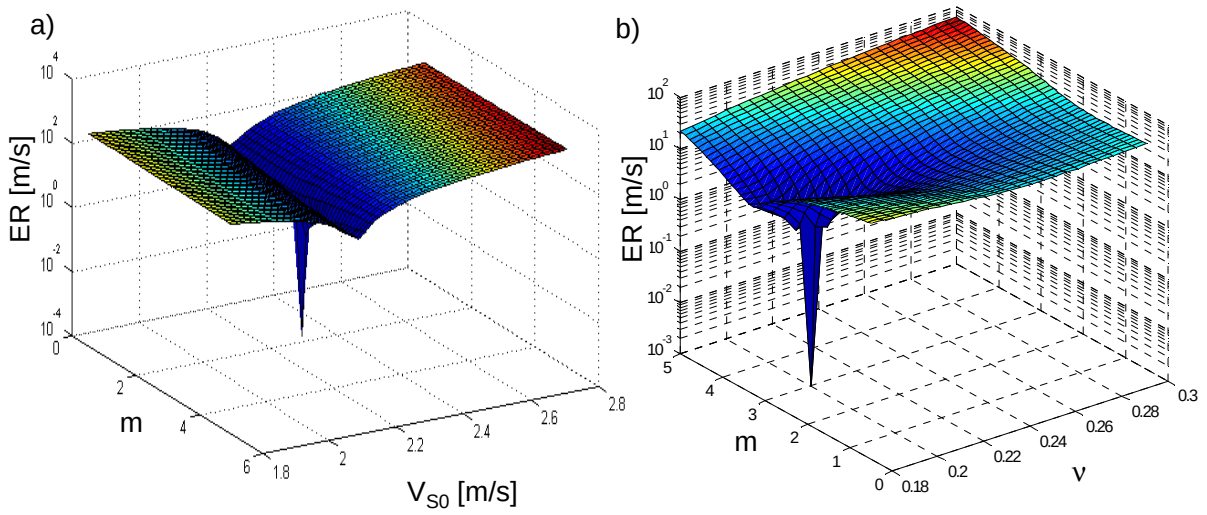

Figure IV.4 The error function for the Gibson's model: a) for a fixed ν, b) for a fixed V_{S0}.

The existence of a single minimum in both cases is very beneficial for the identification procedure. This allows for the use of local optimization algorithm, whose operation is rapid and the obtained results are reliable.

IV.4.2 Tests of the program

The preceded studies of the error function sensitivity confirm the validity of the use of the local optimization for the Gibson's model parameters identification. The inversion procedure is created in the base of the knowledge about the model limitations, its sensitivity and the error function evaluation. In the program named InvGibLSQ the Gibson's model and the gradient local optimization procedure were implemented. The Matlab local optimization function lsqnonlin (available in Matlab's toolbox) was used as previously.

The parameters identification for a given synthetic curve (generated by the same model which is used in the inversion) is the elementary test of the correctness of the algorithm. The values of the parameters in this test were as fallowing $V_{S0} = 2200\ m/s$, $m = 5$ and $\nu = 0.2$. The ranges of the parameters for these studies was as fallowing: from *1800 m/s* to *2800 m/s* for V_{S0} and from *-20* to *+30* for m. The value of the Poisson's ratio, based on the earlier discussion, was established as a constant $\nu = 0.2$. In the Figure IV.5 the result of inverse

problem solution for this case is shown. The developed program is characterized by short duration of calculations in comparison to the programs based on the Haskell's model. The values of the model parameters obtained by inversion exactly match to the values used, which were used to generate the synthetic curve. For other data sets the similarly efficiency of the procedure operating is obtained. In the case of synthetic dispersion curve the accuracy of inversion depends only on the optimization configuration, where level of the acceptance of the solution is defined.

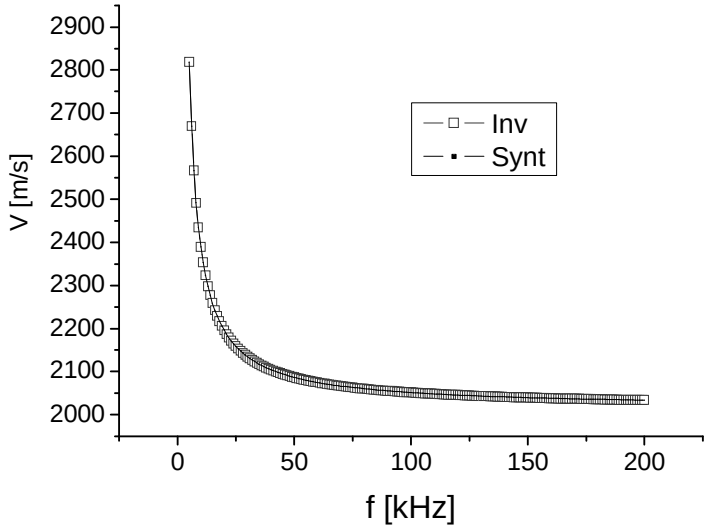

	Synt	Inv (LSQ)
V_{S0} [m/s]	2200	**2200,19**
m	5	**5,002**
ν	0,2	**0,199**

Figure IV.5 The comparison of the dispersion characteristics, synthetic - Synt and theoretical Inv (obtained by the inversion).

The simplicity of the Gibson's model (small number of parameters, the error function with one extremum) determines high effectiveness of the use all of considered optimization algorithms. to solve the inverse problem. Both, stochastic and deterministic algorithms allow as to get the correct results, but the latter provide an easy way to input the limits of the parameters ranges and in most cases are characterized by a shorter duration of calculations.

IV.5 Procedure of the depth of degradation estimations based on the Gibson's model

In this Chapter an algorithm for the determination of the depth of material degradation is presented. In this algorithm the Gibson's model is used. The developed algorithm is called DDS (Degradation Depth Search). As it was shown in the Chapter II.1.4, the Gibson's model assumes a continuous linear change of the shear modulus versus depth. In the proposed

algorithm this property is used but only to a certain finite depth. In considered approach the shear modulus linearly changes up to the border of degradation, and then remains constant - the "healthy" part of the material without degradation (see the Figure IV.6). Considering the degraded material from the surface is assumed that the stiffness of the shaping of the module varies linearly with depth up to the limit of). Given the fact that the depth of the wave penetration into material is related to the wavelength the hypothesis that the Gibson's model will be agreed with the material up to certain wavelength, and then (for deeper zones of material) the discrepancy between the Gibson's model predictions and the waves velocity in that structure of the material will be increasing.

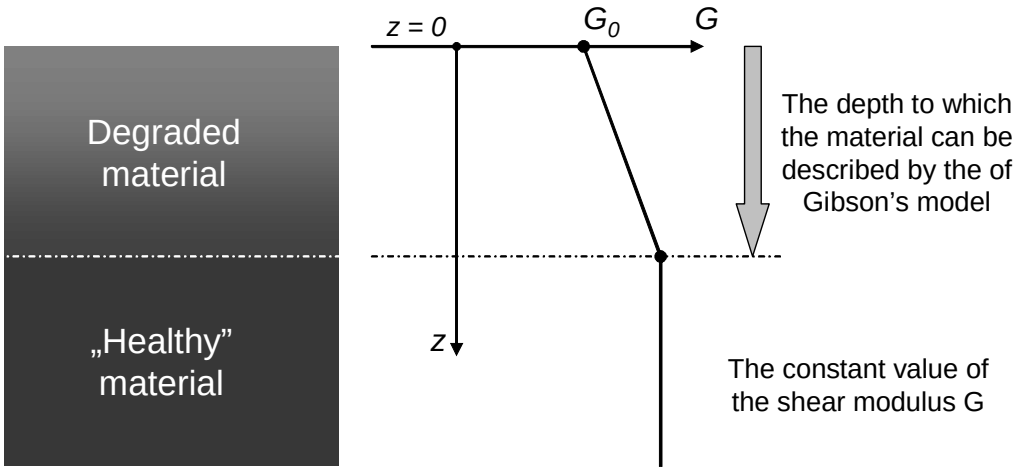

Figure IV.6 The illustration of a partially degraded material (*G* - shear module, *z* - depth).

IV.5.1 Concept of the algorithm

The task of the developed procedure is to find the greatest depth for which the theoretical dispersion curve generated by the Gibson's model fits to the experimental dispersion characteristic obtained for partially depredated material. The fact that the surface wave penetrates into material to the depth approximately equal to wavelength is used for this purpose. For the known wave velocity the depth of the wave penetration can be linked to its frequency. Thus, the decrease of the wave frequency causes the increase of the penetration depth. Finally, the DDS procedure search the lowest frequency for which the theoretical characteristic obtained from Gibson's model match to the experimental characteristic of a partially degraded material. This situation is shown in the Figure II.12, in which the dispersion curve obtained for the partially degraded material (a linear distribution of the G

modulus) corresponds to the part of the characteristics obtained from the Haskell's model (arrow indicated the lowest frequency for which the characteristics are consistent). The implementation of this task requires many repetitions of the Gibson's model inversion. For this purpose, the application described above and named InvGibLSQ was used as a subroutine into DDS program.

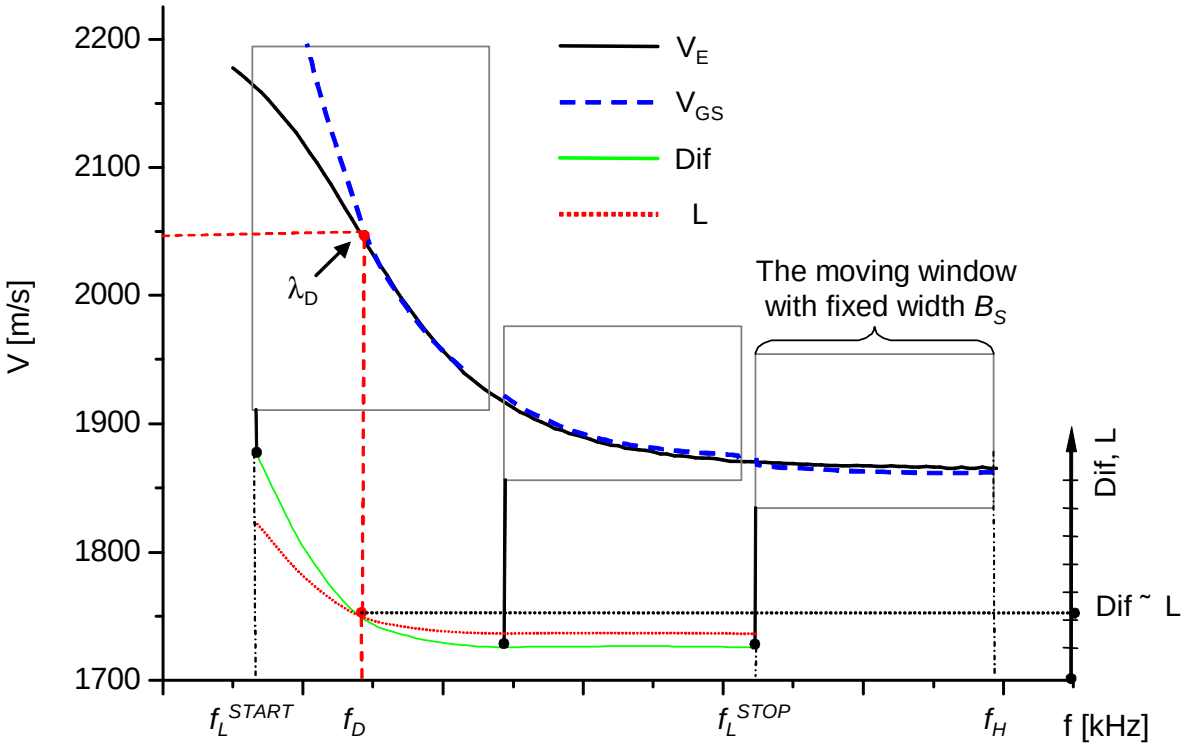

Figure IV.7 The graphic presentation of the DDS procedure operating.

After the program configuration the data for identify V_E are loaded and the main program loop starts working (as illustrated in the Figure IV.7 and on the block diagram in the Figure IV.8). The program runs as follows:

- In the first iteration ($i = 1$) the fragment V_{ES} (width B_S and lower frequencies $f_L^i = f_L^{START}$)of the experimental characteristics V_E is cut out (a window), where $V_{ES}\left(f_L^i\right) = V_E\left(f \in \left(f_L^i, f_L^i + B_S\right)\right)$,
- For the part of characteristic V_{ES} the inverse problem is solved (V_{GS} – result of inversion) , and the error of inversion (Eq. IV.3) is written to fit the variable $Dif(f_L^{START})$ expressed by the relation

$$Dif\left(f_L^i\right) = \frac{\left|V_{ES}\left(f_L^i\right) - V_{GS}\left(f_L^i\right)\right|}{V_{ES}\left(f_L^i\right)} \qquad \text{(IV.3)}$$

- In the next iteration of the window is moved to the now location with the step of Δf and the identification process is carried out for the new position of the window. The error for this iteration is saved as new element of the vector $Dif(f_L^i)$,
- The process is repeated until the window will be transferred to the end of the characteristic ($f_L^i = f_L^{STOP}$). The values of *Dif* are small in the frequency range for which the model is consistent with the experimental characteristics (high frequency) and grow in the range of frequency where the curves are less agrees (low frequency).

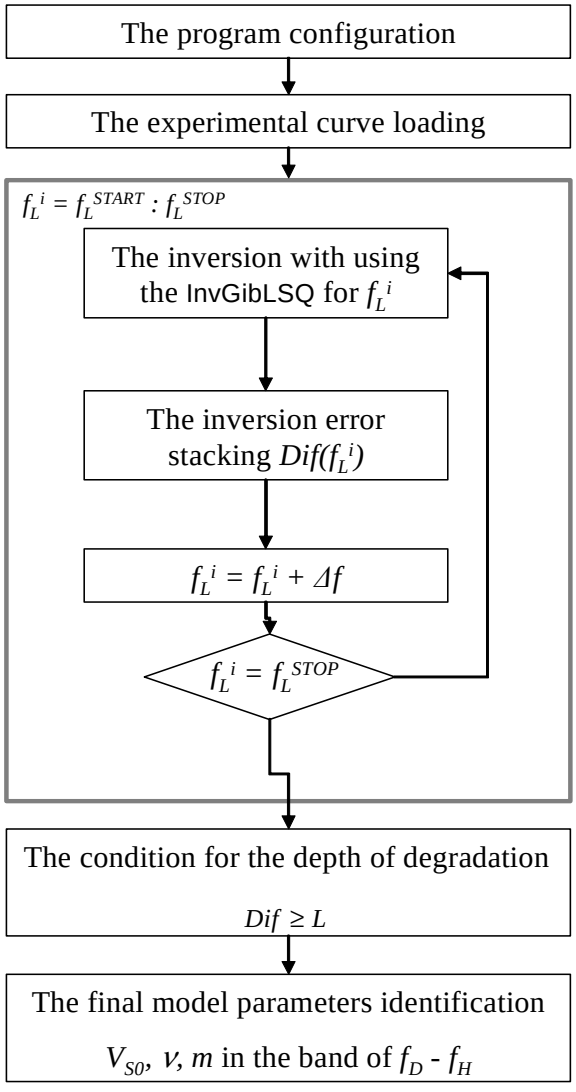

Figure IV.8 The block diagram of the DDS program.

- The acceptation level *L* (curve *L* in the Figure IV.4) is calculated as the average of several (usually 10) consecutive values of the *Dif* vector beginning from the *i-th* iteration (Eq. IV.4), where *a* is a constant factor,

$$L(i) = \frac{a}{10} \cdot \sum_{k=i}^{i+10} Dif\left(f_L^k\right) \qquad \text{(IV.4)}$$

- The "degradation" frequency f_D is the first frequency for which the inequality becomes $Dif < L$. This provides that the model starts to deviate from the characteristics V_E.
- The wavelength λ_D and hence also the depth of degradation $d_{DEG} = \lambda_D$ are determined in the base of frequency f_D and the curve V_E.
- For the most accurate determination of the model parameters (V_{S0}, ν, m) the inverse in the band (f_D - f_H) is proceeded as the last step of DDS.

The factor a in the Equation IV.4 causes that in the curves compliance zone the inequality $L < Dif$ occurs. It was experimentally founded that the best results of the program are obtained for the a from *1.5* to *3*. The adaptive nature of the threshold L causes the reduction the influence of the random fluctuations of the *Dif* curve caused by the noise and measurement errors in the real data processing. Moreover, it was observed that the best results are obtained when the B_S range is about 20-40% band of V_E. Fixed band B_S (fixed-width window) provides the same (in terms of number of samples) conditions for solving the optimization issues in all iterations. Thus, each value of *Dif* can be mutually compared.

In the Figure IV.9a the example of *Dif* curve and the threshold L for the synthetic data are presented, and the results for the real data are shown in the Figure IV.9b. If the curve *Dif* crosses the threshold L in several points the point for the lowest frequency is taken as a result. In the presented example of the real data the algorithm found the value of $f_D = 155kHz$. The wavelength λ_D and in consequences the deep of degradation d_{DEG} is determined in the base of the characteristic $V_E(f = f_D)$. In the next chapter the results of the program operating for the synthetic data are presented.

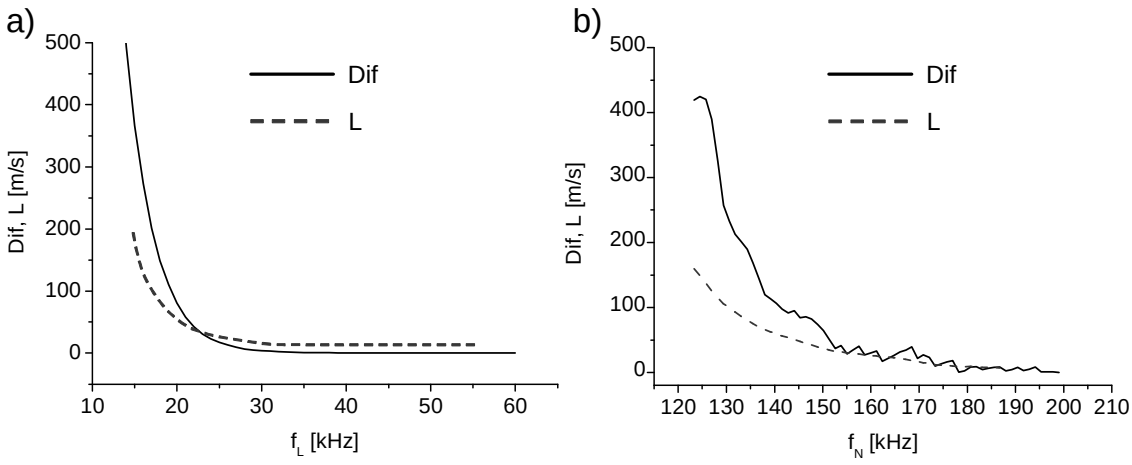

Figure IV.9 The The examples of the *Dif* and *L* curves for: a) the synthetic data, b) the experimental data.

IV.5.2 DDS program verification for the synthetic data

The results presented in the Table IV-3 are the confirmation of the correctness of the procedure DDS. This Table consist the comparison of the results obtained via DDS program with the synthetic data. The 10-layers Haskell's model was the source of the synthetic dispersion curve. The layers parameters are chosen to meet the assumption of stepwise linear changes of the shear modulus versus depth. The thicknesses of all layers are equal, and their sum gives the result of the depth of degradation. The others model parameters were identical for the all presented cases. In the Table IV-3 the obtained results of identification are shown.

The profile of the transversal wave velocity versus depth $V_S(z)$ can be determined if the value of following parameters are known: the transversal wave velocity at the edge V_{S0}, heterogeneity coefficient m. The value of d (depth of degradation) determines the depth up to which the change in the transverse wave velocity occurs.

Table IV-3 The comparison of the results obtained by the DDS program with the theoretical values .

Case	Data	Depth of degradation d [mm]	Transversal velocity V_{S0} [m/s]	Poisson's ratio υ	Heterogeneity coefficient m
1	Synthetic	10	2100	0,30	10
	Identification	10,3	2076	0,35	10,4
2	Synthetic	20	2100	0,30	5
	Identification	19,32	2095	0,28	5,49
3	Synthetic	50	2100	0,30	2
	Identification	51,5	2086	0,31	2,22
4	Synthetic	100	2100	0,30	1
	Identification	96,66	2076	0,34	1,07

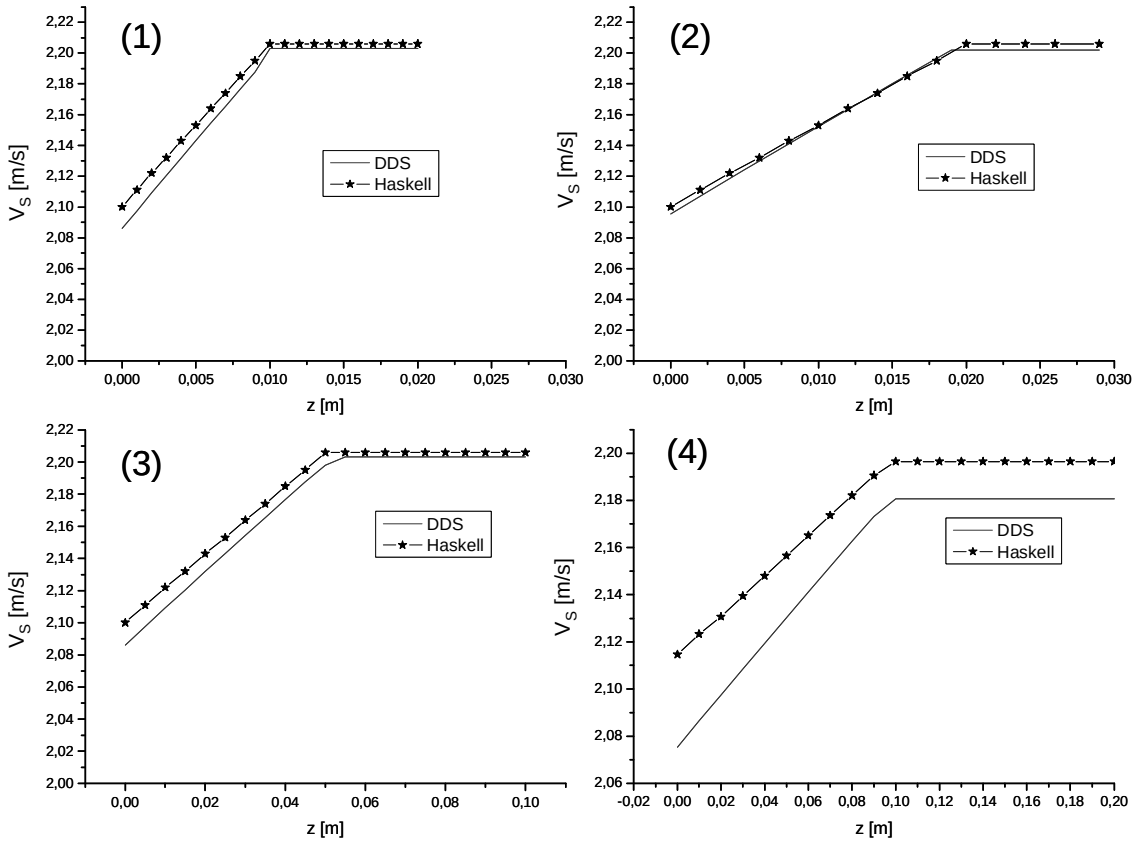

Figure IV.10 The transverse wave velocity profiles obtained via the DDS program for the synthetic data simulated by the Haskell's model and different depths of degradations.

In the Figures IV.10 the transversal waves velocities versus depth obtained for considered cases are presented. In the Chapter V.2 the results of the program operation and the discussion are presented.

IV.6 Point Cloud program

Solving inverse problems in order to reproduce the real structure of the material on the basis of the measured dispersion characteristics is loaded with ambiguity. One of the reason for this ambiguity are measuring inaccuracies and local material inhomogeneities, which result in spread of experimental dispersion curves. The source of ambiguity in the identification is also the used model, which usually in a simplified way describes the tested material. Significant may be the fact, that increase of the number of the model parameters, increase the possibility of the similar solution of identification can be achieved for a different combination of the parameters. This means that different sets of model parameters give similar dispersion characteristics, and thus may have similar value from the standpoint of the

error function. Alike problem of ambiguity is discussed in the literature in the field of seismic [Socco et al 2008, Orozco 2003].

It should be noted, that if the local optimization is used for the identification, exist a probability of finding a local minimum, often near a global minimum. In order to reduce the problem of ambiguity global algorithms can be used. However, their action is much slower without guarantee that the found minimum is a global minimum. The proposed conduct method is to present the results of optimization in the form of a set of solutions (cloud). The developed algorithm can be considered as a hybrid optimization method, because both the stochastic and the deterministic methods are used. The examples of identification with the use of hybrid methods are also practiced for other issues, for example in civil engineering to seek water sources [Kumer et al 2005]. In this Chapter a description of the developed procedure and its tests with synthetic data are shown.

IV.6.1 Concept of the algorithm

The block diagram of the procedure, which was named Point Cloud, is shown in the Figure IV.11. It is the expansion of the earlier described inversion algorithm, which use the Haskell's model and the local optimization procedure LSQ. The stages of the program operation are as follows:

Step I – setting of the program parameters, such as; the number of searched model parameters (number of unknowns - the rest of the model parameters must be precisely determined), the conditions of a single iteration end, the number of identification repetitions, the number of selected results and the limits of selection model parameters. The initial configuration has a crucial influence on the quality and duration of the procedure work. This particularly concerns to the number of optimization parameters.

Step II – loading of the group of experimental curves. As a result of applied spatial averaging in measurements a set of K experimental dispersion characteristics is obtained for each measuring point. Detailed information on this subject can be found in the Chapter III.1. Using in the identification process a set of characteristics rather than one resultant curve let to take into consideration the spread of the measured curves.

Step III – the first iteration of an outer loop involves performing N iterations of an inner loop for the first characteristic from the K set. At the beginning of each iteration of the inner loop, the start parameters of identification e are randomized from an approved range

(Monte Carlo sampling – stochastic approach), then ensues the identification by InvHaskLSQ program which is described in the Chapter IV.3 (LSQ – deterministic approach). Obtained results are recorded in a matrix of solution. The inner loop is repeated *N-times*, which gives *N* sets of searched parameters with assigned to each set the error of identification.

Step IV – execution of the outer loop for all the *K* characteristics, gaining that way *KN* sets of identification parameters with the corresponding errors.

Step V – maintaining the best solutions. At this stage, certain number of the worst solutions is rejected The fitting error (identification error) corresponding to the solution determines the rejection or acceptance of the solution. It should be emphasized that the criterion of the rejection can be defined in several ways, e.g.: rejection of the number of at least matched solutions or rejected all of these solutions, which fitting error exceeds the level set by the user. The algorithm can be also configured in a way that it will be working until a specified number of results (below established error) are obtained. The latter solution gives the best results but it is difficult to predict the duration of the identification.

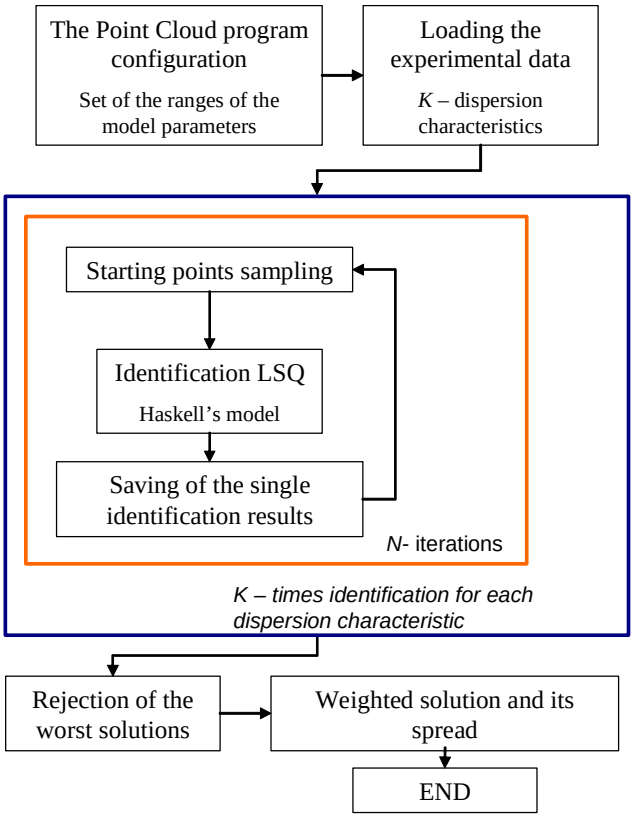

Figure IV.11 The flowchart of the Point Cloud procedure.

Step VI – determining an weighted mean value of the parameters and their spread value. The error of each inversion is the weight taken into account in the mean value

determination. The greater error causes the smaller influence of given solution on the averaged final result. In the Point Cloud program the algorithm for the determination the resultant velocity profile in the form of the weighted mean of the parameters $\overline{p}$ is introduced. The algorithm is according to the equation

$$\overline{p} = \sum_{i=1}^{n} (p_i g_i), \text{ where } g_i = \frac{\frac{1}{b_i}}{\sum_{i=1}^{n} \frac{1}{b_i}} \qquad \text{(IV.5)}$$

where g_i weights are the normalized errors of identification and b_i means fitting error for *i-th* iteration. The graphs in the Figure IV.12 show the Point Could program operation. The structure of the algorithm allows taking into account the spread of the experimental dispersion curves in the process of the inversion by the use of all the measurement curves. Randomly selected boot parameters reduce the risk that the algorithm takes a local minimum as the final solution. Selection of the best solutions only and taking into account their weights increase the accuracy and clarity of the final result.

IV.6.2 Program verification for the synthetic data

The examples of the results obtained for the Cloud Point program for a synthetic data is shown below. The test set consists five theoretical characteristics generated for different (but similar) parameters (see the Table IV-4).

An artificially imposed spread of the dispersion curves was made to give faithfully a real case, in which measured characteristics are also subjected to certain spread. The procedure made 300 identifications in 60 minutes[4]. All fits of the dispersion characteristics are shown in the Figure IV.12a. Taking into account the errors of particular identifications 50 best solutions were selected (Fig. IV.12b).

[4] All calculations in this work were performed on the same computer class AMD Turion(tm).64 X2 1.60 GHz and 2GB memory

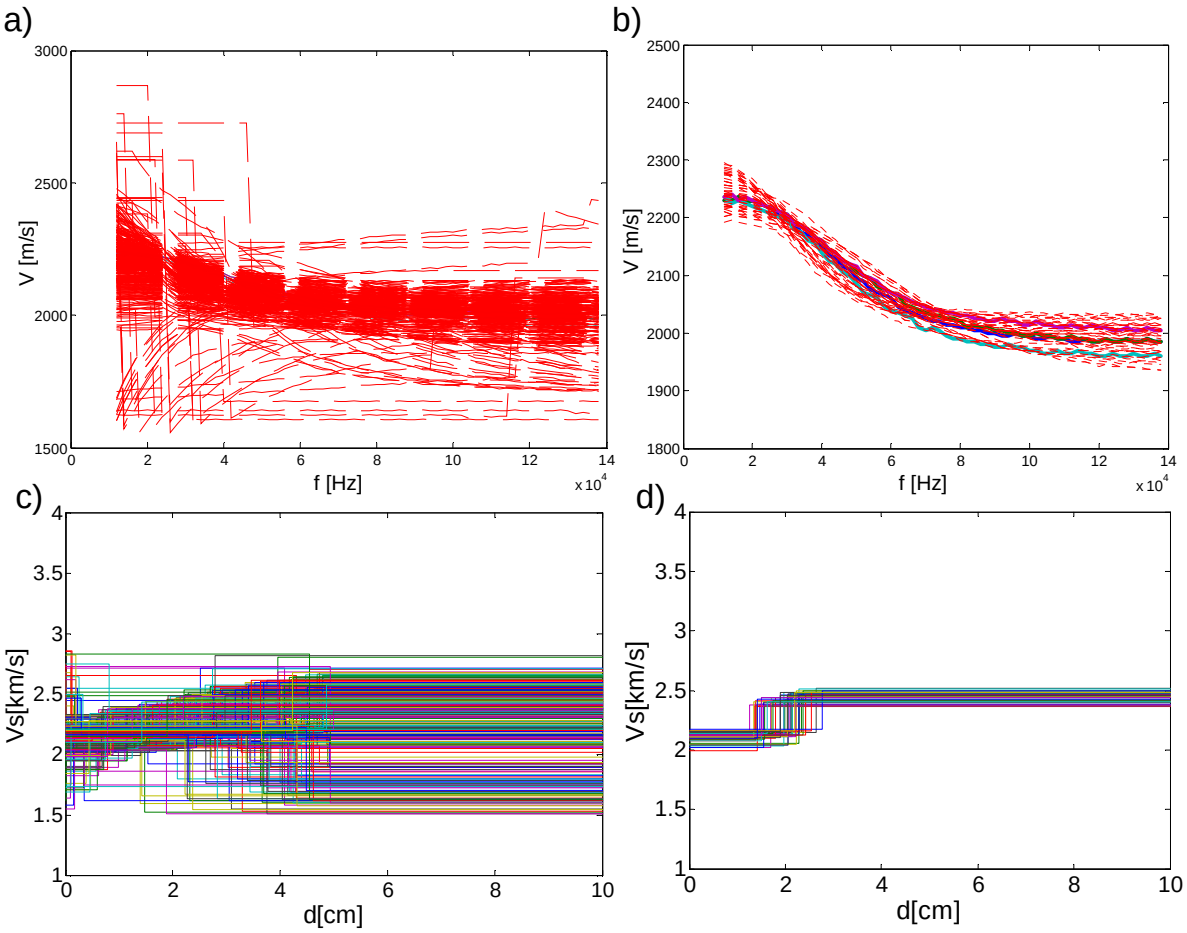

Figure IV.12 The results of the Cloud Point program for synthetic data and three-parameter search. a) the dispersion characteristics for *300* iterations, b) selected *50* best identifications, c) the profile $V_S(z)$ for *300* identifications, d) the profile $V_S(z)$ for *50* best inversions.

In the Figure IV.12c the three searched model parameters for all *300* identifications were shown in the form of the profile of transverse wave propagation velocity *Vs* versus depth. The Figure IV.12d presents profiles for the best solutions selected from all results. The selected solutions are used to calculate the weighted mean values of searched parameters according to the Equation IV.5. A single leap of the velocity V_S in presented profiles, results from the fact that two-layered model was applied. In the Table IV-4 the key parameters of the identification are given. The part of that table named "Synthetic data", contains the model parameters for which the synthetic curves were generated and the values of standard deviation for these parameters (the parameters were changed while generating set of test curves). The parameters of the second layer for all test curves were identical. In the part of the table "Identification" the bold font was used to mark the average values of determined structural parameters along with their standard deviation. Divergences between model values and identification results contain part of the table named "Differences". The smaller discrepancies

than the standard deviation for particular parameters obtained in this test confirms correctness of the developed program operation.

Table IV-4 The parameters and the results of identification obtained from Cloud Point program with three-parameter search.

	Synthetic data			Identification				Differences [%]	
Layer	1	σ [%]	2	1	σ [%]	2	σ [%]	1	2
Longitudinal velocity [m/s]	4280	1,3	4600	4300	-	4600	-	-	-
Transversal velocity [m/s]	2105	2,3	2425	**2115**	**2,0**	**2442**	**1,7**	0,5	0,7
Thickness [cm]	1,91	3,7	-	**1,90**	**20,5**	-	-	0,5	-
Density [kg/m^3]	1900	-	2200	1900	-	2200	-	-	-

In the process of identification, the smaller deviation that the deviation resulting from the spread of synthetic curves may result from the fact, that the program found more accurate solutions for the curves, which are closer to the average synthetic curve.

Table IV-5 The parameters and the results of identification obtained from Cloud Point program with seven parameters search.

	Synthetic data			Identification				Differences [%]	
Layer	1	σ [%]	2	1	σ [%]	2	σ [%]	1	2
Longitudinal velocity [m/s]	4280	1,3	4600	**4153**	**10,4**	**4300**	**9,5**	3,0	6,5
Transversal velocity [m/s]	2105	2,3	2425	**2120**	**2,4**	**2467**	**4,4**	0,7	1,7
Thickness [cm]	1,91	3,7	-	**1,85**	**23,8**	-	-	3,1	-
Density [kg/m^3]	1900	-	2200	**2098**	**7,8**	**2088**	**6,6**	10,4	5,1

A similar verification was performed for more complex model, in which all the seven parameters were assumed as unknown variables of optimization. The same set of the test curves and the identical program configuration (identical conditions for the termination, number of iterations etc.) were used as previously. The obtained results are shown in the Table IV-5. In this test the Cloud Point program needs 110 minutes to solve the task, which is almost twice longer than previously. The biggest differences in matching were with the value of density and velocity of longitudinal wave propagation, which confirms the conclusions presented in the Chapter II.1.5. In case of the others identification variables, i.e. the velocities of transverse wave propagation and thickness of layers, the obtained results are very similar to the results gained with identification with three-parameter model. It means that they are similar to theoretical values (to the parameters for synthetic curves).

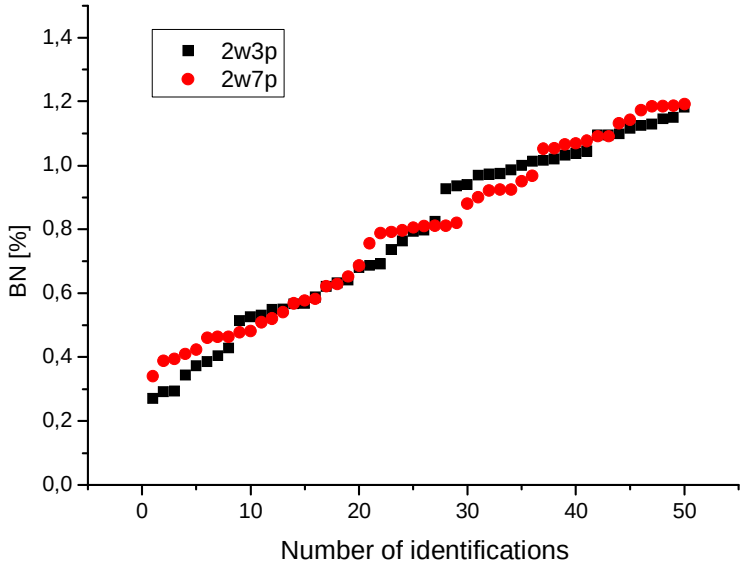

Figure IV.13 The values of standard error *BN* for the best selected results (*2w3p* – three-parameter search, *2w7p* – seven-parameter search).

In the Figure IV.13 the standard errors of identification *BN* (Eq. IV.2) for both analyzed cases (*2w3p – 3* unknowns, *2w7p – 7* unknowns) are presented. The compiled data show that the resulting errors are quite similar in both configurations. The smallest obtained errors are respectively *0,27%* for 2w3p, and *0,34%* for 2w7p. The average errors for selected solutions have identical value which is *0,83%*. On the basis of the error analysis can be concluded, that adding unknowns in the case of inversion with the synthetic curves, slightly affects the accuracy of identification, but significantly extends the time of computations.

IV.7 Identification of the structural parameters on the basis of reflection coefficient characteristic

The solution of the simplified two-parameters model of reflection phenomena can be obtained by the analytical calculations. The special nomogram (Fig. IV.14b) can be generated in the basis of the Equations II.75 and II.76. If the reflection coefficients R_1 and R_2 obtained for two different angles θ_1 and θ_2 are known (Fig. IV.14a) the porosity n and tortuosity α can be determined in the basis of this nomogram.

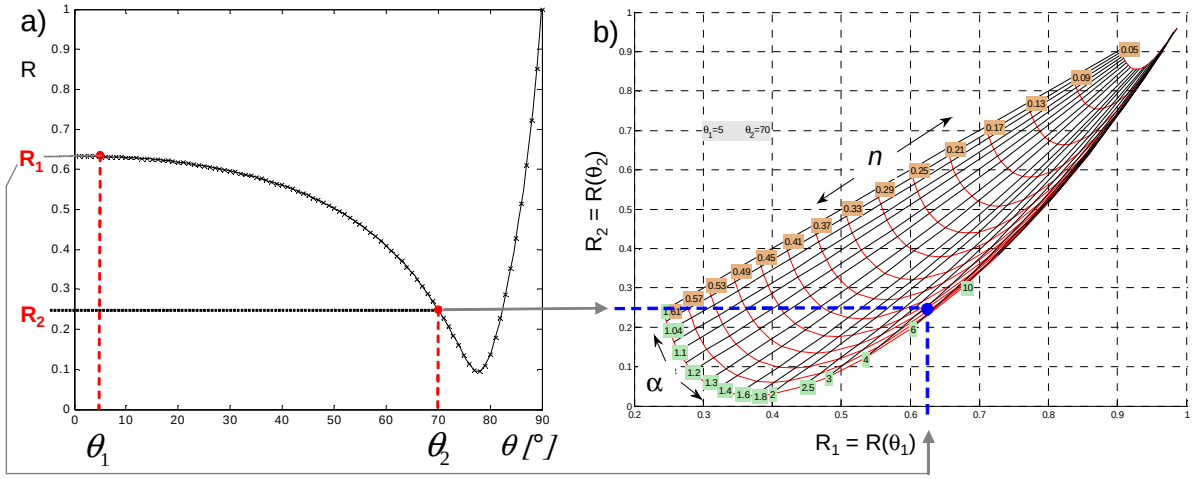

Figure IV.14 The determination of porosity and tortuosity on the basis of the characteristics of R (Fig. a) and the nomogram (Fig. b).

The solution of the reflectometric model with three and more parameters requires the use of the identification procedures. However, it is much simpler issue than the identification with the use of Haskell's model, since there is an analytical solution of the forward model. The use of the identification procedure in the case of two-parameter model increases the curability of the solution, because all characteristic (not two points only) is preceded.

IV.7.1 Concept of the algorithm

In the developed algorithm the model for the generation of the theoretical reflection coefficient characteristics (described in the Chapter II.2.1) is used. The porosity n, the permeability k_0 and the tortuosity α are the structural parameters in this model. Taking into

account the permeability in the model of $R(\theta)$ the model must be described in the following form:

$$R = \left| \frac{\bar{\gamma} \cdot K_0 \cdot l_2 - n \cdot \gamma \cdot \omega^2 \cdot \rho}{\bar{\gamma} \cdot K_0 \cdot l_2 + n \cdot \gamma \cdot \omega^2 \cdot \rho} \right| \tag{IV.6}$$

where:

$$\bar{\gamma} = \omega \sqrt{\left(\frac{\rho}{K_0} \right) \cdot \left(1 - \sin^2(\theta) \right)} \tag{IV.7}$$

$$\gamma = \omega \sqrt{\left(\frac{\rho}{K_0} \right) \cdot \left(\alpha - \sin^2(\theta) + \frac{i \cdot \eta \cdot n}{\rho \cdot k_0 \cdot \omega} \right)} \tag{IV.8}$$

$$l_2 = \left(\frac{\omega \cdot \rho}{K_0} \right) \cdot \left(\alpha + \frac{i \cdot \eta \cdot n}{\rho \cdot k_0 \cdot \omega} \right) \tag{IV.9}$$

where K_0 is the Bulk modulus of the air, ρ is the air density, η is the viscosity of the air, and ω is the circular frequency of the incident wave. The totally open structures are assumed in the model, and therefore the surface flow impedance is $T = 0$. The objective function C in the identification algorithm can be written as:

$$C(n, k_0, \alpha) = \sum_{\theta_{MIN}}^{\theta_{MAX}} \left| R_E(\theta) - R_T(\theta, n, k_0, \alpha) \right| \tag{IV.10}$$

where R_E is the experimental characteristic R_T is the theoretical characteristic.

The inversion in this task uses the SIMPLEX method (Ch. IV.1), which gives good results for the model of three parameters. The vertices of Simplex are three searched parameters. In the program the approach type Point Cloud (i.e. repeatedly calling inversion with randomized starting points) is used. This approach reduces the ambiguity of solutions in the case of lower porosity, for which the model is less sensitive. As the end of the search the criterion of the achievement of the adopted number of solutions matching error below a certain threshold is adopted. This criterion increase a duration of calculations, but very fast forward procedure operation allows to finish the calculations in a relatively short time which not exceeds a few minutes. After the specified number of acceptable iteration the weighted mean and standard deviation for the model parameters are calculated.

IV.7.2 Program verification for the synthetic data

The verification of the procedures for the identification of the structural parameters of the materials based on the reflection coefficient characteristics were carried out for the four synthetic characteristics. The ranges of the model parameters used to generate the theoretical data were chosen to cover the widest possible range of the porous material parameters encountered in the civil engineering. In the Figure IV.15 the example of the inversion for the reflection coefficient characteristics obtained for a high porosity material is shown. In the Table IV 6 the parameters of the synthetic data and the results of inversion obtained for two and three-parameter models are presented. The standard deviations and the errors of algorithms predictions are also shown. For the two-parameter model the porosity and the tortuosity were estimated. This model describes less physical effects (including more simplifications), but it gives a clear solution, regardless of the size of the material parameters.

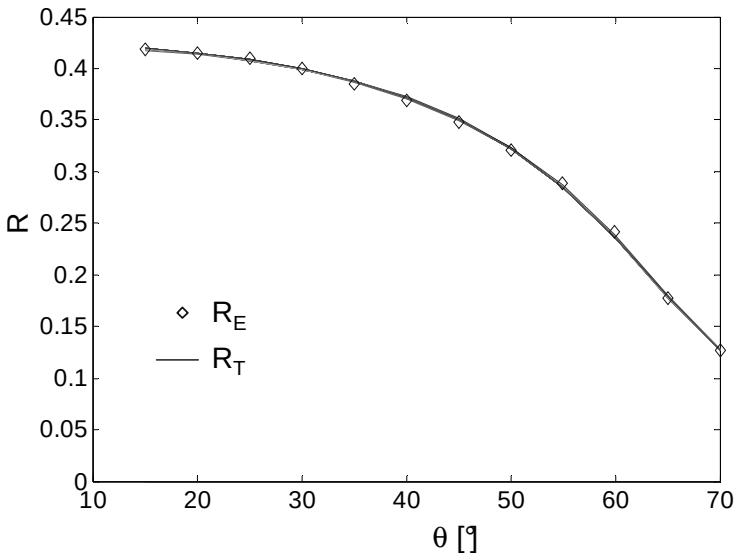

Figure IV.15 The example of the results based on the *R* and three-parameter model (R_E - experimental data, R_T – 20 best solutions).

In the case of the three-parameter model used the best results are obtained for the material with medium and high porosity. This confirms the observations presented in the Chapter II.2.2. For these cases relatively small standard deviation is obtained. In the case of low porosity only permeability was correctly identified (small standard deviation). The mean results obtained for the porosity and the tortuosity do not deviate significantly from the theoretical values but they have a very high standard deviation.

Table IV-6 The results of the material parameters identification on the basis of *R* characteristics and the synthetic data for two and three-parameter model.

Porosity	Model's parameter	Synthetic data	Two parameters model identification		Three parameters model identification		
		Value	Value	Difference [%]	Value	Standard deviation [%]	Difference [%]
Low	Porosity [%]	**20**	**20**	0	**51,7**	172	159
	Tortuosity	**5**	**5**	0,01	**5,13**	97	2,6
	Permeability (exponent)	**-16**	-	-	**-16,36**	2,7	2,3
Medium	Porosity [%]	**30**	**30**	0	**38,8**	30	29
	Tortuosity	**1,6**	**1,6**	0	**3,63**	134	127
	Permeability (exponent)	**-12**	**-**	**-**	**-12,10**	0,8	0,8
Medium	Porosity [%]	**50**	**50**	0	**50**	0,6	0,02
	Tortuosity	**2**	**2**	0	**2**	2	0,5
	Permeability (exponent)	**-11**	**-**	**-**	**-11**	0,09	<0,01
High	Porosity [%]	**80**	**80**	0	**80**	<10e-4	<10e-4
	Tortuosity	**1,1**	**1,1**	0	**1,1**	0,09	0,09
	Permeability (exponent)	**-9**	**-**	**-**	**-9**	0,01	0,01

IV.8 Conclusions

This chapter presents issues concerning the development of procedure for the material parameter estimation based on the experimental data. In order to do that, it was necessary to link theoretical models with optimization algorithms. The analysis, among others things, was referred to choice of optimization method for solving certain issues. The comparison of calculation time shows, that for the considered problem of the surface wave propagation modeling, single solution obtained via the SA algorithm, takes as much time as 60 solutions done by the LSQ procedure. So it seems to be more advantageous to use of repeatedly calling of the local optimization methods, than a single solution using the global algorithm, because the use of global algorithm do not give *100%* credible to find the correct solution. The conducted tests also show that increasing the number of the searched variables, the ambiguity of solution and significantly lengthen the computation time increase too. This is an argument for making an effort to reduce the number of unknowns searched in the inversion.

This chapter presents the author's procedure for calculation the depth of degradation based on Gibson's model, shortly named DDS. The verification carried out for synthetic data,

gave very promising results. Both in terms of estimating the depth of degradation as well as the parameters of considered medium.

The second author's program, whose principle of operation and verification are presented in this Chapter, is the Cloud Point program, which is used to estimate medium parameters using Haskell's model. The conducted tests showed very good compatibility between the parameters obtained in the identification process, with parameters for which test characteristics were generated. This is the first confirmation of correctness for the developed software. The use of the program showed, that in the future development of the Cloud Point program, a certain number of solution characterized by an adequately small error should rather be taken as a criterion for the termination of the identification process. Undoubtedly, a great advantage of the Cloud Point program over a simple identification approach is much less risk of the program termination in the wrong (local) minimum. Other advantage is the possibility to estimate accuracy of identification, on the basis of obtained spreads of searched parameters.

Second part of the Chapter presents the operation and verification of software developed to estimate the parameters of the porous material structure based on the characteristics of reflection coefficient. The program showed that the best results in the case of synthetic data are obtained for the medium and high porosities. That makes the utility of such approach in non-destructive testing is limited to the degenerated concretes and others building materials characterized by a higher porosity such as gas concrete.

Chapter V

Results and Discussion

The effects of the presented work are the measurement systems (SWMD and RMD) used for the material parameters determination. This parameters are important from the standpoint of the non-destructive and non-contact material diagnosis.

In the previous chapters the design and operation of measuring devices were described. Moreover, the features and the tests of developed software used to the material parameters identification are presented. In this Chapter the use of SWMD and RMD is presented for the selected materials. The measurements were performed on the tested materials (laboratory samples) with well-known properties, as well as on the real objects (measurements in the field). The collected data were used, inter alia, to the material parameters identification via the algorithms developed in the work. The measurements do not require the use of identification procedures are presented first. The examples of the identification let to assess the procedures used for the real materials. As the main assessment criterion the accuracy of identification was adopted, i.e. the results convergence with a data obtained by other reference methods, including the destructive measurements.

III.1 Description of the tested materials

The detailed description of the materials used for the measurements is placed below. In some cases of heterogeneous material, the developed software for the material parameters identification was used.

Plexi-Alu sample

For a comprehensive evaluation of the measuring system a special sample was prepared. This sample consists of a block of aluminum with Plexiglas plate glued on the top. This configuration allows us to simulate a multilayer system similar to the heterogeneous (layered) concrete. The sample consists "weak layer" (Plexiglas) with a thickness of *5.5 mm* and the "hard layer" (aluminum) with a thickness of *100 mm*. As glue the epoxy resin was used. The adhesive thickness was approximately *0.05 mm* and its influence of the wave's

dispersion can be neglected. In the Table V-1 the properties of the used materials of the sample are shown. The view of the sample is presented in the Figure V.1a.

Table V-1 The selected properties of the materials used to perform the Plexi-Alu sample.

Material	ρ [kg/m^3]	V_L [m/s]	V_T [m/s]	V_R [m/s]	d [mm]
Aluminum[5]	2800	6420	3104	2910	100
Plexiglas[6]	1180	2450	1320	-	5,5
Epoxy resin[7]	1158	2500	1112	-	~0,05

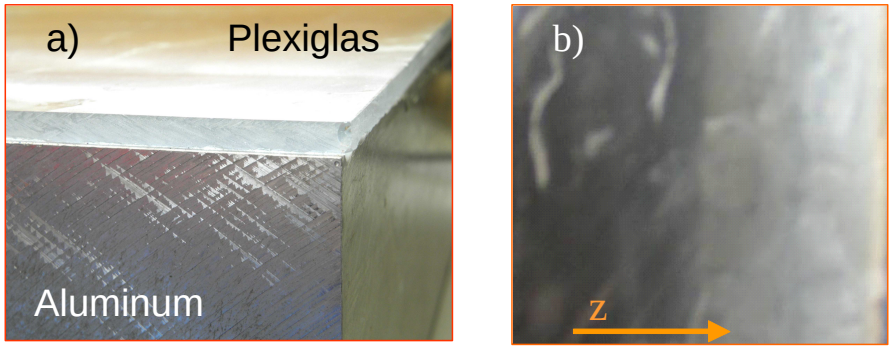

Figure V.1 The tested materials (photographs): a) Plexi-Alu sample, b) cement mortar (the arrow shows the direction of increasing porosity).

Cement mortar with variable porosity

The presented beam of cement mortar with dimensions of *50x20x7,4 cm* is a tested material with a relatively well-defined structure (Fig. V.1b). The sample has a varying porosity versus depth *z*. In order to obtain information about the density, porosity, and velocity as a function of the depth the cylindrical sample (diameter of 36.5 mm) was cut out form the beam. Then the sample was cut into discs with a thickness of *~16 mm*. Each of the discs, with some approximation, represents the material features from the depth from which it was extracted. The *2.5 mm* thick cutting blade was used to cut the disks, and the disks correspond to the depths of *8 mm*, *27 mm*, *45.5 mm* and *64 mm*. For each disc the longitudinal and the transverse wave velocity measurements were performed. For this measurement the echo method and the transducer with a center frequency of *0.5 MHz* where used. The density

[5] Measurements of longitudinal and transversal waves velocities are made in the laboratory on the same sample as the measurement of the surface wave propagation, the method of transition was used in the measurement with error of ~0.1%
[6] Measurements of longitudinal and transversal waves velocities are made in the laboratory on the same sample as the measurement of the surface wave propagation, the echo method was used in the measurement with error of ~0.1%
[7] Source of data. [Wu T.,. Liu Y. 1999]

and the porosity of each disk were also measured. In the Table V-2 the disks parameters are shown.

Table V-2 The parameters of the cement mortar beam of various porosity.

Parameter \ Disk	***1***	***2***	***3***	***4***
Thickness [mm]	16,5	16,0	16,1	16,1
V_P *[m/s]*	4459	4414	2875	2198
V_S *[m/s]*	2463	2270	1464	1073
υ	0,280	0,320	0,335	0,344
Mass [g] Saturated state	39,95	35,94	30,17	25,51
Mass [g] Dry state	36,62	31,73	21,76	14,43
Mass [g] under water	22,54	19,17	13,18	8,62
Volume [cm^3][8]	17,41	16,77	16,99	16,89
Density [g/cm^3][9]	2,295	2,143	1,775	1,510
Porosity [%]	19,1	25,1	49,6	66

Concrete beams prepared in the SENSO project

Much of the experimental presented in this work was carried out in the frame of the SENSO project ("Stratégie d'Evaluation Non destructive pour la Surveillance des Ouvrages en béton" - Strategy in the non-destructive testing for the concrete structures protection), funded by the French Government (*1996-1999*). The laboratory preparation of the concrete beams (samples) was one of the stages of the research in the project. The parameters of the samples were chosen to cover a wide range of the typical concretes used in civil engineering. The samples were prepared in the nine groups, which corresponds to the different types of concrete. Each group is consisted of the eleven identical samples, this gives a set of *99* concrete samples. The samples were fabricated as a homogeneous concrete without reinforcement. All samples of a group were cast at the same time and have the same dimensions of *12x25x50 cm*. In the Table V-3 the characteristics of all groups are given.

[8] calculated from the mass of displaced water
[9] calculated from the mass of displaced water

The SENSO project several teams from different laboratories were attended in order to study the same samples by different methods of the diagnostic. The following methods of NDT were used; the electrical resistivity method [Lataste et al 2009], the capacitance method, the GPR method [Dérobert et al 2009], infrared and acoustic methods (ultrasonic). The group of acoustic methods were used, among others, the measurements of propagation velocity by Impact-echo method, the method of transition, the surface wave propagation methods [Abraham et al 2009, Piwakowski et al 2009]. For the attenuation measurements the back scattering method [Garnier et al 2009] and the surface wave propagation method were used. The measurement data obtained from each method were then stocked and linked with the results of the destructive methods.

Table V-3 The characteristic of the groups of concrete samples.

Groupe	**G1**	**G2**	**G3**	**G3a**	**G4**	**G5**	**G6**	**G7**	**G8**
W/C ratio	0,31	0,47	0,57	0,59	0,57	0,57	0,58	0,63	0,90
Type of Aggregates	Round Siliceous					Crushed Siliceous	Crushed limestone	Round Siliceous	
Size of Aggregates [mm]	0-14	0-14	0-14	0-14	0-20	0-14	0-14	0-14	0-14
Porosity [%]	12,5	14,3	15,5		14,2	15,2	14,9	16,9	18,1
Young's modulus [GPa]	35,8	30,9	29,5		30,8	33,3	39,4	29,2	22,9
Compression strength [MPa]	77,2	55,6	45,8		46,8	53,3	44,5	44,3	27,5

The last stage of data processing in the SENSO project was the fusion of the stocked data [Ploix et al 2009], The data fusion was used to correlate the stocked data for the evaluation of such concrete parameters as; the Young's modulus, the compressive strength, the porosity and the water content. The detailed information about the SENSO project can be found in numerous publications [NDTC'09 2009].

The following are the results of measurements of the propagation velocity and the attenuation of surface waves obtained by the SWMD system are presented below. Moreover the data collected in the frame of SENSO project were used as a component of data library in the concrete parameters identification proceeded by the data fusion. The measurements of the ultrasonic wave propagation using the SWMD were made along and adjacent to the selected

measuring profile shown in the Figure V.2. The measurements were performed for varying degrees of water saturation. As shown in the Table V-3, the beams were characterized by a porosity range from *12.5 %* to *18.1 %* and by different water saturations, (*0%*, *40%*, *60%*, *80%*, and *100%*). This allows determine the influence of the porosity and the water presence in concrete on the attenuation and the velocity of surface wave. The water content in concrete is an important aspect, because the concrete structures are often used in the conditions different humidity. The common humidity for concretes contains from a few percent for objects subjected to strong sunlight for 100% humidity for underwater building. The influence of the size and type of aggregate used in the samples fabrication is also considered.

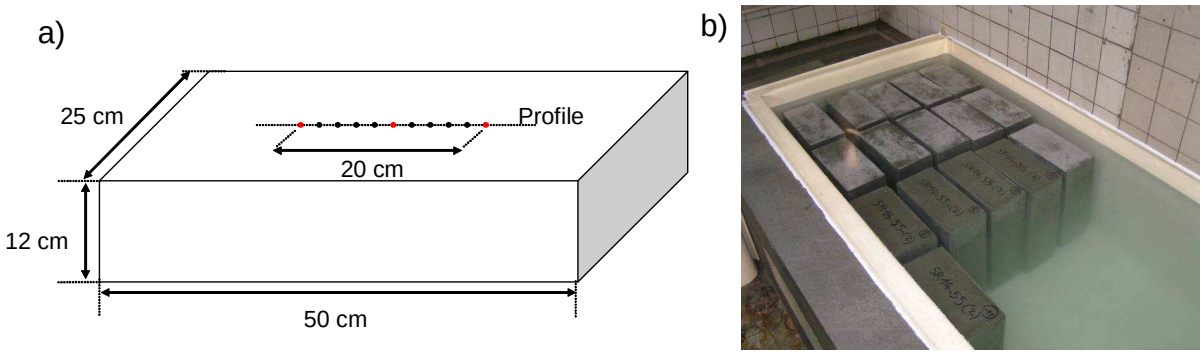

Figure V.2 The tested concrete beams: a) the beam size and location of the measurement profile, b) the beams subjected to total saturation by fresh water.

Port infrastructure in St. Nazaire (France)

The span of the transport dock in the port of St. Nazaire in France was one of the studied object in the SENSO project, as shown in the Figure V.3. Figure V.3 The concrete span of the transport ramp in the port of St-Nazaire, a) the zones of measurements are indicated by the arrows, b) the example of the SW propagation measurement realized by SWMD.

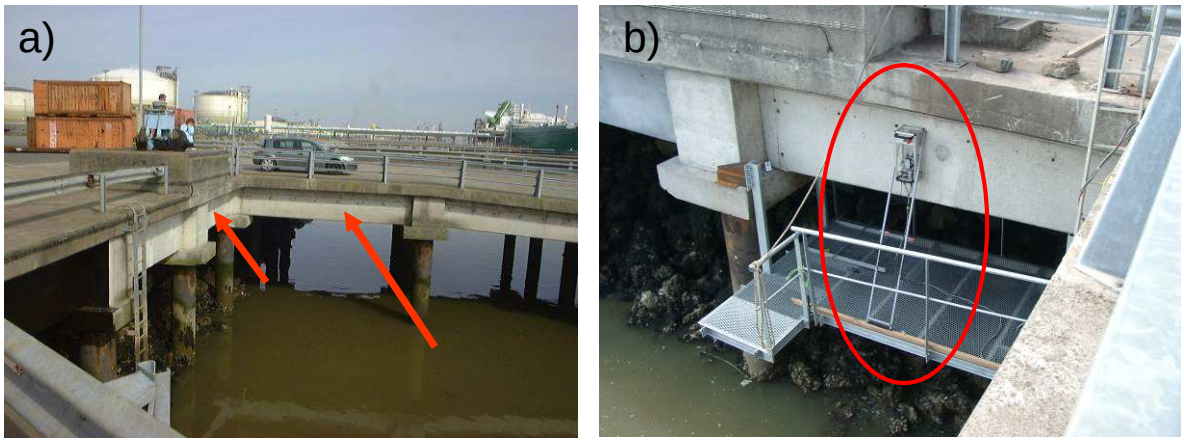

Figure V.3 The tested concrete beams: a) the beam size and location of the measurement profile, b) the beams subjected to total saturation by fresh water.

Built in 1992, the port infrastructure is exposed to salt water and in consequences to the process of degradation by the chlorine ions. One of the objectives of the research was to determine the depth of the chloride ion penetration and related to this the structural degradation. By these measurements the tests of the developed diagnostic tools for the real object were allowed. An important advantage of this place is the known profile of degradation of chlorine obtained on the basis of destructive testing. This means, that the comparison of the results of the measurements with the reference data is possible.

Gas concrete samples for the reflectometric measurements

As shown earlier, the reflectometric method works well for materials with relatively high porosity (greater than "healthy" concrete) at the moment. Because of this, the reflectometric method was tested on the gas concrete samples produced by three different companies (YTONG, Solbet, H+H). The gas concrete has a relatively high porosity and the permeability comparable with normal concrete, so from the standpoint of the gas and other substances transport (e.g. moisture) can be considered as a physical model of degraded concrete. In the Table V 4, the parameters of the tested gas concretes are presented.

Table V-4 Some of the gas concretes parameters used in the measurements.

	Density [kg/m^3]	**Volumetric porosity [%]**	**Permeability 10^{-13}m^2**
YTONG	563	76	2.92
SOLBET	560	77	2.70
H+H	550	72	8.49

V.2 Test results for the concrete beams

In the SENSO project the performances of the SWMD system were evaluated for the different types of concrete in different conditions. The obtained results of measurements were compared with the results form another methods used in the SENSO project. The range of measurements in the SENSO project is discussed in the Chapter V.1. The experience gained in this way was very useful for the hardware and software upgrades, which increase the infield measurements. The following section presents the results of the SW propagation measurements realized on the concrete samples described above. In the analysis of the results the influence of the structural parameters of medium on the wave velocity and attenuation were examined. During a few sessions of measurement almost *320* different samples were tested. Assuming that on each sample *11* measuring profiles were performed, and each profile consisted of *15* points almost *53,000* signals was recorded and processed.

Such a large number of measurements let us to average the results reasonably well. Moreover, the repeatability of measurements can be checked and the influence of the concrete heterogeneity on the final result can be reduced. The statement of the various factors influence on the measurement of the surface wave propagation was carried out. The considered factors were the type and the state of concrete and their exploitation process. The values of the apparent velocity of SW and the value of attenuation obtained experimentally where used (Chapter III.1.2).

Effect of water content on the wave propagation velocity

In the Figure V.4a the changes of the apparent velocity of the SW V_A as a function of the volumetric water content W in the concretes of different porosity is presented. In this case the volumetric water content is in the range from *0%* to *16%* which corresponds to the degree of saturation from *0%* to *100%*. It should be noted that the saturation value of *0%* and *100%* are the approximated values. Such saturations are impossible to achieve because of e.g. the presence of the closed pores.

The results for the samples from the group G1 are different from the others. This can by explained by the low porosity ($P = 12.49\%$) of this type of concrete, and in consequences the difficulties in the water saturation. For the curves with the water content above ~4% the linear tendency is observed. For the value $W<4\%$ the influence of capillary effects increases and causes the change of the curves tendency [Villain et al 2009].

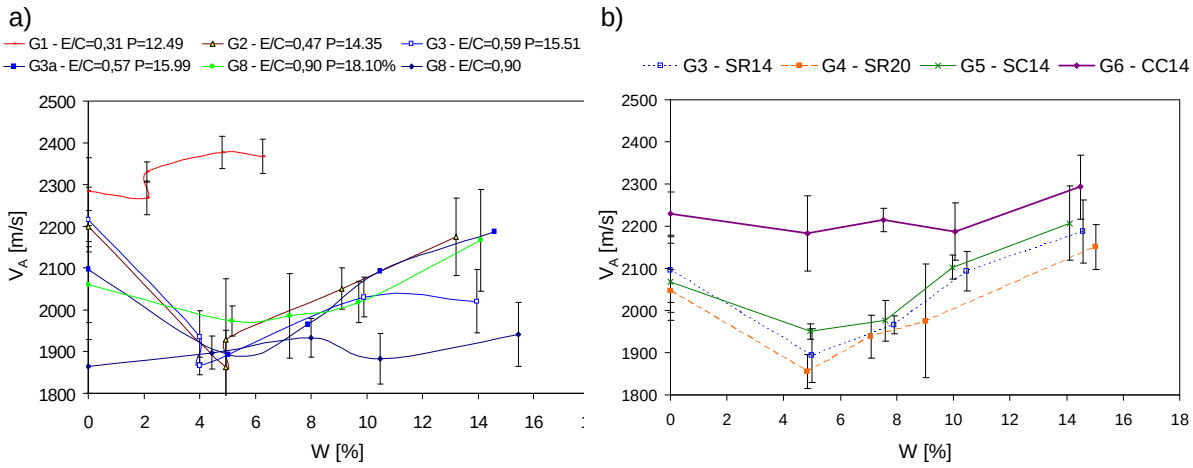

Figure V.4 The velocity V_A in the concrete as a function of water content W depending on the porosity P (a) and the type of the used aggregate (b).

In the Figure V.4b the changes of V_A velocity as a function of the volumetric water content in the concrete of almost the same porosity and the identical type and size of aggregates are shown.

In the basis of the results presented above three groups of concrete (G3, G4, G5) show very similar tendencies of $V_A(W)$ and only in the case of the concrete based on the limestone aggregate (G6) the highest velocities and the lowest saturation influence are observed (the highest located curve). The comparison of the results for the groups G3 and G4, which differ only in the aggregate size, (*14 mm* and *20 mm* respectively) only a slight increase in velocity (about 3%) in the case of finer aggregate can be seen.

Effect of porosity on the wave propagation velocities

The porosity influence on the velocity of surface wave propagation was compared for the various degrees of the water saturation *S*. The groups of samples based on the same type and size of aggregates was chosen to this comparison. For the two extreme states of saturation (Fig. V.5a) i.e. dry concrete (S = 0%) and concrete completely saturated (S = 100%) the decrease in velocity with increasing porosity is observed. The comparison of the plotted trend lines shows only a small difference between these two extreme degrees of saturation.

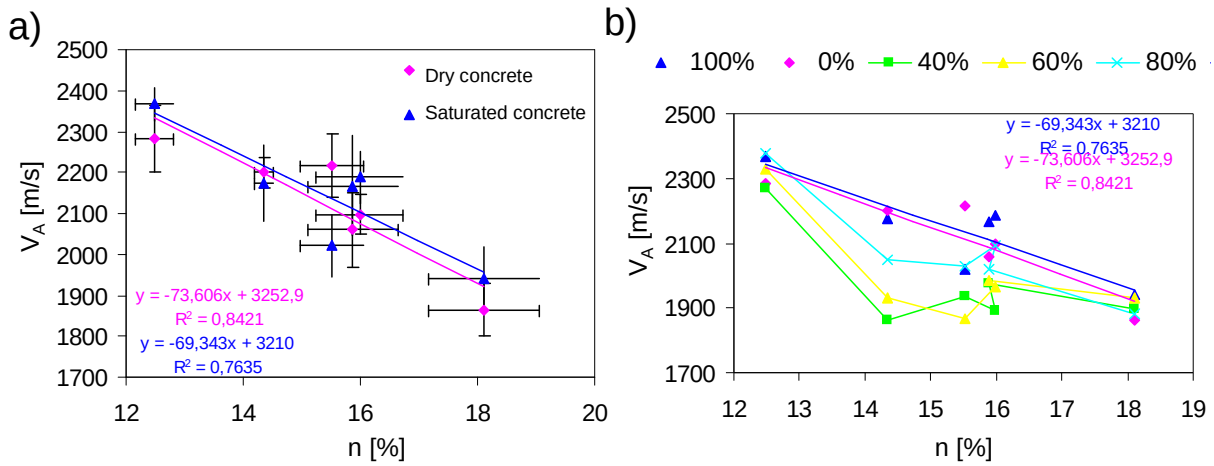

Figure V.5 The porosity influence on the velocity of surface wave propagation for the beams of the groups G1, G2, G3, G3A, G7, G8, a) at the saturations of 0% and 100% only, b) at all tested stages of saturation.

In the Figure V.5b the relation between the wave velocity and the porosity is shown for the partially saturated concretes. Generally, the decrease of the velocity with increasing porosity is observed but the characteristic are much more irregular especially in the middle range of porosities. To minimize the ambiguity of the relation between the velocity and the porosity caused by the humidity the one of method of humidity determination (e.i. the electrical method) can by used.

Influence of size and shape of the aggregate

The collected data allowed assessing the influence of some parameters of the aggregate used in production of concrete on the velocity of surface wave propagation,. The results presented below were characterized by spread from 3% to 6%, it means, greater than the influence of particular factors on velocity V_A (for the clarity of charts presentation the error bars are hidden). The Figure V.6a shows the dependence between the velocity of surface waves and the size of aggregate. The analysis shows a slight decrease in the velocity with an increase in the size of aggregate. Almost the same tendency is seen at all levels of water saturation. Larger aggregate causes a decrease in velocity of about *0,5-1%*.

Analyzing the influence of a type of used aggregate, it was observed that the concrete made with limestone aggregate has a higher wave velocity than the concrete made with siliceous aggregate. Moreover, it was noticed that the study of surface wave propagation is less sensitive to the moisture content in case of the concretes containing limestone aggregate (Fig. V.6b). Maximum differences in velocity caused by a different aggregates reach *11%* for partial saturation (*40%* and *60%*). Another considered factor was a study of influence of

aggregate shape on SW velocity. The Figure V.6c shows, that the influence of the aggregate shape on the velocity of surface waves is negligible and does not exceed 3%. In real conditions information about the aggregate's type, size and shape used in the production of concrete are relatively easy to determine. If there is no detailed documentation containing this type of data, it suffices to knock off or grind down a small fragment of the tested construction.

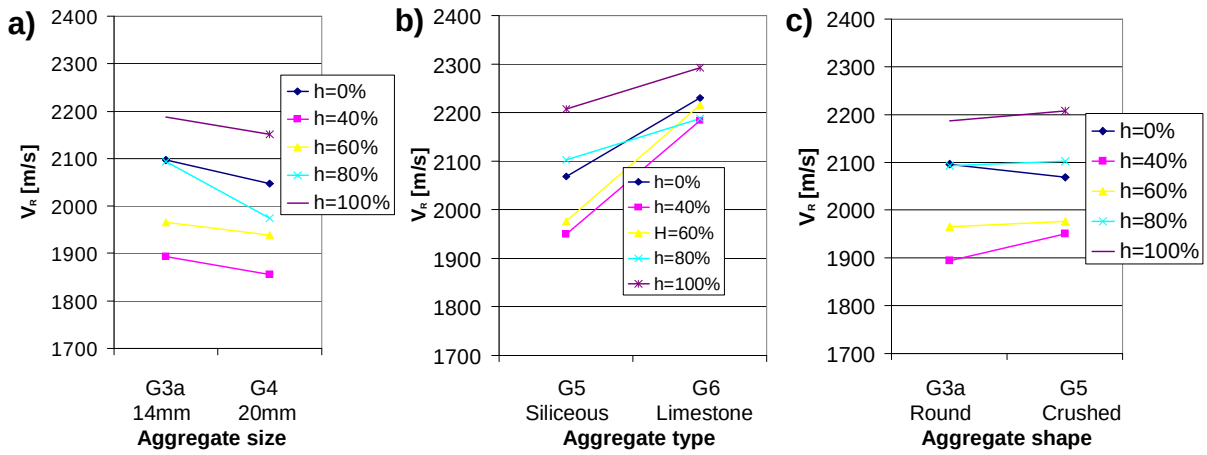

Figure V.6 The aggregates parameters influence on the surface wave propagation velocity for the case of different of; a) size of aggregate, b) type of aggregate, c) shape of aggregate.

Velocity relates to mechanical parameters of concrete

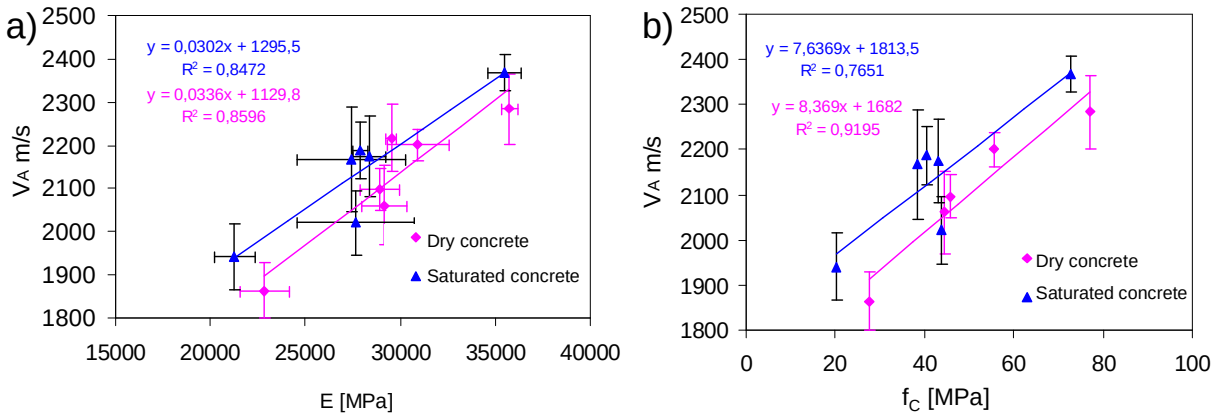

Figure V.7 The SW velocity V_A relates to mechanical parameters of concrete a) for Young's modulus, b) for compressive strenght.

The summary of the velocity of surface waves related to the Young's modulus E (Fig. V.7a) and the compression strength f_C (Fig. V.7b) is presented below. The groups of concrete of the same type of aggregate (groups G1, G2, G3, G3a, G7, G8) but in two extreme states of water saturation were selected for this analysis. In both cases (E and f_C) a quasi linear increase

of the parameter value with increase of the velocity V_A is observed. At the same time, it should be noticed that dry concretes have the higher parameter value of E and f_C at the same velocity than the saturated concretes. This shows that the saturation may have a significant influence in determining mechanical parameters of the concrete, based on the velocity of surface wave propagation.

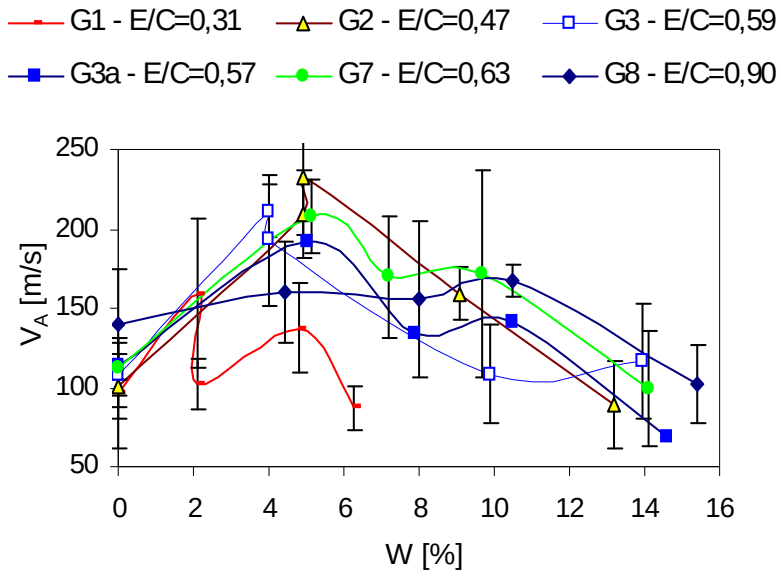

Figure V.8 The attenuation depending on the volumetric water content for different groups of concrete.

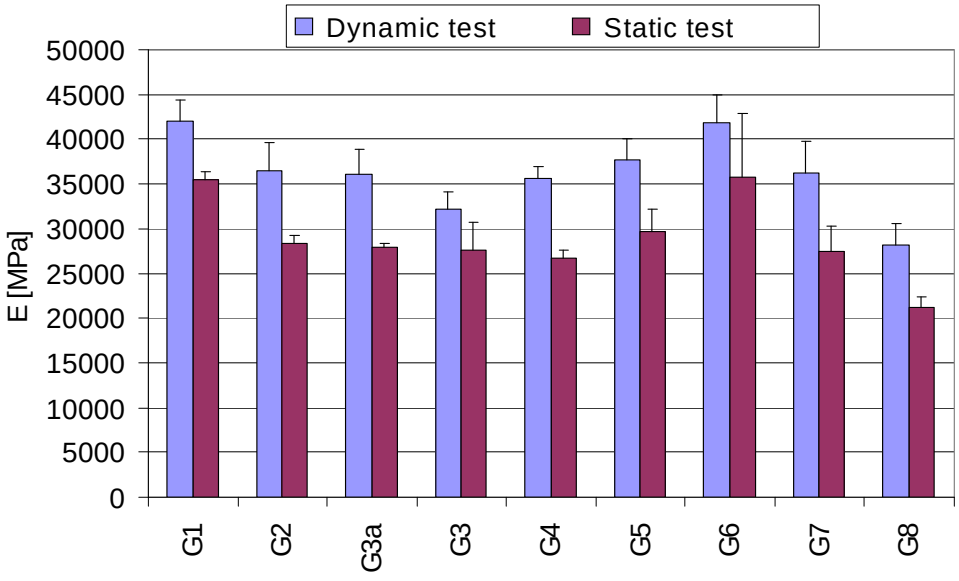

Figure V.9 The values of Young's modules for different groups of concrete beams (saturated concrete).

In the Figure V.8 the surface wave attenuation as a function of changes of water saturation for concretes with different water to cement ratio (W/C), and in consequence of different porosity was shown. It can be easily noticed, that for dry concrete and completely

saturated, the attenuation takes very similar values. The materials partially saturated show slightly higher attenuations. During processing of the recorded signals, the repeatability of velocity value (relatively small spread) was observed. On the other hand the obtained attenuation characteristics are less repeatable and show no noticeable regularity. Drawing a conclusion that on existing stage of measurement method development and signals processing, the use of information contained in attenuation is difficult because of the interpretation problems and unreliability.

The limited size of the samples tested in laboratory, allowed to measure the velocity of longitudinal waves using transmission method. Combined with known density it allowed determining the value of Young's modulus *E* according to the equation I.2. In the Figure V.9 the comparison of the value for Young's modulus determined by destructive methods (static measurement), and calculated in the basis of ultrasonic methods (dynamic measurement) for all tested groups of concrete samples is presented. The obtained results show very good correlation between non-destructive and destructive measurements. Comparing the results we observe that all the values of dynamic measurements are higher of about *20%* than the static measurements. Similar situation was observed in the previous research concerning values of Young's modulus determining on the basis of ultrasonic measurements [Popovics 1995]. The collected results compose a knowledge base, which can be used, inter alia, as a source of data of concretes and in the procedures of identification to restrict the range of changes of particular parameters. The obtained conclusions can be also used as a correction of results in parametric identification, which does not include, for example the humidity.

V.3 Results of identification based on the surface wave propagation measurements

The ultimate purpose of the developed system of measurements is the identification of material parameters using experimental data. The results of the identification can be useful arguments for diagnostic decisions. The solution of the inverse problem, which is a component of this identification, was carried out for the measurements data performed both in the laboratory and in the field. The materials, for which the identification was taken, are described in the previous subsection. In the case of measurements of surface wave propagation, the identification result is generally the velocity profile of transverse wave as a function of depth. If for tested material is also known the value of density and velocity of

longitudinal wave propagation (for many materials such as rocks, there is a relation between the velocities of longitudinal and transverse wave), then it is possible to estimate the Poisson's ratio ν (Eq. I.1) and the Young's modulus E (Eq. I.2).

The laboratory measurements of the sample Plexi-Alu

Dispersion characteristics obtained from the measurements of two layered sample Plexi-Alu was used to assess the procedures of identification. Low attenuation and homogeneous structure of layers in the sample, allow obtaining strong signals of high signal to noise ratio. It is advantageous from the standpoint of their processing and identification of material parameters. Program DDS with implemented Gibson's model and the Cloud Point program with Haskell's model were used for identification. The case of Plexi-Alu structure is not so good example for the application of the Gibson's model. The reason is that, the tested sample consists of two layers of very different properties. Whereas in the model the continuous change of properties is assumed.

Table V-5 The results of identification using the DDS program for the Plexi-Alu sample.

	First layer thickness (degradation) *d [mm]*	Transversal wave velocity at the surface V_{S0} *[m/s]*	Poisson's ratio υ	Heterogeneity coefficient m
Reference data	5,5	1320	Plexi - 0,30 Alu - 0,35	-
Identification	8,4	1266	0,5	71,72
Differences	56%	5%	43%	-

The results obtained from the DDS program are shown in the Table V.5. The reference data come from the measurements made by others methods. Comparing the results of identification with the reference values can be seen, that relatively precisely was set only the velocity of transverse wave in the top layer V_{S0}. Whereas the value of the degradation depth (in that case it should correspond to the thickness of Plexi layer) and the Poisson's ratio differ significantly from the real values. Despite the obvious differences of the model and the macrostructure of the sample, in that case the identification was carried out to establish the predictions of the DDS program. And also, to compare the results of both programs used (DDS and Cloud Point). The relatively large leap of parameters results in very high heterogeneity coefficient, which in effect can be the reason for substantial error of the degradation depth evaluation. Despite the obvious discrepancies, the results show that the

developed procedure provides sensible order of magnitude for some of searched parameters. The same experimental dispersion characteristics obtained for the sample Plexi-Alu, was used to identify the parameters using the Cloud Point program. The macrostructure in the form of one layer on a half-space was adopted in the model. The searched parameters were: the transversal wave velocity in the first layer, the thickness of the first layer and the of transversal wave velocity in the second layer (half-space). The other parameters of the system were taken as known and equal to the reference values. The obtained results are shown in the Table V-6.

Table V-6 The results of identification using the Cloud Point program for the Plexi-Alu sample.

	Reference data				Identification results					
Layer	V_p	V_s	ρ	d	V_s	Differences	σ	d	Differences	σ
	[m/s]	[m/s]	[kg/m^3]	[mm]	[m/s]	[%]	[%]	[mm]	[%]	[%]
I (Plexi)	2450	**1320**	1180	**5,5**	**1394**	5,6	0,9	**6,0**	9,1	1,5
II (Alu)	6420	**3104**	2800	100	**3191**	2,6	4,2	-	-	

The Cloud Point program made *500* iterations. The level of standard identification error with the *BN < 0,5%* (Eq. IV.2) was chosen as a preliminary criterion for the best result choice. The pre-established threshold *BN* was not acquired by any identification. Therefore, the characteristics of the distribution of *BN* errors was used (Fig. V.10) to choice *23* results characterizing by the least errors (in the initial, linear range of *BN* curve).

The Table V-6 also contains the differences between the obtained parameter values and the corresponding reference data. As well as the standard deviation σ expressed as a percentage. The results of the Cloud Point program show, significantly better compatibility in relation to the results obtained with the DDS program. The evidences of it are considerably lower values of differences and standard deviations for particular parameters. In a case of identification V_S for the first layer and its thickness *d*, the higher values of differences than standard deviation were observed. That may be caused by a systematic measurement error (e.g. inaccurately putting of the SWMD on the tested surface) or insufficiently precisely matched of the parameters taken as known (layers densities).

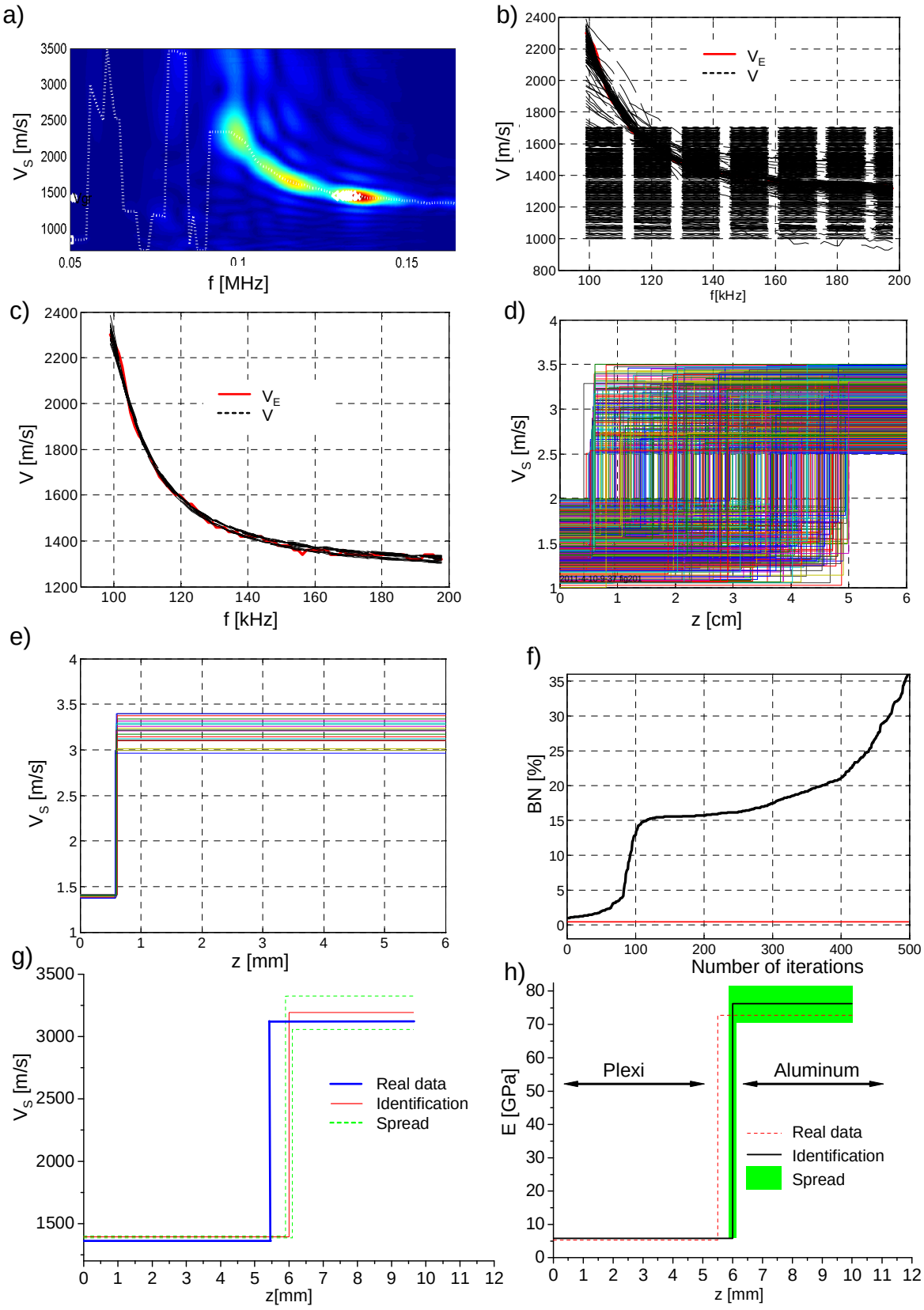

Figure V.10 The stages of the parameter identification realized for the Plexi-Alu sample (described in the text).

The stages of the identification process realized by the Cloud Point program are shown in the Figure V.10, and their results are:

a) *V-f* map obtained from the experimental data,

b) Modelling of the dispersion characteristics *V(f)* for all (*500*) identifications along with the experimental characteristics $V_E(f)$,

c) *23* best fitted *V(f)* to $V_E(f)$,

d) The transverse velocity profiles as a function of depth $V_S(z)$ for all identifications,

e) Profiles for the best selected identifications,

f) The *BN* value as a function of number of identifications (red line indicate the acceptance threshold of *0.5%*),

g) the average profile $V_S(z)$ with the spread and the reference real profile,

h) the Young's modulus profile versus depth *E(z)* determined on the basis $V_S(z)$.

The vertical sections of the characteristics from the Figures d, e, g and h are used only to show the layer borders of the system. Using the previously given equation (I.1 and I.2) and the values of the longitudinal velocity and density, the values of Young's modulus for particular layers were estimated. The obtained values are similar to the reference data of tested sample, as shown in the Figure V.10h. Analyzing the BN course (Fig.V.10f) is shown that about 80 iterations is characterized by a relatively small error, and then follows irregular growth of the BN value. Such changes of BN curve can be an indicator of how to choose the acceptance threshold. Establishing the criteria of optimal configuration of the Cloud Point program, requires further work.

Laboratory measurements of the cement mortar sample

The measurements of heterogeneous cement mortar sample carried out with the surface wave method showed, that the only opportunity to observe the presence of waves, gives the test conducted on the side of the samples of higher density. Thus, this case is unusual in comparison with the degraded materials, because for the tested mortar, mechanical parameters fall along with the depth. The advantage of this example is that, the change of the property follows in a continuous manner. Attempts to identify the structural parameters using the Haskell's model did not give the correct results. It is connected with the numerical difficulties of finding the root of dispersion equation in the Haskell's model. The developed

numerical procedure for solving the Haskell's model turned out to be unreliable in a case of material in which there is the sudden decrease of parameters value with depth.

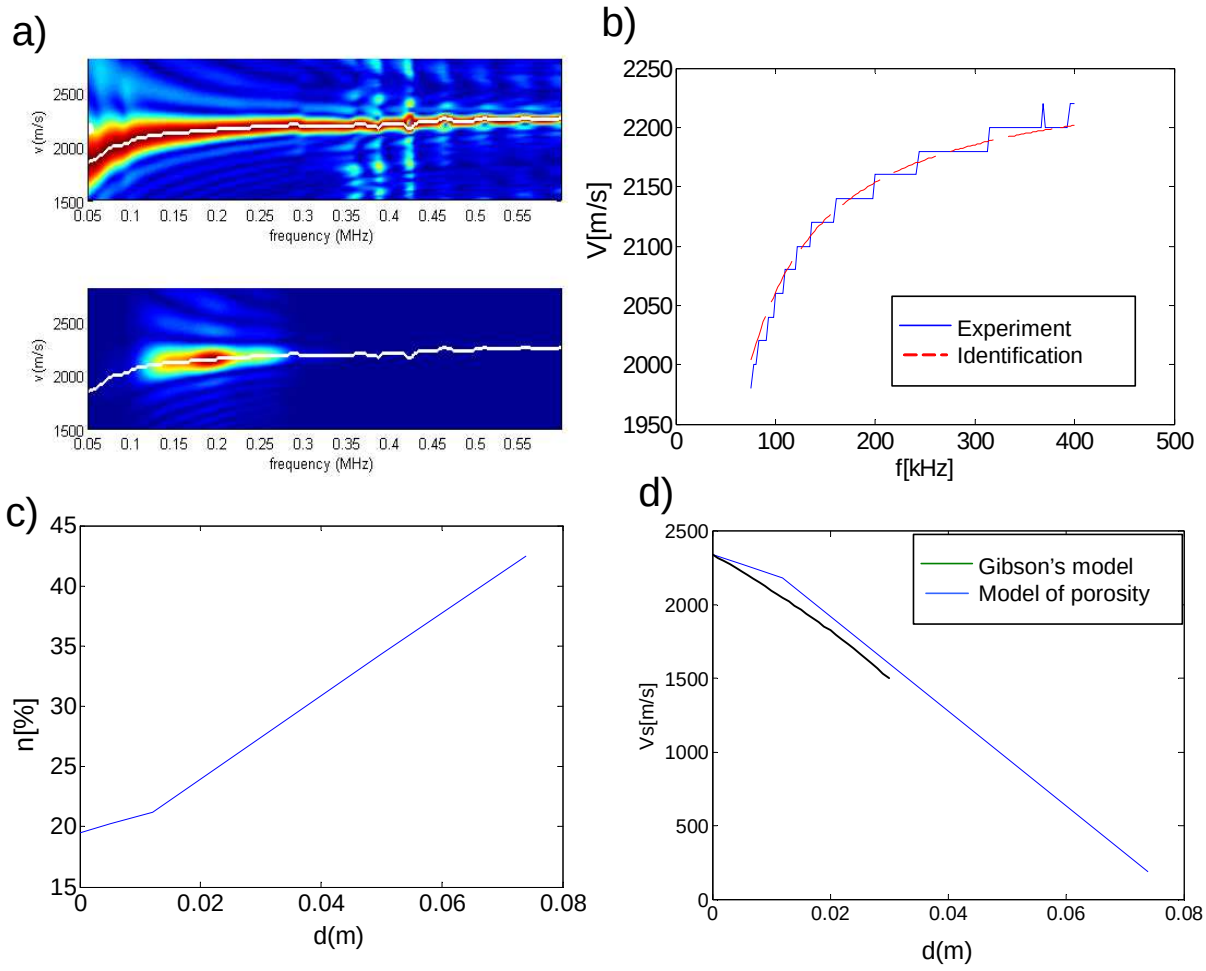

Figure V.11 The data and results of parameter identification of cement mortar sample with the use of the Gibson's model, a) one of the *V-f* experimental map (shown in different sensitivity scale), b) the dispersion characteristics obtained by the measurements and identification, c) the distribution of porosity as a function of depth, d) the profile of transverse wave velocity obtained by the identification and by the model of porosity.

In this case, much better results were obtained while using the Gibson's model. In the identification the basic program InvGibLSQ was used to solve the inverse problem. Using in that case the DDS procedure is unjustified, because in the tested material the change of parameters occurs in the full depth. Therefore, there is no such depth, which could be acknowledged as the limit of degradation. The Figure V.11a shows experimental dispersion characteristics determined for tested sample. In the procedure of identification the modelling dispersion characteristics was matched to the experimental characteristics using the Gibson's model. The result of that match is shown in the Figure V.11b.

Using the information about the porosity *n* obtained from destructive tests (Fig. V.11c) combined with a model describing the dependence of the velocity of transversal wave V_S and porosity of the equation $V_S=V_{S0}(1-bn)$ (*b* is constant) [Goueygou and al. 2009a] the velocity profile of transverse wave propagation versus depth was obtained. That profile correlates very well with the profile obtained by identification. Both profiles are shown in the Figure V.11d. The shown profile of velocity obtained by the Gibson's model reaches only to depth of *~3 cm*. The limitation is the largest wavelength which results from lower frequency of modeling dispersion characteristics (*70 kHz*).

Field measurements in St.Nazaire

The measurements carried out on the concrete elements of port ramp in St.Nazaire (France) and identification of material parameters based on these measurements, is a one of the most important fragment of the experimental part of this thesis in a field research. The presented example is a complex test of the system (starting from realization of the measurements and data processing, and ending on the process of parametric identification) on a real object. In addition, this concrete was independently tested in a destructive manner, thanks to that, the more important parameters including the depth of "degradation" are known. Thus it is possible to compare the results of identification with the reference data. The main objectives of the research were to determine the depth of degradation caused by the disadvantageous action of chloride ions, and also establish the profile of transversal wave propagation versus depth and estimates the degree of degradation. The Equation V.1 was used to determine the degree of degradation *SD*.

$$SD = \frac{V_{S2} - V_{S1}}{V_{S2}} x100\% \qquad \text{(V.1)}$$

where V_{S1} and V_{S2} indicate the velocity of transversal wave, respectively at the surface of degraded layer and in the deep material. The process of solving the inverse problem was carried out with the use of DDS program and the Cloud Point program. It means, that using both the Gibson's and the Haskell's models. In the configuration of the Haskell's model was adopted a system of two layers and for both layers the velocities of transversal waves and densities were established as constants. Obtained results are given in the Table V-7.

Table V-7 The results of identification for the concrete from St. Nazaire.

Result	Degradation depth d [mm]	Transversal wave velocity at the surface V_{S1} [m/s]	Transversal wave velocity in deep V_{S2} [m/s]	Degradation degree [%]	BN [%]
Real	36-40	2530	No data	No data	-
DDS identification	32	2529	2830	10,6	0,96
Cloud Point identification	23,7	2632	2799	6,0	2,24

In the Figure V.12a is shown the result of the destructive testing of the distribution of the content of chloride ions versus depth with marked critical level [SENSO 2009]. The depth was assumed as the end of the "degraded" area, for which the content of chloride ions falls below the critical level. The Figure V.12b shows measured characteristics of surface waves attenuation. The two shown curves are the average values for two methods of averaging. In one case, the average attenuation characteristics, is calculated from the attenuations of all time signals. In the other case, attenuation is calculated from the averaged time signals. The selected reliable range indicates the area of good signal noise ratio. In this scope, the two curves overlap and the attenuation characteristics may be described by linear dependence (Eq, II.38). The tested concrete is characterized by high level of attenuation reaching 150 dB/m, which gives the average coefficient *Q=16.6*. In such situation, it is appropriate to take into account the influence of attenuation into dispersion according to the approach proposed in the Chapter II.1.7. In the Figure V.12c the experimental dispersion characteristics V_E is shown and the characteristic of the dispersion caused only by structure macrohomogeneity V. This curve is obtained after taking into consideration the influence of attenuation according to approximation proposed in the Chapter II.1.7. In the Figure V.12d is shown the reconstructed profile of transversal wave velocity as a function of depth obtained from the DDS program (the Gibson's model). Figure V.12e shows the profile of transversal wave velocity V_S obtained with the use of the Cloud Point program (the Haskell's model). The values of the Young's modulus E versus depth (Fig.V.12f) were calculated with use the longitudinal wave velocity density obtained by other measurements (available in the project SENSO).

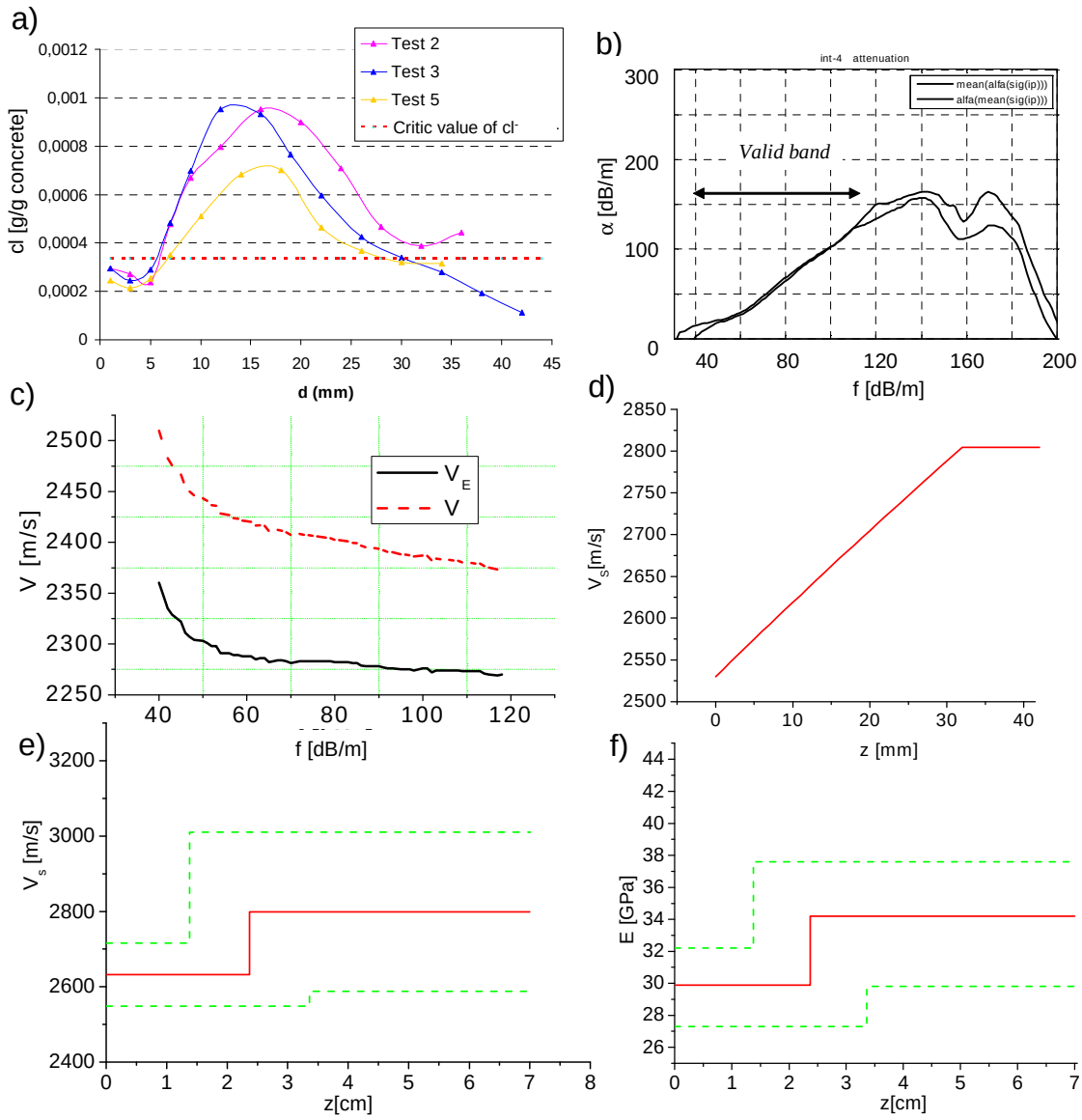

Figure V.12 The results of research for the concrete of port ramp in St.Nazaire; a) the distribution of the chloride ions content, b) the attenuation characteristics, c) the dispersion characteristics with and without an attenuation effect, d) the velocity profile Vs determined by the DDS program, e) the velocity profile Vs determined by the Cloud Point program (green dotted lines indicate the limits of standard deviation, red solid line indicates the average parameter value)..

Comparing the obtained results (Table V-7) can be stated, that the results acquired with the use of the DDS program are more similar to real values than the results obtained by the Cloud Point program. It should be noticed, that in this case measured material is characterized by continuous change of parameters versus depth (which may provide continuous rather than sudden concentration change of chloride ions). Such structure is closer to the description of the Gibson's model rather than the Haskell's. Identification of the transverse wave velocity in the top layer it is also better when using the DDS program. The

theoretical model in the Cloud Point program was configured in the two layer system. As the unknowns were assumed all seven parameters, such as the density, the velocity of longitudinal and transverse wave propagation for both layers, and the thickness of the top layer. The results of identification by the Cloud Point program were charged with standard deviation, which were respectively *3,2%*, *7,5%* and *41,8%* for the identification of velocity V_{S1}, V_{S2} and depth *d*. The two layered structure of the Haskell's model is less adequate to the considered material case, than the structure with a continuous change of parameters (like in the Gibson's model). It makes that more identification discrepancies of parameters may occur when the Cloud Point program is used, rather than the DDS.

V.1 Results of identification based on the characteristics of reflection coefficient

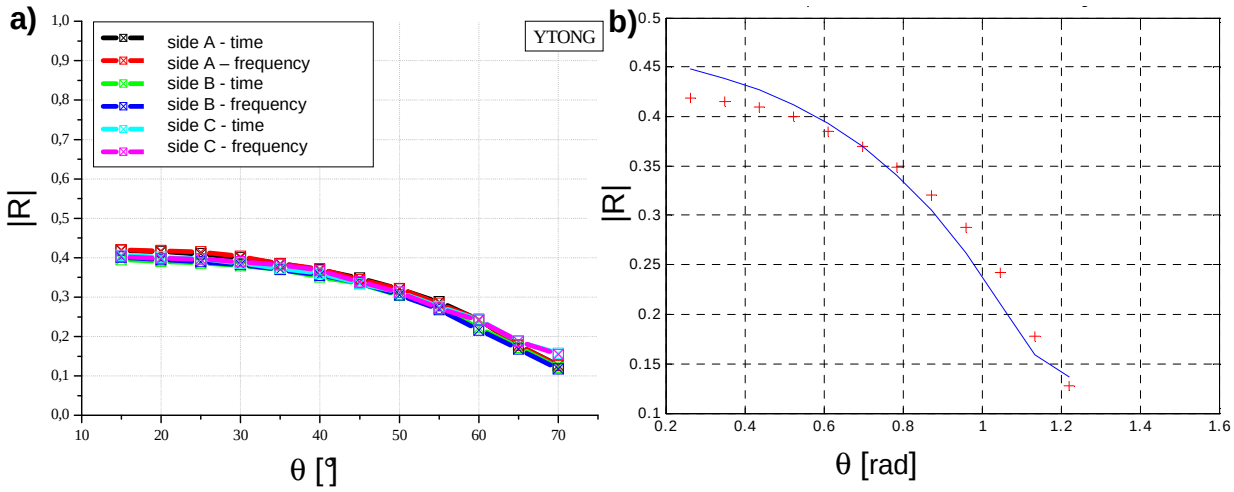

Figure V.13 The characteristic of the reflection coefficient versus incidence angle, a) the experimental results for different sides of tested sample, b) the results of the identification (model - solid line, the experiment - dotted line).

The reflectometric measurements which allow obtaining the characteristic of reflection coefficient *R*, were performed for wide range of materials. However, taking into account the conclusions from the model analysis (Chapter II.2.2) and the obtained experimental results, can be stated, that at present stage of this method development the correct results are obtained for a small number of real cases including gas concrete YTONG. Results for two other gas concretes are not reliable due to very large spread. The reason this dispersion may be actual material heterogeneity, but this issue requires further study. Figure V.13a shows the characteristics of reflection coefficient for a sample of gas concrete YTONG, which was

tested on three sides. The graph in the Figure V.13b shows experimental averaging curve (dotted line) and the curve obtained by identification (solid line).

Table V-2 The results of identification for gas concrete measurements.

YTONG	Tortuosity	Volumetric porosity [%]	Permeability [m^2]
Real data	No data	76	$2.92*10^{-13}$
Identification	2,66	65-75	$8.10*10^{-11}$

Comparison of the results of identification and real values are presented in the Table V-8. Good inversion results were obtained for porosity and significant discrepancy concerns permeability. The real value of tortuosity is not known for the tested sample. Attempts of identification other cement materials (mortars or concretes) did not give satisfactory results in respect of repeatability and compatibility of obtained parameters with expected values (real). That confirms conclusions of model sensitivity analysis carried out in the Chapter II.2.2.

V.5 Discussion about the experiences in use of the measurement systems

Experiences gained during the development of measurement systems, subsequent implemented modifications, and also carried out measurements resulted in knowledge, which might affect the quality of ongoing research. This is especially important when testing degraded concretes characterized by large heterogeneity and high attenuation. The most important experiences connected with SWMD system are shown below:

- positioning the SWMD system towards the surface. It turns out to be very important to set in parallel the SWMD system towards tested surface. Mistake in parallelism of setting, cause a change in length of propagation path in the air (the distance between the receiver and the surface sample) during displacing of the receiver. Thus causing in error of wave velocity measurement. For the position error about *1.5 mm* in the length of measurement profile of *200 mm*, the velocity error is about *3%*,
- spatial averaging. Due to the strong heterogeneity encountered in concrete materials, is recommended to apply the spatial averaging of tested material, as referred to the Chapter

III.1. This is done by registration of following profiles in different places of tested object. Distance between the positions of successive profiles must be large enough, so that areas of propagation in each profile do not overlap. The limitation is the size of tested area.

- use of valid band. During the signal processing, is recommended to use measurement data only for frequencies from valid band. The valid band both for velocity and attenuation is the range of the frequencies with good signal-noise ratio, as referred to the Chapter III.1.2.

Important observations gathered for the RMD system are as follows:

- setting of RMD system. Large impact on the quality of obtained results has (possibly accurate) setting of the device towards tested material, so that the transducers' axis of rotation lies exactly on the surface,
- measurement conditions. Significant influence on signal propagation has thermal movements of air. It is worth to use covers or if possible carry out measurements in closed rooms/chambers,
- signals averaging. The use of several (up to dozen or so) measurement repetitions and their averaging, allows to significantly reduce the influence of random errors (e.g. derived from the air fluctuations).
- reference measurement. It is worth to carry out measurements on the glass standard just before the measurement of tested material, in order to maintain similar conditions of propagation (parameters of the air).

V.6 Conclusions

In this chapter are presented the results of the use the developed measurement systems and programs for the structural and mechanical identification of diagnostic parameters of material. Obtaining reliable final results requires a correct operation of measuring devices, software for signals acquisition and data processing. That concerns also the programs realizing identification of the material parameters. The compatibility of the results obtaining on the basis of proposed measurements with the reference data is the criterion of correctness of system operating as a whole. The presented results apply to both measurement methods developed in the thesis. The main focus in the presentation of results is put on the measurement of surface wave propagation. Because the reflectometric method requires further development and at present stage, only rare materials gives the satisfactory results. It means

that, the parameters, potentially possible to determine using the reflectometric method, such as porosity or permeability should be determined by other methods at the moment.

In the case of tested materials using surface waves were presented the results of research for the macro-homogeneity modeling materials (sample of Plexi-Alu, sample of cement mortar), reference materials (a set of concrete beams from the SENSO project) and for real structure (measurement in St.Nazaire). Wide range of the tests, allows evaluating the operation of the system as a whole, but also the individual's elements of it. The research conducted on the test materials, is the first stage of verification of procedures. And the confirmation is the results of field measurements from the port in St.Nazaire, which are in a considerable degree compatible with independent real data collected for the tested construction. On the basis of the experimental part of realized study, may be drawn following conclusions:

- the results obtained by identification for the data from St.Nazaire indicate, that important influence on the accuracy of the Cloud Point program has the quality of experimental data. Especially spread of dispersion characteristics. That is why a great emphasis should be placed on quality and scrupulosity of the measurements carried out,
- diversified results of identification obtained in dependence on model used (Haskell's or Gibson's model) suggest, that the choice of optimal model for solving particular issue requires a deep analyze,
- the tests on concrete beams within SENSO project are a knowledge base of an influence of different factors (properties of concrete) on surface wave propagation. Thanks to information collected it may be concluded, which properties of tested material may be neglected and which should be taken into account, because of little influence on surface wave propagation.
- based on the ultrasonic measurements, presented calculations of Young's modulus quite well correlate real values,
- the information about attenuation of ultrasonic waves in concrete was used for taking into account the attenuation influence on dispersion for a strongly attenuated concrete,
- the data concerning the attenuation may be a source for additional suggestions about the quality of tested material,

It is worth to add, that beyond presented work, the SWMD system was successfully used while searching defects of composite structures [Safinowski and al. 2006]. The showed results of reflectometric measurements concern only one selected material, for which quite

good results were obtained. It limits its range of uses on the present stage of method development. The previous experiments connected with the measurements of reflection coefficient characteristics, show substantial potential of the applications of this approach in non-destructive diagnostic. Nevertheless, full usage of reflectometric method requires its further development in both of the theoretical and the experimental sides.

Chapter VI

Summary and final conclusions

The issue of developing measurement tools connected with non-destructive and non-contact diagnostics of structural and mechanical degradation of building materials - concretes in particular was discussed. After a through analysis of the literature dealing with non-destructive concrete diagnosis (Chapter I), the focus was put on developing two methods which use ultrasonic waves propagation - the methods are based on the analysis of surface wave propagation ie heterogeneous system and on reflection of the waves from a porous material. In connection with the methods chosen in Chapter II, three models describing the discussed propagation phenomena are dealt with. Two of these models (Haskell's model and Gibson's model) describe the propagation of surface waves and the third one deals with the wave reflection phenomena. These models together with appropriate software were used to research the sensitivity of the models. The influence of different parameters on the calculations was checked. In the theoretical part regarding the surface waves propagation an attempt to approximate the component of dispersion caused by attenuation was made. An analysis of sensitivity of the reflectometric model has shown the limited possibility of its use to strongly porous materials (strongly degraded concretes and gas concretes).

To realize the experimental part of this work, two computer operated measurement devices had to be designed and constructed – they were discussed in Chapter III. In the process of the work a portable non-contact surface wave propagation device (SWMD) and a portable non-contact reflection characteristic measurement device (RMD) were built. The devices can be used both in a laboratory and during field work. Using air as the medium of conduction for the wave between the ultrasound transducers and the material made the measurement non-contact and do not need any coupling material, thus they are non-invasive. In this part the advanced elements of signal processing used for measurements realization were shown. The attempted effect of the quantitative diagnostics was to estimate the state of the material by checking its material parameters. Linking the measurement data with the correct models describing the wave phenomena is needed to evaluate the problem of degraded concrete materials. To realize this step it was necessary to solve the inverse problem with the use of optimization procedures. Chapter IV deals with the choice and implementation of a few

optimization methods for the sake of the investigated structure. Two Self-developed programs were presented: the Cloud Points program – using the Haskell's model and the DDS program based on the Gibson's model- used to learn the depth of degradation. Both developed programs were tested on a specially prepared synthetic data.

The realization of the research on the real materials (chapter V) was an important opportunity to verify the proposed diagnostic tools. The results support the accuracy of operating of all elements of the systems discussed: the measurement device, applied data processing and the methods of the material parameters identification. The data collected on the samples in the SENSO project comprise knowledge bases in the influence of some parameters of concrete on the propagation of surface waves. The research done in laboratory conditions and in the field conditions have shown some shortcomings of the tools built in terms of their mechanics and software. The findings may point to the directions of the prospective works. It regards both the development of the presented techniques and the measurement devices as well as the signals processing and the methods of parametric identification. In the hardware part of the system responsible for surface wave measurement (SWMD) the fallowing things have to be considered:

- rebuilding the SWMD to apply a second transmitting transducer, which could enable us to conduct measurements in both directions of the profile. This would let us adjust the errors of the device positioning according to the tested surface by the use of signal processing,
- miniaturisation of the controller unit and the power amplifier. It is possible with the dynamic development of electronic components along with the knowledge acquired about the hardware requirements,
- improvement of the acoustic isolation between the transmitting and the receiving transducers in order to decrease the influence of the wave reaching directly through the air on the received signal,
- supplementing the SWMD system with the ability to measure other parameters such as the measurement of concrete humidity.

In the hardware part of the reflectometric measurement system (RMD) certain developments should be taken into consideration:

- developing an easier and more precise system of positioning of the device according to the sample,

- enclosing the device with the screens decreasing the influence of the environment on the measurement,
- adjusting the device to enable it to work on vertical (walls) and inverse horizontal (ceilings) sites.

Apart from the mentioned suggestions, the RMD system needs much research in order to asses its real usefulness and possible applications.

The software used for signal acquisition and data processing can be optimized to work faster. Tools that enable to suggest to the user the necessity of retaking the failed measurements could be applied to the software. They could be also able to reject the less accurate results to give a clearer image of the gathered measurement data. The improvements connected with parametric identification techniques at this stage of the research can include only the procedures using the Haskell's model such as:

- code victimization to solve the Haskell's model, which would hasten its work and therefore shorten the time of the identification process.
- implementation of other optimization procedures such as: Genetic Algorithms, and thus continuing research on choosing the right method of solving the inverse problem.
- formulating a procedure based on the use of other models which could describe a degraded material.

BIBIOGRAPHY

Abraham O., Villain G., Lu L., Cottineau L., Durand O. (2009), *A laser interferometer robot for the study of surface wave sensitivity to various concrete mixes*, NDTCE'09, Non-Destructive Testing in Civil Engineering Nantes, France, June 30th – July 3rd, 2009.

ACI 228.1R-95, (2002), *In-Place Methods to Estimate Concrete Strength*, ACI Manual of Concrete Practice, American Concrete Institute, Farmington Hills MI, 2002.

Aki K., Richards P. G. (1990), *Quantitative Seismology*, Freeman and Co., New York 1990.

Amborski, K. (2009), *Podstawy metod optymalizacji*, Oficyna Wydawnicza Politechniki Warszawskiej, Warszawa 2009.

Arndt R., Jalinoos F. (2009), *NDE for corrosion detection in reinforced concrete structures – a benchmark approach*, NDTCE'09, Non-Destructive Testing in Civil Engineering Nantes, June 30th – July 3rd, 321-326, France 2009.

Attenborowugh K., (1982), *Acoustical characteristics of porous materials*, Phys. Reports, 82, 3, 179-227 1982.

Balayssac J.P., Laurens S., Arliguie G., Ploix M. A., Breysse D., Dérobert X., Piwakowski B. (2009), *NDE for corrosion detection in reinforced concrete structures – a benchmark approach*, NDTCE'09, Non-Destructive Testing in Civil Engineering Nantes, June 30th – July 3rd, 391-398, France 2009.

Bergmann L. (1948), *Ultrasonic and their Scientific and Technical Applications*, Wiley, New York 1948.

Biot M. A. (1956), *Theory of propagation of elastic waves in a fluid-saturated porous solid. I. Low-frequency range, II. Higher-frequency range*, Journal of the Acoustic Society of America, 28, 2, 168-178, 179-191, 1956.

Boiero D., Wisen R., Socco L.V. (2006), *Scale property Monte Carlo driven inversion of surface wave data*, Near Surface, Helsinki 2006.

BS (1881), *Recommendations for the assessment of concrete strength by near-to-surface tests*, British Standards Institution, Part 207 London 1881.

Brouwer J. Helbig K. (1998), *Shallow High-Resolution Reflection Seismics*, Elsevier Science Ltd., Oxford 1998.

Bungey J. H., Millard S. G. (1996), *Testing of concrete in structures,* Third edition, Chapman & Hall, 1996.

Carter R. G., Gablonsky J. M., Patrick A. Kelley C. T., Eslinger O. J. (2002), *Algorith;s for noisy problems in gas transmissions pipeline optimization,* Optimization and Engineeering 2 139-157, 2002.

Cartz L. (1995), *Nondestructive Testing, Radiography, Ultrasonic, Liquid Penetrant, Magnetic Particle, Eddy Current,* ASM International®, 1995.

Castagnede B., Aknine A., Melon M., Dopellier C. (1998), *Ultrasonic characterization of the anisotropic behavior of air-saturated porous materials,* Ultrasonics, 36, 323-341, 1998.

Coleman, T.F., Li Y. (1994), *On the Convergence of Reflective Newton Methods for Large-Scale Nonlinear Minimization Subject to Bounds,* Mathematical Programming, Vol. 67, Number 2, pp 189-224, 1994.

Cook R., A. (1991), *Fundamentals of mercury intrusion porosimetry and its application to concrete materials science,* Master of Science Thesis, Cornell University, 1991.

Clemena G. G., Malhotra V. M., Carino N.J. (1991), *Short-Pulse Radar Methods in Handbook on Nondestructive Testing of Concrete,* Press, Baca Raton CRC pp. 253-274 , FL, 1991.

Dal Moro G., Forte E., Pipan M., Sugan. M (2006), *Velocity spectra and seismic-signal identification for surface-wave analysis,* Near Surface Geophysics, pp. 243-251, 2006.

Dal Moro G., Pipan M., Gabrielli P. (2007), *Rayleigh Wave Dispersion Curve Inversion via Genetic Algorithms and Posterior Probability Density Estimation,* Journal of Applied Geophysics 61, pp. 39-55, 2007.

Declercq NF., Briers R., Degrieck J., Leroy O. (2005), *The history and properties of ultrasonic inhomogeneous waves,* IEEE Transactions on Ultrasonics, Ferroelectrics, and Frequency control Vol. 52 NO. 5, pp. 776-791, May 2005.

Dérobert X., Villain G., Cortas R., Chazelas J. (2009), *EM characterization of hydraulic concretes in the GPR frequency-band using a quadratic experimental design,* NDTCE'09, Non-Destructive Testing in Civil Engineering Nantes, June 30th – July 3rd, France 2009.

Fellah Z. E. A., Berger S., Lauriks W., Depollier C., Aristegui C., Chapelon J.-Y. (2003), *Measuring the porosity and the tortuosity of porous materials via reflected waves at oblique incidence* J. Acoust. Soc. Am. 113, 5, 2424-2433, 2003.

Feng S., Sugiyama T., Yamanaka H. (2005), *Effectiveness of multimode surface wave inversion in shallow engineering site investigation,* Exploration Geophysics 36, pp. 26-33, 2005.

Figg J. (1989), *Concrete surface permability: Measurement and meaning,* Chemistry and Industry, 714-719. , Now York. 1989.

Findeisen S., Szymanowski W., Wierzbicki A., (1987), *Teoria i metody obliczeniowe optymalizacji,* PWN 1987.

Finkel D. E. (2003), *DIRECT Optimization Algorithm User Guide,* Center for Research in Scientific Computation North Carolina State University Raleigh, NC 27695-8205, North Carolina 2003.

Floudas, C.A, Pardalos, P.M., (eds.), (2009), *Encyclopedia of Optimization,* 2nd edition, Springer 2009.

Garnier V., Corneloup G., Toppani E., Leygonie M., (2000), *Non-Destructive Evaluation of Concrete Damage by Ultrasound*15th WCNDT, Roma 2000.

Garnier V., Chaix J., Payan C. (2009), *Improvement of new wave propagation techniques to characterize concrete* [NDTCE'09].

Gurevich B., Schoenberg M., (1999), *Interfae conditions for Biot's equations of poroelasticitv,* J. Acoust Soc. Am , 105, 2585-2589, 1999.

Gibson R.E. (1967), *Some Results Concerning Displacements and Stresses in a Non-Homogeneous Elastic Half-Space,* Geotechnique 17 58-67, 18 275, 19 160 1967.

Goueygou M., Lafhaj Z., Soltani,F. (2009a), *Assesment of porosity of mortar using ultrasonic Rayleigh waves,* NDT&E International Vol. 42 pp. 353-360, 2009.

Goueygou M., Piwakowski B., Ould Naffa S., Buyle-Bodin F. (2002), *Assessment of broadband ultrasonic attenuation measurements in inhomogeneous media,* Ultrasonics, pp. 77-82, 2002.

Goueygou M., Soltani F., Lafhaj Z., Piwakowski B. (2009b), *Effects of geometrical diffraction on non contact measurements of ultrasonioc attenuation in cement based materials* Submitted to NDTCE'09, Non-Destructive Testing in Civil Engineering Nantes, , June 30th – July 3rd, France 2009.

Goupillaud P. L. (1976), *Signal design in the 'Vibraseis' technique."* Geophysics 41, pp. 1291-1304, 1976.

Halleux B. D. (2000), *Notes sur le contrôle non destructif,* Université Catholique de Louvain, Louvain-la-Neuve 2000.

Hala J., Schabwicz K. (2005), M*ethodology of neural identification of strength of concrete,* ACI Materials Journal, Vol. 102, no. 6, pp. 459-464, 2005.

Haskell N. A. (1953), *The disperstion of surface waves on multilayered media*, Bulletin of the Seismological Society of America 43, 17-34 1953.

Hoffren H., Karppinen T., Hæggström E., (2004), *Measuring porosity and tortuosity of rocks by means of air-borne ultrasound,* AGU Fall Meeting, San Francisco, USA 2004.

Hoffren H., Karppinen T., Kohout T., Hæggström E., (2005), *Plastic foam porosity characterization by air-borne ultrasound, Review of Progress in Quantitative Nondestructive Evaluation,* Brunswick, Maine, USA 2005.

Hubbard S.S., Zhang J.Y., Monteiro P. J. M., Peterson J. E., Rubin Y. (2003), *Experimental detection of Reinforcing Bar Corrosion Using Nondestructive Geophysical Techniques,* ACI Mat.J., Vol. 100, No. 6, pp. 501-510, 2003.

Jung Y., Kundu T., Ehsani M. R. (2002), *A Now Nondestructive Inspection Technique for Reinforced Concrete Beams,* ACI Materials Journal / May-June 2002.

Kaczmarek M., Safinowski P., Piwakowski B. (2009), *Non-contact ultrasonic porosymetry* NDTCE'09, Non-Destructive Testing in Civil Engineering Nantes, France, June 30th – July 3rd, pp. 529-534, 2009.

Kaszyński J. (2003) *Ultradźwiękowe badania betonu z uwzględnieniem strefy zbrojenia i zarysowania,* Wydawnictwo uczelniane Politechniki Szczecińskiej, 2003.

Kirkpatrick S., Gelatt C. D., Jr., Vecchi M. P. (1983), *Optimization by Simulated Annealing,* Volume 220, Number 4598, Science 13 May 1983.

Klimis N. (1988), *Etude en laboratoire de l'atténation des ondes longitudinales – Application à la caractérisation géotechnique des roches,* Rapports des Laboratoire LCPC, Ministère de l'équipement; Série : géotechnique – mécanique des sols – sciences de la terre GT28 ; Avril 1988.

Kosecki A., (2010), *Optimisation d'une source vibratoire pour la détection des cqvites souterraines par sismique réflexion haute résolution,* PhD Ecole Centrale de Lille, 2010.

Kosecki A., Piwakowski B., Driad-Lebeau L. (2010), *High Resolution Seismic Investigation In Salt Mining Context.* Revue Acta Geophysica Vol. 58/1, pp.15-33, 2010.

Klauder J. R., Price A. C., Darlington S., Albershim W. J. (1960), *The theory and design of chirp radars,* Bell System Tech. Journal Vol. 39, pp. 745-807, 1960.

Klimis N. (1988), *Etude en laboratoire de l'atténuation des ondes longitudinales, Application à la caractérisation géotechnique des roches,* Rapports des laboratoires, Publié par LCPC, 58 bd Lefebvre – 75732 ¨PAEIS CEDEX 15 sous le numéro3558, 1988.

Krstulovic-Opara N., Woods R. D., Al-Shayea N., (1969), *Nondestructive Testing of Concrete Structures Using the Rayleigh Wave Dispersion Method,* ACI Materials Journal /January-February 1996.

Kuc R. (1981), *Digital filter models for media having linear with frequency loss characteristics,* Journal of the Acoustical Society of America Vol. 69, pp. 35-40, 1981.

Kuc R. (1983), *Generating a Minimum-Phase Digital Filter Model for the Acoustic Attenuation of Soft Tissue,* IEEE Utrasonics Symposium, Atlanta, Expanded Abstracts KK-1, 1983.

(Kumar) Mahinthakumar G., Sayeed M. (2005), *Hybrid Gnetic Algorithm – Local Search Methos for Solving Groundwater Source Identification Inverse Problem,* J. Water Tesour. Plng. and Mgm. 131, 45 2005.

Kusiak, J., Danielewska-Tułecka, A., Oprocha, P., (2009), *Optymalizacja. Wybrane metody z przykładami zastosowań,* Wydawnictwo Naukowe PWN 2009.

Lai G. C. (2098), *Simultaneous inversion of Rayleigh phase velocity and attenuation for near surface site characterisation,* PhD thesis Georgia Institute of Technology, 1998.

Lai G. C., Rix G. J., Foti S. Roma V. (2002), *Simultaneous measurement and inversion of surface wave dispersion and attenuation curves,* Soil Dynamics and Earthquake Engineering, Vol. 22. pp. 923-930, 2002.

Lamb H. (1917), *On waves in an elastic plate,* Proc. Roy. Soc., Vol. 93 PT series A. pp. 114-128, 1917.

Lataste J., Laurens S., Moczko A. (2009), *Some elements for improving interpretation of concrete electrical resistivity,* [NDTCE'09].

Litniewski J., Nowicki A., Klimonda Z., Lewandowski M. (2007), *Sound Fields for Coded Excitations in Water and Tissue: Experimental Approach,* Ultrasound in Biology and Medicine, Vol. 33, Issue 4,. pp. 601-607, 2007.

Lowe M. J. S. (1995), *Matrix Techniques for Modeling Ultrasonic Waves in Multilayered Media,* IEEE Transactions on Ultrasonics, Ferroelectrics, and Frequency control Vol. 42 NO. 4 JULY 1995.

Mavko C., Mukerji T., Dvorkin J. (2003), *The Rock Physics Handbook – Tools for Seismic Analysis in Porous Media,* Cambridge University Press 2003.

McMechan G. A., Yedlin M. J. (1981), *Analysis of dispersive waves by wave field transformation,* Geophysics Vol. 48. NO. 6, pp. 869-874, June 1981.

Mehta P. K. (1997), *Durability – Critical Issues for the furure,* Concrete International, 27-33, 1997.

Mehta P. K., Monteiro P. J. M. (2006), *Concrete, Microstructure, Properties and Materials,* The McGraw-Hill Companies, Inc. Third edition, 2006.

Miller G. F., Pursey H. (1955), *In situ nondestructive testing of concrete* SP-82, ACI International Conference, Ottawa, 831, 1955.

Mindess S. (2001), *Editorial,* Matériaux et Structures Vol. 34, pp. 450 10-2001.

Misaridis T. Jensen J.A. (2005), *Use of Modulated Excitation Signals in Medical Ultrasound. Part II: Design and Performance for Medical Imaging Applications,* IEEE Transactions on Ultrasonics, Ferroelectrics, and Frequency control Vol. 52(2), pp. 192-207, 2005.

Moczko A. (2006) *Współczesne metody diagnostyki istniejących konstrukcji betonowych.* Materiały Budowlane, nr 12, str. 21-24, 2006.

Moré, J. J. (1977) *The Levenberg-Marquardt Algorithm: Implementation and Theory*, Numerical Analysis, ed. G. A. Watson, Lecture Notes in Mathematics 630, Springer Verlag, pp. 105-116, 1977.

(NDTCE'09) Abraham O., Derobert X.. (2009), *Non-Destructive Testing in Civil Engineering NDTCE'09*, Wydane przez LCPC, pod numerem C1502542, Francja 2009.

Nelder J.,-Mead R. (1965) *A simplex method for function minimization,* Computer Journal Vol. 7 pp. 308-313, 1965.

Neville, A.M. (2000) *Właściwości betonu,* Polski Cement, Kraków 2000.

Neuenschwander J., Schmidt, Th. Luthi, Romer M. (2006), *Leaky Rayleigh wace investigation on mortar samples,* Ultrasonics Vol. 45, pp 50-55, 2006.

Nowicki A. (2010) *Ultradźwięki w medycynie – wprowadzenie do współczesnej ultrasonografii,* Roztoczańska Szkoła Ultrasonografii, 2010.

Orozco M. C. (2003) *Inversion method for spectral analysis of surface waves (SASW),* PhD Georgia Institute of Technology, 2003.

Owino O. J., Jacobs L. J. (1999) *Attenuation measurement in cement-based materials using laser,* J.Eng. Mech.. pp. 637-645, June 1999.

Park C. B., Miller R. D., Jianghai X. (1998) *Multichannel analysis of surface waves* Geophysics, Vol 64, N°3, pp. 800-808, 1998.

Pettunen C. D., Jones D.R., Stuckman B. E. (1993), *Lipschitzian optimization without the lipschitz constant,* Journal of Optimization Theory and Application, Vol. 79(1), pp. 157-181, October 1993.

Piwakowski B., Fnine A., Goueygou M., Buyle-Bodin F. (2004), *Generation of Rayleigh waves into mortar and concrete samples,* Ultrasonics, Vol 42, Issues 1-9, pp 395-402, 2004.

Piwakowski B., Safinowski P. (2009), *Non-destructive non-contact air-coupled concrete evaluation by an ultrasound automated device,* NDTCE'09, Non-Destructive Testing in Civil Engineering Nantes, France, June 30th – July 3rd, pp. 603-608, 2009.

Ploix M-A., Garnier V., Breysse D., Moysan J. (2009), *Possibilistic NDT data fusion for evaluationg concrete structures,* NDTCE'09, Non-Destructive Testing in Civil Engineering Nantes, June 30th – July 3rd, 348-354, France 2009.

Popovics J. S. (1995), *Comment on "Determination of elastic constants of a concrete specimen using transient elastic waves"*, J. Acoust. Soc. Am. 98, 2142-2148 1995.

Ranachowski Z. (1990), *Wyznaczanie naprężeń krytycznych w betonie przy pomocy zautomatyzowanych pomiarów metodą emisji akustycznej***,** Praca doktorska, Instytut Budownictwa Politechniki Wrocławskiej, Wrocław, 1990.

RAP 2010 *Nieinwazyjna Diagnostyka Penetracji Degradacji Materiałów Konstrukcyjnych* Raport merytoryczny z realizacji projektu badawczo rozwojowego Nr. R04 009 02 Bydgoszcz 2010.

Rayleigh L. (1885), *On waves propagation along the plane surface of en elastic solid,* Proc. London Math. Soc., Vol. 17, 1885.

Reichling K., Raupach M., Wiggenhauser H., Stoppel M., Dobmann G., Kurz J. (2009), *BETOSCAN – Robot controlled non-destructive diagnosis of reinforced concrete decks,* NDTCE'09, Non-Destructive Testing in Civil Engineering Nantes, June 30th – July 3rd, 425-439 , France 2009.

Rihaczek A. W. (1969), *Principles of High-Resolution Radar*, McGraw-Hill, New Jork 1969.

Rix G. J., Lai G. C. (2000), *In situ measurement of damping ratio using surface waves,* Jurnal of Geotechnical and Geoenvironmental Enginierng, Processing of the ASCE, Vol. 126(5): 472-480, 2000.

Runkiewicz L. (2002), *Badania Konstrukcji Żelbetowych,* Diagnostyka Techniczna wyd. Biuro Gamma. Waraszawa 2002.

Ryden N., Lowe M. J. S., Cawley P. (2009) *Non-contact surface wave testing of pavements using a rolling microphone array,* pp. 561-566, [NDTCE'09]

Safinowski P., Kosecki A., Piwakowski B. (2006), *Diagnostic of composites using ultrasonic waves, Papier invité.* Proceedings of Conference: Scientific and technical aspects in high performance sailing., pp 20 – 30, Barcelone 2006.

Safinowski P., Piwakowski B., Kaczmarek M., Kosecki A., (2008), *Caractérisqtion du béton à l'aide de la réflectométrie ultrasonore*, COFREND 2008, Toulouse 20-23 mai 2008.

Schabowicz K., Hoła J. (2008), *Nondestructive Elastic-Wave Tests of Post-tensioned Concrete Girders in Road Bridge*, 17th World Conference on Nondestructive Testing, Shanghai, China, 25-28 Oct 2008.

Schevenels, M., Badsar, S., Degrande, G. (2009). *The use of the SASW method to determine the shear wave velocity and the material damping ratio of shallow soil layers*, 71st EAGE Conference & Exhibition incorporating SPE EUROPEC 2009.

SENSO (2009), *Projet ANR SENSO - Stratégie d'Evaluation Non destructive pour la Surveillance des Ouvrages en béton - Rapport Final – Septembre 2009,* LMDC – Université de Toulouse 2009.

Shannon C. E. (1949), *Communication in the presence of noise,* Proc. Institute of Radio Engineeris , Vol. 37, no. 1, pp. 10-21, Jan. 1949.

Shiyan J. (2009), *Etude expérimentale des incertitude stochastiques pendent l'évaluation du béton à l'aide des ondes de surface ultrasonores,* Diplôme Master Ecole Centrale de Lille, 2009.

Socco L. V., Boiero D. (2008), *Improved Monte Carlo inversion of surface wave data,* Geophysical Prospecting, Vol. 56, pp. 357-371, 2008.

Stachurski A., Wierzbicki A. P. (1999), *Podstawy optymalizacji,* PWN Warszawa 1999.

Stadnicki J. (2006), *Teoria i praktyka rozwiązywania zadań optymalizacji,* WNT Warszawa 2006.

Szelążek J. (2001) *Postępy w ultradźwiękowych badaniach naprężeń,* Praca habilitacyjna IPPT PAN 4/2001.

Thomson W. T. (1950), *Transmition of elastic waves through a stratified solid medium,* J. Appl. Phys., Vol. 21, pp.89-93, 1950.

Vardoulaskis I. (1981), *Surface waves in a half-space of submerged sand,* Earthquake Engineering and Structural Dynamics, Vol. 9, 329-342, 1981.

Vardoulakis I., Verros Ch. (1988), *Dispersion low of Rayleigh-type waves in a compressible Gibson half-space*, International Journal for Numerical and Analytical methods in Geomechanics, Vol. 12, 639-655, 1988.

Viktorov I. A. (1967), *Rayleigh and Lamb Waves*, Plenum Press, New-York 1967.

Villain G., Derobert X., Abraham O., Coffec O., Durand O., Laguerre L., Baltazart V. (2009), *Use of ultrasonic and electromagnetic NDT to evaluate durability monitoring parameters of concrete*, NDTCE'09, Non-Destructive Testing in Civil Engineering Nantes, France, June 30th – July 3rd, 343-348, 2009.

Wardany R., A. (2005), *Caractérisation non destructive des structures en béton au moyen des ondes dispersives de Rayleigh et de Lamb*, Thése de doctorat (Ph :D) Spéciqlité: génie civil; Sherbrooke (Québec) Canada, 2005.

Wathelet W., Jongamans D. Ohrnberger M. (2004), *Surface-wave inversion using a direct search algorithm and its application to ambient vibration measurements*, Near Surface Geophysics, pp. 211-221, 2004.

Weil G. J., Malhotra V. M., Carino N.J. (1991), *Infrared Thermographic Techniques, Handbook on Nondestructive Testing of Concrete*, pp. 253-274 CRC Press, Baca Raton, FL, 1991.

Wu T.-T., Liu Y.-H. (1999), *Inverse determination of thickness and elastic properties of a bonding layer using laser-generated surface waves*, Ultrasonics 37 (1999) 23-30, 1999.

Xia J., Miller R. D., Park Ch. B. (2006), *Estimation of shear wave velocity in a compressible Gibson half-space by inverting Rayleigh wave phase velocity*, Surveys in Geophysics Vol. 27: pp. 1-17, 2006.

Yilmaz O. (1987), *Seismic Signal Processing*, Society of Exploration Geophysicists, 1987.

Yang W. Y., Cao W., Chung T-S., Morris J. (2005), *Applied numerical methods using MATLAB*, A JOHN WILEY & SONS, INC., Publication 2005.

Zhu, J. Y., Popovics, J. S. (2001), *Non-contact detection of surface waves in concrete using an air-coupled sensor*, in Review of Progress in QNDE, Vol. 20B, edited by D. O. Thompson and D. E. Chimenti, AIP Conference Proceedings, American Institute of Physics, Melville, pp.1261-1268, New York 2001.

Zoubeir L., Guillaume R., Kaczmarek M., Skoczyla. F. (2007), *Experimental determination of intrinsic permeability of limestone and concrete: Comparison in situ and laboratory results*, Building and Environment (BEJ) Vol. 42 (8) pp. 3042-3050, 2007.

APPENDIX I

Chosen detail of optimization methods

Bisection method

The method of an even division know also as the bisection method is an easy way to solve non-linear equations. Balzano Cauchy's proposition is used in this method, it says that if a continuous function *f(x)* has reverse signs at the both ends of a closed range *[a;b]* there has to be at least one radical of the equation *f(x) = 0*. From the above proposition *2* obligatory conditions can be surmised. Firstly, the function *f(x)* in a chosen closed range *[a;b]* has to be continuous, secondly the product *f(a)f(b)<0* has to be achieved. The graphic illustration of the non-linear equation with the use of the bisection method of Equal division was shown in the Figure A1.1.

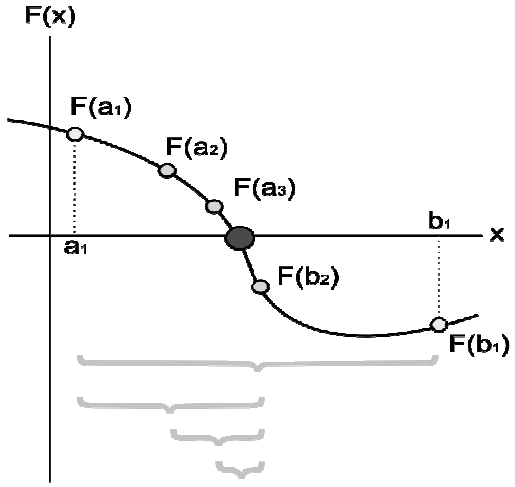

Figure A1.1 The graphic illustration of the bisection method[10].

The work of the procedure is as follows, the range *[a;b]* is divided into *2* in the point $x_1 = a + b/2$ when the function equals *f(x₁) = 0*, then x_1 is the searched result of the equation. If the result is different the range *[a;b]* is divided into *2* equal parts *[a;x₁]* and *[x₁;b]* and the products *f(a)f(x)* and *f(x)f(b)* are checked. If there is at least one zero point one of the products will be a negative number. It then becomes the new range of the search in which the division procedure is repeated. There are two conditions of ending the algorithm. One of them is

[10] Gpraph form : http://pl.wikipedia.org/w/index.php?title=Plik:Bisection_method.png&filetimestamp=20050826130956

finding an x_n for which the equation $f(x_n) = 0$. The algorithm finishes its work a lot earlier when it finds a relatively small number (approximation of a radical) [Yang at al. 2005]. The algorithm is characterized by a big speed of work but a problem occurs when the function of the target has more than one rout. For example – if there are *2* zero points crossings in a given range and in consequence the ends of the range would have an identical sign the algorithm will not find any solution. Some constraints of applying the method of bisection are – looking for zero point crossings and not the extremes of the function which makes it necessary (in the classical view on the optimization) to use a derivative of the target's function not the function itself.

In the presented work, the method of bisection was only used in solving the problem based directly on the Haskell's model described in the Chapter II. 1.2. It lets us quickly find the radicals of the dispersive equation for quasi Reyleigh waves (multiple modes) by solving multiple dispersive equations for the entire range of frequencies. In Matlab environment there exists a built-in procedure of searching the zero point of a non-linear function "fzero". Nevertheless for the use of this work a procedure realising code was made. The work of the code was successfully tested by comparing results with the method of the Simulated Annealing which is appropriate for the same purpose. The bisection method is however more time effective.

Gradient Methods

The gradient methods are come under the category of the deterministic first order optimization methods. One of the gradient methods is the Newton method. The work of the procedure begins in a start point x_0 chosen by the user included in the domain *D*, in which the direction of the search is calculated, it is represented by the vector d_k the points of the following interations are calculated according to the equation

$$x_{k+1} = x_k + d_k \qquad \text{(A.1)}$$

If the criteria of the stop of the algorithm are fulfilled a new interation begins and a new direction of the search is calculated for the recently set point x_{k+1}. The process is repeated as long as of the criteria of ending is achieved. The direction of the minimum search in the Newton's method is calculated with the use of a Taylor's series of the objective function according to the given *x* point in accordance with the equation

$$f(x+\delta) = f(x) + \nabla f(x)^T \delta + \frac{1}{2}\delta^T \nabla^2 f(x)\delta + O(\delta^2) \quad SD = \frac{V_{S2} - V_{S1}}{V_{S2}} x100\% \qquad \text{(A.2)}$$

where $\nabla f(x)$ means the gradient of the objective function, $\nabla^2 f(x)$ is the Hess matrix (called Hesjan as well), and the ingredient $O(\delta^2)$ is the rest of the value of δ^2. Supposing that the rest in the solution (A.2) is negligibly small, square approximation of the objective function *f(x)* in accordance with the $_{xk}$ point.

$$F_k(\delta) = f(x_k) + \nabla f(x_k)^T \delta + \frac{1}{2}\delta^T \nabla^2 f(x_k)\delta \tag{A.3}$$

Then, the direction of search can by calculated

$$d_k = \min_{\delta} F_k(\delta) = -\frac{\nabla f(x_k)}{\nabla^2 f(x_k)} \tag{A.4}$$

Substituting (A.4) to (A.1) the recurrent equation of the Newton's method can be formulated

$$x_{k+1} = x_k - \frac{\nabla f(x_k)}{\nabla^2 f(x_k)} \tag{A.5}$$

In the presented work as a basic algorythm to solve the inverse issue the "Isqnonlin" (LSQ) procedure was used. It is available in the optimizing toolbox in the Matlab environment. The procedure may be successfully used in solving both the dispersive equations as well as the identification of parameters in the reflectometry. The "Isqnonlin: function is often used to rapidly establish with optimizing procedures the local minimum of a function. The LSQ procedure requires defining the *C* vector which is a margin of the experimental values V_E and the *V* ea a forecasts of the model for the vector *P* of the established model parameters. The operation of calculation Euclideans norm of the *C* vector which is a objective function is done inside the LSQ procedure. There are certain requirements of ending the optimization and their configuration is possible by dint of the "optimset" function. The most important parameters of the function are:

'TolFun' – it establishes the minimal value of the function which is needed to end the calculations. Ending the procedure of this reason is most beneficial, it guarantees reaching the matching with high accuracy, The value of this parameter has to be established on the basis of the experience of the user. The main factors influencing the value are: the quality of the experimental data and the resolution of the model. To make it easier, you can assume a very small value of i.e. 10-2 and take into consideration the quality of the matching show by a graphic.

'DiffMinChange' – establishes how big changes of the function are acceptable. Stopping because of this parameter may happen when a function has a valley with a flat bottom – so many parameters with an identical value of the function will occur. The research done has shown that the value of this parameter should be inside the range 10-3

'TolX' – determines the minimal change of the model parameters. It makes it possible to end the optimization w a situation when the value of a found minimum does not fullfill the criterion 'TolFun'. This kind of a situation can occur when the experimental data contain noise or the used model does not require making a set approximation - in this case it is impossible to reflect id ideally. Ending the search because of this reason does not guarantee that the found minimum is correct.

It depends from the configuration if the function can work as an algorithm of Large-scale optimization [Coleman 1994] or as Medium-scale optimization [Moré 1977]. In the first example the Newton method is used which lets us solve non-linear equations with the use of combined gradients. The advantage of using large scale optimization method in the Isqnonlin procedure is the readiness to define the borders of the search for the whole vector of the search parameters. In the case of Medium-scale optimization including the borders of the search range is much more complicated. It can be done by including an accurately formulated function of an added penalty to the target of the function. The vital condition to end the search is reaching the assumed value of the minimum of the target function and it usually means that the global extreme was found – the best possible solution. In the case of real data which include noise it is very difficult to fulfill. Therefore it happens that the optimizing procedure ends because the changes of the *P* parameter are smaller than the set values in the options of the procedure. In this case, there is risk that the algorithm is stuck in the local minimum. It has to be established then if the value of the reached minimum is acceptable. The graphic visualisation of the matching may be very helpful. It may suggest the presumptive end of the calculations. It is also possible that the algorithm would find a blurred minimum "a flattened" minimum of the target. In this situation, the algorithm ends the search because of the zero values of the gradients. Another condition of finishing the calculation is the breaching of the assumed number of the iterations of the procedure or the number of recollections of the target function which means an incorrect solution to the task.

Simplex Method

The simplex Method is also called the Nelder-Mead's method from the names of its creators, is one of the direct methods [Nelder and others 1996], it means that it uses directly the objective function and not its derivative. It is a local optimization method. The work of the method does not require counting the derivatives of the objective function which decreases the amount of time needed. For a *N*-dimension problem the work of the procedure requires *N+1* points in a *N*-dimension space, on the basis of which a simplest geometrical figure can be built in this space (it is called simplex). For a one dimension space problem it would be a segment for a two dimension problem it would be a triangle etc. The process of searching the minimum is based on setting a new point of the top of the simplex by reflecting the highest point according to the opposite face (a point in the case of a segment). Additionally the procedure may decrease or increase the newly obtained simplex to find the minimum of the function faster. The simplex becomes smaller and smaller approaching the minimum. The optimizing ends when the size of the simplex are smaller than the established border values. In the Matlab environment the Simplex method is implemented in the "fminsearch" function.

Simulated Annealing method

One of the methods used in the work of optimizing global methods is the method of Simulated Annealing (SA) Published in 1983, which authors are S. Kirkpatrick, Ch. Gallet and M. Vecchiego [S. Kirkpatrick at all. 1983]. The work of the method can be compared to the operation of heat development of metals in which annealing leads to the reduction of the internal stress which appeared due to an abrupt hardening. In the SA method an analogy between the energies of atoms of the improved metal and the target function occurs. Reaching the minimum of the function can be compared to a free cooling of a processed metal. One of the advantages is the fact that the target function does not have to be differential nor even linear. The disadvantage of this method is relatively high time consumption before reaching the solution.

Scheme of the SA algorithm at work is shown in the picture A1.2. Its work begins with choosing a start point from the range of search and setting the parameters of work for the algorithm such as the starting temperature, the lowering temperature modulus or the cooling model. The value of the temperature corresponds to the probability with which the starting sample points are accepted. The higher of temperature caused the bigger probability of acceptance. From the space around the last and the best solution, (at the first iteration it is the

starting point) a new neighbor is reached (a new range of searched parameters). If the value of the function for the new point is bigger than for the previous point then it is saved as the candidate for the solution. Next, for the new point, the acceptance function is calculated which depends from the value of the target function for both the old and the new solution and from the temperature corresponding to a given iteration. The acceptance function says if the search of a new neighbor in the next iteration starts form the old or the new solution. It is also worth noting that the lower the temperature, the lower the probability of changing the starting point in the search of a new solution. The value of the temperature in lowered after each iteration, so at the beginning of the work of the algorithm the starting point is often changed, and at the end at a lower temperature it stays unchanged. Such situation makes the algorithm SA work more locally at the end than at the beginning when the temperature was high.

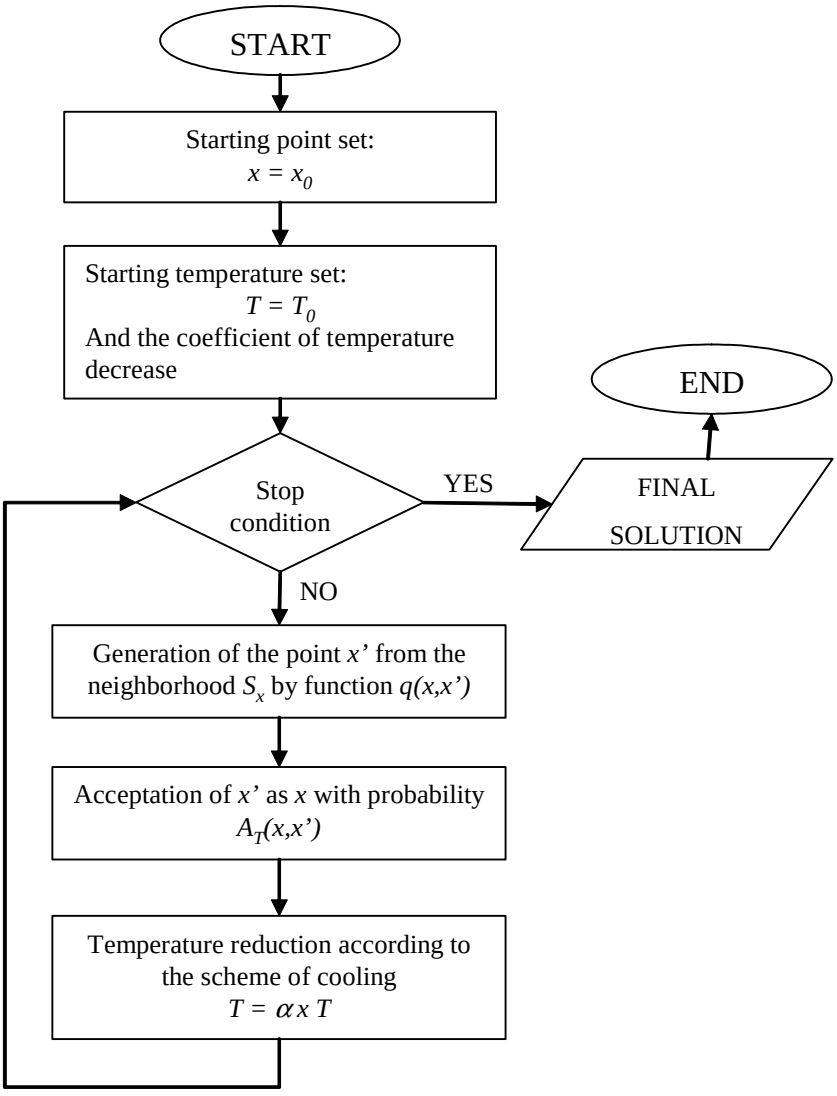

Figure A1.2 The block diagram of Simulated Annealing method..

Ending a single iteration takes place after finding a set number of neighbors. A new iteration begins with a lower temperature. An assumed model of cooling is responsible for the way of lowering the temperature. There are different mechanisms of cooling in the common use. In most of them the temperature is lower with every iteration, although oscillation methods are sometimes used. The algorithm ends its work when the value of the function is below a set level or when the lowest possible temperature is achieved.

DIRECT Method

Optimization algorithm called DIRECT belongs to a group of algorithms of global action. For the first time appeared in Pettunen's work [Pettunen and al. 1993]. The destiny of the algorithm was to solve the global optimization problems with certain restrictions of parameters and an objective function with real values. The name DIRECT comes from the shortening of the phrase "DIviding RECTangles", which describes the way the algorithm reaches the minimum of the objective function. DIRECT is the direct algorithm and therefore as SA, does not require the knowledge of gradients of the objective function. These types of algorithms work well in situations where there is no information about the objective function and it should be treated as a "black box". An example of DIRECT being used to solve a real industrial problem is shown i.a. in Carter's work [Carter and al. 2002].

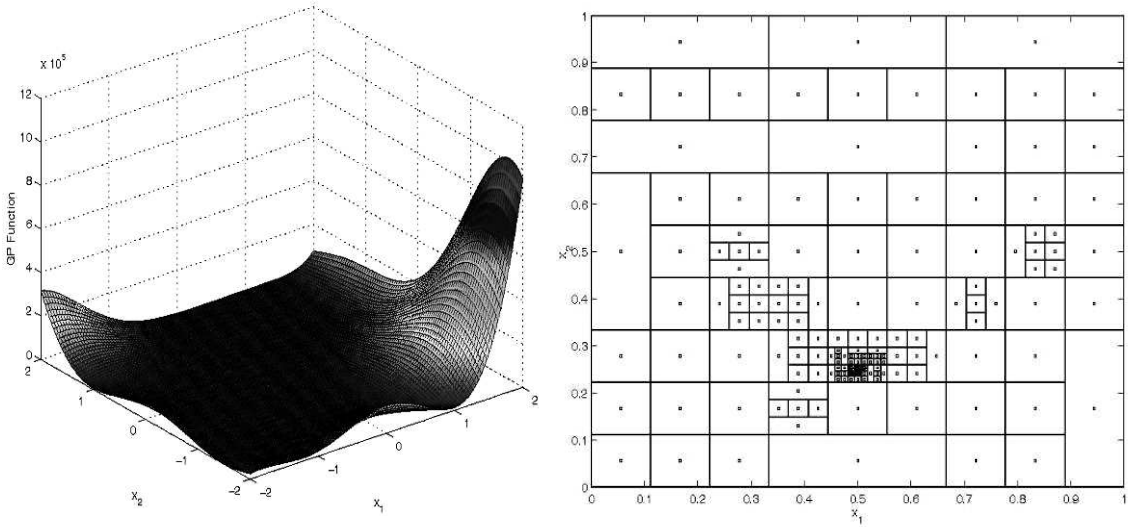

Figure A1.3 The graphical mapping of the search space division in the DIRECT method (on the right) realized on the example of a test function "Goldenstein-Price (on the left) [Finkel 2003].

Functioning of the algorithm is to divide the search space into smaller and smaller subspaces. In two-dimensional problem it will be exactly dividing the rectangle into smaller rectangles. In each iteration, selected rectangles are divided into three equal parts. And for each of them is determined centre of gravity for which is calculated the value of objective function. After division, follows the selection of potentially optimal rectangles. The value of the objective function for the center of gravity and the size of rectangle are taking into account as the selection criteria. It is possible that more than one rectangle meets the selection criteria. All potentially optimal rectangles are divided into three equal parts along the long side, which completes the iteration. The procedure is repeated until set number of iteration is used up, or the less value of objective function than established threshold is achieved. Graphic representation of the DIRECT method while searching a minimum of test function “Goldenstain-Price” is shown in the Figures A1.3 and A1.4.

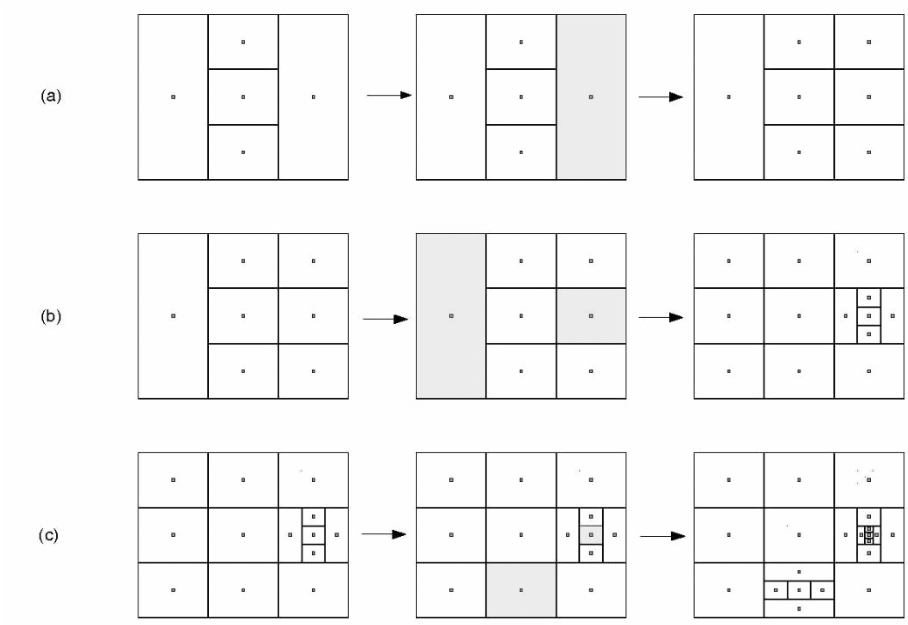

Figure A1.4 The block diagram of Simulated Annealing method..

APPENDIX II

Details of identification with the use of Haskell's model with synthetic data.

To test the researched procedures of identification of the model's parameters, A configuration with two and three layers was considered (including the half-space). In the simplest example of a heterogeneous system with two layers, the number of searched parameters was reduced to three: the velocity of the transversal wave for two layers and the thickness of the first layer. The rest of the parameters were assumed to be constant. The dispersion curves were generated with the use of the Haskell's model as well. In all the examples *1 kHz* was assumed for the scale of frequencies.

Identification procedure for the 2 layers – 3 parameters (2w3p) model configuration - LSQ method

The graphic result shows the Figure A2.1 and the number values are put in the table where Synt – means the synthetic data, Inv – the date obtained from the inversion. The numbers at individual parameters show the number of the layer i.e. V_{S2} is the velocity of the transversal wave in the second layer. Only the values in bold were the subject of identification.

The minimal value of the error function is *46,5* which gives us a normalized error BN of *0,033%* (according to the Equation IV.2) despite the fact that an ideal match should give a value of *0*. It is worth noticing that even for such a small number of variables the algorithm does not always find the right results, and the result shown is the most accurate of a few ones. It was noticed that when searching for *3* parameters most of the found results may be considered accurate (close approximation of the synthetic curve) despite different deviations of curve fit. The biggest advantage of this procedure is the small amount of time consumed for calculations – in this example it was approximately 4,2 minute.

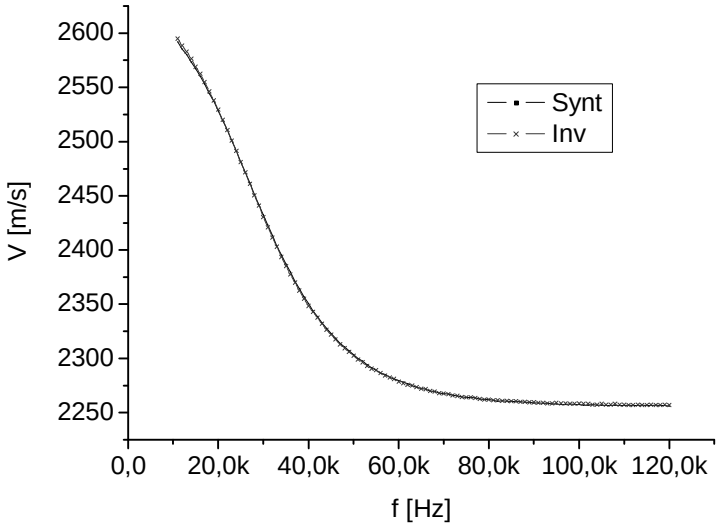

	Synt	Inv (LSQ)
V_P1 [m/s]	3900	3900
V_P2 [m/s]	4500	4500
V_S1 [m/s]	2500	**2501**
V_S2 [m/s]	3000	**3007**
d1 [cm]	3	**3,04**
$\rho 1$ [kg/m^3]	2000	2000
$\rho 2$ [kg/m^3]	2100	2100
BN [%]		0,033
Czas obliczeń [s]		252

Figure A2.1 The example of identification procedure with LSQ method for the model in a configuration: *2* layers *3* parameters (2w3p).

Identification procedure for the 2 layers – 3 parameters (2w3p) model configuration - SA method

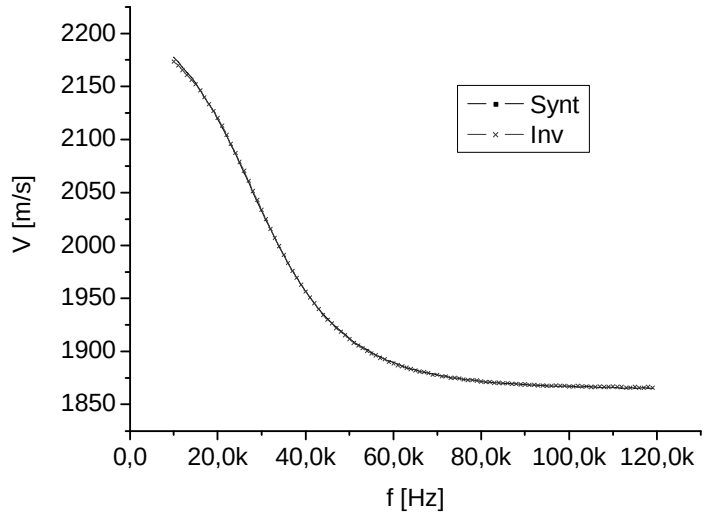

	Synt	Inv (SA)
V_P1 [m/s]	4000	4000
V_P2 [m/s]	4600	4600
V_S1 [m/s]	2000	**2005**
V_S2 [m/s]	2400	**2395**
d1 [cm]	2,5	**2,55**
$\rho 1$ [kg/m^3]	2000	2000
$\rho 2$ [kg/m^3]	2000	2000
BN [%]		0,027
Czas obliczeń [s]		3240

Figure A2.2 The example of identification procedure with SA method for the model in a configuration: *2* layers *3* parameters (2w3p).

To compare the usage of the local optimization procedure with the global procedure for parameters identification, the same task was solved with the use of the Simulated Annealing method. The dispersion characteristics fit with the parameters found was shown in the Figure A2.2. The minimal value of the objective function is close to the result for the local procedure and equals *58,5* which gives a fit error of *0,027%*. A disadvantage of global

procedures is a noticeable amount of time consumed for the realization of the tasks, it amounted to *54* minutes – ten times longer than in the case of the LSQ method. In the process of calculation the same computer was used.

Identification procedure for the 2 layers – 7 parameters (2w3p) model configuration - LSQ method

Decreasing the number of searched parameters makes the identification procedure faster, but in the real conditions it requires the knowledge of a group of parameters or their approximation. If the approximation is wrong the procedure of identification would not find the correct result. In the test below, the identification of all seven parameters for a two-layer structure was conducted. The calculations were done on the basis of LSQ method. The results of identification were shown in the Figure A2.3. Comparing the parameters it can be claimed that the worst match was obtained for the longitudinal wave velocity. It confirms the results of sensitivity research of Haskell's model described in the Chapter II.1.3. It must be remembered that the larger number of variables the more ambiguous the result is. It is important to know that both the velocity of the transversal wave and the thickness of the layer were estimated correctly. The minimal value of the function is comparable with the results received in the previous examples and equals *71,25* which gives a fit error of *0,021*. The time of calculation in comparison with a three parameter model was *10* minutes longer.

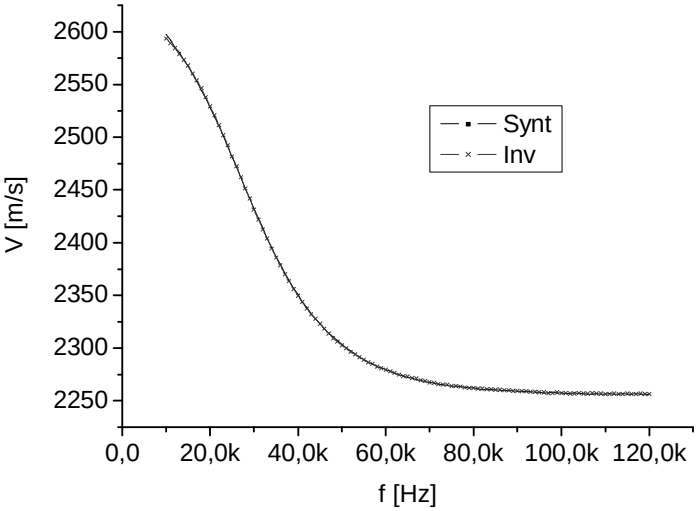

	Synt	Inv (LSQ)
V_P1 [m/s]	*3900*	***4470***
V_P2 [m/s]	*4500*	***4854***
V_S1 [m/s]	*2500*	***2437***
V_S2 [m/s]	*3000*	***2893***
d1 [cm]	*3*	***3,12***
$\rho 1$ [kg/m^3]	*2000*	***1999***
$\rho 2$ [kg/m^3]	*2100*	***2038***
BN [%]		*0,021*
Czas obliczeń [s]		*600*

Figure A2.3 The example of identification procedure with LSQ method for the model in a configuration: 2 layers 7 parameters (2w7p).

Identification procedure for the 2 layers – 7 parameters (2w7p) model configuration - SA method

The results obtained for identifications of seven parameters with the Simulated Annealing method are slightly less reliable than the results obtained thanks to the LSQ method. Similar to the previous experiences, large differences are for the longitudinal wave velocities and the density of layers. The example is characterized by a larger value of the objective function's minimum found which equals *355*, it results with an fit error *0.062%*. That is why more differences in identified parameters occur. The time used for leading the identification process amounted to *75* minutes – *7* times longer than in the case of LSQ method for the same task.

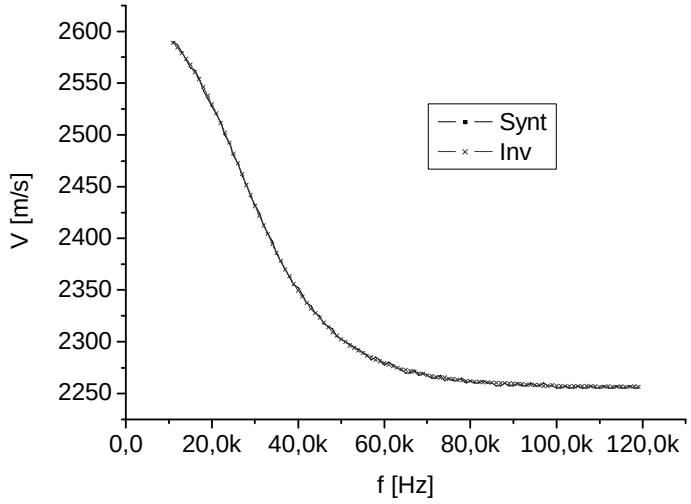

	Synt	Inv (SA)
V_P1 [m/s]	3900	**4842**
V_P2 [m/s]	4500	**5167**
V_S1 [m/s]	2500	**2414**
V_S2 [m/s]	3000	**2942**
d1 [cm]	3	**2,70**
$\rho 1$ [kg/m^3]	2000	**2440**
$\rho 2$ [kg/m^3]	2100	**1960**
BN [%]		0,062
Czas obliczeń [s]		4500

Figure A2.4 The example of identification procedure with LSQ method for the model in a configuration: 2 layers 7 parameters (2w7p).

Identification procedure for the 3 layers – 5 parameters (3w5p) model configuration – LSQ method

The next test of the optimization procedure was conducted on a three-layer model searching for five parameters. In the process of identification the values of transversal wave propagation velocity in different layers and thickness of these layers were assumed. The results of curve fitting process and the assumed parameters are shown in the Figure A2.5. The normalized fit error in this case equaled *0,098%* - three times more than in the case of *2*-layer model. Despite that, the comparison of the results of the identification with the synthetic

results is satisfying, especially for the transversal wave velocity in particular layers. The identification of Layers' thickness was set with a minor error only. The time of the calculation - *16* minutes – is *4* times longer than in the case of the *2*-layer model with *3* parameters searched.

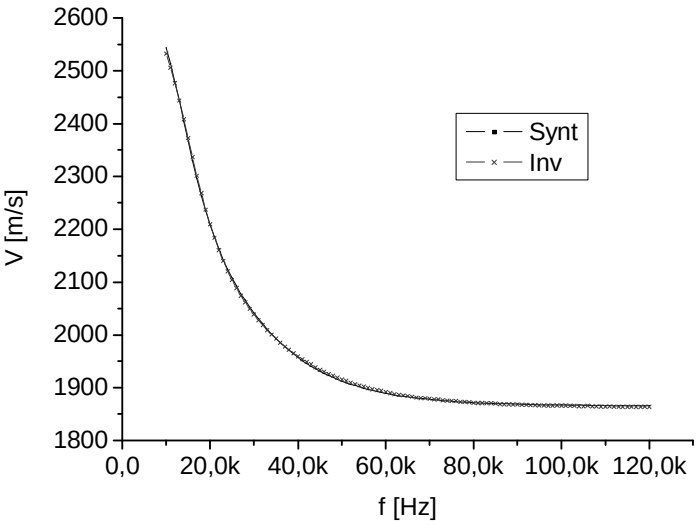

	Synt	Inv (LSQ)
V_P1 [m/s]	4000	4000
V_P2 [m/s]	4600	4600
V_P3 [m/s]	5200	5200
V_S1 [m/s]	2000	**1999**
V_S2 [m/s]	2400	**2337**
V_S3 [m/s]	3000	**2955**
d1 [cm]	2,5	**2,32**
d2 [cm]	4	**3,59**
$\rho 1$ [kg/m^3]	2000	2000
$\rho 2$ [kg/m^3]	2000	2000
$\rho 3$ [kg/m^3]	2100	2100
BN [%]		0,098
Czas obliczeń [s]		960

Figure A2.5 The example of identification procedure with LSQ method for the model in a configuration: 3 layers 5 parameters (3w5p).

Identification procedure for the 3 layers – 5 parameters (3w5p) model configuration - SA method

A similar procedure of identification for a three-layer model with five searched parameters was conducted with the use of SA method. The obtained match and parameters are shown in the Figure A2.6. It is characterized by a relatively small value of the objective function equaling *178,5* which gives an error of matching of *0,082%*. The time of the calculation for this example is *97* minutes – *6* times longer than in the case of LSQ procedure. It has to be mentioned that a good matching was acquired every time which supports the thesis that algorithms which work globally do not guarantee obtaining an accurate result.

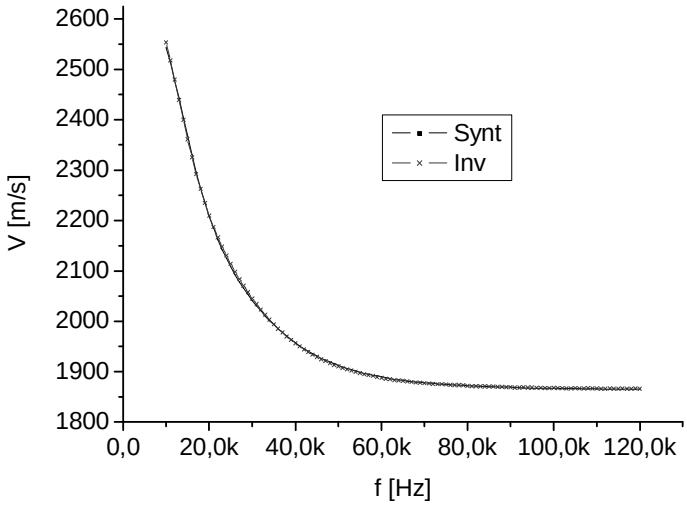

	Synt	Inv (SA)
V_P1 [m/s]	4000	4000
V_P2 [m/s]	4600	4600
V_P3 [m/s]	5200	5200
V_S1 [m/s]	2000	**2001**
V_S2 [m/s]	2400	**2459**
V_S3 [m/s]	3000	**3052**
d1 [cm]	2,5	**2,63**
d2 [cm]	4	**4,56**
$\rho1$ [kg/m³]	2000	2000
$\rho2$ [kg/m³]	2000	2000
$\rho3$ [kg/m³]	2100	2100
BN [%]		0,082
Czas obliczeń [s]		5820

Figure A2.6 The example of identification procedure with SA method for the model in a configuration: 3 layers 5 parameters (3w5p).

Résume de la thèse de doctorat

L’objectif principal de cette thèse est de développer deux méthodes de diagnostic des dégradations mécaniques et structurales du béton au moyen d'ultrasons. Les techniques choisies pour les mesures sont non-destructives et sans contact, permettant ainsi les situations où l’accès au corps d’épreuve est limité à une seule face. Les sujets considérés dans ce mémoire, nécessaires à la réalisation des objectifs de la thèse, sont les suivants :

- l’adaptation de deux modèles de propagation des ondes de surface dans des milieux hétérogènes (modèle de Haskell et modèle de Gibson), afin de générer les caractéristiques de la dispersion du matériau analysé ;

- l’adaptation du modèle réflectométrique, afin de générer les caractéristiques du coefficient de réflexion des ondes acoustiques sur la surface du matériau ausculté,

- le développement de deux systèmes de mesures automatisées : SWMD – système pour la mesure de la propagation des ondes du surface, RMD – système pour la mesure réflectométrique ;

- le développement de logiciels pouvant résoudre le problème inverse (inversion des caractéristiques de dispersion),

- la réalisation de plusieurs mesures en laboratoire et in situ pour la vérification du fonctionnement des systèmes développés.

Le travail est présenté dans six chapitres et deux annexes.

Le premier chapitre contient une introduction générale et définit les problèmes à résoudre et les objectifs du travail. Dans ce chapitre sont présentés : un état des lieux du domaine de diagnostic du béton, ainsi que les principaux problèmes et enjeux liés à ce sujet, une présentation et une analyse des méthodes non-destructives utilisées pour le diagnostic du béton.

Si l'on prend en compte le fait que les structures en béton sont soumises à des processus naturels de vieillissement et d'usure, pilonnés par l'influence défavorable de l'environnement et des conditions de fonctionnement souvent anormales, il devient évident qu'il est nécessaire d'assurer la sécurité de leur utilisation par la détection et l'indication de la localisation des dommages potentiels. Habituellement l'affaiblissement commence par la couche de surface. Au fil du temps, la dégradation s'étend en profondeur et peut affecter la zone de renfort, ce qui provoque une corrosion accélérée et excessive, qui à son tour peut avoir un impact significatif sur le risque de l'effondrement structurel. Signaler le problème au plus tôt est alors un enjeu majeur. Il est important et même nécessaire de surveiller et de diagnostiquer l'état de la construction. Cela nécessite des outils appropriés : des méthodes et équipements de test, une technologie, un enregistrement, un traitement de résultats ; le tout assuré par des systèmes d'aide au diagnostic, précis et fiables.

Les méthodes employées pour la surveillance et le diagnostic de l'état des ouvrages en béton peuvent se faire de façon destructive ou non-destructive. Le procédé non-destructif est depuis longtemps le sujet d'une forte demande et présente des avantages indéniables. La majorité des méthodes non-destructives fait appel à des ondes ultra-sonores, néanmoins il n'existe encore aucun « système » totalement opérationnel, crédible et fiable, destiné au diagnostic de l'état de la couche supérieure de béton. Après avoir présenté cette motivation, le chapitre justifie le choix de deux méthodes non-destructives (la méthode des ondes de surface et la méthode de réflectométrie).

Le deuxième chapitre contient une description des trois modèles de propagation des ondes ultrasonores. Les deux premiers, utilisés en géophysique : le modèle de Haskell et le modèle de Gibson, conviennent à la modélisation de propagation des ondes de surface (OS) dans les matériaux hétérogènes. Le troisième modèle est basé sur le phénomène de réflexion des ondes ultra-sonores par la surface d'un matériau poreux.

Le modèle de Haskell permet de générer des caractéristiques de dispersion des ondes de surface dans un milieu hétérogène. La prise en compte de l'hétérogénéité est réalisée par une composition de plusieurs couches homogènes. Il faut souligner que dans le but de résoudre ce modèle, il est nécessaire d'utiliser les outils d'optimisation numériques, car la solution analytique n'existe pas. Le modèle de Gibson décrit la propagation des OS dans un milieu hétérogène caractérisé par un changement linéaire du module de cisaillement en fonction de la profondeur.

Le troisième modèle exploite le phénomène de réflexion des ondes ultra-sonores et il est basé sur la théorie simplifiée de Biot.

Ce chapitre contient aussi une étude de la sensibilité de ces modèles. Il s'agit d'analyser l'impact des paramètres définissant le matériel physique ou structurel sur les résultats.

Dans le troisième chapitre, sont présentés les outils expérimentaux construits dans le cadre de ce travail afin de mettre en œuvre les techniques de diagnostic. Il s'agit de deux systèmes : le premier sert à l'étude de la propagation des ondes de surface et le second est utilisé pour les essais en réflexion ultra-sonore. Le développement de ces systèmes originaux sous-entend :

la réalisation de deux dispositifs automatisés pour mesurer les ondes de surface («SWMD») et les ondes réfléchies par la surface du béton (« RMD »),

le développement d'un logiciel à interface graphique pour contrôler le « SWMD » et le « RMD » - application de signaux à fréquence variable de type « chirp »

Ce chapitre contient aussi la description des différents essais de test effectués grâce à ces outils. Tout comme le chapitre précédent, le troisième chapitre est terminée par les conclusions.

Le quatrième chapitre est consacré aux méthodes d'identification des paramètres mécaniques et structuraux du béton à partir des mesures ultra-sonores. Le développement des algorithmes d'estimation de la valeur des paramètres mécaniques et structurels du béton dégradé basés sur les modèles y est présenté. Il contient, entre autres : une description des algorithmes (procédures) utilisés pour évaluer la profondeur de la dégradation et les paramètres qui déterminent la structure des matériaux testés, les résultats des vérifications et des essais effectués avec des données synthétiques et les conclusions du travail effectué. Les méthodes stochastiques et déterministes sont utilisées. En plus, deux programmes originaux pour résoudre les problèmes inversés sont développés. Le programme « Cloud Point » réalise l'inversion multiple avec l'utilisation du modèle de Haskell. Le deuxième programme, nommée « DDS » ; utilise le modèle de Gibson pour l'estimation de la profondeur de la dégradation.

Le cinquième chapitre contient une présentation et une analyse des résultats obtenus lors des mesures in situ et en laboratoire grâce aux outils de diagnostic développés. Avant de passer aux tests, une description des matériaux testés est présentée.

La mise en œuvre d'une grande série de mesures sur plusieurs échantillons de béton dans des conditions de laboratoire, ainsi que les mesures sur les ouvrages y sont présentés. Les mesures ont notamment été effectuées dans le projet « SENSO ». Les conclusions du travail sont formulées, comme précédemment, à la fin du chapitre.

Le sixième chapitre constitue une conclusion globale sur le travail effectué. Il présente aussi des perspectives pour les travaux ultérieurs.

Deux annexes complètent ce mémoire. La première présente le détail des méthodes d'optimisation, la seconde fournie le détail des procédures d'essai pour l'identification des paramètres du modèle de Haskell.

Abstract

Diagnostic ultrasonore de la dégradation mécanique et structurale du béton

Le travail présenté dans ce mémoire concerne le développement d'outils pour le diagnostic non-destructif et sans contact de l'état (dégradation) des matériaux de construction, principalement du béton. La thèse est focalisée sur deux techniques d'évaluation utilisant la propagation des ondes ultra-sonores : l'étude de la propagation des ondes de surface et l'analyse des coefficients de réflexion en fonction de l'angle d'incidence (réflectométrie). La partie théorique du travail présente les bases de la modélisation des phénomènes considérés, ainsi que la mise en œuvre des modèles décrits dans la résolution des problèmes inverses. Un logiciel utilisant des algorithmes d'optimisation pour l'identification des paramètres du modèle sur la base des données de mesure est développé dans le cadre ce travail. La partie expérimentale présente le développement de deux systèmes de mesures ainsi que leur utilisation en laboratoire et sur le terrain. Le but de cette partie est non seulement de développer des outils expérimentaux mais aussi de les rendre opérationnels pour une utilisation courante. Les applications des outils développés pour le diagnostic sont discutées sur la base d'exemples de résultats obtenus en laboratoire et in situ. Ils permettent de spécifier les paramètres tels que la profondeur de la dégradation, la vitesse des ondes de surface et des ondes transversales en fonction de la profondeur pour le matériau testé ainsi que la perméabilité de surface, la porosité et la tortuosité du matériau testé.

Mots-clefs : ultrasons, ondes de surface, la réflectométrie, systèmes de mesure, diagnostic de matériaux, d'identification, béton, CND, l'optimisation

Ultrasonic diagnostic of mechanical and structural degradation of concrete

The present work concerns the development of tools for non-destructive and non-contact diagnostic of state (degradation) of construction materials, mainly concrete. Attention is focused on two complementary techniques using the propagation of ultrasonic waves, i.e. the study of surface waves propagation and the analysis of reflection coefficients as a function of incidence angle (reflectometry). The theoretical part of the thesis shows the foundations of modelling the considered phenomena, as well as the implementation of the described models in solving the inverse problems. Software developed for this work uses optimization algorithms for identification of model parameters based on the measurement data. The chapters concerning the experimental work shows the construction of two measurement systems developed according to assumptions, including their possible use in both laboratory and field conditions. Applications of the developed diagnostic tools are discussed based on the examples of the results obtained in the laboratory and for the real objects. They allow to specify the parameters such as the depth of degradation, velocity of surface and S-waves as functions of the depth for the tested material and surface permeability, porosity and tortuosity of tested material.

Keywords: ultrasounds, surface waves, reflectometry, controlled measurement systems, diagnostic of materials, identification, concrete, NDT, optimization.